

**Dynamic Lateral Response of Single Piles Considering
Soil Inertia Contribution**

By

Gustavo E. Pacheco-Crosetti, MSCE

A thesis submitted in partial fulfillment of the requirements for the degree of

DOCTOR OF PHILOSOPHY
in
Civil Engineering

UNIVERSITY OF PUERTO RICO
MAYAGÜEZ CAMPUS
May 2007

Approved by:

Ricardo López-Rodríguez, PhD
Member, Graduate Committee

Date

José A. Martínez-Cruzado, PhD
Member, Graduate Committee

Date

Miguel A. Pando-López, PhD
Member, Graduate Committee

Date

Luis E. Suárez-Colche, PhD
President, Graduate Committee

Date

Victor Snyder-Sevits, PhD
Representative of Graduate Studies

Date

Ismael Pagán-Trinidad, MSCE
Chairperson of the Department

Date

*To Ernesto W. Pacheco,
my father, my friend, my guide and master.*

Abstract

The most widely used model to perform the analysis of piles under lateral loads consists in modeling the pile as a series of beam elements and representing the soil as a group of unconnected, concentrated springs perpendicular to the pile (*Discrete Winkler Model*). The literature review shows that the soil stiffness and damping properties are included in a dynamic analysis through lumped springs and dashpots, but a lumped mass to represent soil inertia is not included.

The objective of this investigation is to perform an analytical and numerical study of the dynamic response of the pile-soil system under lateral loads (considering the soil as a semi-infinite half space), in order to develop a rational method that includes the soil contribution to the system inertial properties through a series of lumped masses, consistent with the Discrete Winkler Model, and to evaluate the importance of such lumped mass in the system response.

A simplified lumped model, consistent with the Winkler hypothesis, was obtained by performing an approximation of the continuous (plane strain) model developed by Novak. In the proposed approach, the pile-soil interaction is taken into account through three frequency independent elements: a spring with stiffness k_a , a mass with value m_a , and a dashpot with coefficient c_a . The spring-mass-dashpot coefficients k_a , m_a , and c_a that represent the soil can be obtained by means of simple equations.

The proposed lumped model was used to demonstrate that a lumped soil mass is not required for small soil Poisson's ratios. However, the soil mass is important for high soil Poisson's ratios, as may be the case of saturated soils (for $\nu = 0.5$ the required soil lumped mass is in the same order of the pile mass contribution).

Resumen

El modelo más usado para efectuar el análisis de pilotes bajo carga lateral consiste en modelar el pilote como una serie de elementos de viga (flexionales), y representar al suelo como un grupo de resortes concentrados, desconectados, perpendiculares al pilote (*Modelo Discreto de Winkler*). La revisión bibliográfica muestra que las propiedades de rigidez y amortiguamiento del suelo son incluidas en un análisis dinámico por medio de resortes y amortiguadores concentrados, pero las propiedades de inercia del suelo no son consideradas por medio de una masa concentrada.

El objetivo de esta investigación es desarrollar un estudio analítico y numérico de la respuesta dinámica del sistema suelo-pilote bajo cargas laterales (considerando el suelo como un espacio semi-infinito), para desarrollar un método racional que incluya la contribución del suelo a las propiedades de inercia del sistema, a través de una serie de masas concentradas, consistentes con el Modelo Discreto de Winkler, y evaluar la importancia de esta masa concentrada en la respuesta del sistema.

Se realizó una aproximación al modelo continuo (de estado plano de deformaciones) desarrollado por Novak, para obtener un modelo simplificado consistente con las hipótesis de Winkler. La interacción suelo-pilote se tiene en cuenta a través de tres elementos independientes de la frecuencia: un resorte de rigidez k_a , una masa de valor m_a , y un amortiguador de constante c_a . Estos tres coeficientes se obtienen por medio de expresiones sencillas.

Este modelo se usó para demostrar que para razones de Poisson bajas no se requiere una masa concentrada de suelo. Sin embargo, para razones de Poisson altas, como es el caso de suelos saturados, la masa de suelo es importante (para $\nu = 0.5$ la masa concentrada de suelo es del mismo orden que la contribución de masa del pilote).

Acknowledgements

I would like to thank everybody who contributed to the development of this project:

- God, for giving meaning to every journey.
- Blanca, my wife, and Natalia, my daughter, for their support, their love, and their enormous sacrifice during the last five years. They are the center of my universe, and a continuous source of strength, peace and happiness.
- My family in Argentina (my father Ernesto, my mother Anita, my brother Gastón, and my sister Gabriela), for their love, continuous presence, and for always being a source of inspiration and encouragement.
- Dr. Luis Suarez, for his support, guidance, sharp comments and suggestions, and for his friendship. He has always been a role model, both as a professor and as a person.
- The members of my graduate committee, Drs. López, Martínez and Pando, for their time and support. Dr. Pando gave me a deep insight into the behavior of piles, and provided me with very useful references.
- Dr. Carlos Prato and Victor De Napoli, for their kindness in providing me the documents describing the dynamic tests they performed over piles under lateral loads.
- Dr. Pedro Arduino, who gave me some useful references. We have shared studies and friendship for more than 14 years.
- The Faculty Members of the Civil Engineering department at UPR-Mayagüez, for the exquisite learning experience I have had during my graduate studies.
- My classmates, for their friendship and stimulating talks. Juan Carlos Morales, Orlando Cundumi, Fabián Consuegra, and Jorge Botero not only provided a deeply estimated friendship, but also an indispensable support to complete my classes when I got sick.
- Eduardo Veras, for his friendship, his support and diligence sending me some papers from Florida, and for his encouragement.
- The Polytechnic University of Puerto Rico (PUPR), for the support and accommodation provided to help me pursue graduate studies.

- Susana Concepción-Nieves, from the PUPR Library, for her support and diligence obtaining several papers I have requested that were not available in PR.
- The administrative personnel of the Civil and Environmental Department at PUPR, for their support and understanding: José Borrageros, Amado Vélez, Iris Rosado, and Carmen Rodríguez.
- My colleague, partner and friend José A. Martinez, for his support and understanding during these years.

Table of Contents

1	Introduction.....	1
1.1	Justification.....	1
1.2	Objectives and Scope.....	2
1.3	General Procedures and Methods	3
1.3.1	Soil Model Proposed for this Work	4
1.3.2	Proposed Numerical Implementation	6
2	Literature Review and Background	7
2.1	Analytical Models for Piles under Static Lateral Load.....	7
2.1.1	Beam on Elastic Foundation Approach	7
2.1.1.1	The p-y Method.....	11
2.1.1.2	The Wedge Model.....	14
2.1.1.3	New Developments in BEF	15
2.1.2	Elastic Continuum Approach.....	16
2.1.3	The Finite Element Approach.....	18
2.2	Analysis of Piles under Dynamic Lateral Loads.....	21
2.2.1	Winkler Approach.....	21
2.2.2	Continuum Approach.....	27
2.2.3	Finite Element Approach	30
3	Numerical Evaluation of the Soil Inertia Contribution to the Soil-Pile System	
	Response	34
3.1	Case Study	34
3.2	Dynamic Response to be Evaluated.....	35
3.3	Analysis Package, Type, and General Parameters.....	36
3.4	General Comments on the Finite Element Model to be Adopted.....	36
3.5	Two Dimensional Analysis.....	37
3.5.1	Boundary Conditions	38
3.5.2	FEM Mesh	39
3.5.3	System Response	40
3.5.4	Discussion of the 2D Results	43
3.6	Three Dimensional Model	45
3.6.1	Boundary Conditions	45
3.6.2	FEM Mesh	49
3.6.3	System Response	51
3.6.4	Discussion of the 3D Results	61
3.6.5	Comments on the 3D Model Analysis Applicability	64

4	Lumped Soil Model for Dynamic Soil-Pile System Response	66
4.1	Dynamic Stiffness and Flexibility of a SDOF System	66
4.2	Novak's Dynamic Stiffness to Model Soil-Pile Interaction	74
4.3	Equivalent Lumped Model	78
4.3.1	Lumped Coefficients Definition	79
4.3.2	Determination of the Lumped Coefficients	81
4.3.3	Lumped Coefficients Analysis.....	91
4.4	Pile Element Matrices	98
4.4.1	Classical Beam Element with Lumped Soil.....	98
4.4.2	Classical Beam Element with Distributed Soil	101
4.4.3	Refined Beam Element with Distributed Soil.....	104
5	Proposed Lumped Model Validation/Verification.....	107
5.1	Lumped Dynamic Stiffness Approximation of Novak Continuum Model for Plane Strain	107
5.2	Pile with Lumped Model vs Pile with Novak Model	112
5.2.1	Lumped vs Novak Model for Different Soil Poisson's Ratios	119
5.2.2	Lumped vs Novak Model for Different Pile Radius	121
5.2.3	Lumped vs Novak Model for Different Soil Modulus of Elasticity	123
5.3	1D Stiffness Method Model vs. 3D FEM Model.....	126
5.4	Modeling of Experimental Pile Test with Lumped Soil Model.....	130
5.5	The Effect of Poisson's Ratio in the 3D FE System Response.....	133
5.6	Comparison to other Models.....	136
5.6.1	Damping Coefficient.....	136
5.6.2	Stiffness Coefficient.....	140
5.7	Final Comments	143
6	Applications of the Proposed Lumped Model	144
6.1	Effect of the Pile Stiffness on the System Response	144
6.2	Effect of the Radiation Damping on the System Response	146
6.3	Analysis of the Mass Effect on a 3D FE Model System Response	148
6.3.1	Effect of the Mass Distribution on a System of Springs in Series.....	149
6.3.2	Effect of the Mass Distribution on a MDOF System.....	151
6.3.3	Effect of the Mass Distribution on a Pile-Soil System	153
6.3.4	Discussion of the Results – FE Model Propagation Damping.....	158
6.3.4.1	2D FE Model Subjected to an Impulsive Force.....	158
6.3.4.2	Effect of Parallel Springs without Distributed Masses	162
6.3.4.3	Effect of the Mass in a 3D Truss	163
7	Conclusions and Recommendations	165
7.1	Summary and Conclusions	165
7.2	Recommendations.....	171

8	References.....	173
8.1	Books	173
8.2	Class Notes.....	174
8.3	Technical Manuals, Guides and Reports	174
8.4	Research Reports and Thesis	176
8.5	Papers.....	177
A	Soil Deposit and Pile Natural Frequencies	183
A.1	Soil Deposit Natural Frequencies, Wave Length, and FEM Element Size	183
A.2	Pile Natural Frequencies and Modal Shape	186
B	FEM Analysis in SAP.....	193
B.1	Analysis Type	193
B.2	Step by Step Model Generation	193
C	FEM Boundary Spring Constants	201
D	Lumped Equivalent Coefficients for Novak Model.....	205
D.1	Case of $D = 0.0$ and $\nu = 0.5$	207
D.2	Case of $D = 0.0$ and $\nu = 0.45$	214
D.3	Case of $D = 0.0$ and $\nu = 0.35$	221
D.4	Case of $D = 0.0$ and $\nu = 0.3$	228
E	Pile Element with Distributed Soil Parameters.....	235
E.1	Classical Beam Element	235
E.1.1	Element Stiffness Matrix	241
E.1.2	Element Mass Matrix	244
E.1.3	Element Damping Matrix	245
E.2	Refined Beam Element	246
E.2.1	Refined Element Stiffness Matrix.....	250
E.2.2	Refined Element Mass Matrix	254
E.2.3	Refined Element Damping Matrix.....	256
E.3	Analysis of Convergence to the Natural Frequency	257
E.3.1	Classical Beam Element with Lumped Mass Matrix.....	260
E.3.2	Classical Beam Element with Consistent Mass Matrix	262
E.3.3	Refined Beam Element with Consistent Mass Matrix.....	264

F	Programs for Approximate Model Verification.....	267
F.1	FRF Using Novak Plane Strain Soil Dynamic Stiffness.....	267
F.2	FRF Using Lumped Soil Dynamic Stiffness	270
F.3	FRF Comparing Novak and Lumped Models.....	272
F.4	FRF Comparing Novak and Lumped Models for Different v	275
F.5	FRF Comparing Novak and Lumped Models for Different ρ	279
F.6	FRF Comparing Novak and Lumped Models for Different E	282
F.7	FRF Implemented in SAP	285
F.7.1	SDOF System	285
F.7.2	Pile + Lumped Soil System	288
F.8	Dynamic Stiffness of Pile Top for Di Napoli and Prato Test	290
F.9	Damping Coefficient Comparison	293
F.10	Stiffness Coefficient Comparison	298
G	Influence of Pile Stiffness on the FRF of Pile Head.....	309
G.1	FRF Comparing Pile Alone and Pile + Soil for Different Radius	309
H	Influence of Radiation Damping on the FRF of Pile Head.....	312
H.1	FRF Comparing Pile Alone and Pile + Soil for Different C_a	312
I	Influence of the Soil Mass Distribution	315
I.1	FRF For a System with Springs in Series	315
I.2	FRF For a System with Springs in Parallel.....	316
I.3	FRF For a Pile-Soil System with Springs in Series	318
I.4	FRF For a Pile-Soil System with Springs in Parallel.....	322
I.5	FRF For a Pile-Soil System with Single Spring	325

List of Figures

Figure 2.1 Subgrade Reaction Modulus Model: (a) Pile and Soil representation, (b) Effect of a partial uniform pressure over the soil model	8
Figure 2.2: Finite-Difference Discretization for the Analysis of Laterally Loaded Piles (Poulos and Davis, 1980)	10
Figure 2.3: Typical p-y Curve for Ductile and Brittle Soil (FHWA, 1997)	11
Figure 2.4: Schematic of Pile-Soil Model for the p-y Approach (FHWA, 1997).....	12
Figure 2.5: Distribution of contact stresses against a pile before and after lateral deflection (Reese and Van Impe, 2001)	13
Figure 2.6: Lateral loading and resistance components on a drilled shaft (Wallace et al, 2001).....	14
Figure 2.7: Wedge Model Configuration and Distribution of Soil-Pile Reaction along Deflected Pile (Ashour and Norris, 2000).....	15
Figure 2.8: General Pile Discretization for the Analysis of Soil as a Continuous. Stresses acting on (a) pile, (b) soil adjacent to pile (Poulos and Davis, 1980).....	17
Figure 2.9: Example of a Three-Dimensional Finite Element Mesh for a Single Pile System (Yang and Jeremic, 2002)	19
Figure 2.10: Example of a Finite Difference Mesh for a Soil–Pile System: (a) 3D View, (b) Close-up of sleeved zone (Ng and Zhang, 2001)	20
Figure 2.11: p-y Method for Modeling Hysteretic Damping and Cyclic Degradation in Soil (Brown et al., 2001)	22
Figure 2.12: Hysteretic Cycle using Masing’s Rules (Suarez, 2003)	23
Figure 2.13: Models to Analyze Radiation Damping for a Horizontally Vibrating Pile (Wang et al., 1998).....	24
Figure 2.14: BNWF Model with Different Damping Effects	24
Figure 2.15: Hybrid Dynamic Winkler Model for Lateral Pile Response (Nogami and Koganai, 1988)	25
Figure 2.16: Schematic for the Nonlinear HDWM (Nogami et al., 1992)	26
Figure 2.17: Model for Seismic Analysis of Pile-Supported Bridge (Hutchinson et al., 2004)	27
Figure 2.18: Discrete Planes and Free-Field Boundary Conditions (Klar and Frydman, 2002).....	32
Figure 2.19: Example of a 3D FE Mesh and Boundary Elements for the Dynamic Analysis of a Soil–Pile System: (a) top view, (b) elevation (Maheshwari et al., 2004).....	33
Figure 3.1: 2D FEM Model.....	39
Figure 3.2: FEM Model Node Identification near Pile Top	39
Figure 3.3: FRF for the 2D Model without Soil Mass.....	41
Figure 3.4: FRF for the 2D Model with Soil Mass.....	41
Figure 3.5: FRF for the 2D Model with and without Soil Mass, and no Lateral Supports	42
Figure 3.6: 2D FEM Mesh with Partial Soil Mass Assignment	42
Figure 3.7: FRF for the 2D Model with Partial and Full Soil Mass Assignment, and no Lateral Supports ..	43
Figure 3.8: Dashpot Elements to Simulate Radiation Damping in the FE Cut-off Boundaries.....	46
Figure 3.9: Rectangular Soil Island Dimensions	47
Figure 3.10: Isometric View of the FEM 3D Model Mesh	49
Figure 3.11: Front View of the FEM 3D Model Mesh (long dimension).....	50
Figure 3.12: Right View of the FEM 3D Model Mesh (short dimension)	50
Figure 3.13: FRF for the 3D Model without Soil Mass.....	52
Figure 3.14: FRF for the 3D Model with Soil Mass.....	52
Figure 3.15: FRF for the 3D Model with and without Soil Mass, and no Lateral Supports	53
Figure 3.16: FRF for the 3D Model with Soil Mass, and Dashpots in the Lateral Cutoff Boundaries.....	54
Figure 3.17: 3D FEM Mesh with Partial Soil Mass Assignment	55
Figure 3.18: FRF for the 3D Model with Partial Soil Mass and no Lateral Supports	56
Figure 3.19: FRF for the 3D Model with Soil Mass, and Springs and Dashpots in the Lateral Cutoff Boundaries.....	57
Figure 3.20: FRF for the 3D Model without Soil Mass, and Rollers in the Lateral Cutoff Boundaries	58
Figure 3.21: FRF for the 3D Model with Soil Mass, and Rollers in the Lateral Cutoff Boundaries.....	59

Figure 3.22: FRF for the 3D Model with Soil Mass, and Springs-Dashpots Elements in the Lateral Cutoff Boundaries, together with Soil and Pile Natural Frequencies	60
Figure 4.1: SDOF System	66
Figure 4.2: Free Body and Kinetic Diagrams	67
Figure 4.3: Dynamic Stiffness Components (Phase Diagram)	69
Figure 4.4: Variation of Real and Imaginary Components of $Kd(\omega)$ as a Function of Load Frequency ω ...	70
Figure 4.5: Variation of $ Kdr(\omega) $ as a Function of Load Relative Frequency ωr , for Different Damping Ratios.....	71
Figure 4.6 : Phase Angle ϕ a Function of Load Relative Frequency ωr , for Different Damping Ratios.....	72
Figure 4.7: Variation of $ Hr(\omega) $ as a Function of Load Relative Frequency ωr , for Different Damping Ratios.....	73
Figure 4.8: Horizontal Stiffness and Damping Parameters S_{u1} and S_{u2}	76
Figure 4.9: Comparison of Approximate (Novak) vs. More Rigorous Approach (Aboul-Ella and Novak, 1978)	78
Figure 4.10: Real Part of $f(a_0, \nu, D)$ for $\nu = 0.5$ and $D = 0.0$ (red), Data Points (Green), and Polynomial Approximation (Blue)	84
Figure 4.11: Imaginary Part of $f(a_0, \nu, D)$ for $\nu = 0.5$ and $D = 0.0$ (red), Data Points (Green), and Polynomial Approximation (Blue)	84
Figure 4.12: Real Part of $f(a_0, \nu, D)$ for $\nu = 0.48$ and $D = 0.0$ (red), Data Points (Green), and Polynomial Approximation (Blue)	86
Figure 4.13: Real Part of $f(a_0, \nu, D)$ for $\nu = 0.47$ and $D = 0.0$ (red), Modified Data Points (Green), and Polynomial Approximation (Blue)	86
Figure 4.14: Variation of Regression Coefficients with Poisson's Ratio [0.3-0.5]	87
Figure 4.15: Variation of Regression Coefficient α_m with Poisson's Ratio [0.3-0.5]	88
Figure 4.16: Real Part of $f(a_0, \nu, D)$ for $\nu = 0.30$ and $D = 0.0$ (red), and Horizontal Line Approximation (Blue) using Inflection Point	89
Figure 4.17: Real Part of $f(a_0, \nu, D)$ for $\nu = 0.30$ and $D = 0.0$ (red), Horizontal Line Approximation (Blue) using the Mean Value, and Selected Data Points (green).....	90
Figure 4.18: Variation of Regression Coefficients with Poisson's Ratio [0-0.3]	90
Figure 4.19: Variation of Regression Coefficients with Poisson's Ratio [0.5-0.0]	92
Figure 4.20: Dimensionless FRF for $\xi = 0.2$	94
Figure 4.21: Dimensionless FRF for $\xi = 1.5$	95
Figure 4.22: Dimensionless FRF for $\xi = 10.0$	95
Figure 4.23: Dimensionless FRF for Different M and ξ	96
Figure 4.24: Effect of ν in the Propagation of P-Waves.....	97
Figure 4.25: Pile Element DOF	98
Figure 4.26: Pile Element with Lumped Soil Parameters.....	101
Figure 4.27: Pile Element with Distributed Soil Parameters	102
Figure 4.28: Refined Beam Element with Distributed Soil Parameters	105
Figure 5.1: Coefficient of Determination for Different Poisson's Ratios.....	109
Figure 5.2: Coefficient of Determination of the Imaginary Part for Different Poisson's Ratios.....	111
Figure 5.3: Coefficient of Variation of the Real Part for Different Poisson's Ratios.....	112
Figure 5.4: Pile Analytical Model and Element Matrices	113
Figure 5.5: FRF of Pile without Soil Contribution	114
Figure 5.6: Soil-Pile Analytical Models.....	115
Figure 5.7: Pile-Soil System FRF Using Novak Model	116
Figure 5.8: Pile-Soil System FRF Using Lumped Model.....	117
Figure 5.9: Comparison between Lumped FRF (red) and Novak FRF (blue).....	117
Figure 5.10: FRF with and Without Soil Contribution.....	118
Figure 5.11: Comparison Between Lumped FRF (red) and Novak FRF (blue) for Different Soil Poisson's Ratios $[0.20 \leq \nu \leq 0.30]$	119

Figure 5.12: Comparison Between Lumped FRF (red) and Novak FRF (blue) for Different Soil Poisson's Ratios [$0.32 \leq \nu \leq 0.42$]	120
Figure 5.13: Comparison Between Lumped FRF (red) and Novak FRF (blue) for Different Soil Poisson's Ratio [$0.44 \leq \nu \leq 0.50$]	121
Figure 5.14: Comparison Between Lumped FRF (red) and Novak FRF (blue) for Different Pile Radius [$1.0 \text{ ft} \leq r_o \leq 6.0 \text{ ft}$]	122
Figure 5.15: Comparison Between Lumped FRF (red) and Novak FRF (blue) for Different Pile Radius [$7.0 \text{ ft} \leq r_o \leq 10.0 \text{ ft}$]	123
Figure 5.16: Comparison between Lumped FRF (red) and Novak FRF (blue) for Different Soil Elastic Modulus [$200 \text{ ksf} \leq E \leq 2200 \text{ ksf}$]	124
Figure 5.17: Comparison between Lumped FRF (red) and Novak FRF (blue) for Different Soil Elastic Modulus [$2600 \text{ ksf} \leq E \leq 3800 \text{ ksf}$]	125
Figure 5.18: 1D Model Implemented in SAP2000	127
Figure 5.19: FRF of Pile Head using the 1D Model	127
Figure 5.20: FRF of Pile Head: 3D vs. 1D Models	128
Figure 5.21: FRF of Pile Head: 3D vs. 1D Models with Reduced Damping	129
Figure 5.22: Load Cell Fixed to the Pendulum and Accelerometer Fixed to Pile Top (De Napoli and Prato, 2006)	130
Figure 5.23: Tested Pile Group Layout (De Napoli and Prato, 2006)	131
Figure 5.24: Real and Imaginary Components of the Dynamic Stiffness. Pile P3D30. Directions N-S and E-W (E-O) (De Napoli, 2006)	132
Figure 5.25: Real and Imaginary Components of the Dynamic Stiffness Obtained Numerically with the Lumped Model	132
Figure 5.26: 3D FE Model FRF for Different Poisson's Ratios	134
Figure 5.27: 3D FE Model Static Flexibility for Different Poisson's Ratios	134
Figure 5.28: 3D FE Model Static Stiffness for Different Poisson's Ratios	135
Figure 5.29: 1-D Radiation Damping Model	136
Figure 5.30: Ratio between Damping Coefficients C_a and C_B for Different Poisson's Ratio of the Soil	138
Figure 5.31: Ratio between Damping Coefficients C_a and Modified C_B for Different Poisson's Ratio of the Soil	139
Figure 5.32: Relative Stiffness k_a/k_h for Different Modulus of Elasticity of the Soil	141
Figure 5.33: Relative Stiffness k_a/k_h for Different Poisson's Ratio of the Soil	142
Figure 5.34: Relative Stiffness k_a/k_h for Different Modulus of Elasticity of the Soil and the Pile for Soil Poisson's Ratio $\nu = 0.4$	142
Figure 5.35: Relative Stiffness k_a/k_h for Different Modulus of Elasticity of the Soil and the Pile for Soil Poisson's Ratio $\nu = 0.3$	143
Figure 6.1: Comparison between Pile Alone FRF (red) and Pile with Soil FRF (blue) for Different Pile Radius	145
Figure 6.2: Comparison between Pile Alone FRF (red) and Pile with Soil FRF (blue) for Different Pile Radius	146
Figure 6.3: Effect of Different Damping Coefficient Value on the System FRF	147
Figure 6.4: FRF for the 3D Model with and without Soil Mass, and no Lateral Supports	148
Figure 6.5: Models used to Analyze the Effect of the Added Mass in a System of Springs in Series	150
Figure 6.6: Effect of the Mass Distribution in a System of Springs in Series	150
Figure 6.7: Models used to Analyze the Effect of the Added Mass in a System of Springs in Parallel	152
Figure 6.8: Effect of the Mass Distribution in a System of Springs in Parallel	153
Figure 6.9: Piles Models to be Analyzed	154
Figure 6.10: FRF of the Pile without Soil Contribution	156
Figure 6.11: FRF of the Pile with Soil Contribution. $M_a \approx 10 \text{ Mp}$	156
Figure 6.12: FRF of the Pile with Soil Contribution. $M_a \approx 100 \text{ Mp}$	157
Figure 6.13: Impulsive Ramp Function	159
Figure 6.14: Points for Response Calculation	159
Figure 6.15: Displacement Time Histories of two Nodes when the Soil Mass is Neglected	160

Figure 6.16: Response of First and Last Point when Soil Mass is Considered.....	161
Figure 6.17: Response for all Points when Soil Mass is Considered	161
Figure 6.18: System with Parallel Springs with no Added Masses	162
Figure 6.19: FRF for the System with Parallel Springs with no Added Masses.....	163
Figure 6.20: 3D Truss Model View.....	164
Figure 6.21: FRF of Pile Top in the 3D Truss Model	164
Figure 7.1: Analytical Model for the Proposed Lumped Soil Representation.....	168
Figure A.1: Maximum Element Size for 4 th Natural Frequency.....	184
Figure A.2: Maximum Element Size for 8 th Natural Frequency.....	185
Figure B.1: Template Selection and Mesh Parameters.....	194
Figure B.2: Soil Mesh	195
Figure B.3: Soil Mesh (Area Elements) and Pile (Frame Elements).....	195
Figure B.4: Load Case Definition	196
Figure B.5: Analysis Case Definition.....	197
Figure B.6: Setting the Parameters to be Plotted - a.....	198
Figure B.7: Setting the Parameters to be Plotted - b.....	199
Figure B.8: Setting the Parameters to be Plotted - c.....	199
Figure B.9: Frequency Response Function.....	200
Figure C.1: Rectangular Soil Island Dimensions	201
Figure C.2: Computation of Coefficients β for x plane	203
Figure C.3: Computation of Coefficients k and K for x plane	204
Figure E.1: Pile Element with Distributed Soil Parameters.....	235
Figure E.2: Beam Element Shape Functions (Battini, 2006).....	236
Figure E.3: Refined Pile Element with Distributed Soil Parameters.....	246
Figure E.4: Normalized Coordinate Sistem.....	247
Figure E.5: Refined Beam Element Shape Functions - a	248
Figure E.6: Refined Beam Element Shape Functions - b	249
Figure E.7: Refined Beam Element Shape Functions - c	250
Figure E.8: First Natural Frequency vs Number of Elements (ne).....	258
Figure E.9: Second Natural Frequency vs Number of Elements (ne).....	258
Figure E.10: Third Natural Frequency vs Number of Elements (ne)	259
Figure E.11: Fourth Natural Frequency vs Number of Elements (ne).....	259
Figure F.1: Link Element DOF vs. Global Coordinates.....	285
Figure F.2: SDOF Problem	286
Figure F.3: SDOF System SAP Model.....	287
Figure F.4: SDOF Problem SAP Response vs. Analytical Response.....	288
Figure F.5: SAP Link Element Definition for 1D Pile with Soil Model	289

List of Tables

Table 3.1: Values of Elastic Modulus E for Different UBC Site Types	35
Table 3.2: Equivalent Elastic Properties for the 2D Model	38
Table 3.3: Elastic Properties for 3D Model	45
Table 3.4: Dashpot Coefficients for the Cut off Boundaries	47
Table 3.5: Spring Coefficients for Cutoff Boundaries.....	48
Table 3.6: Soil Stratum and Pile Natural Frequencies and Wavelengths	61
Table 4.1: Regression Coefficients α_k , α_m , and α_c for ν [0.5-0.31].....	88
Table 4.2: Regression Coefficients α_k , α_m , and α_c for ν [0.3-0.0].....	91
Table 4.3: Damping ratio ξ for ν [0.50-0.30]	93
Table 5.1: Coefficient of Determination for Different Poisson's Ratios [0.31-0.50]	109
Table 5.2: Coefficient of Determination and Coefficient of Variation for Different Poisson's Ratios [0.31-0.50]	111
Table F.1: Link Element DOF vs. Global DOF	285

1 Introduction

This chapter presents the justification of the developed research project, and the objectives and scope of the work, together with a brief discussion of the methodology adopted to develop the project.

1.1 Justification

Foundation systems composed by isolated piles or pile groups are extensively used to support different types of structures placed over soft soil layers, where shallow foundations are not appropriate because they do not provide the required capacity, or may experience too large settlements.

These pile foundations have to be designed to support lateral loads due to earthquakes, wind, and vehicle impact loads, among others. The most widely used model to perform the analysis of piles under lateral loads consists in modeling the pile as a series of beam elements, and considering the pile-soil interaction by representing the soil as a group of unconnected, concentrated springs perpendicular to the pile (*Discrete Winkler Model*). In order to consider soil non-linear behavior, the springs can have a varying stiffness given through a non-linear load-deflection relationship that depends on the type of soil and type of pile, known as *p-y curves*.

To adequately address pile response under earthquake actions, or to analyze heavy vibratory machine foundations, it is often required to perform a dynamic analysis of the pile for transverse (lateral) vibrations. For a dynamic analysis it is critical to have an adequate representation of the system stiffness (force-deflection relationships), and adequate representation of the system mass involved in the vibration phenomena. Up to now, the Winkler model that is generally used only takes into account the mass of the pile, and does not consider the possible soil mass contribution to the inertia characteristics of the system.

The literature review (presented in Chapter 2) shows that the soil stiffness and damping properties are included in a dynamic analysis through lumped springs and dashpots, but a lumped mass to represent soil inertia is not included. The objective of this investigation is to perform an analytical and numerical study of the dynamic response of the pile-soil system under lateral loads (considering the soil as a semi-infinite half space) in order to assess the importance of the soil mass in the system response, and develop a rational method that includes the soil contribution to the system inertial properties through a series of lumped masses, consistent with the Discrete Winkler Model.

1.2 Objectives and Scope

The main objective of this investigation is to assess the importance of the soil mass in the soil-pile system response and to develop a rational method to include the soil contribution to the inertial properties of a soil-pile system under dynamic lateral loads, through lumped masses consistent with the discrete Winkler model. This would lead to a better representation of the dynamic soil-pile interaction.

After performing the analytical studies necessary to develop a procedure for the inclusion of the soil mass into the system, a series of worksheets and computer programs were developed in order to perform the dynamic analysis of the system response. This allows validating the method developed by comparing the results to those of more complex analyses, such as a 3D Finite Element Method (performed with robust commercial packages such as SAP2000), or to the ones obtained by experimental results. They also allow performing some parametric studies and applications.

After performing the verification and validation of the model, and the evaluation of some case studies, conclusions regarding the significance (or not) of including soil inertial properties in the analysis are presented, the accuracy of the proposed model is discussed, and recommendations for possible future work are developed.

In order to limit the scope of the project, the analysis focuses on a single pile located in a homogeneous soil deposit, evaluated as a semi-infinite half space. The pile has a straight axis, circular cross section, and is placed vertically. The soil was assumed not saturated, so pore pressure effects (including liquefaction) were not an issue.

1.3 General Procedures and Methods

Following is a list of the primary tasks conducted during this research:

- a) Develop a thorough study and literature review of relevant topics (piles under static and dynamic lateral loads, seismic-soil-pile interaction, soil-structure interaction, lumped models of piles). The summary of the findings are presented in Chapter 2.
- b) Perform a numerical study of the influence of the soil mass on the system response by performing a dynamic analysis of 2D and 3D Finite Element Models of a case study of a pile in a sand deposit. The study is performed without considering the soil mass, including the soil mass, and including a partial zone of soil with mass. The main objective is to compare the response of the system with and without the soil mass, in order to assess the impact of the soil inertial properties on the pile-soil system response, and to compare the results with partial soil mass and with full soil mass, in order to assess if a lumped mass model is able to replicate the system response. The results are presented in Chapter 3.
- c) Propose an approximation and perform a regression analysis of the complex dynamic stiffness model developed by Novak. The model, one of the most accepted and used in the literature, is based on a continuous approach that considers the soil as a homogeneous, elastic, semi-infinite medium, and the pile as a straight vertically placed element with flexural deformations and rigid cross section. The objective is to obtain an analytical expression for the equivalent lumped mass that allows for the use of a discrete beam on elastic foundation (BEF) model that considers soil inertia properties. The appropriate pile stiffness, mass and damping matrices required to perform a 2D stiffness analysis are derived. These results are presented in Chapter 4.

d) The accuracy of the simplified discrete model obtained is validated by means of a series of numerical tests. To this end several worksheets and programs are developed in MathCad and Matlab. The validations performed are:

- Examination of the accuracy of the regression analysis performed by computing the appropriate regression analysis statistical parameters
- Evaluation of the accuracy of the discrete model for representing the continuous model by analyzing the response of a case study. Then, in order to generalize the results, a series of parametric studies are performed, where soil and pile characteristics are varied in a wide range.
- Comparison of the results of the discrete model versus the results of a 3D FEM analysis, for a case study.
- Comparison of the results of the discrete model with experimental results.
- Evaluation of the effect of the Poisson's Ratio in the system response in a 3D FEM model, to analyze if these results contribute to explain the variation of the mass coefficient found in the simplified model.
- Comparison of the simplified model stiffness and the damping coefficients to corresponding coefficients presented in the literature.

These analyses are presented in Chapter 5.

e) Development of applications (analyses and parametric studies) of the simplified lumped model. This is reported in Chapter 6.

f) Drawing conclusions and, based on the findings, preparation of recommendations. The conclusions and recommendations are presented in Chapter 7.

Some comments regarding the adopted soil model and numerical procedures are presented in the following subsections.

1.3.1 Soil Model Proposed for this Work

The Beam on Elastic Foundation approach (Winkler model, or subgrade-reaction approach) was adopted to model the soil in this study. Despite the disadvantages of the

model (i.e. lack of continuity of the soil model because the displacements at a point of a soil are not influenced by stresses and forces at other points within the soil), this approach has been widely employed in foundation engineering practice as confirmed by diverse authors (e.g. Poulos and Davis, 1980; El Naggar and Novak, 1996; Wang et al., 1998; Mostafa and El Naggar, 2002). In addition, it is the procedure recommended in many technical reports such as the publications of the Federal Highway Administration (Lam and Martin, 1986; FHWA, 1997; FHWA, 1998), the reports of the U.S. Army Corps of Engineers (USACE, 1991; USACE, 1998; Mosher and Dawkins, 2000), the publications of the Transportation Research Board (Brown et al., 2001), and the Naval Facilities Engineering Command (NFEC, 1986).

Some of the advantages of the subgrade-reaction approach can be summarized as follows:

- It has been proven to be a versatile technique.
- Simple numerical algorithm implementation.
- Fast problem modeling and solution computation.
- Ability to take into account factors such as the variation of soil stiffness with depth and the layering of the soil profile (vertical soil inhomogeneity).
- Ability to simulate nonlinearity (through the *p-y curves*), and hysteretic degradation of the soil surrounding the pile by simply changing the modulus of subgrade-reaction.
- Large body of knowledge: the considerable amount of past experience gained in applying this approach to practical problems, and the availability of a number of empirical correlations to determine the modulus of subgrade-reaction.

Its extensive use in the current analysis of piles has been one of the principal reasons for selecting this methodology for the present research project. The discrete BEF model has the potential to provide a rational way to address the soil inertial contribution to soil-pile interaction.

1.3.2 Proposed Numerical Implementation

Regarding the numerical implementation, although the Finite-Difference Method (FDM) has been widely used by many authors (as described in Section 2.1.1), the Stiffness Matrix Approach (one dimensional Finite Element Method - FEM) was adopted, since this approach is considered more suitable and general for the current study.

According to Bowles (1996) the following is a summary of the main disadvantages of the FDM:

- Boundary conditions are difficult to introduce in the FDM, requiring fictitious nodes.
- The FDM would require all nodes to have equal spacing in order to use the same recurrent equation. Better pile design data is obtained when closer spacing is used near the pile head.
- The FDM end and interior equations are not the same.
- The FDM equations for the pile head depend on whether it is free or either its translation and/or rotation are restrained.
- The FDM matrix is full (not scattered).
- Variable pile cross sections are not easily handled by the FDM.

On the other hand, as reported by Bowles (1996), the FEM has the following advantages:

- The FEM matrix is always symmetric and banded.
- The FEM delivers translation and rotation of pile nodes.
- The FEM elements can have length and cross section that vary from one element to the next.
- Boundary conditions and load points can be easily specified in the FEM.
- FEM programs for piles under lateral loads can be easily adapted to other similar type of problems, such as beams on elastic foundation, lateral piers, and in-take towers, among others.

2 Literature Review and Background

A review of soil-pile behavior under lateral loads is presented in the following sections. The purpose of this chapter is to present the current state of the art and practice in the analysis of piles under static and dynamic lateral loads, pointing out some milestones in this development, rather than be a comprehensive review of all the papers and reports related to these topics. The chapter has two major sections, which are relevant to the proposed research topic and will serve as theoretical background and reference: the modeling of piles under static lateral loads, and the analysis of piles under dynamic loads.

2.1 Analytical Models for Piles under Static Lateral Load

As described by Poulos and Davis (1980) and Fleming et al. (1992), there are three major approaches for the load-deflection prediction of laterally loaded piles.

2.1.1 Beam on Elastic Foundation Approach

This model was originally proposed by Winkler in 1867. The model, also known as *Beam on Elastic Foundation* (BEF) and *Beam on Winkler Foundation* (BWF), proposes that the deflection (v) at any point of the soil in contact with the pile is linearly related to the contact pressure (p) at that point, and independent of the contact stresses at other points. In other words, the model represents the soil as a series of unconnected linearly-elastic distributed springs (Aristizábal-Ochoa, 2003), as shown in Figure 2.1. The pile is modeled as a beam-column element.

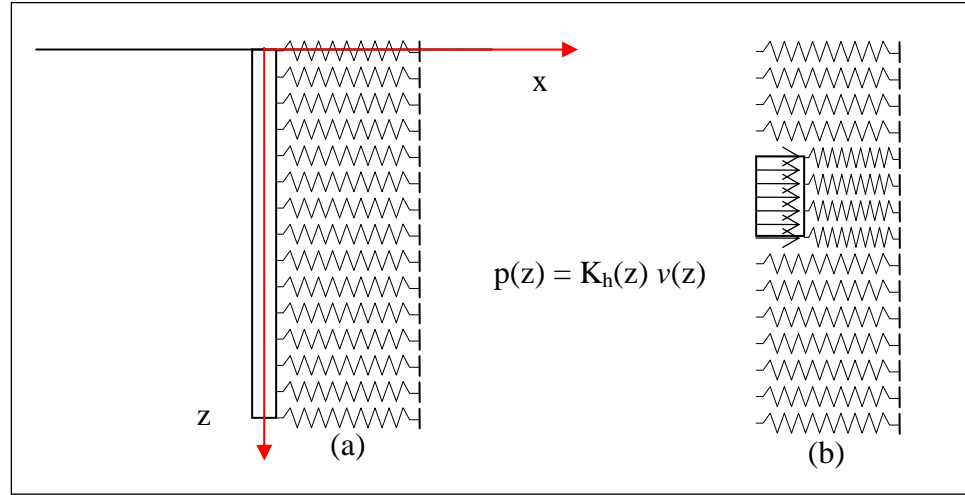


Figure 2.1 Subgrade Reaction Modulus Model: (a) Pile and Soil representation, (b) Effect of a partial uniform pressure over the soil model

The spring modulus of the model is the soil *Modulus of Lateral (Horizontal) Subgrade Reaction*, K_h , in units of [force/length³]. K_h represents the horizontal pressure (or horizontal force acting on a unit vertical area; or the distributed force along the pile length, acting on a unit length) required to produce a unit horizontal displacement. K_h depends on the soil type, depth, and foundation size, among others.

The differential equation of equilibrium of a beam (pile) subjected to a distributed load w is given by:

$$E_p I_p \frac{d^4 v}{dz^4} = -w = -p d = -K_h v d$$

$$E_p I_p \frac{d^4 v}{dz^4} + K_h d v = 0 \quad (1)$$

where:

- E_p = pile modulus of elasticity
- I_p = pile cross section moment of inertia
- d = pile diameter
- w = soil reaction per unit length over the pile (distributed load)
- p = soil pressure over the pile
- K_h = soil lateral subgrade-reaction modulus
- v = lateral displacement of the pile

Analytical (Closed Form) Solutions have been obtained for this equation for the case of K_h constant with depth, and specific boundary conditions (e.g., Hetenyi, 1946; Scott, 1981, presents the Hetenyi solution in a detailed way). These solutions, although limited regarding practical applications, provide a significant insight into the pile response and the factors that affect the soil-pile interaction. Vesić (1961) presented a rigorous analysis of beams resting on an elastic, isotropic half-space medium, obtaining analytical solutions (deflection, slope, bending moment, shear force, and contact pressure) for infinite beams acted upon by a concentrated load and by a couple. He compared these solutions with the Winkler model solutions, and recommended values for the subgrade reaction modulus so that the Winkler solution can provide reasonably accurate results. He also demonstrated that the Winkler model gives reasonably accurate results for long and medium length beams. Kagawa (1992) performed a dimensional analysis to evaluate factors affecting the subgrade reaction modulus K_h , and proposed a procedure to determine an average value of K_h as a function of the soil Young's modulus that may be used for pile analysis based on the BEF.

Numerical Solutions by means of the *Finite Difference Method* (FDM) have been proposed and implemented since the early fifties (e.g. Palmer and Thompson, 1948; Gleser, 1953; Reese and Matlock, 1956). In this method, the basic differential equation (1) is written in finite-difference form, and the solution is found at discrete points. A general discrete model for the FDM is shown in Figure 2.2. The discretization of the solution by means of the FDM has the disadvantages that it is difficult to introduce general boundary conditions at the pile top and tip, and that the elements must be uniform in size.

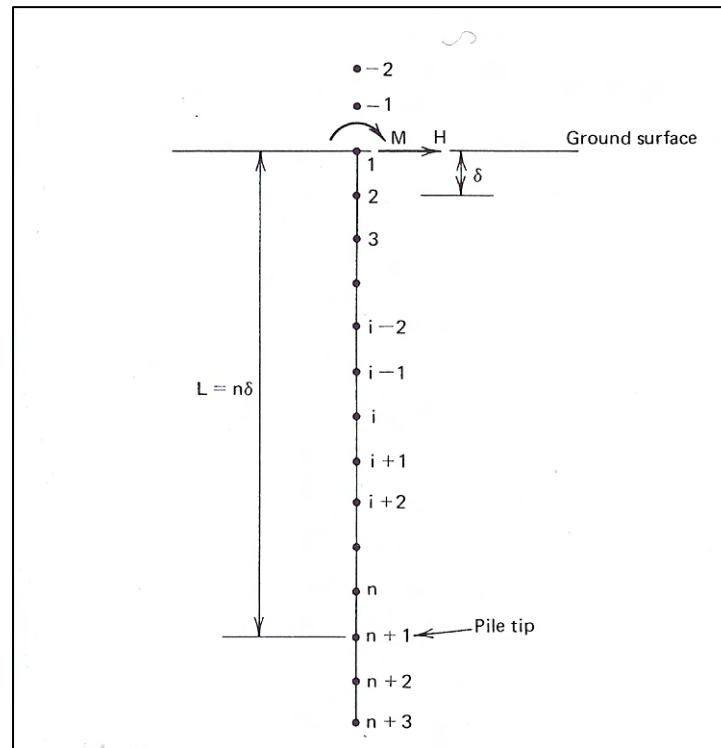


Figure 2.2: Finite-Difference Discretization for the Analysis of Laterally Loaded Piles (Poulos and Davis, 1980)

Numerical Solutions by means of the *Finite Element Method* (FEM) with *One Dimensional Elements* (1D elements), or beam elements, may be obtained from foundation engineering books (e.g. Bowles, 1974; and Bowles, 1996). This analysis is most often referred to as the *Stiffness Method*.

Some authors have used the BEF to propose a complete design process for piles. The work by Broms (1964a/b, 1965) is perhaps the best known of these approaches, where the BEF is used to predict deflections under working loads, and a method to estimate ultimate load resistance is also provided by assuming a number of simple ultimate states for the pile-soil system.

2.1.1.1 The p-y Method

The original BEF model by itself does not account for the nonlinear response of the soil. The most widely-employed approach to consider the nonlinear nature of soil response is the *p-y Method*, where the spring stiffness value is variable, allowing consideration of a non-proportional relationship between the soil resistance per unit pile length (p) and the lateral displacement (y) (see Figure 2.3).

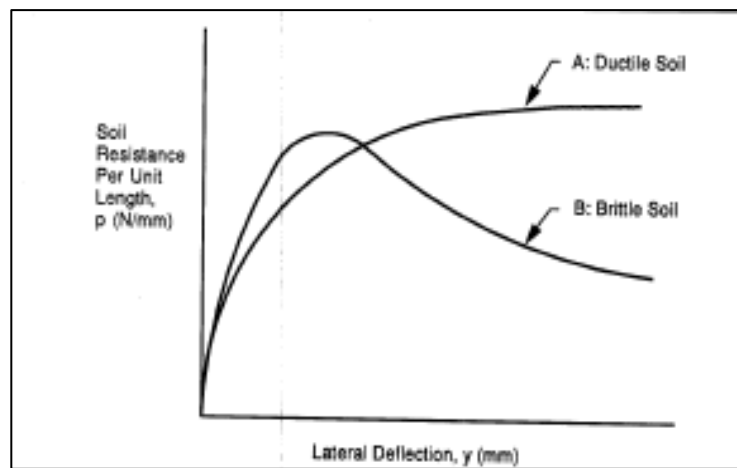


Figure 2.3: Typical p-y Curve for Ductile and Brittle Soil (FHWA, 1997)

The *p-y* approach was developed by Reese, Matlock and coworkers. In a series of papers, they described how to construct the *p-y* curves for different soils and depths based on experimental results, how to develop a solution by the FDM, and how to develop a computer program (Matlock and Reese, 1960; Reese, 1977; and Matlock, 1970). Figure 2.4 shows a schematic of the soil-pile modeling and the corresponding *p-y* curve for each non-linear spring.

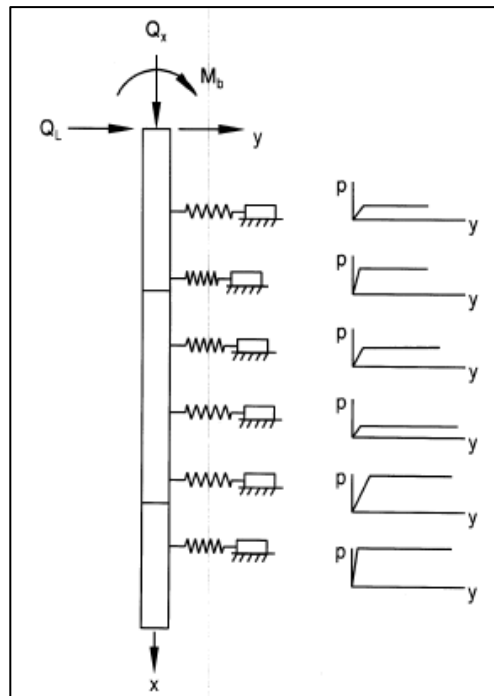


Figure 2.4: Schematic of Pile-Soil Model for the p-y Approach (FHWA, 1997)

It is important to point out that p is not the contact stress (as in the original Winkler model), but the resultant of the contact stresses (with complex distribution) and the friction (adhesion) along the pile perimeter for a given depth, resulting in a contact (interaction) load per unit length of pile. Figure 2.5 shows a distribution of contact stresses prior to and after pile lateral deflection. The value of p depends on soil type, pile type and shape, depth, and value of the deflection y (since the response is non-linear). Figure 2.6 represents the complexity of the factors involved (for the case of a drill shaft).

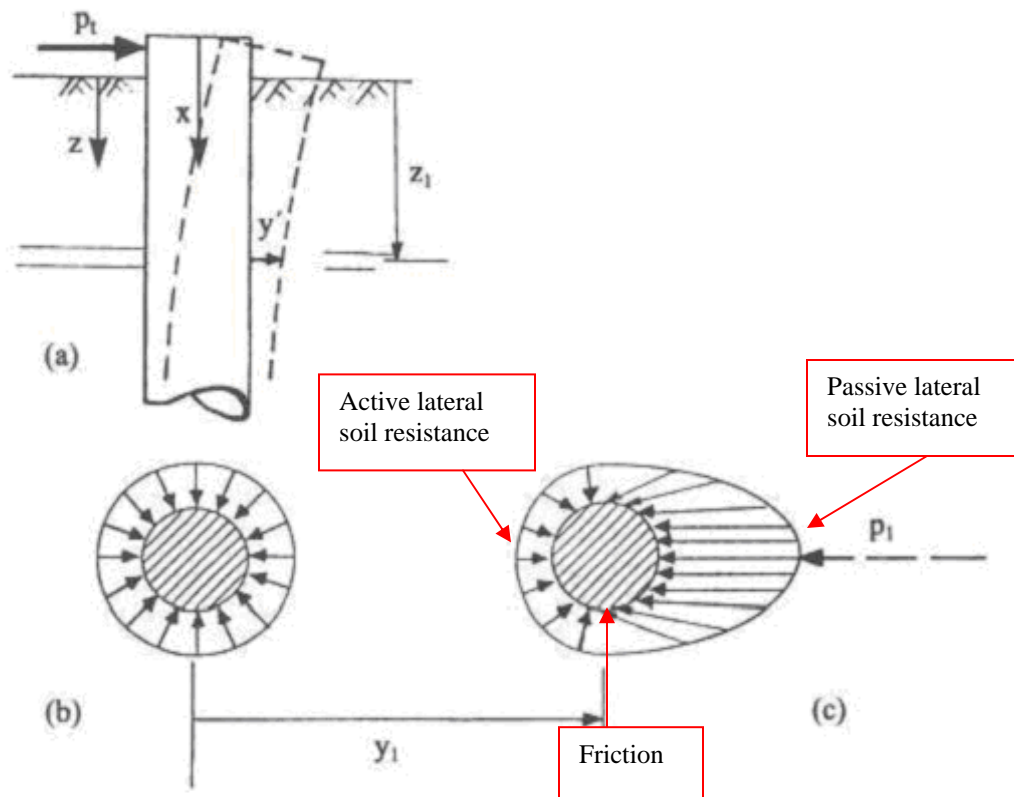


Figure 2.5: Distribution of contact stresses against a pile before and after lateral deflection (Reese and Van Impe, 2001)

The p-y method is sometimes referred to in the literature as the *Beam-on-Nonlinear-Winkler Foundation* (BNWF) framework to model soil-pile interaction (e.g. Wang et al., 1998; Hutchinson et al., 2004), or as the *Load-Transfer Approach* (Basile, 2003).

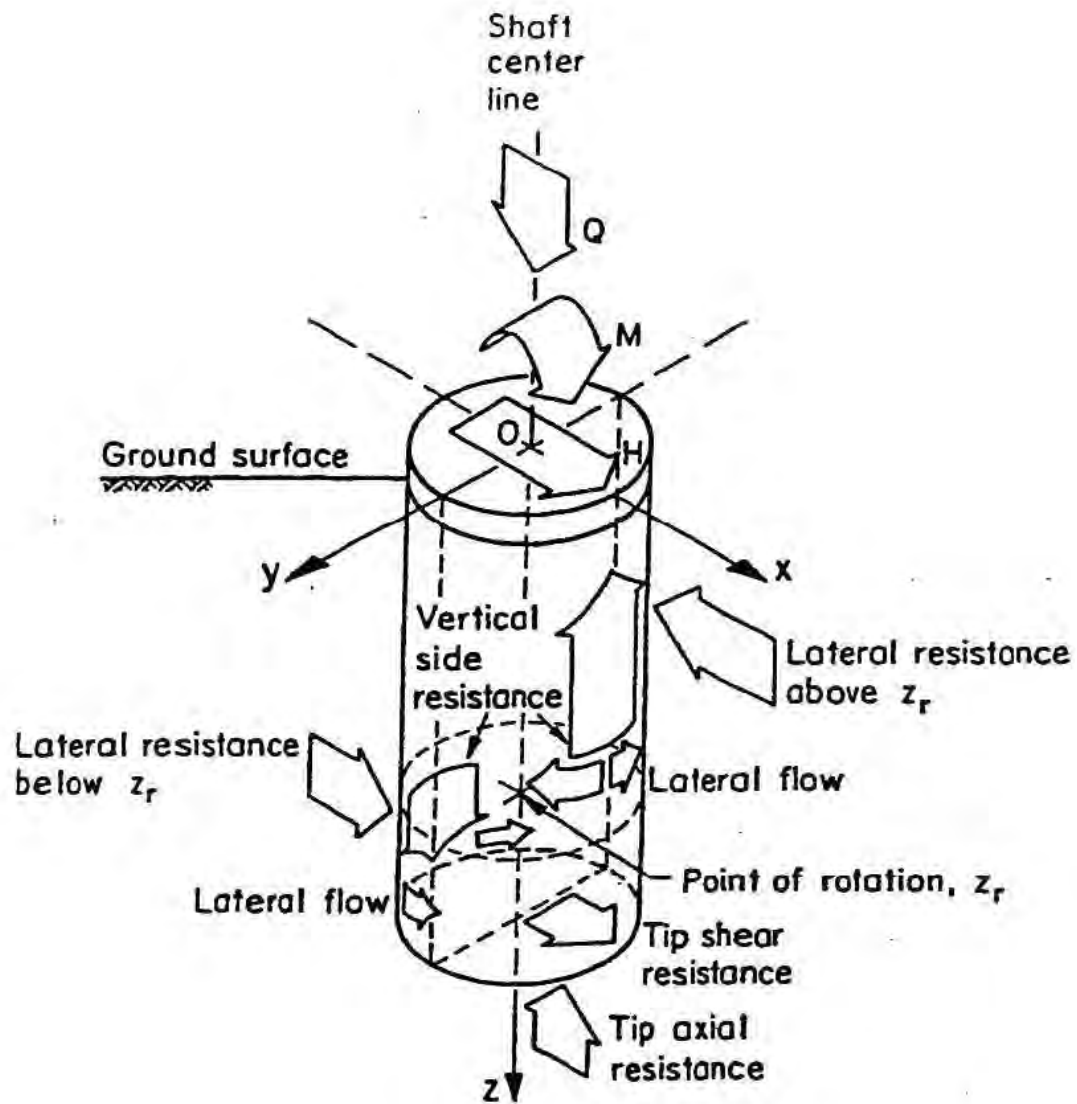


Figure 2.6: Lateral loading and resistance components on a drilled shaft (Wallace et al, 2001)

2.1.1.2 The Wedge Model

The p - y curves of Matlock-Reese were established based on the results of field tests on instrumented piles. Ashour, Norris, and coworkers (Ashour et al., 1998; Ashour and Norris, 2000) developed the *Strain Wedge Model*, which allows the assessment of nonlinear p - y curve response of laterally loaded piles based on an 3D soil-pile interaction

response through a passive wedge soil developing in front of the pile (Figure 2.7). This approach permits to relate the stress-strain-strength behavior of the layered soil in the 3D wedge model to the 1D BNWF model parameters. In this way, the nonlinear response may be obtained from an analysis that considers the actual conditions of the soil-pile system (pile diameter, soil stratification, etc.)

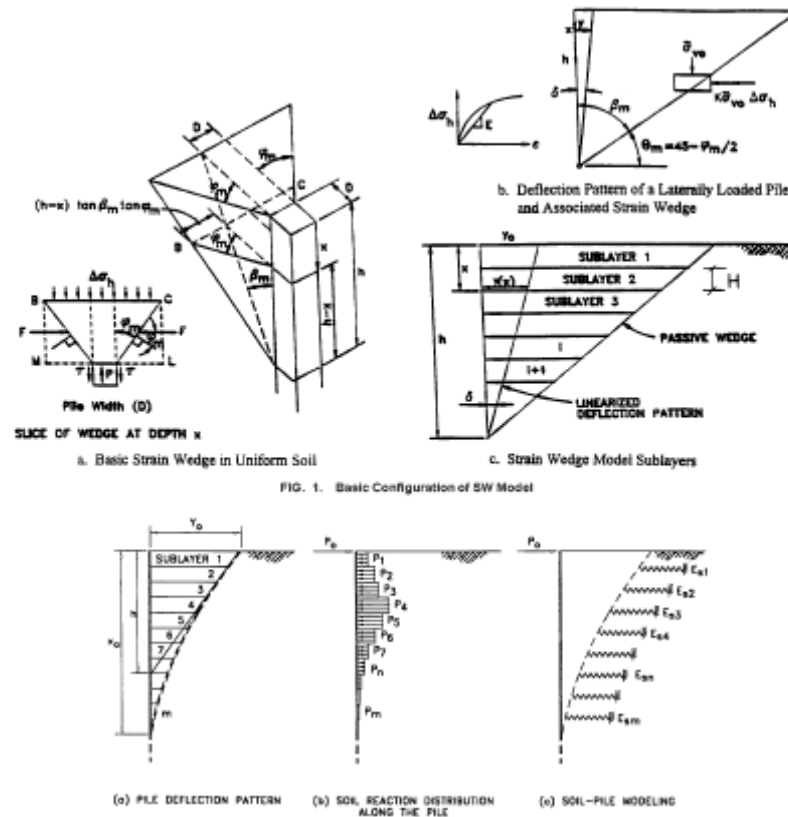


Figure 2.7: Wedge Model Configuration and Distribution of Soil-Pile Reaction along Deflected Pile (Ashour and Norris, 2000)

2.1.1.3 New Developments in BEF

The BEF analysis using the Winkler model to predict soil-pile behavior under static lateral loads continues to be a research topic. A few examples of recent developments are mentioned here. Shen and Teh (2004) proposed a variational approach (similar to the Ritz method) to perform the analysis of a laterally loaded pile in a soil with subgrade reaction modulus increasing with depth. Hsiung (2003) presented the theoretical solution for the

maximum bending moment and deflection for laterally loaded piles in a uniform subgrade reaction modulus soil that yields. Kim et al. (2004) conducted lateral field tests on instrumented piles located in a site in Korea, in order to obtain p-y curves and analyze the influence of the installation method and head restraint conditions in the soil-pile response.

2.1.2 Elastic Continuum Approach

The representation of the soil as a homogeneous elastic continuum has also been proposed for the analysis of the soil-pile interaction.

Some authors developed *Plane Strain Models* (e.g. Davis and Booker, 1971) for the analysis of limit pile capacity. These solutions are relevant for the case of shallowly-embedded sheet piling, and may be also accurate for a group of piles closely spaced in a single long row (i.e. wall footing). Plane Strain Models are also used for modeling the 3D system as a series of parallel horizontal planes in plane strain.

Other authors developed *Three Dimensional Elastic Models* (e.g. Douglas and Davis, 1964; Spillers and Stoll, 1964; Poulos, 1971, 1972). These models are based on *Mindlin's Solution* for the horizontal displacement caused by a horizontal point load within the interior of a semi-infinite elastic-isotropic homogeneous mass (this solution can be found in Elasticity handbooks, such as the one by Poulos and Davis, 1974). Since Mindlin's solutions become singular when evaluating the displacement corresponding to the point where the load is located, integral solutions over a predefined area, representing a fraction of the pile surface, are used (Douglas and Davis, 1964; Spillers and Stoll, 1964; Basile, 2002). These solutions are generally known as *Green Functions*, and define the displacement field due to an assumed loading system (pattern) associated with the pile-soil interaction.

Poulos and Davis (1980) presented the implementation of the model proposed by Poulos (1971, 1972). In this model the pile is assumed to be a thin rectangular vertical strip divided in elements, and it is considered that each element is acted upon by uniform horizontal stresses (see Figure 2.8) which are related to the element displacements through the integral solution of Mindlin's problem. Finally, they solved the differential equation of equilibrium of a beam element on a continuous soil with the Finite Difference Method (FDM), in which the soil pressures over each element are unknown variables. After obtaining the pressures, the displacements are found.

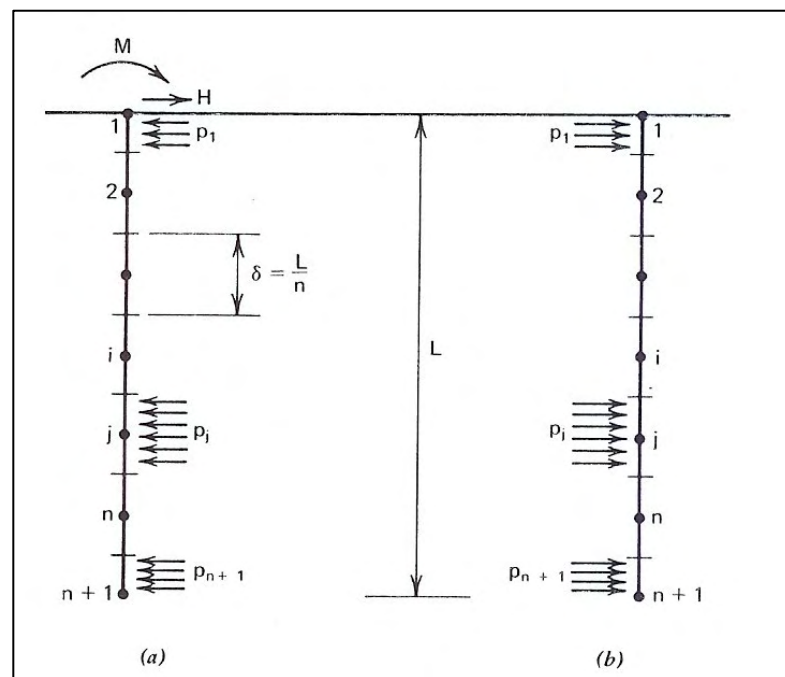


Figure 2.8: General Pile Discretization for the Analysis of Soil as a Continuous. Stresses acting on (a) pile, (b) soil adjacent to pile (Poulos and Davis, 1980)

The model has the advantage that it is able to take into account the continuous nature of soil, the semi-infinite dimension of the half-space, and the boundary conditions along the unloaded ground surface. Although yielding of soil may be introduced by varying the soil elastic modulus, this approach does not permit to consider local yielding and layered soil conditions (without stretching Mindlin's Solution for a homogeneous half-space). In this regard, Spillers and Stoll (1964) proposed the computation of the maximum permissible load by any suitable yielding condition (for instance, a wedge model for the top part of

the soil, where the displacements are larger and yielding of soil occurs), together with the elastic solution and an iterative process to verify that the maximum load is not exceeded at any point. It was mentioned that two of the drawbacks of the discretization by means of the FDM is the difficulty to introduce general boundary conditions at pile top and bottom, and the required uniform size of the elements. As reported by Basile (2002), this soil model was also used for the *Boundary Element Method* (BEM) analysis of piled foundations.

2.1.3 The Finite Element Approach

In order to obtain the solution of laterally loaded flexible piles in an elasto-plastic soil mass, the *Finite Element Method* (FEM) has been proposed and implemented to perform a numerical analysis of the soil-pile system.

As reported by Poulos and Davis (1980), the first attempts included two-dimensional finite element models in the horizontal plane (Baguelin and Frank, 1979), axi-symmetric geometries (Banerjee and Davies, 1978), and general three-dimensional finite element analysis (Desai and Appel, 1976).

Some recent publications include the work by Yang and Jeremic (2002), who used 3D FE models of a laterally loaded pile embedded in uniform and layered soil profiles in order to numerically obtain p-y curves and compare them to experimental ones (Figure 2.9).

The FE method has the ability of permitting to account for soil nonlinearity by applying appropriate constitutive models, such as the Drucker-Prager formulation (Ben Jamma and Shiojiri, 2000; Yang and Jeremic, 2002), and to use gap-elements to model possible pile-soil separation. These modeling capabilities are usually available in robust general purpose FEM programs (such as ABAQUS and ANSYS) or special geotechnical engineering oriented codes (e.g. PLAXIS).

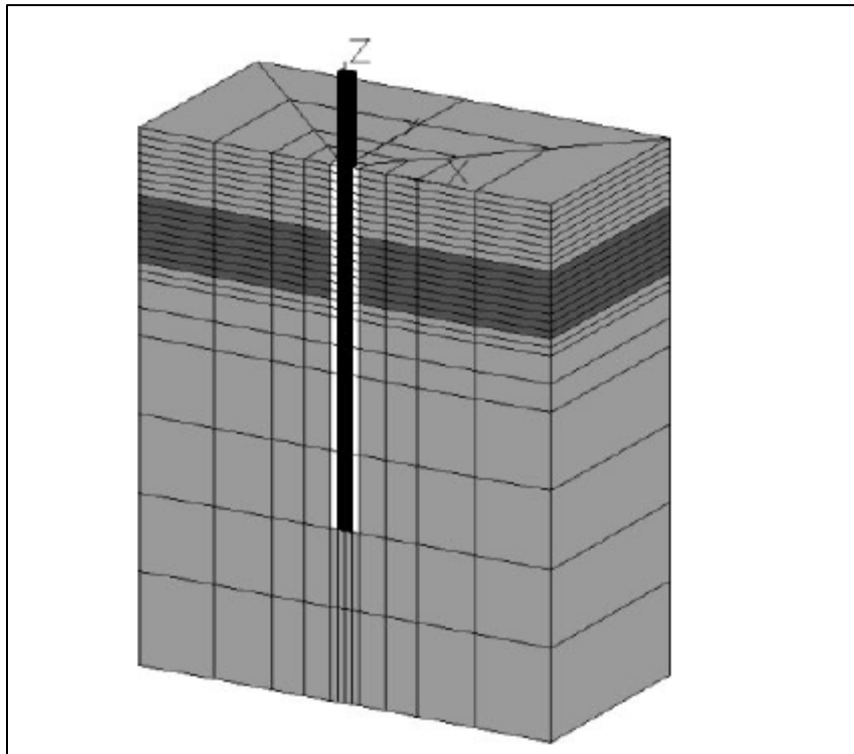


Figure 2.9: Example of a Three-Dimensional Finite Element Mesh for a Single Pile System (Yang and Jeremic, 2002)

There is a general agreement (e.g. Poulos and Davis, 1980; Kagawa, 1992; El Naggar and Novak, 1996; Wang et al., 1998; Mostafa and El Naggar, 2002) that the FEM analysis is impractical for the design of anything but extremely expensive structures, due to the cost of the specialized software, the time consuming model generation, the time required for the non-linear analysis, the difficulty in the interpretation of the result in terms of common pile (beam) variables, and the uncertainties associated with soil non-linear modeling in 3D.

Finally, it is appropriate to mention that in the last years a powerful 3D Finite Difference Method program called Flac3D (Itasca Consulting Group, Inc, 1996) has been used to solve complex geotechnical engineering problems. However, the program has rarely been used for pile analysis. An example is the work by Ng and Zhang (2001), who used a 3D FDM model to analyze the behavior of piles placed on a cut slope. In particular, they

investigated the effect of the sleeving (annulus of compressible material that is usually constructed between the piles and the adjacent soil to minimize the transfer of lateral load from the buildings to the shallow depths of the slope) on the pile performance (Figure 2.10).

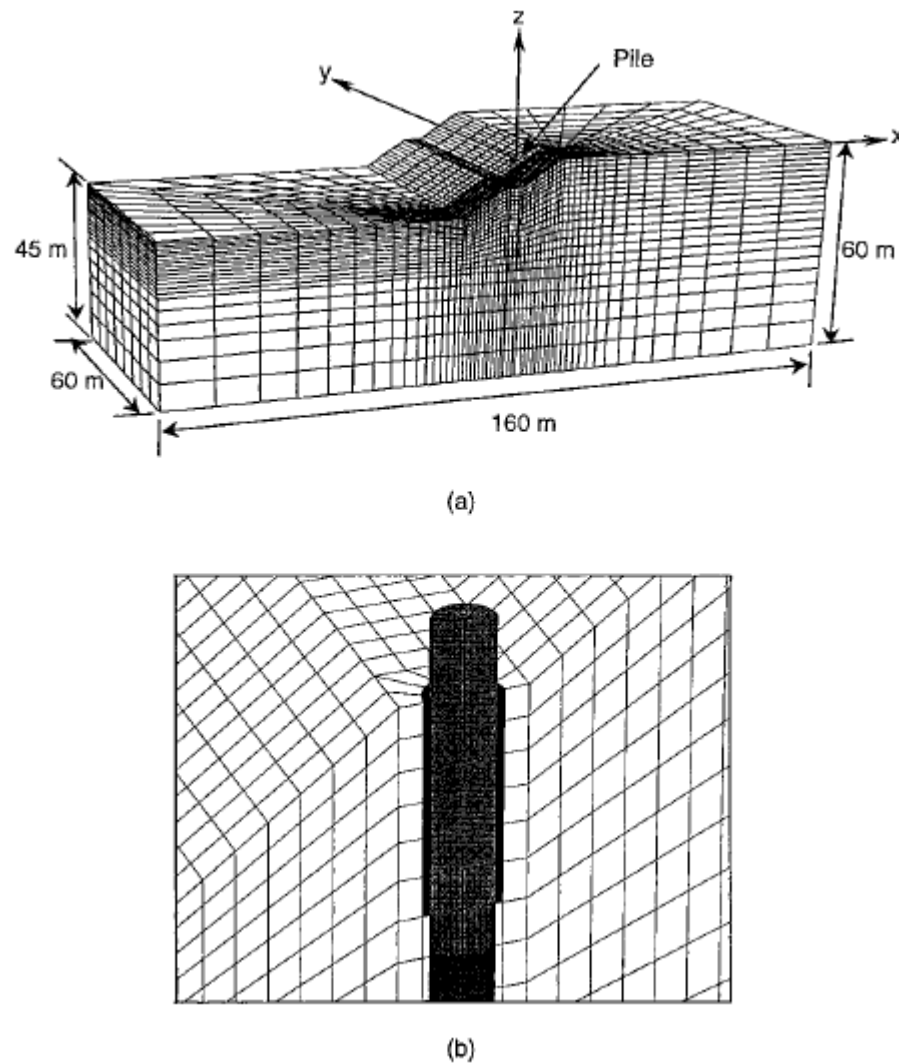


Figure 2.10: Example of a Finite Difference Mesh for a Soil-Pile System: (a) 3D View, (b) Close-up of sleeved zone (Ng and Zhang, 2001)

2.2 Analysis of Piles under Dynamic Lateral Loads

Similar approaches as those described in Section 2.1 have been proposed and implemented for the dynamic analysis of single piles under horizontal loads (e.g., seismic excitations). They are the Finite Element Method (FEM) and the Boundary Element Method (BEM) that treat the soil as a continuous medium, the Beam on Nonlinear Winkler Foundation (BNWF), that treats the soil as a series of disconnected springs, and the Continuum Approach, that provides closed form solutions by considering the soil as an infinite semi-space. A brief description of these approaches is presented in this section, with particular emphasis in seismic analysis.

2.2.1 Winkler Approach

Considering that both piles and soil can behave in a nonlinear manner during extreme events, the use of p - y methods for defining the lateral stiffness of pile-soil model for seismic analysis (secant stiffness as a function of pile deformation) has been used since the seventies (Matlock et al., 1978). This model has been used by several authors (e.g. PoLam et al., 1998; Wang et al., 1998; Hutchinson et al., 2004). Appropriate p - y models which take into account cyclic soil degradation should be used. Since the classic *Linear Modal Analysis* cannot be applied due to the expected nonlinear response, an *Iterative Nonlinear Time-Domain Analysis* can be used to perform this analysis (Brown et al., 2001).

The energy dissipation inherent to material behavior, known as *Material Damping*, may be modeled as a dashpot in parallel with a spring that represents soil stiffness. This is the well known Kelvin-Voigt model for visco-elastic materials.

The energy dissipation due to soil nonlinear behavior, known as *Hysteretic Damping*, can be considered in the p - y model by allowing the unloading path to differ from the loading

path (Brown et al., 2001), as shown in Figure 2.11. This figure also shows a way to consider soil degradation, namely the reduction in soil strength as the loading cycles progress.

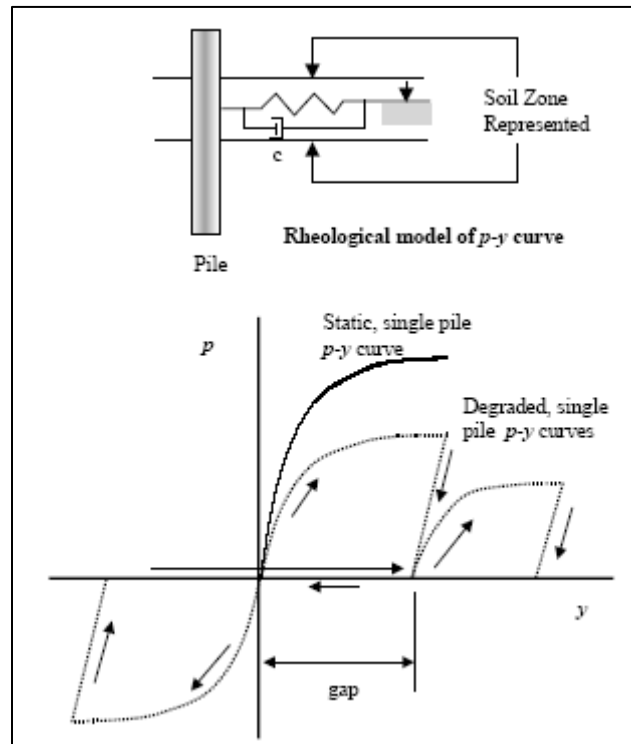


Figure 2.11: p-y Method for Modeling Hysteretic Damping and Cyclic Degradation in Soil (Brown et al., 2001)

When a soil is subjected to cyclic symmetric loads a *Hysteresis Cycle* is produced in the stress-strain response, which has acute angles where the load inverts. The hysteresis cycle may be defined using *Masing's Rules* (Suarez, 2003). The p-y curve, that may be considered as the constitutive equation of the soil, is used as the *backbone curve* or *skeleton curve*, and its shape is used to define the cycle (Figure 2.12): curve oa is reproduced in bca, curve ob is reproduced in adb (both with double amplitude and double ordinates). The hysteretic damping is related to the energy dissipated by cycle, which is equal to the enclosed area. A detailed description of this model is presented by Suarez (2003).

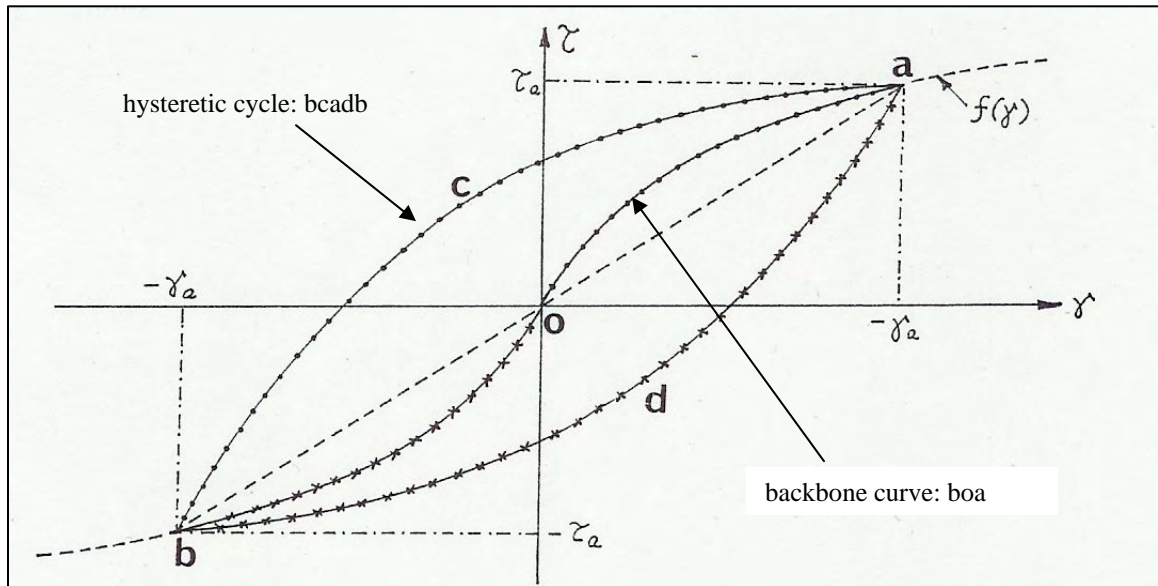


Figure 2.12: Hysteretic Cycle using Masing's Rules (Suarez, 2003)

The loss of energy in the soil-pile system due to out-going stress waves that travel from pile-soil interface to infinity, known as *Radiation Damping*, has been considered by a number of researchers, as reported by Wang et al. (1998). Berger et al. (1977) proposed a simplified approach, assuming that the pile cross section (that moves horizontally) only generates one dimensional (1D) P-waves traveling in the direction of shaking, and 1D SH waves traveling perpendicular to the pile (Figure 2.13 a). Novak et al. (1978) proposed a more rigorous model, assuming a plane strain state for the soil (considered as homogeneous, isotropic, and linearly elastic) and analyzed the pile undergoing uniform harmonic vibrations in an infinite medium. Because the pile is considered infinitely long, massless and rigid, the problem reduces from 3D to 2D, as a rigid circular disc vibrating in an infinite elastic plane (Figure 2.13 b). Gazetas and Dobry (1984a, 1984b) proposed a simplified model by assuming that compression-extension waves propagate in the two quarter planes along the direction of shaking, and that SH-waves propagate in the two quarters perpendicular to the direction of shaking (Figure 2.13 c). For each of the previous approaches, a dashpot coefficient “C” can be determined. A damper with this coefficient is placed in parallel with the non-linear spring element.

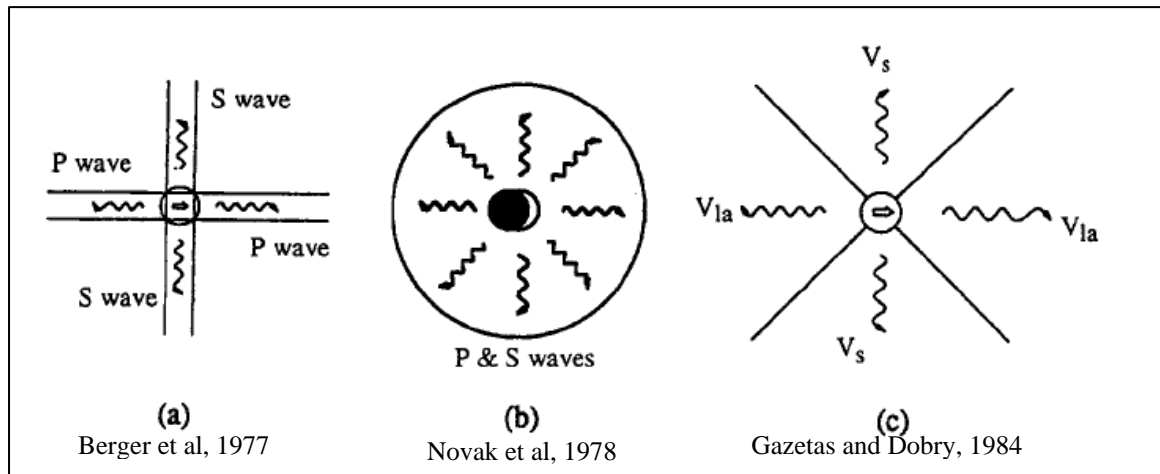


Figure 2.13: Models to Analyze Radiation Damping for a Horizontally Vibrating Pile (Wang et al., 1998)

Figure 2.14 summarizes the modeling of stiffness and damping for a pile-soil system when using a beam on nonlinear Winkler foundation model (e.g. Kagawa and Kraft, 1980a, 1981; Badoni and Makris, 1996).

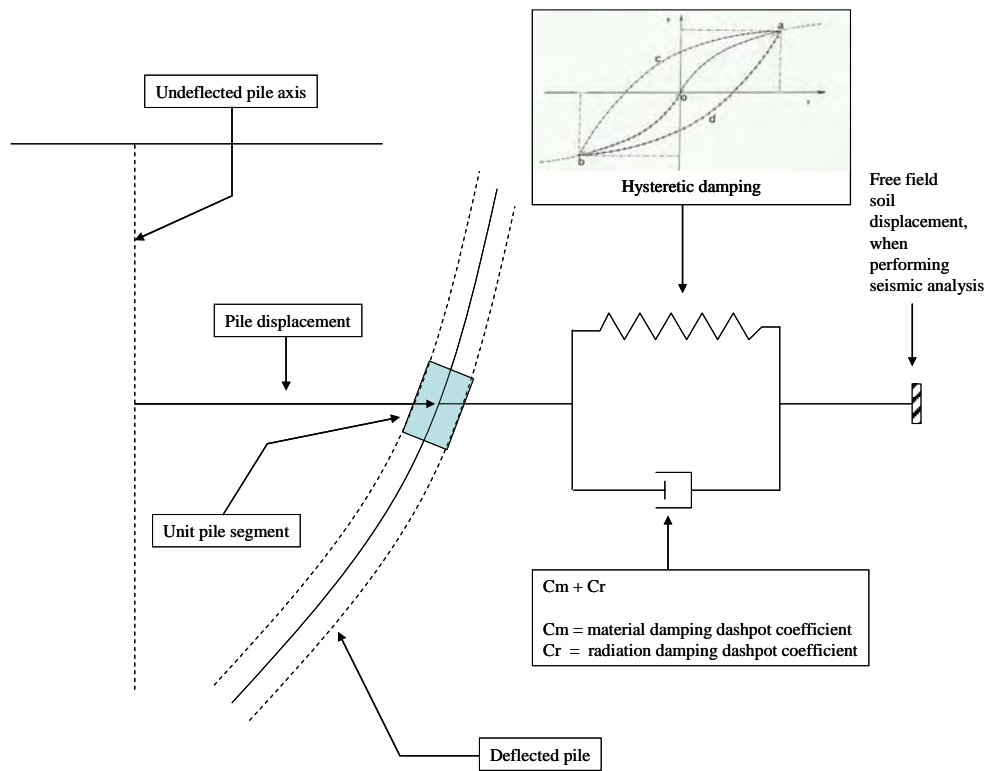


Figure 2.14: BNWF Model with Different Damping Effects

Several authors have proposed a Winkler model based on a continuum solution, most of them considering the soil as an isolated horizontal plane in a plane strain state of stresses. These solutions are considered a very good approximation of the real 3D behavior for frequencies higher than the fundamental natural frequency of the soil deposit, as demonstrated by Nogami and Novak (1980). Nogami and Koganai (1988) proposed a time-domain method to calculate the flexural response of linear single piles, based on plane strain solutions, but consisting of a series of springs and dashpots (as shown in Figure 2.15). This modified Winkler model, sometimes referred to as the *Hybrid Dynamic Winkler Model (HDWM)*, was validated for a wide range of frequencies. They proposed a model in which the soil mass is included through a soil radius (as a cylinder around the pile), but the value of this soil radius was never addressed in the paper.

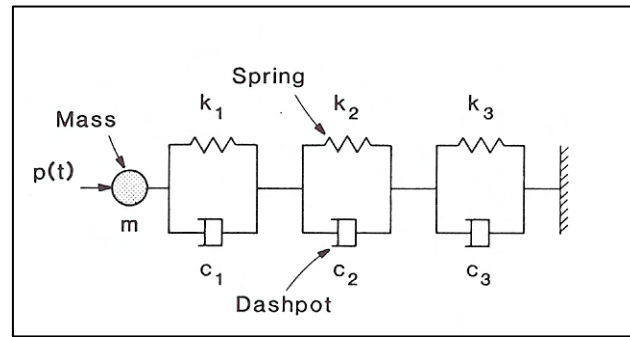


Figure 2.15: Hybrid Dynamic Winkler Model for Lateral Pile Response (Nogami and Koganai, 1988)

This model was then extended by Nogami et al. (1992) for the nonlinear dynamic analysis of soil-pile interaction, by dividing the soil medium in two regions (Figure 2.16). The *near field region* in the vicinity of the pile shaft, where strong nonlinear soil response occurs, is represented by a nonlinear spring and a gap element. The *far field region*, where the behavior is primarily linear elastic, is represented by the series of springs and dashpots proposed by Nogami and Koganai (1988). Again, they proposed a model where the soil mass is included through a soil radius (as an annular cylindrical region around the pile). Here also the typical value of the soil radius was not addressed in the paper (it is only mentioned that it was artificially taken). A simpler model based on this approach was proposed by El Naggar and Novak (1995, 1996) and used by Mostafa and El Naggar

site response analysis, can be done using a program like SHAKE (Schnabel et al., 1972; Idriss and Sun, 1992). 2) Second, the free field motion is applied to the soil-pile system as boundary support movements at the end of each spring element. This allows consideration of the effects of varying motion due to the vertical propagation of the ground shaking. As an example, Figure 2.17 shows the scheme of the model used by Hutchinson et al. (2004) for the inelastic seismic analysis of extended pile-shaft-supported bridge structures. It is important to note that no lumped masses were used to consider soil inertial contribution to system response in this work.

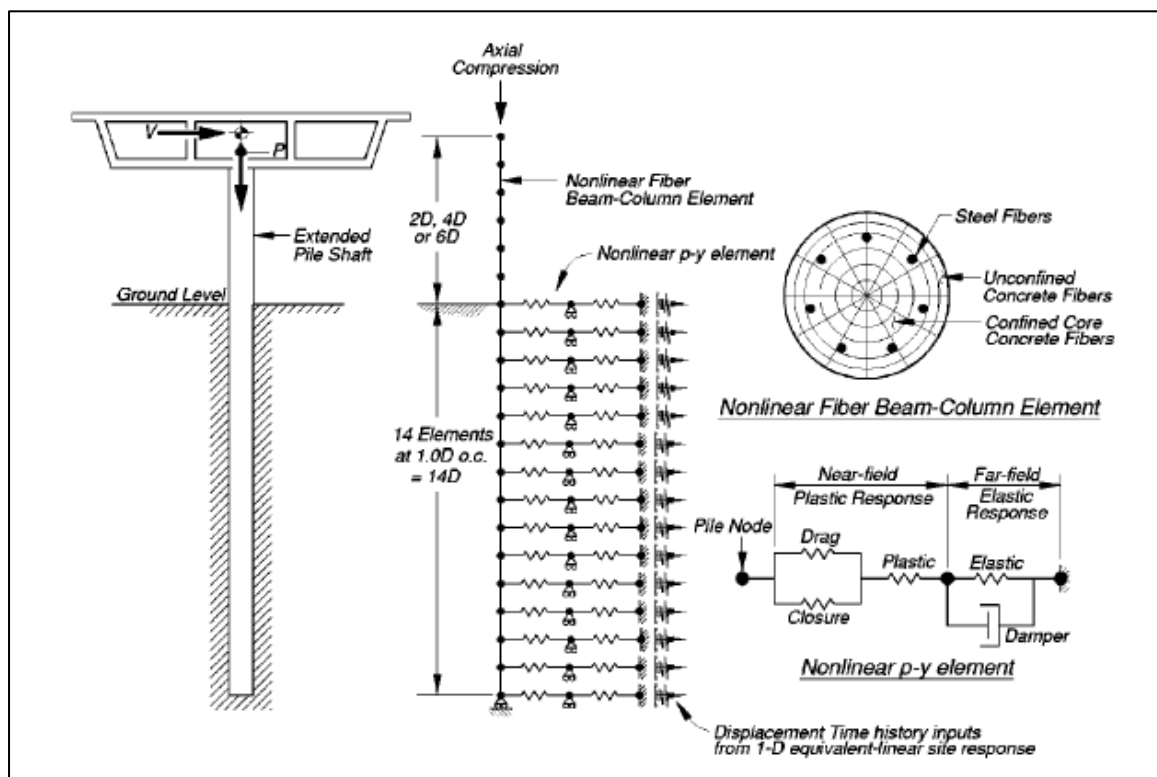


Figure 2.17: Model for Seismic Analysis of Pile-Supported Bridge (Hutchinson et al., 2004)

2.2.2 Continuum Approach

The mayor advantage of the continuum approach over the BNWF and the FEM is that it automatically includes the radiation of energy to infinity, known as *Radiation Damping*,

through the complex expression of the pile impedance function (stiffness). The disadvantages are that, in general, it is only applicable to visco-elastic materials, although material damping may be considered by using the complex form of the material properties, or Lamé's constants. Another drawback is that the nonlinear behavior can only be accounted for by changing the elastic modulus of the full space, i.e. it does not allow for local yielding. Finally, the boundary conditions are limited and the soil characteristics have to be simple, i.e. the soil must be homogeneous or with homogeneous layers.

Despite its limitations, this analysis is extremely useful to acquire a better understanding and insight of the soil-pile interaction phenomenon, and to obtain analytical expressions of parameters such as the subgrade reaction modulus (Vesić, 1961), that can be used in the Winkler models.

Following is a brief description of some publications that are considered relevant for the purpose of the present project:

Novak (1974) presented an approximate continuum approach to account for soil-pile interaction: it is assumed that the soil is composed of a set of independent horizontal layers of infinitesimal thickness, which extend to infinity. As each plane is considered independent, this model may be viewed as a generalized Winkler model. The planes are homogeneous, isotropic, and linearly elastic, and are considered to be in a plane strain state. Using Baranov's solution for the horizontal soil reaction to a rigid circular disc with harmonic horizontal displacement (representing a pile cross section), Novak formulated the differential equation of the damped pile in horizontal vibration. He found the steady-state (particular) solution for harmonic motion induced through pile ends, and used this solution to find the dynamic stiffness of the pile head for different boundary conditions. According to Novak, the dimensionless parameters that control the soil-pile system response are: (a) the specific mass of the soil " ρ " over the specific mass of the pile " ρ_p " (mass ratio ρ/ρ_p), (b) the ratio between the shear wave velocity of the soil " V_s " and the

longitudinal wave velocity of the pile “vc” (wave velocity ratio V_s/v_c), (c) the ratio of the length of the pile “L” to the pile radius “ro” (slenderness ratio L/r_o), and (d) the frequency of the load “ ω ” (expressed as a dimensionless parameter $a_o = r_o \omega \sqrt{\rho/G}$, where G is the shear modulus of the soil). Then he presented the equivalent stiffness and damping constants for a pile head, and for a pile group considering a rigid pile cup at pile heads. He presented a numerical example, and compared the response of a spread footing to an identical footing resting on piles, reaching the following conclusions: (a) pile foundations are more rigid, having higher natural frequencies, smaller damping, and larger resonant amplitudes than spread footings; (b) pile (and spread footing) embedment can reduce resonant amplitudes; (c) piles can reduce settlements, but they cannot eliminate vibrations, so the dynamic analysis of pile foundations is as important as for shallow foundations. As stated by Klar (2003), as the frequency tends to zero, the stiffness obtained from the Novak solution (1974) tends to zero. Moreover, as the frequency increases Novak’s solutions tends to Tajimi’s solution (based on a more rigorous 3D analysis). Due to the fact that for higher frequencies waves tend to propagate more horizontally, Novak’s model tends to capture the actual behavior. Therefore Novak’s solution can provide good results for high frequencies and poor results for very low frequencies and static conditions.

Nogami and Novak (1980) investigated the coefficients of dynamic soil reaction to pile motion treating the soil as a three-dimensional continuum, in order to compare to the Winkler model (where the soil is modeled as discrete springs and dashpots). The assumptions used were: (a) homogeneous soil stratum underlain by a rigid bedrock; (b) linear viscoelastic soil material with constant hysteretic damping; (c) cylindrical elastic pile driven to the bedrock; (d) no vertical soil movement; (e) no relative soil-pile movement at soil-pile interface; and (f) harmonic motion. They reached the following conclusions: (a) even in homogeneous soil media, the local stiffness and damping of the soil can vary greatly with depth, frequency, and relative pile/soil stiffness; (b) at frequencies higher than the fundamental frequency of the soil deposit, the 3D solution is similar to the plane strain solution (2D) proposed by Novak (1974). For these

frequencies, the soil medium can be treated accurately with the Winkler hypothesis (uncoupled springs and dashpots along the pile); and (c) the Winkler hypothesis works better for stiffer piles and deeper soil deposits.

The results from the previous works have been used to model the stiffness and damping effects of the dynamic soil-pile response in a Winkler model, analyzing the pile dynamic stiffness (impedance), but they were not clearly used to consider the contribution of the soil mass to the dynamic response in a discrete Winkler model.

2.2.3 Finite Element Approach

As pointed out by Wolf (1985), for static loading, a fictitious boundary at a sufficient distance from the structure (pile) where the response is expected to vanish from a practical point of view, can be introduced, leading to a soil with finite domain. This finite domain is meshed, and pin supports (displacements restraints) are assigned to the boundary nodes. However, for dynamic loading, the fictitious boundaries can reflect waves originating from the vibrating structure (pile) back into the discretized soil region, instead of letting them to propagate toward infinity. Special attention has to be paid in placing adequate radiation damping capabilities at the soil FEM boundaries.

Some recent publications that are considered relevant as references for the present study are briefly summarized in the following paragraphs:

Wu and Finn (1997a, 1997b) proposed a “*quasi-three-dimensional finite element method*”, where the soil is modeled using eight-node brick elements having only one translational DOF at each node, in the direction of shaking. The element stiffness, mass and damping matrices are obtained from a simplified differential equation of dynamic equilibrium in the direction of shaking. The simplifications came from the study of the shear wave propagation in the vertical direction, and the analysis of the components of stress (or strain) that may be neglected. The pile is modeled with classical two-node beam

elements. Dynamic soil-pile interaction is considered by enforcing displacement compatibility between the pile and soil. They report that the proposed FEM is both accurate and efficient.

Bentley and El Naggar (2000) developed a 3D finite element model that considers the soil nonlinear behavior (by means of the Drucker-Prager yielding criteria), discontinuity conditions at the soil-pile interface (by means of contact elements that allow slippage and gapping), energy dissipation (by means of Kelvin elements), wave propagation (by introducing the excitation at the bottom of the model), and actual in situ stress conditions (geostatic stresses). They used the model to evaluate the kinematic soil-pile interaction, comparing the free-field soil response with the response of the soil-pile system. They performed the analysis by applying earthquake excitations with low dominant frequencies, and found that although the response is slightly amplified for elastic soils, the pile-head response closely resembles the free field response for elastoplastic soils.

Klar and Frydman (2002) used a series of plane strain FE models in horizontal planes to model the 3D response. Figure 2.18 shows the different planes and the boundary conditions schematically.

Maheshwari et al. (2004) used a 3D FE model to obtain the pile response under seismic excitation and a load applied to the pile cap, considering the effects of material nonlinearity in the soil and separation at the soil–pile interface on the dynamic behavior of a single pile and pile groups. Figure 2.19 shows one of the FE mesh used for this study.

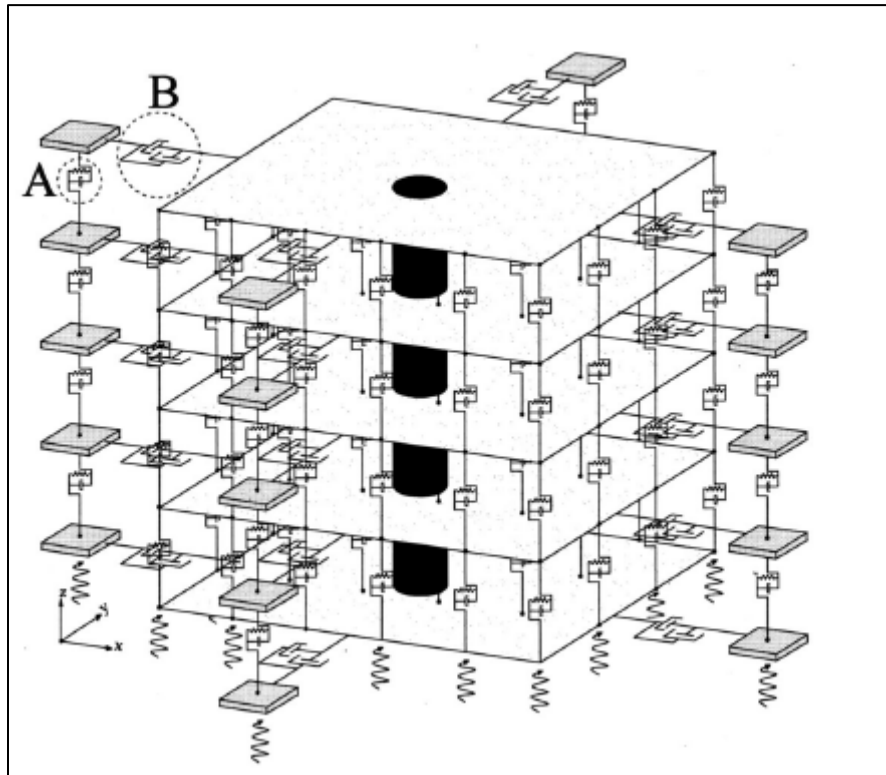


Figure 2.18: Discrete Planes and Free-Field Boundary Conditions (Klar and Frydman, 2002)

It is appropriate to mention that the *Boundary Element Method* (BEM) has been increasingly used in the investigation of laterally loaded piles. Examples are the work by Ben-Jamma and Shiojiri (2000), who used a hybrid of Thin Layer Element and Finite Element methods to analyze the total soil-substructure system and obtain the dynamic response of single piles embedded in an infinite half-space. The benefits of the BEM for pile structure interaction modeling and analysis were emphasized by Basile (2003).

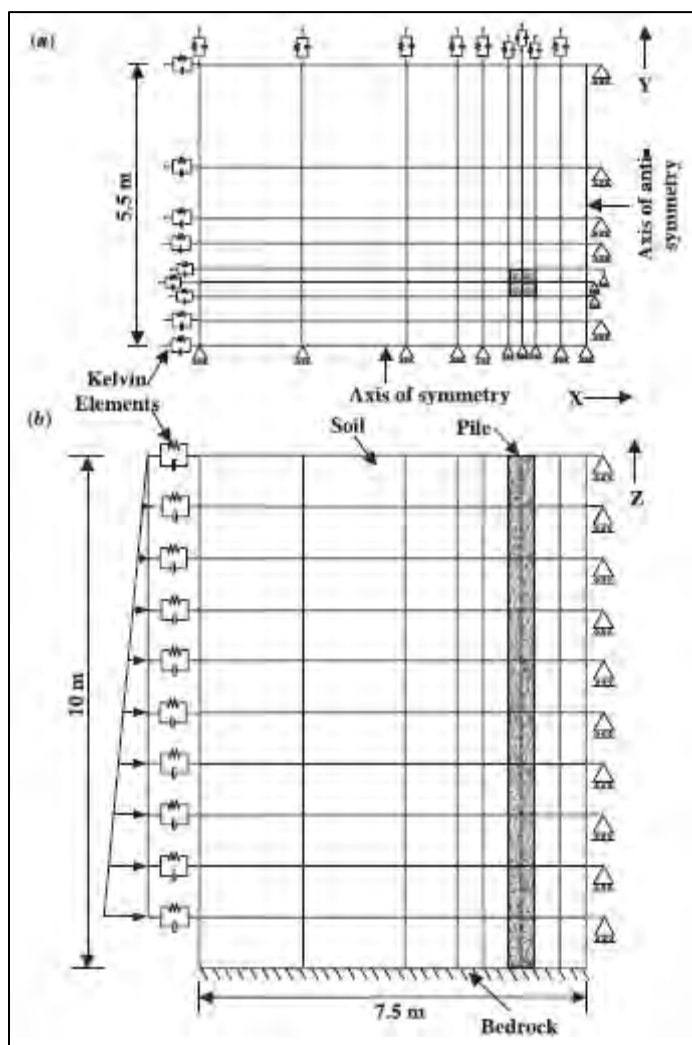


Figure 2.19: Example of a 3D FE Mesh and Boundary Elements for the Dynamic Analysis of a Soil-Pile System: (a) top view, (b) elevation (Maheshwari et al., 2004)

3 Numerical Evaluation of the Soil Inertia Contribution to the Soil-Pile System Response

The objective of this chapter is to evaluate in a preliminary form the importance of the soil inertia properties in the soil-pile system behavior. To this end, a set of representative soil and pile characteristics will be selected, and the dynamic flexibility of the pile head will be obtained by means of a Finite Element Method (FEM) steady state analysis. Two types of analysis will be performed: one considering the soil mass and the other neglecting it. The response of both analyses will be compared in order to address the impact of the soil mass. The effect of the cutoff boundary conditions will also be evaluated.

3.1 Case Study

In order to perform the analysis, average soil properties corresponding to a dense sand deposit will be selected. These values were obtained by consulting the Soil Mechanics, Soil Dynamics, and Foundation books from Barkan (1962), Bowles (1996), Cernica (1995), Coduto (2001), Das (1999), and Poulos and Davis (1980). The adopted values for the soil material properties are as follows:

$$\begin{aligned} E_s &= 12 \text{ ksi} && \text{(soil modulus of elasticity or Young's modulus)} \\ \gamma_s &= 110 \text{ pcf} && \text{(soil specific weight)} \\ \nu_s &= 0.3 && \text{(soil Poisson's ratio)} \end{aligned}$$

The depth of the sand soil deposit considered is 30 ft. It is assumed that the soil deposit rests on a rigid rock, and that its properties are constant with depth.

It is appropriate to mention that in order to have a soil with a *shear wave velocity* V_s in the range of soil profile type SD of the Uniform Building Code (International Code Council, 1997), the modulus of elasticity E should be adopted between two to eight times higher than the values recommended in the previous cited books, as shown in Table 3.1.

This is probably due to the fact that a secant modulus is usually provided as the reference value in the literature.

Table 3.1: Values of Elastic Modulus E for Different UBC Site Types

$g = 32.2 \text{ [ft/s}^2\text{]}$ gravity acceleration

Soil Type	γ [pcf]	ν	Vs [ft/sec]		G [ksi]		E [ksi]		E [MPa]	
			>	<	>	<	>	<	>	<
SA	130	0.2	5000		700.91		1682.19		11578.88	
SB	125	0.25	2500	5000	168.49	673.96	421.22	1684.89	2899.36	11597.44
SC	120	0.25	1200	2500	37.27	161.75	93.17	404.37	641.29	2783.39
SD	115	0.3	600	1200	8.93	35.71	23.21	92.86	159.79	639.15
SE	110	0.3		600		8.54		22.20		152.84

Assumed values

UBC tabulated values

$$V_s = \sqrt{\frac{G}{\rho}} \quad \rho = \frac{\gamma}{g} \quad G = \frac{E}{2(1+\nu)}$$

The pile foundation used in this chapter was based on a reinforced concrete pile, with a *compressive strength* $f'_c = 4000 \text{ psi}$, corresponding to a normal strength concrete, and the following material properties:

$E_p = 3600 \text{ ksi}$ (pile modulus of elasticity)

$\gamma_p = 150 \text{ pcf}$ (pile specific weight)

$\nu_p = 0.2$ (pile Poisson's ratio)

The pile has a 1-ft square cross section, and an embedded length of 30 ft.

3.2 Dynamic Response to be Evaluated

In order to evaluate the effect of the soil inertia properties in the system behavior, the *dynamic flexibility* of the pile head will be considered. The dynamic flexibility is defined here as the horizontal pile head displacement due to the excitation of a unit harmonic load at the pile top for different load vibration frequencies. This quantity is also known as the *Frequency Response Function (FRF)* of the pile head.

3.3 Analysis Package, Type, and General Parameters

The computer program SAP2000 was selected to perform the FE analysis required to obtain the Frequency Response Function. Although SAP2000 is not among the most frequently used software packages for pile-soil interaction problems, it was selected due to its availability, its friendly graphical user interface, and its adequate capabilities for the present analysis.

The analysis to be performed in order to obtain the FRF is designated as *Steady State Analysis* in SAP2000. Appendix B presents a detailed step-by-step process to perform the analysis for one of the two dimensional cases considered and presented later in section 3.5.

For the present study, the default damping model available in SAP2000 was adopted: a hysteretic damping constant for all frequencies, with a stiffness-proportional coefficient of 0.05.

3.4 General Comments on the Finite Element Model to be Adopted

The FE mesh will be adopted considering the case studies reviewed in the literature (i.e. Maheshwari et al., 2004) and the recommendations given by soil-structure interaction specialists (i.e. Lysmer, 1979). For example, Lysmer (1979) states that the element size should be related to the highest frequency, f_{\max} [hz], of the wave that must be transmitted correctly through the finite element model. The shortest *wavelength*, λ_s which occurs in the system is:

$$\lambda_s = \frac{V_s}{f_{\max}} \quad (3.1)$$

where V_s is the *shear wave velocity*. Lysmer recommends that the maximum element size be limited to $\lambda_s / 8$. For the data adopted for this case study, an element size of 2 ft would be adequate to transmit harmonic waves with a frequency up to the fourth natural

frequency of the one-layer uniform soil deposit, and an element size of 1 ft would be adequate to transmit a wave with a frequency up to the eighth soil deposit natural frequency (see computations in Appendix A).

When performing a 2D analysis, the soil will be represented with rectangular planar elements, and with brick solid elements when performing a 3D analysis. It is important to have in mind that the type of analysis to be performed will focus on the effects of the soil mass in the system response when the system remains in the linear elastic range. The contact problems between pile and soil are considered not important for this purpose, therefore frame lineal elements are considered adequate to model the pile. For other type of analysis, it would be more appropriate to model the pile with plane (2D) or solid (3D) elements, and model the soil-pile interface with contact elements.

Regarding the model size (macro-idealization), Lysmer (1979) states that, as far as the motion of the structure is concerned, the boundaries of the soil volume should be located far enough away from the structure to simulate the infinite extent of the deposit. The author recommends placing the lateral boundaries at a distance of two or more times the depth of the soil profile away from the edge of the structure. Although these recommendations were intended for the analysis of superstructures that may be partially embedded, they will be used herein as a guidance. Considering the 30 ft soil deposit depth, the boundaries will be placed 60 ft away from the pile. The mesh obtained is more extended than those used in the several papers reviewed in which the FEM was used as the analysis technique.

3.5 Two Dimensional Analysis

A beam (frame) element was adopted for the pile, and plane stress elements for the soil, with 1 ft thickness. In order to model plane strain conditions, the elasticity modulus E and Poisson's ratio ν of both concrete and soil were replaced by the well known equivalent

elastic constants that allow to obtain plane strain solutions from plane stress analysis (Ugural and Fenster, 1995):

$$\begin{aligned} E_{eq} &= \frac{E}{1-\nu^2} \\ \nu_{eq} &= \frac{\nu}{1-\nu} \end{aligned} \quad (3.2)$$

The resulting equivalent properties for the sand soil and the reinforced concrete (RC) are presented in Table 3.2:

Table 3.2: Equivalent Elastic Properties for the 2D Model

Material	E [ksi]	ν	Eeq [ksi]	veq
Soil	12	0.3	13.19	0.429
RC	3600	0.2	3750.00	0.250

3.5.1 Boundary Conditions

The soil will be considered fully restrained at the bottom edge, in order to model a rigid bedrock below the sand deposit. The top edge will be considered free. The two lateral edges should represent the continuity of the soil deposit as an infinite half space. The model will be taken wide enough in order to approximately represent this condition. In order to verify this statement, two boundary conditions will be considered: free and restrained against horizontal movement. If the two conditions give similar results, a more refined lateral boundary condition, that should give results somewhere in between these two cases, is not required since it will not change the general conclusions of the analysis of the results. A more advanced and commonly used boundary condition is to represent the elastic continuity by means of horizontal springs and to use dashpots to represent the radiation damping. These boundary conditions will be implemented in the 3D model.

3.5.2 FEM Mesh

Following the criteria described in section 3.4, the full FE model is 120 ft wide and 30 ft high, the finite element mesh representing the soil is composed of 2ft x 2ft rectangular elements, and the pile consists of 2ft frame elements. The resulting FE mesh is shown in Figure 3.1. The FE model contains 15 frame elements and 900 plane stress elements, having 976 nodes and 1976 *degrees of freedom* (DOF) corresponding to two translations of each soil node and two translations and one rotation of each pile node.

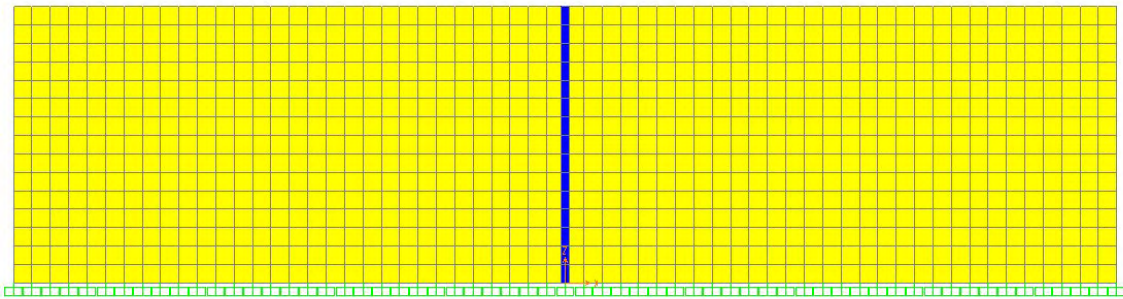


Figure 3.1: 2D FEM Model

Figure 3.2 presents a zoom in of the FE model for the pile top, in order to show the numbering of the node whose motion will be studied. The pile top corresponds to node 496 in this model, and its steady state response will be obtained.

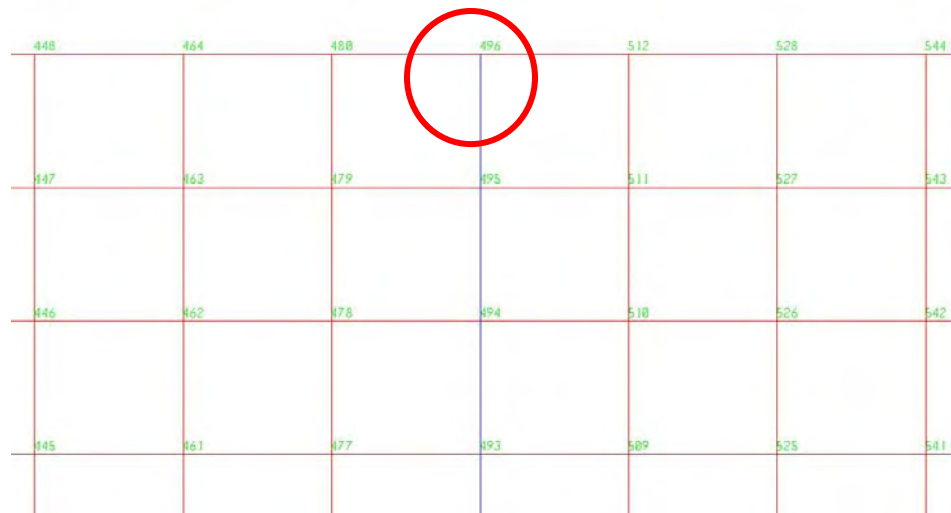


Figure 3.2: FEM Model Node Identification near Pile Top

3.5.3 System Response

As stated in section 3.2, the system response to be evaluated is the dynamic flexibility of the pile head (i.e., the horizontal pile displacement due to a unit harmonic load for different load vibration frequencies). This response will be designated as *FRF* (*Frequency Response Function*). It is obtained by means of the Steady State Analysis option in SAP2000 (see Appendix B for details).

This response will be presented in charts (Figures 3.3 through 3.7), by plotting the magnitude of the horizontal displacement of the pile top, in $[ft]$, against the frequency of the load, in $[Hz]$. The following nomenclature will be used in these graphs:

SM = Soil Mass

NO SM = Soil Mass is not included in the analysis

YES SM = Soil Mass is included in the analysis

LS = Lateral Support

NO LS = There are not Lateral Supports at the model edge

YES LS = There are Lateral Supports at model edge

In order to obtain a high resolution, 400 frequency increments were specified for each analysis. The mass of the pile is always included in the analyses.

Figure 3.3 presents the results of the model without the inclusion of the soil mass, for the two boundary conditions evaluated. Figure 3.4 presents the results of the model considering the soil mass, for the two boundary conditions evaluated. Figure 3.5 presents the results of the model first considering and next neglecting the soil mass, leaving the lateral edges without lateral supports.

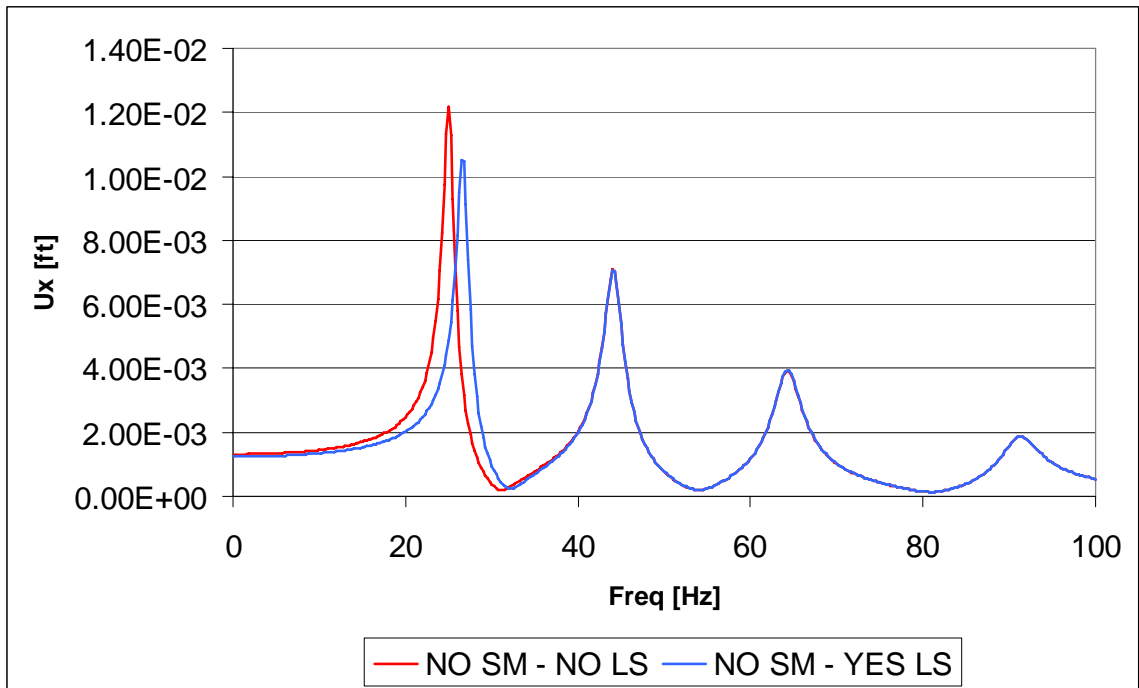


Figure 3.3: FRF for the 2D Model without Soil Mass

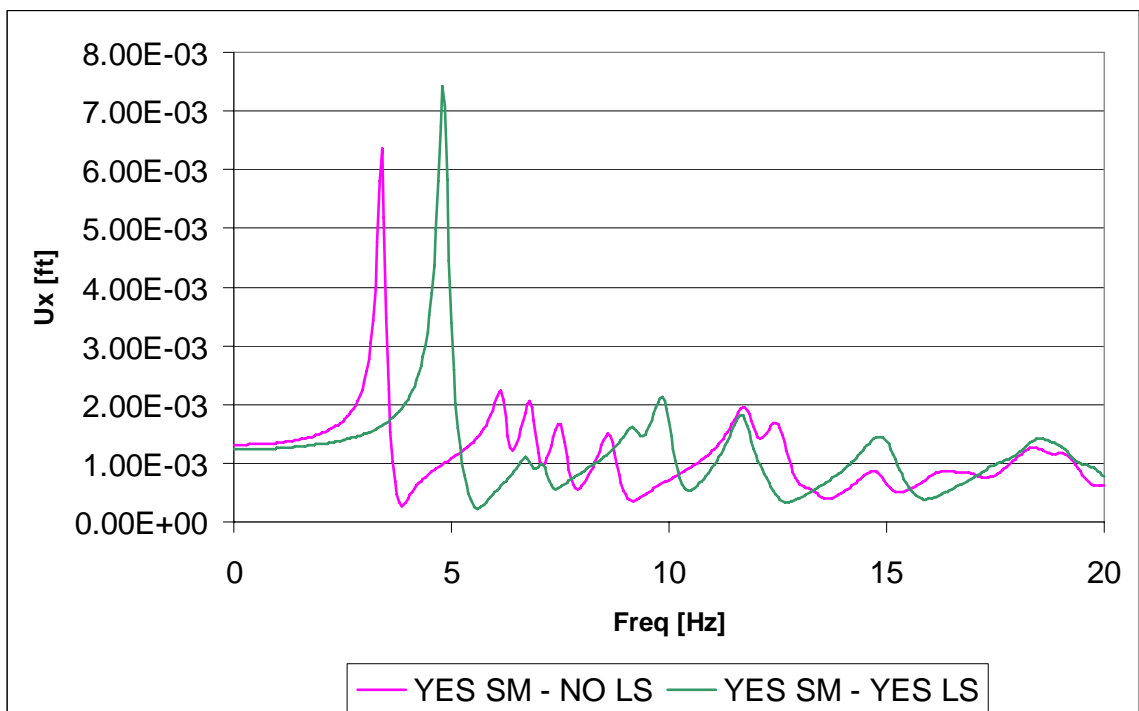


Figure 3.4: FRF for the 2D Model with Soil Mass

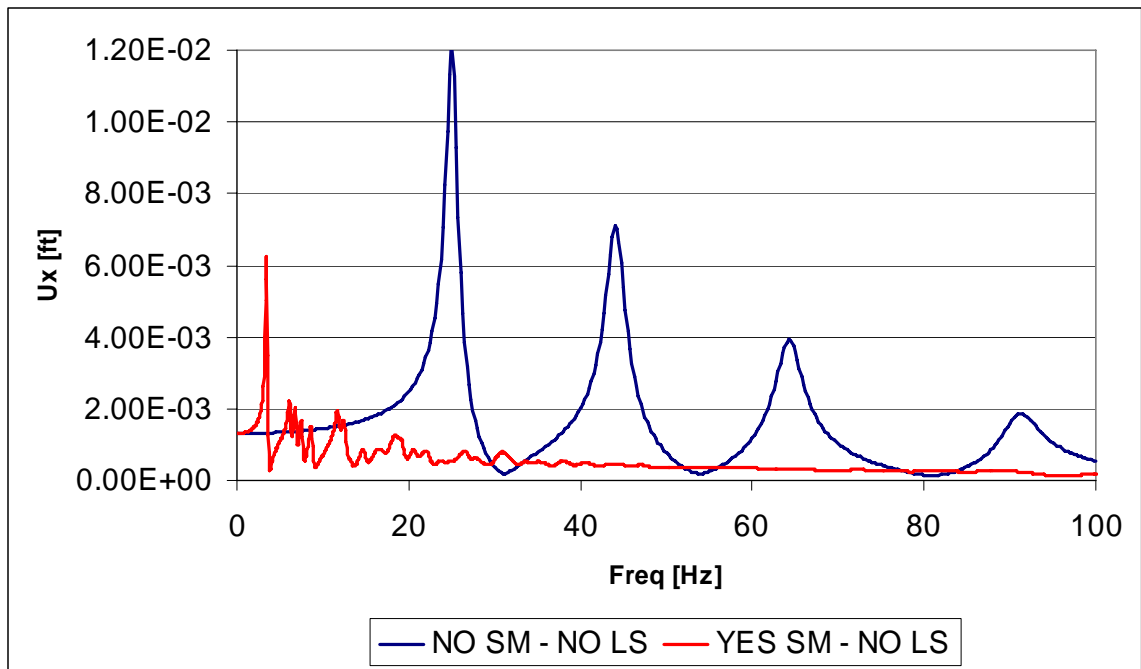


Figure 3.5: FRF for the 2D Model with and without Soil Mass, and no Lateral Supports

Figure 3.6 presents the soil model with two zones, one zone adjacent to the pile was arbitrary selected to be 20 ft wide and corresponds to the zone where soil mass will be considered (red). The other zone, away from the pile, 40 ft wide, in which the soil will be considered massless (orange). Figure 3.7 presents the results of this model with partial mass assignment along with the function obtained when the full soil deposit mass is included.

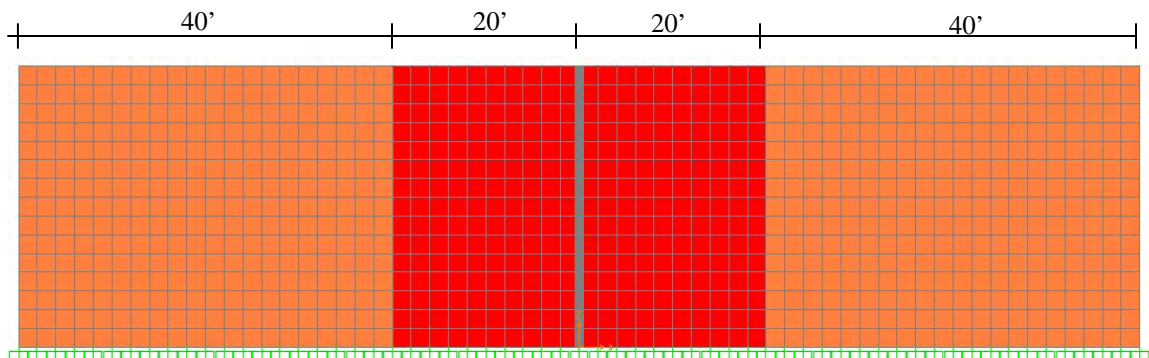


Figure 3.6: 2D FEM Mesh with Partial Soil Mass Assignment

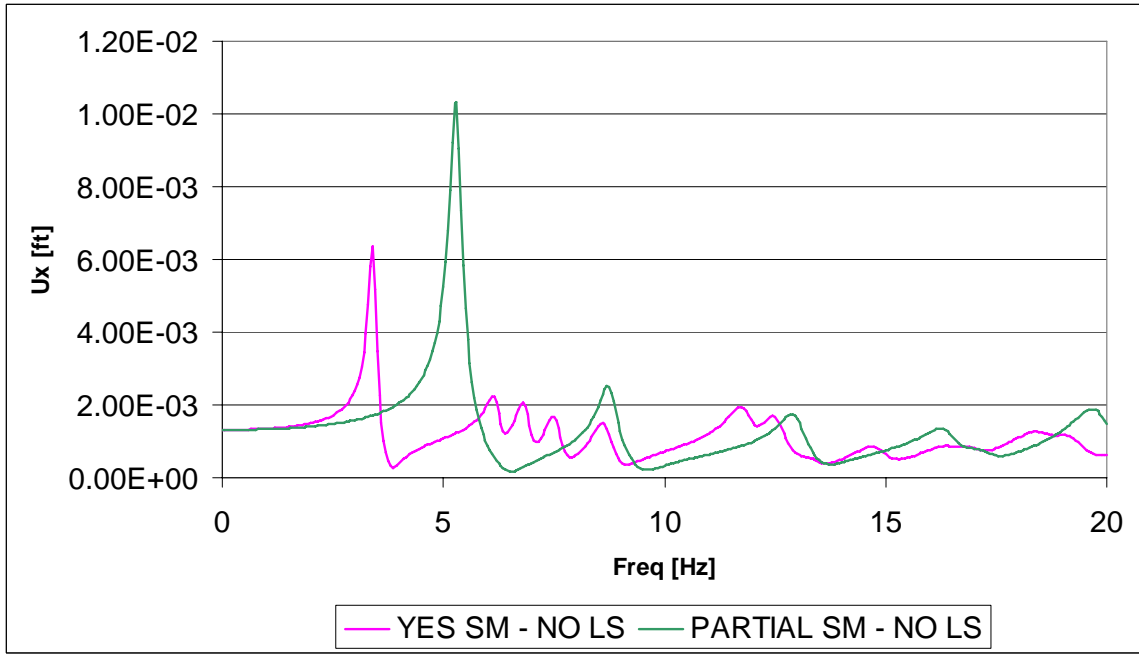


Figure 3.7: FRF for the 2D Model with Partial and Full Soil Mass Assignment, and no Lateral Supports

3.5.4 Discussion of the 2D Results

From Figures 3.3 and 3.4, it is evident that the effect of the fixed lateral support is to produce a shift of the peaks of the FRF to the right. This implies an increase in the natural frequencies of the system, which correspond to the peaks of the FRF. This situation is expected since the system is stiffer (more rigid) due to the presence of the lateral supports that restraint the horizontal movement. The natural frequencies increase as the stiffness increases, as shown in the following expression that gives a natural frequency of a multi degree of freedom (MDOF) system:

$$\omega_j^2 = \frac{\{\phi_j\}^T [K] \{\phi_j\}}{\{\phi_j\}^T [M] \{\phi_j\}} \quad (3.3)$$

where:

ω_j = system natural frequency corresponding to the j^{th} vibration mode

$\{\phi_j\}$ = system j^{th} vibration mode (eigenvector)

$[K]$ = system stiffness matrix

$[M]$ = system mass matrix

Figures 3.3 and 3.4 also show that the general behavior of the pile-soil systems is similar for both boundary conditions, and the first two natural frequencies are comparable in both cases. This leads to the conclusion that, for the analyses to be performed, it is not necessary to consider a more refined elastic lateral support. Free boundary supports will be considered for the remaining analyses.

Figure 3.5 presents the resulting FRF (in magnitude) for the system with and without the soil mass. As expected (see equation 3.3), the presence of the soil mass reduces the natural frequencies (i.e. the frequencies where the peaks of the FRF occur). This figure shows that the inclusion of the soil mass produces a significant qualitative and quantitative change in the behavior of the pile-soil system. This leads to the conclusion that the soil mass plays an important role in the dynamic response.

Figure 3.7 shows a comparison between the magnitude of the FRF for the system with a partial assignment of the soil mass (the mass nearest to the pile) and the FRF of the system with full soil mass assignment. The figure shows that the system with partial mass assignment partially captures the general behavior of the system with the full soil mass assigned, and that the first natural frequencies of both models are relatively close. This leads to the conclusion that a partial soil mass assignment may result in a reasonable good estimate of the first natural frequency, and of the overall system response.

3.6 Three Dimensional Model

The results of analyses similar to the ones presented in section 3.5, but considering a three dimensional (3D) soil model, are presented here. Table 3.3 shows the elastic material properties to be used for the soil and the RC pile:

Table 3.3: Elastic Properties for 3D Model

Material	E [Ksi]	ν
Soil	12	0.3
RC	3600	0.2

3.6.1 Boundary Conditions

The soil will be considered fully restrained in the bottom edge, in order to model a rigid bedrock below the sand deposit. The top edge will be considered free. The lateral edges will be considered with five different boundary conditions: free, restrained against horizontal movement, with roller supports (vertical movement restrained), with *dashpots* that model the radiation damping due to waves traveling in the semi-infinite medium, and with spring-dashpot to model both the soil continuity and the radiation damping. The latter conditions will be considered to evaluate the effect of the radiation damping in the system response (an effect not evaluated in the 2D analyses).

As stated by Arduino (2005), to simulate the radiation condition, the *cut off boundaries* must include normal and tangential energy absorption elements. These absorption elements are usually represented by dashpots, and are usually known as Lysmer boundary conditions. Properly calibrated, these elements absorb the propagating waves in such a way that any incident wave produces zero energy being reflected back into the domain. The dashpot coefficients are determined in terms of the material properties of the semi-infinite domain, as shown in Figure 3.8. As presented by Mengi and Tanrukulu (1993), the original dashpot proposed by Lysmer and Kuhlemeyer (1969) included dimensionless

constants a and b ($C_n = a \rho v_p$, $C_t = b \rho v_s$). However, it was found that using optimized values for these constants (in order to minimize the reflected energy) does not bring major improvements to the performance of viscous boundary conditions as compared to simply taking $a = b = 1$. These last values were adopted for the present work.

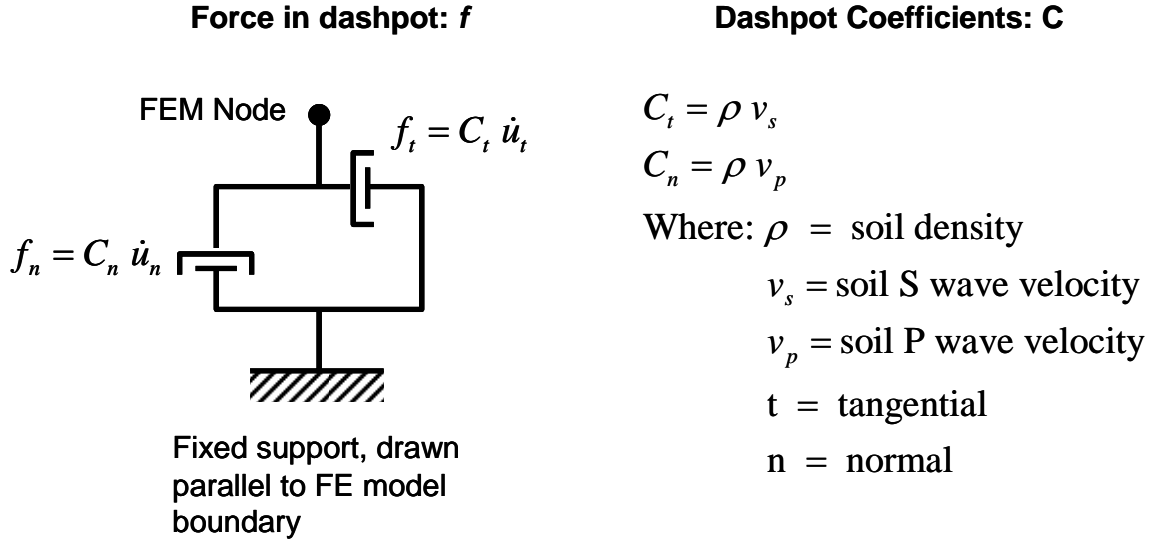


Figure 3.8: Dashpot Elements to Simulate Radiation Damping in the FE Cut-off Boundaries

The dashpot coefficients presented in Figure 3.8 have to be multiplied by the *influence area* “ A ” of each node of the FE boundary in order to obtain a concentrated dashpot coefficient, resulting in: $C_T = C_t A$ and $C_N = C_n A$, where the capital subscript represents nodal concentrated values. Because the mesh of the FE model is uniform of size 2’x2’x2’, an internal node will have an influence area of $A = 4 \text{ ft}^2$, an edge node of $A = 2 \text{ ft}^2$, and a corner node of $A = 1 \text{ ft}^2$. Table 3.4 summarizes the values of the dashpot coefficients to be used in the model, for each of the of influence areas stated before.

Table 3.4: Dashpot Coefficients for the Cut off Boundaries

E [Ksi]	ν	γ [pcf]	G [Ksi]	Vp [ft/sec]	Vs [ft/sec]
12	0.3	110	4.62	711.22	441.08

C_n [psf / (ft/sec)]	C_t [psf / (ft/sec)]
2429.63	1506.79

A [ft ²]	C_N [lb / (ft/sec)]	C_T [lb / (ft/sec)]
4	9718.52	6027.17
2	4859.26	3013.59
1	2429.63	1506.79

The spring constants used to model the unbounded nature of the soil medium will be obtained following the approach proposed by Luco (2004). Luco obtained expressions for the average distributed spring constant to be applied at the boundaries of a rectangular soil island or truncated region of dimensions $2a_x \times 2a_y \times a_z$, as depicted in Figure 3.9, carved out of the half space. In the present FE model, $a_x = 60$ ft, $a_y = 30$ ft, and $a_z = 30$ ft.

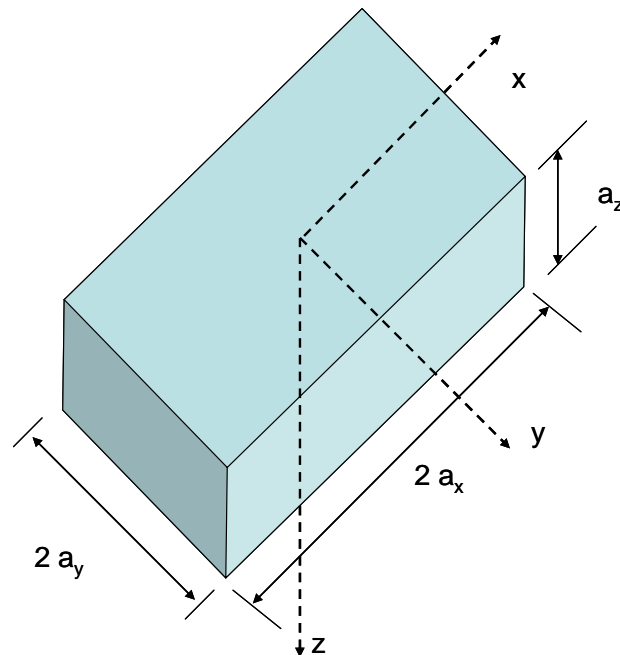


Figure 3.9: Rectangular Soil Island Dimensions

The average distributed springs constants to be applied at the region boundaries are obtained from the following equation:

$$k_{ij} = \frac{G}{a_i} \beta_{ij} \quad (3.4)$$

where:

k_{ij} = distributed spring constant

$i = x, y, \text{ or } z$ = plane in which the spring is placed (represented by its normal)

$j = x, y, \text{ or } z$ = direction in which the spring acts

a_i = dimension in the i direction

β_{ij} = coefficient that depends on the Poisson's ratio of the soil and the block dimensions

These coefficients have to be multiplied by the *influence area* “ A ” of each node of the FE boundary in order to obtain a concentrated spring coefficient. This leads to the following expression: $K_{ij} = k_{ij} A$, where the capital letter represents nodal concentrated values. Because the size of each FE is 2'x2', an internal node will have an influence area of $A = 4 \text{ ft}^2$, an edge node of $A = 2 \text{ ft}^2$, and a corner node of $A = 1 \text{ ft}^2$.

Appendix C presents the computations of the coefficients β , k and K . Table 3.5 summarizes the values of the spring coefficients to be used in the model, for each one of the values of influence areas A stated before.

Table 3.5: Spring Coefficients for Cutoff Boundaries

$A \text{ [ft}^2\text{]}$	$K_{xx} \text{ [lb / ft]}$	$K_{xy} \text{ [lb / ft]}$	$K_{xz} \text{ [lb / ft]}$
4	87080	24260	24260
2	43540	12130	12130
1	21770	6064	6064
$A \text{ [ft}^2\text{]}$	$K_{yx} \text{ [lb / ft]}$	$K_{yy} \text{ [lb / ft]}$	$K_{yz} \text{ [lb / ft]}$
4	49410	88160	37900
2	24700	44080	18950
1	12350	22040	9475

3.6.2 FEM Mesh

Following the criteria described in section 3.4, the FE model is 120 ft long, 60 ft wide, and 30 ft tall. The finite element mesh representing the soil is composed of 2ft x 2ft x 2ft solid elements, and the pile is modeled with frame elements with 2ft length. The resulting FEM mesh is shown in an isometric view in Figure 3.10, in a front view in Figure 3.11 (xz plane, long dimension of the model), and in a right view in Figure 3.12 (yz plane, short dimension of the model).

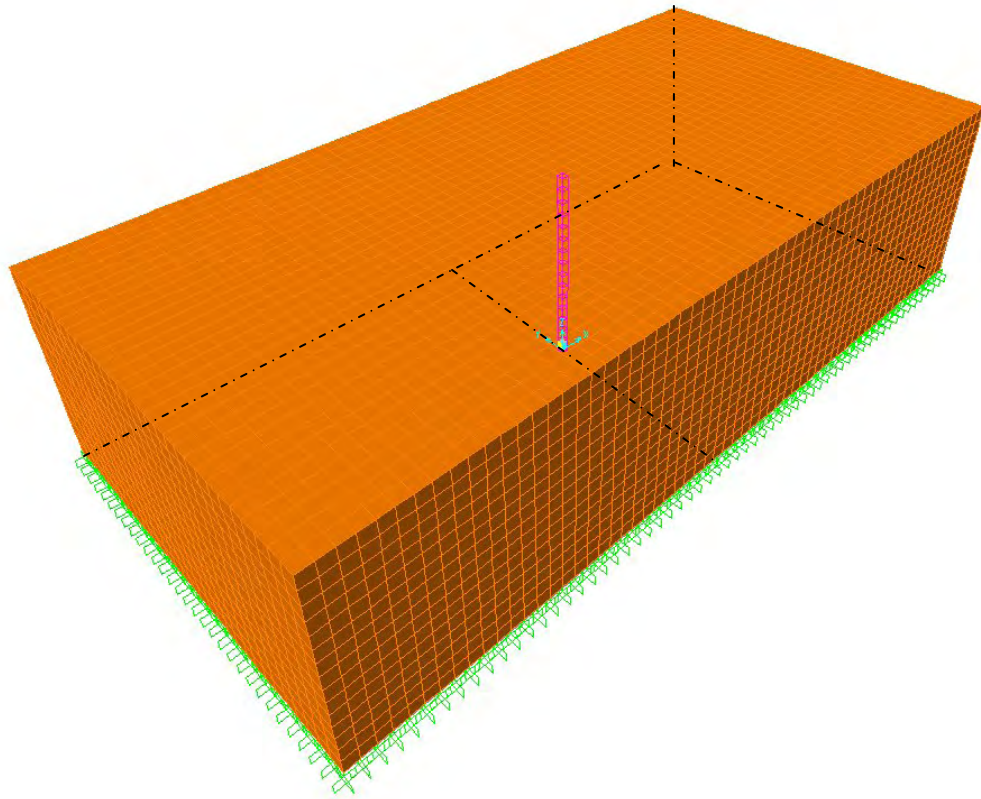


Figure 3.10: Isometric View of the FEM 3D Model Mesh

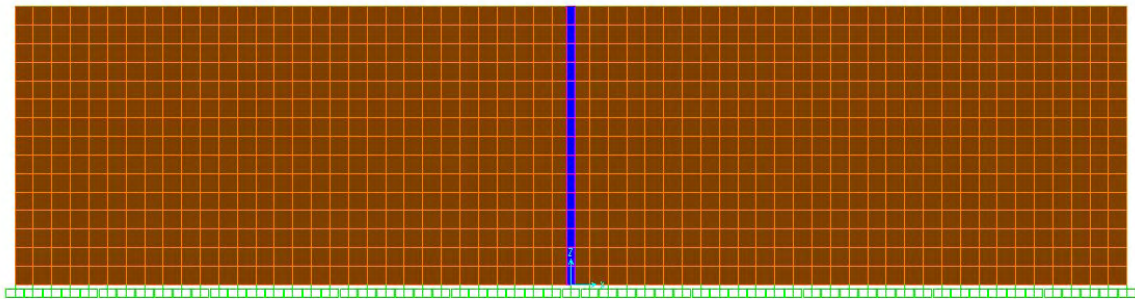


Figure 3.11: Front View of the FEM 3D Model Mesh (long dimension)

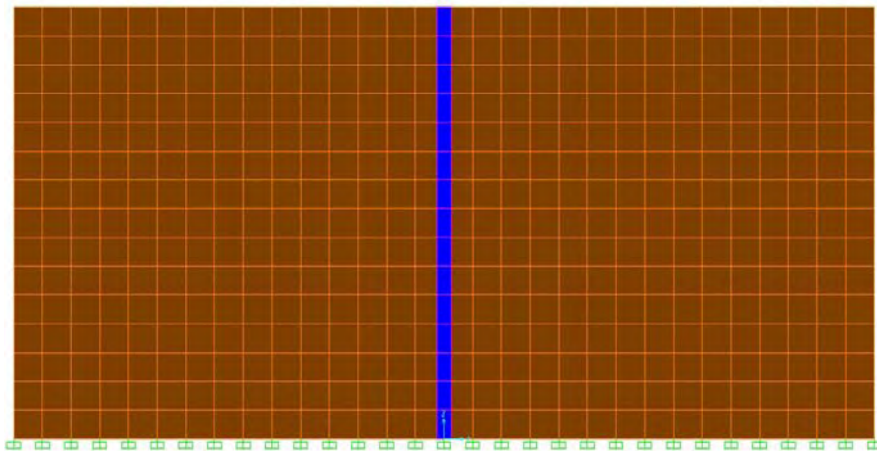


Figure 3.12: Right View of the FEM 3D Model Mesh (short dimension)

The resulting FE model has 15 frame elements and 27000 solid elements, 30256 nodes, and 90813 *degrees of freedom* (DOF), corresponding to three displacements at each soil node, and three displacements and three rotations at each pile node. The steady state response at the pile top, which corresponds to node 15136 in this model, will be obtained. The magnitude of the force applied at the top of the pile in the x (long) direction is 1 kip.

3.6.3 System Response

As stated in section 3.2, the system response to be evaluated is the dynamic flexibility of the pile head (the horizontal pile displacement due to a unit harmonic load, for different load vibration frequencies). The dynamic flexibility curve is also known as the *FRF* (*Frequency Response Function*).

This response will be presented in charts that show the magnitude of the horizontal displacement of the pile top as a function of the frequency of the load. The following nomenclature will be used in these graphs:

SM = Soil Mass

NO SM = Soil Mass is not included in the analysis

YES SM = Soil Mass is included in the analysis

LS = Lateral Support

NO LS = No Lateral Supports are present at the model edge

YES LS = Lateral Supports are present at the model edge

DP = Dashpot (radiation damping)

NO DP = No Dashpots are present at the model edge

Yes DP = Dashpots are present at the model edge

RS = Roller Support

Yes RS = Roller Supports are present at the model edge

In order to obtain a detailed response while at the same time keeping the computing time at reasonable levels, 100 frequency increments were specified for each analysis.

Figure 3.13 presents the results of the model when the soil mass is neglected, for two lateral boundary conditions: free and fixed. Figure 3.14 presents the FRF curve considering the soil mass, for the same two lateral boundary conditions. Finally, Figure 3.15 displays the results including and neglecting the soil mass, with the lateral edges without lateral supports (free).

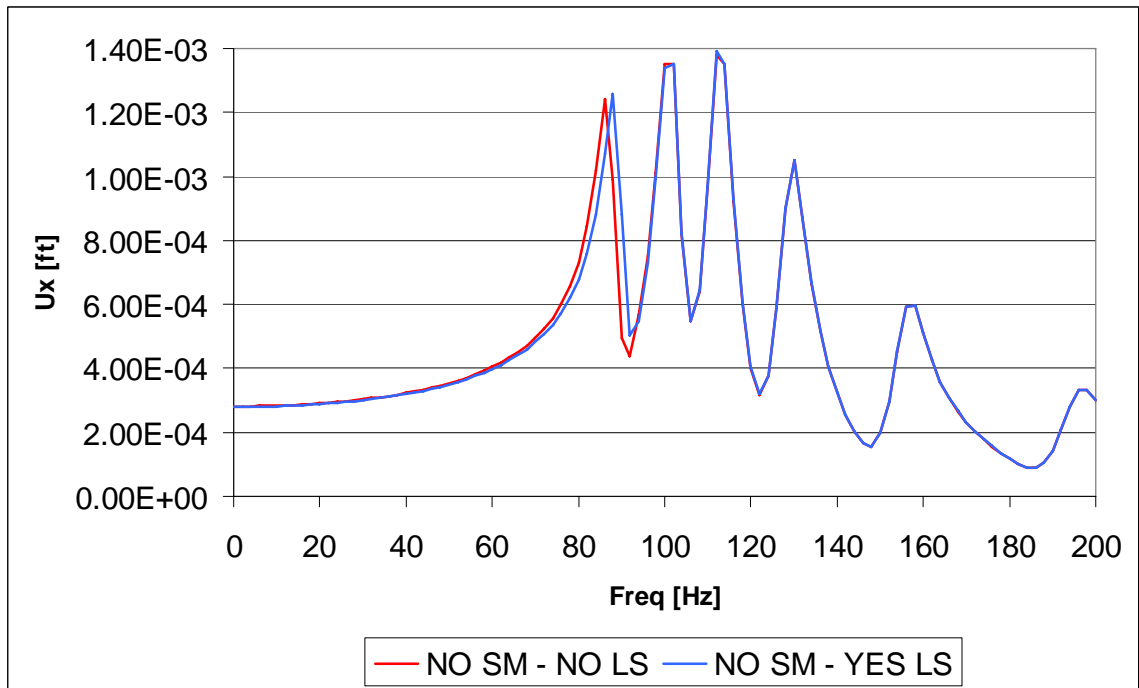


Figure 3.13: FRF for the 3D Model without Soil Mass

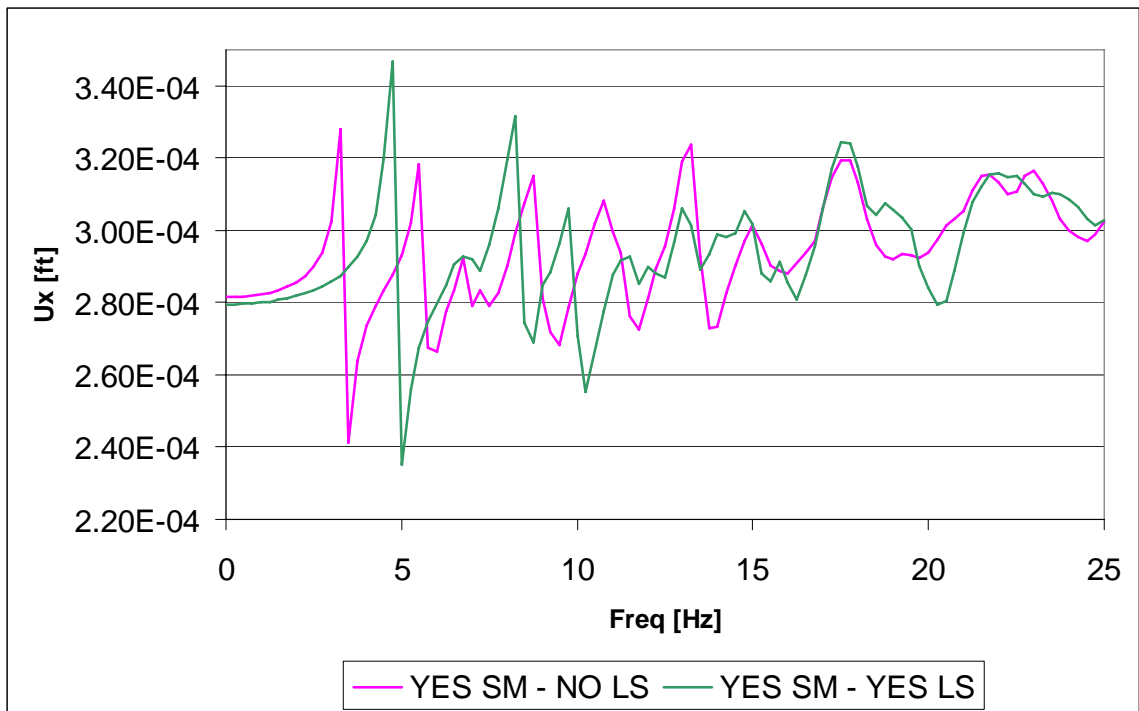


Figure 3.14: FRF for the 3D Model with Soil Mass

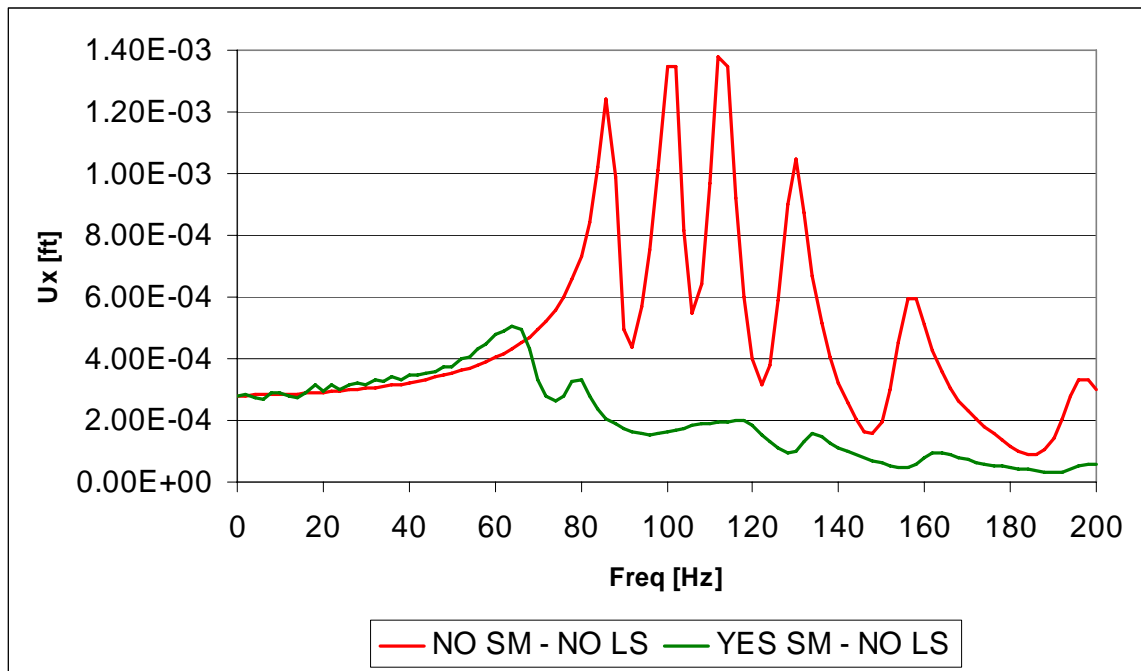


Figure 3.15: FRF for the 3D Model with and without Soil Mass, and no Lateral Supports

Figures 3.16 a and b present the amplitude of the top pile displacement for the FE model that considers the soil mass and also dashpots in the cutoff boundaries to simulate the radiation damping, for two different load frequency ranges. In both charts the response is plotted against the one obtained by considering free lateral edges, without the dashpots. The first figure (Figure 3.16a) displays a zoom of the dynamic flexibility for the lower frequency range (0 to 25 Hz). It is important to mention that for both frequency ranges (0 to 25, and 0 to 200 Hz), the same number of frequency increments (100) was used in the analysis: Figure 3.16a is more detailed than the lower range of Figure 3.16b, capturing some peaks not present in Figure 3.16b.

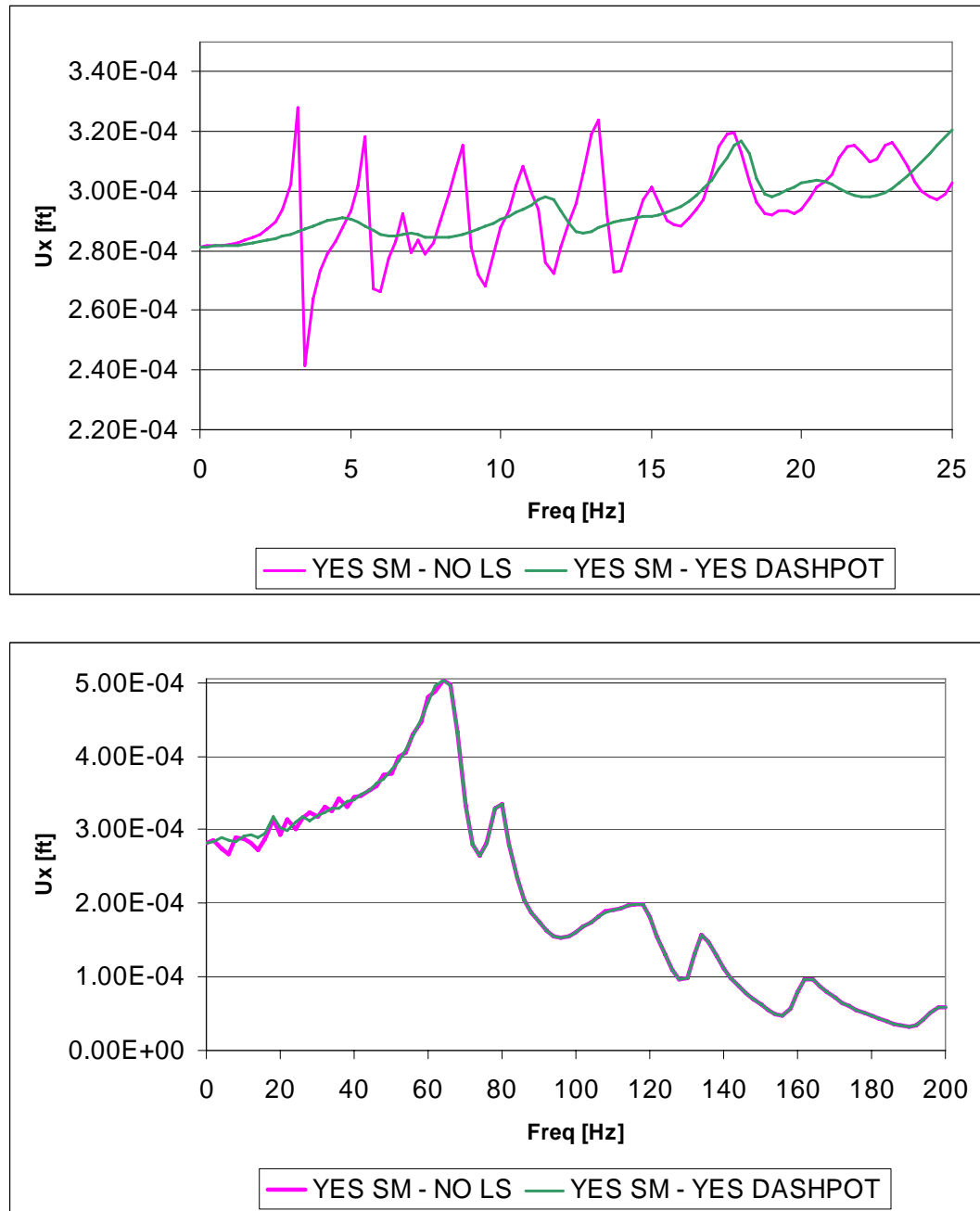


Figure 3.16: FRF for the 3D Model with Soil Mass, and Dashpots in the Lateral Cutoff Boundaries

Figure 3.17 presents the soil model with two zones, one near the pile (40 ft wide x 40 ft long) in which soil mass will be considered (shown in red), and the other away from the pile (the remaining of the soil island) in which the soil will be considered massless (the orange zone).

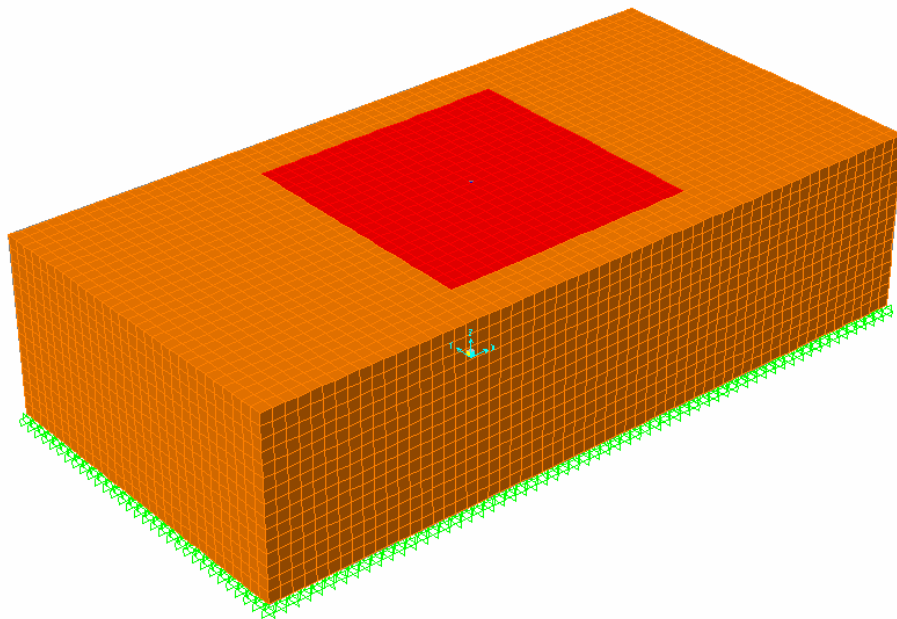


Figure 3.17: 3D FEM Mesh with Partial Soil Mass Assignment

Figures 3.18 a and b present the displacement of the pile top with this partial mass assignment for the soil. Each figure corresponds to two different load frequency ranges. In both charts the response is plotted against the displacements obtained considering all the soil deposit with mass.

Figures 3.19 a and b show the results corresponding to the FE model that considers soil mass and springs and dashpots in the cutoff boundaries to simulate the semi-infinite nature of the soil medium and the radiation damping. Again, there are two figures to better appreciate the response in two different load frequency ranges. In both charts the response is plotted against the one obtained considering free lateral edges.

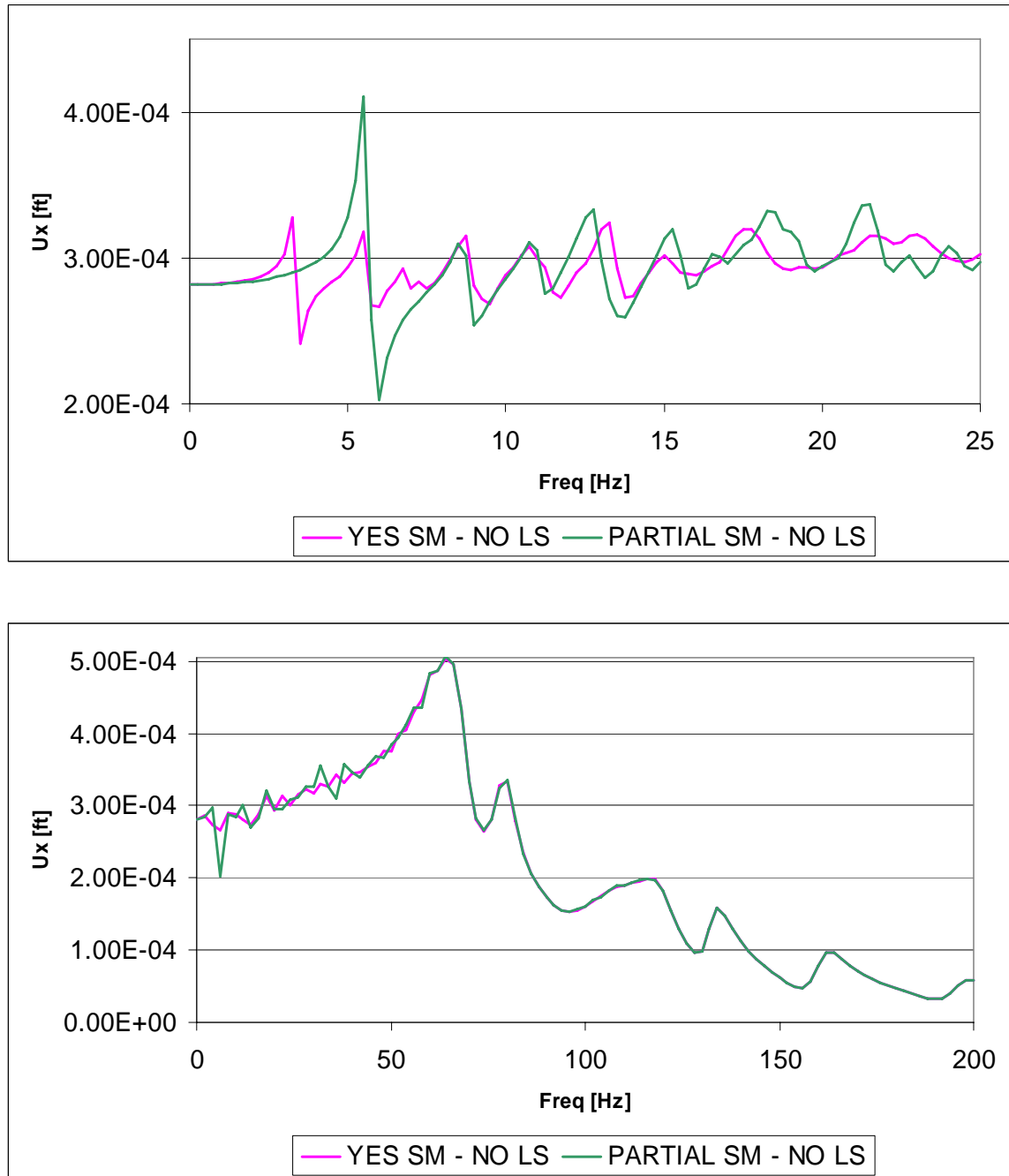


Figure 3.18: FRF for the 3D Model with Partial Soil Mass and no Lateral Supports

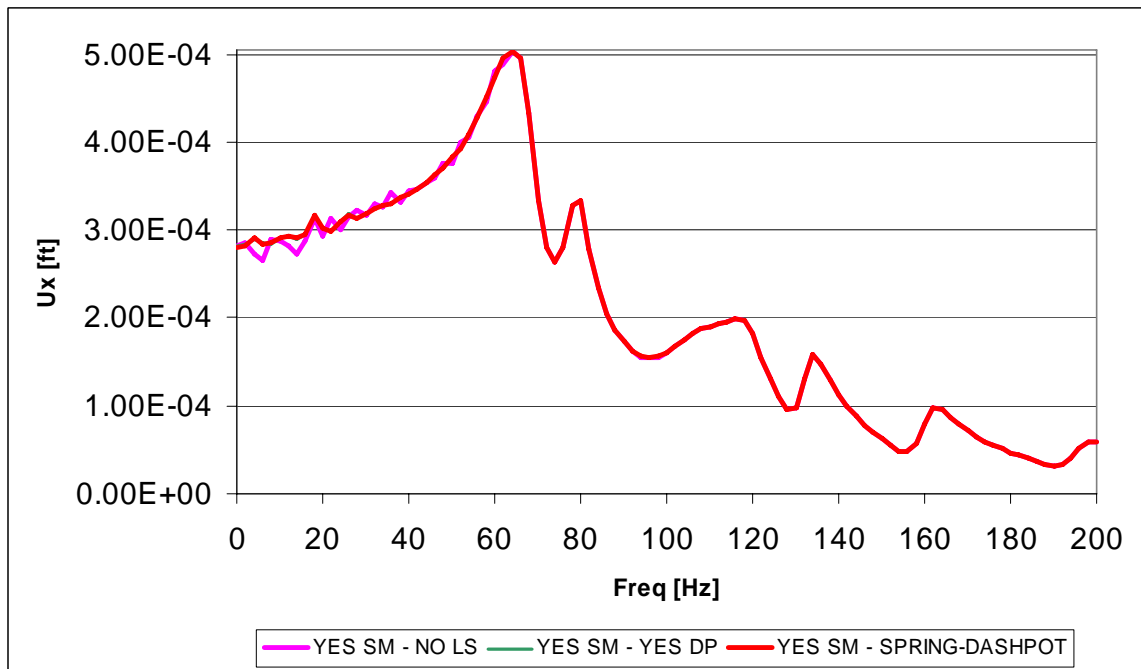
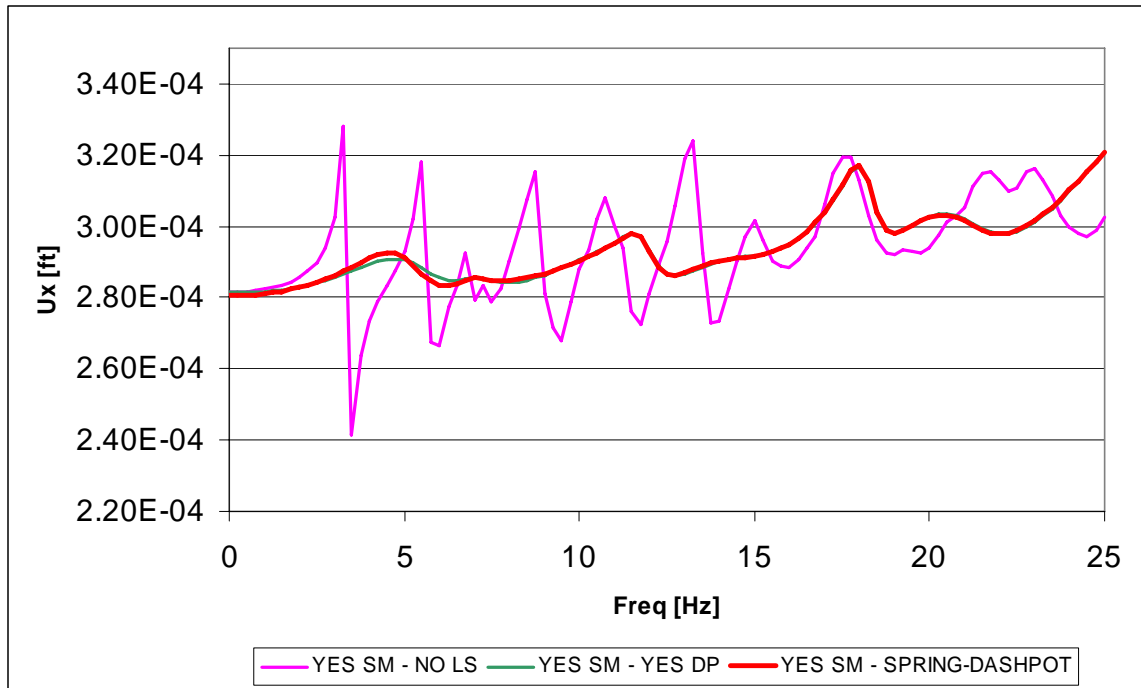


Figure 3.19: FRF for the 3D Model with Soil Mass, and Springs and Dashpots in the Lateral Cutoff Boundaries

Figure 3.20 presents the results of the model when the soil mass is neglected, and with roller supports at the cutoff boundaries. These results are plotted against the FRF magnitude obtained for the model with free nodes at the lateral edges, for comparison.

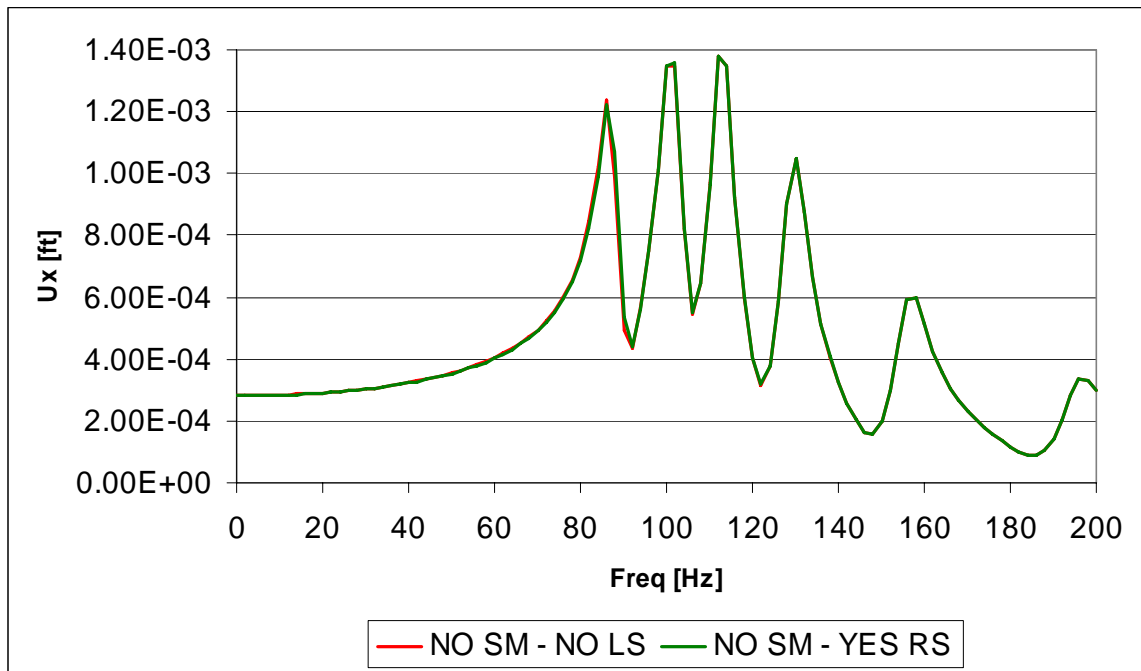


Figure 3.20: FRF for the 3D Model without Soil Mass, and Rollers in the Lateral Cutoff Boundaries

Figures 3.21 a and b present the FRF curve considering the soil mass, for two different frequency ranges, when the model lateral edges are restrained by roller supports. These results are plotted against the FRF obtained for the model with free nodes at the cutoff boundaries, for comparison.

Finally, Figure 3.22 presents the FRF of the system considering soil mass and with springs and dashpots in the cutoff boundaries, together with the soil deposit natural frequencies and the pile natural frequencies (as computed in Appendix A, considering both as continuous systems). Table 3.6 presents the computed natural frequencies, the wavelengths, and the ratio between the wavelengths of the pile and the soil for coincident (or more precisely, similar) natural frequencies.

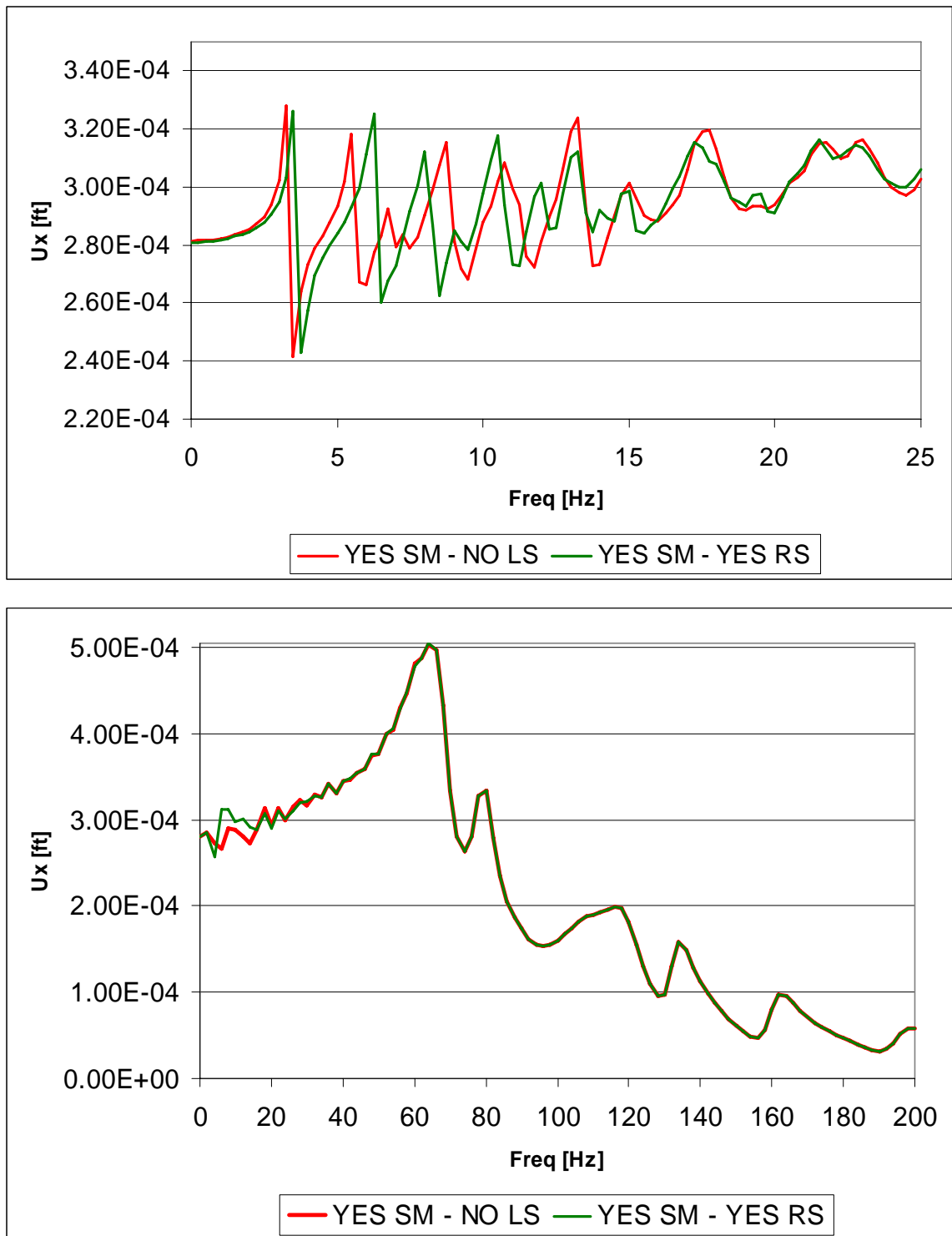


Figure 3.21: FRF for the 3D Model with Soil Mass, and Rollers in the Lateral Cutoff Boundaries

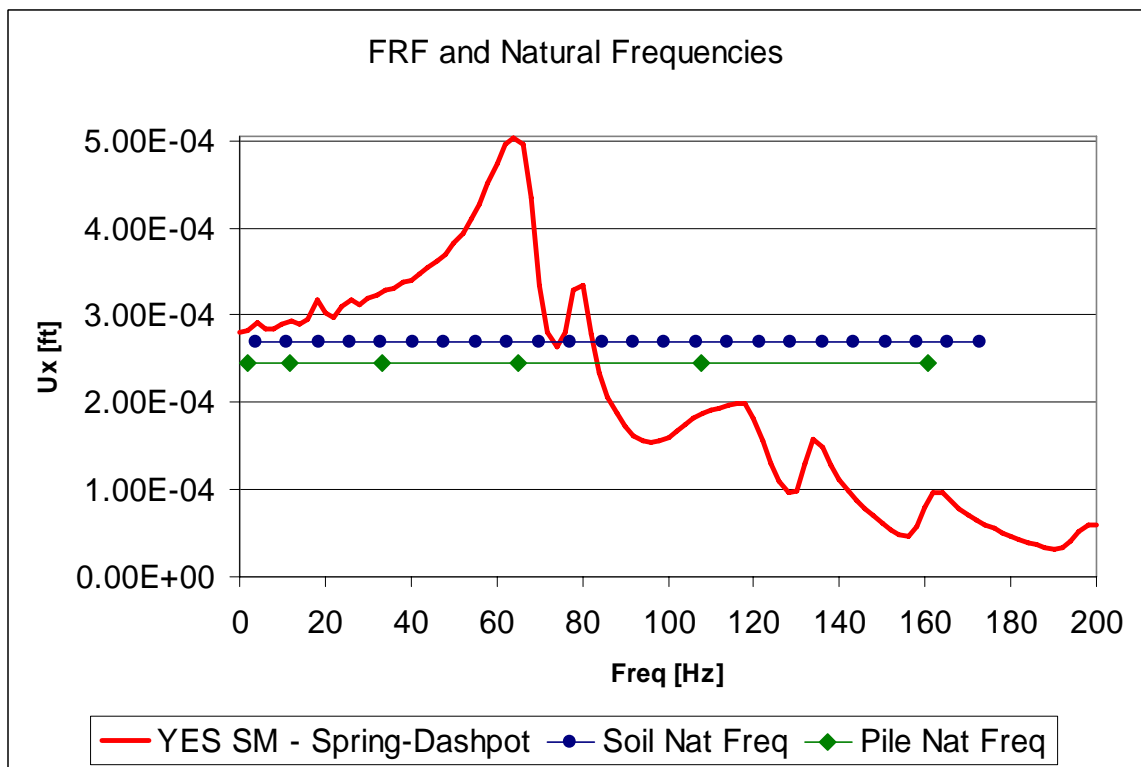
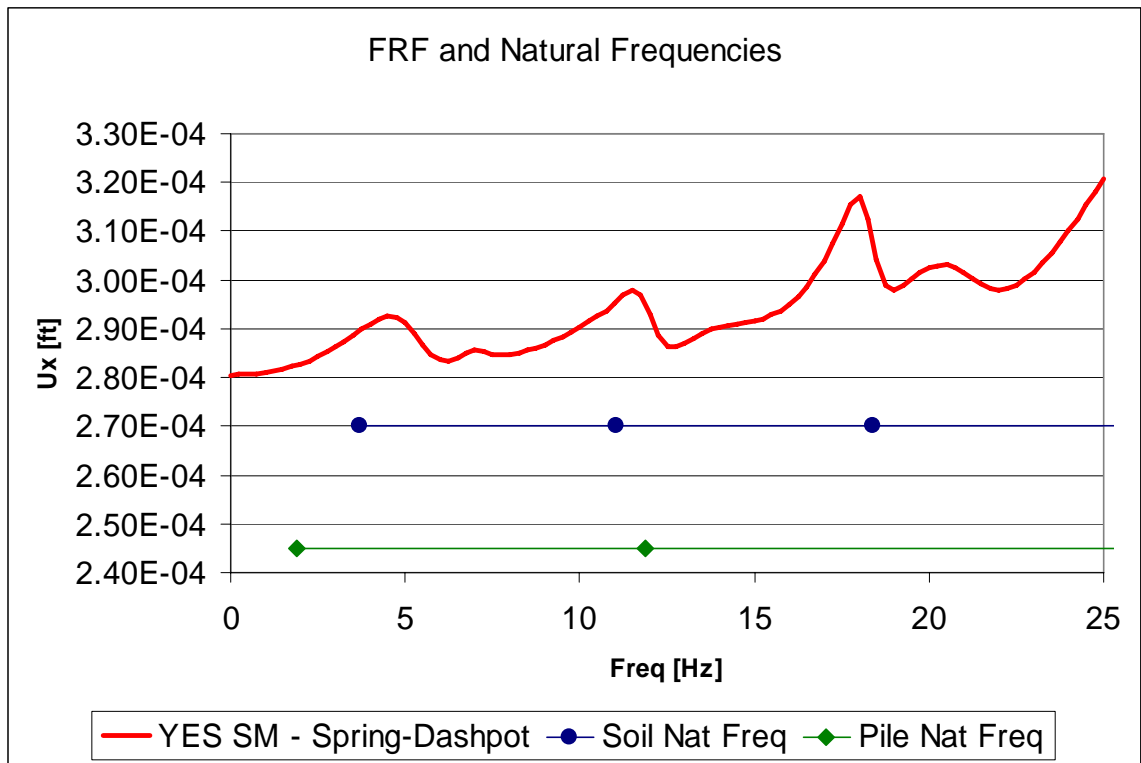


Figure 3.22: FRF for the 3D Model with Soil Mass, and Springs-Dashpots Elements in the Lateral Cutoff Boundaries, together with Soil and Pile Natural Frequencies

Table 3.6: Soil Stratum and Pile Natural Frequencies and Wavelengths

Soil Natural Frequencies			Pile Natural Frequencies			λ_p / λ_s
i	f_i [Hz]	λ_s [ft]	i	f_i [Hz]	$\approx \lambda_p$ [ft]	
1	3.68	120.00	1	1.89	240	
2	11.03	40.00	2	11.87	30	0.75
3	18.38	24.00	3	33.22	21	1.58
4	25.73	17.14	4	65.11	15	2.12
5	33.08	13.33	5	107.63	12	2.90
6	40.43	10.91	6	160.78	10	3.58
7	47.78	9.23				
8	55.14	8.00				
9	62.49	7.06				
10	69.84	6.32				
11	77.189	5.714				
12	84.54	5.217				
13	91.892	4.8				
14	99.243	4.444				
15	106.594	4.138				
16	113.946	3.871				
17	121.297	3.636				
18	128.648	3.429				
19	135.999	3.243				
20	143.351	3.077				
21	150.702	2.927				
22	158.053	2.791				
23	165.405	2.667				
24	172.756	2.553				

3.6.4 Discussion of the 3D Results

Examining Figures 3.13 and 3.14, it is evident that the effect of the lateral support is to produce a shift of the peaks of the FRF to the right. This implies an increase in the natural frequencies of the system, which corresponds to the peaks of the FRF. This situation is expected since the system is stiffer (more rigid) due to the presence of the lateral supports that restraint the horizontal movement, and the natural frequencies increase as the stiffness increases.

These figures also show that the general behavior of the systems is similar for both boundary conditions, and the first two natural frequencies are comparable in both cases. This leads to the conclusion that, for the type of analysis considered, it is not necessary to use a more refined elastic lateral support. Free boundary supports seem appropriate for the remaining analyses.

Figure 3.15 presents the resulting FRF for the system with and without the soil mass. As expected, the presence of the soil mass reduces the natural frequencies. However, this figure also shows that the inclusion of the soil mass produces a significant qualitative and quantitative change in the dynamic behavior of the system. This leads to the conclusion that the soil mass plays an important role in the dynamic response of the pile. It also reveals that, for the case analyzed, the general effect of the mass was quite similar to a damper: the FRF peaks were smothered in addition to the shift in their locations to the left (at least in the first two peaks).

Figure 3.16 shows the FRF for the system with soil mass and with dashpots in the lateral cutoff edges compared to the response of the same system without the dashpots. It is evident that these dashpots have an important impact in the system response at low frequencies, but not at high frequencies. The effects of the dashpots were to smooth the FRF peaks (lowering the system displacement response), to eliminate some of them (probably associated with rebounding of waves in the cutoff boundaries), and to produce a shift in the peaks location.

Figure 3.18 shows the FRF for the system with a partial assignment of the soil mass (to the soil nearest to the pile) compared to the FRF of the system with full soil mass assignment. The figure shows that the system with partial mass assignment captures the general behavior of the system with the full soil mass assigned. This leads to the conclusion that a partial soil mass assignment may result in reasonable good estimates of the overall system response.

Figure 3.19 presents the FRF for the system with full soil mass assignment, and springs and dashpots in the cutoff boundaries. The figure also includes the response of the system with free cutoff boundaries, and with dashpots in the cutoff boundaries. The figure shows that there is not a significant difference between the system with dashpots only and the system with springs and dashpots, reflecting that the soil island has been taken large enough so the soil half space is adequately represented. The dashpots appear to be more important in order to model the boundary conditions of the problem.

Figures 3.20 and 3.21 presents the FRF for the system with free edge nodes and with roller supports at the edge nodes. In Figure 3.20 the soil mass is neglected, and in Figure 3.21 the soil mass is included. The figures show that the response for these two boundary conditions are similar, and practically identical for the frequency range of interest (where the principal peaks of the FRF are located). A similar outcome was obtained in the analysis that includes springs at the boundaries (where the vertical springs play a similar role than the roller supports). This situation leads to the conclusion that the soil island has been taken large enough so the soil half space is adequately represented, and that roller supports are not required to draw valid conclusions on the system response.

Figure 3.22 presents the FRF for the system with full soil mass assignment, and springs and dashpots in the cutoff boundaries, together with the soil and pile natural frequencies. It can be appreciated that for frequencies near soil and pile natural frequencies, the FRF experiences a peak. When soil and pile have closely located natural frequencies and their wave length ratio is close to an integer (the pile approximated wave length, obtained from its natural modal shape, is a multiple of soil wave length), as presented in Table 3.6, the FRF peak is higher, probably due to the fact that soil and pile modes can couple more effectively.

Finally, a brief comparison between the 2D and the 3D analysis will be presented. By comparing Figures 3.3 and 3.13 (2D model vs 3D model without soil mass) one can appreciate a significantly different behavior, with a clear shift of the natural frequencies

to the right for the 3D model. This situation may be explained considering that although the 3D model is more flexible it has much less mass involved (due to the fact that the pile is of finite cross section vs the infinite length in the out of plane direction of the 2D model). It is appropriate to point out that the static displacement is smaller in the 3D model since the unit load is distributed in the 60 ft width (in the transverse direction, y axis) soil mass; however the 2D model is equivalent to have a unit load every ft of soil width.

By evaluating figures 3.4 and 3.14 (2D model vs 3D model with soil mass) it is possible to appreciate a considerably different response of both systems. Although the first peak of the FRF is placed near the same value for both cases, the response of the 3D has a series of closely located peaks, probably due to out of plane vibration modes in this range of frequencies.

These findings lead to the conclusion that, when performing a FEM analysis, a 2D FEM analysis may be appropriate to draw general conclusions of the pile-soil behavior, and to gain insight on the system response and parameters affecting the system behavior. But a 3D FEM analysis would be required in order to develop more accurate conclusions, since it is a more realistic representation of the system.

3.6.5 Comments on the 3D Model Analysis Applicability

The FEM analysis was first performed on a PC with a Pentium IV processor, 3.2 Ghz of speed, 512 MB of RAM, and 143 GB of hard drive (101 GB free). This is considered, at the present moment, a quite robust PC for any small to midsize engineering firm (either a Structural Engineering or a Geotechnical Engineering firm).

When performing the 3D analysis, and due to the size of the problem, each frequency analyzed in order to obtain the dynamic flexibility of pile top lasted more than 20 minutes. For 100 frequency increments the analysis lasted for around 38 hours.

The required analysis time, added to the time consumed during the model generation, verification, modification (a process delayed due to the automatic redrawing of the model performed by the program after each editing step), and saving, made the 3D analysis complicated and probably not recommended for any practical purpose in an engineering firm. Considering a seismic time history analysis (with several time increments) that includes material nonlinearities (so each increment of time implies an iterative process, and the necessity of a more refined model for the pile and the soil-pile contact surface), it would easily require more than 2 days per analysis.

The above mentioned situations related to a 3D FEM analysis lead to the conclusion that simpler, yet accurate for design purposes, models are still required for practical purposes in an engineering firm.

The required time to perform each FE analysis was also used to decide that the FEM is not the desired tool to perform parametric analyses that may result in the definition of a lumped soil mass. The definition of an analytical expression for the lumped soil mass will be obtained from the approximation of a continuous model, as presented in Chapter 4.

4 Lumped Soil Model for Dynamic Soil-Pile System Response

The objective of this chapter is to derive an expression of the soil mass contribution to the soil-pile system response consistent with the Winkler Simplified Model.

The *Dynamic Stiffness* of a lumped *Single Degree of Freedom* (SDOF) *System* is presented first. Then, the expression for the dynamic stiffness of the pile-soil system derived by Novak is described. Novak made this development considering an infinite soil layer of unit thickness under a *Plane Strain State*. The Novak's expression will be manipulated in order to obtain an equivalent lumped model expression.

4.1 Dynamic Stiffness and Flexibility of a SDOF System

Let us consider a lumped single degree of freedom (SDOF) system, consisting of a rigid body of mass M (lumped mass) constrained to move along the X axis. The mass is attached to a fixed support by a spring of stiffness K and a dashpot of constant C , as shown in Figure 4.1. The system is subjected to damped forced harmonic vibrations by the action of a force with harmonic variation in time $F(t) = F_o e^{i\omega t}$, and the system response (position as a function of time) is described through the coordinate $X(t)$.

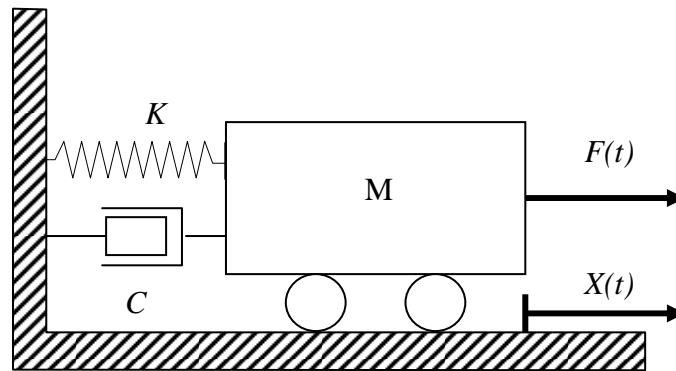


Figure 4.1: SDOF System

Figure 4.2 presents the *free body diagram* (FBD) and the *kinetic diagram* of the rigid body, corresponding to a positive displacement, a positive velocity, and a positive acceleration, where:

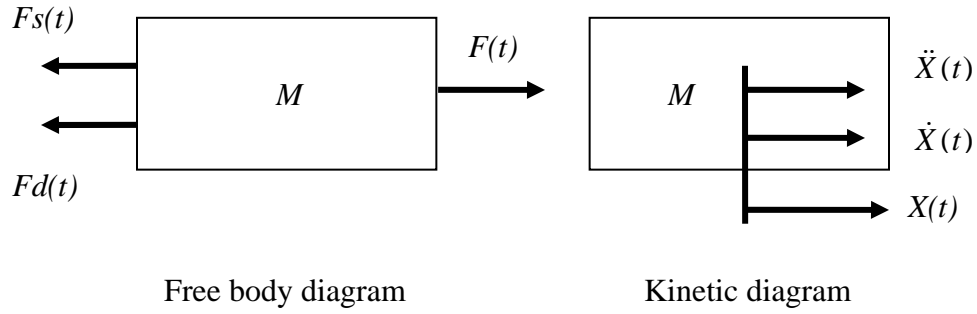


Figure 4.2: Free Body and Kinetic Diagrams

$F(t)$ = applied dynamic force

$Fs(t)$ = spring force = $K X(t)$

$Fd(t)$ = damping force = $C \dot{X}(t)$

Applying Newton's second law, the equation of motion for the rigid body is:

$$F(t) - Fs(t) - Fd(t) = M \ddot{X}(t) \quad (4.1)$$

$$M \ddot{X}(t) + C \dot{X}(t) + K X(t) = F(t)$$

The complementary solution of equation (4.1), obtained from the homogeneous second-order differential equation of motion, results in a transient solution exponentially decaying with time, and will not be considered here. $X(t) = X_o e^{i\omega t}$ is proposed for the particular solution, or steady state solution, of equation (4.1). Replacing $X(t)$ in (4.1) leads to:

$$M i^2 \omega^2 X_o e^{i\omega t} + C i \omega X_o e^{i\omega t} + K X_o e^{i\omega t} = F_o e^{i\omega t}$$

$$\left[K - \omega^2 M + i \omega C \right] X_o = F_o \quad (4.2)$$

$$Kd(\omega) X_o = F_o$$

The complex function $[K - \omega^2 M + i \omega C]$ that relates the displacement and the force magnitude is referred as the *system dynamic stiffness* or *impedance* “ $Kd(\omega)$ ”. One can give a physical meaning to $Kd(\omega)$ as the amplitude of the harmonic force that must be applied to a SDOF system to obtain a unit steady state harmonic displacement.

$Kd(\omega)$ has a real component $Kdd(\omega)$ (also known as the *direct dynamic stiffness*) and an imaginary component $Kdq(\omega)$ (also known as the *quadrature dynamic stiffness*), as shown in equation (4.3) and Figure 4.3.

$$\begin{aligned} Kd(\omega) &= \left[K - \omega^2 M + i \omega C \right] \\ Kdd(\omega) &= K - \omega^2 M \\ Kdq(\omega) &= \omega C \end{aligned} \quad (4.3)$$

It can be seen from equation (4.2) that X_o results in a complex function of ω , meaning that the displacement is not in phase with the force, and that the imaginary component of the stiffness (due to the system damping) is responsible for the phase angle ϕ with which the displacement lags the force.

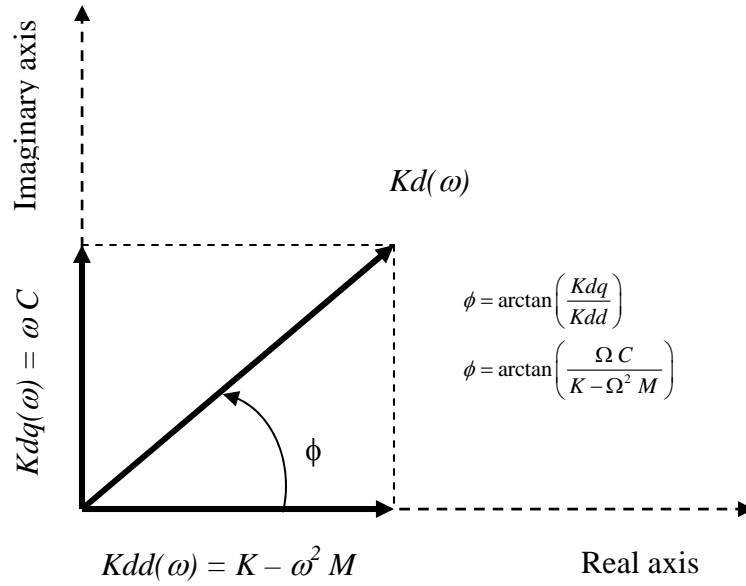


Figure 4.3: Dynamic Stiffness Components (Phase Diagram)

Another way of representing the dynamic stiffness is to use a polar system of reference giving its module $|Kd(\omega)|$ (vector length) and phase angle $\phi(\omega)$ as described in equation 4.4, instead of giving its component in a Cartesian system of coordinates ($Kdd(\omega)$ and $Kdq(\omega)$). In the expressions of $|Kd(\omega)|$ and $\phi(\omega)$ it is usual to take K out of the radical, and make a change of variables considering that $K/M = \omega_n^2$, and $C/K = 2\xi/\omega_n$, where ω_n is the system natural frequency and ξ is the system damping ratio.

$$\begin{aligned}
 |Kd(\omega)| &= \sqrt{(K - \omega^2 M)^2 + (\omega C)^2} = K \sqrt{\left[1 - \left(\frac{\omega}{\omega_n}\right)^2\right]^2 + \left[2\xi \left(\frac{\omega}{\omega_n}\right)\right]^2} \\
 \phi(\omega) &= \arctan\left(\frac{\omega C}{K - \omega^2 M}\right) = \arctan\left(\frac{2\xi \frac{\omega}{\omega_n}}{1 - \left(\frac{\omega}{\omega_n}\right)^2}\right) \\
 Kd(\omega) &= |Kd(\omega)| e^{i\phi(\omega)}
 \end{aligned} \tag{4.4}$$

Figure 4.4 presents in a qualitative way the variation of the real component $K_{dd}(\omega)$ and the imaginary component $K_{dq}(\omega)$ of the dynamic stiffness with the frequency of the load ω . The real component has a parabolic variation, and it becomes zero when the frequency of the load coincides with the natural frequency of the system $\omega n = \sqrt{K/M}$ (resonance condition). It is important to notice that, in a damped system, the dynamic stiffness does not become zero at resonance, since the imaginary component (which has a linear variation with ω) has a finite value equal to $\omega n C$.

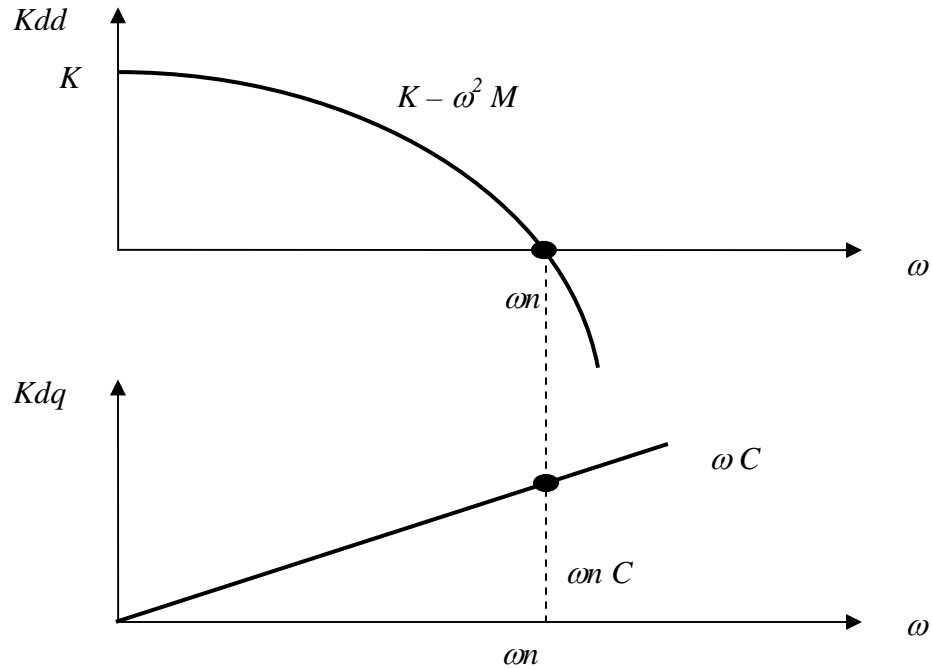


Figure 4.4: Variation of Real and Imaginary Components of $Kd(\omega)$ as a Function of Load Frequency ω

The ratio of the dynamic stiffness to the static stiffness may be called the *relative dynamic stiffness* $Kdr(\omega) = Kd(\omega)/K$:

$$Kdr(\omega) = \frac{Kd(\omega)}{K} = \left[1 - \omega^2 \frac{M}{K} + i \omega \frac{C}{K} \right] = \left[1 - \left(\frac{\omega}{\omega n} \right)^2 + i 2 \xi \frac{\omega}{\omega n} \right]$$

The direct (or real) and quadrature (or imaginary) components of the relative stiffness are:

$$K_{ddr}(\omega) = 1 - \left(\frac{\omega}{\omega n} \right)^2$$

$$K_{dqr}(\omega) = 2 \xi \frac{\omega}{\omega n}$$

The modulus of the relative (or non-dimensional) dynamic stiffness is:

$$|K_{dr}(\omega)| = \sqrt{\left[1 - \left(\frac{\omega}{\omega n} \right)^2 \right]^2 + \left[2 \xi \left(\frac{\omega}{\omega n} \right) \right]^2} \quad (4.5)$$

Figure 4.5 shows the variation of $|K_{dr}(\omega)|$ with the frequency ratio $\omega r = \omega/\omega n$, for different damping ratios ξ (5%, 10%, 20%, 30%); it can be seen that $|K_{dr}(\omega)|$ is minimum near resonance ($\omega r = 1$).

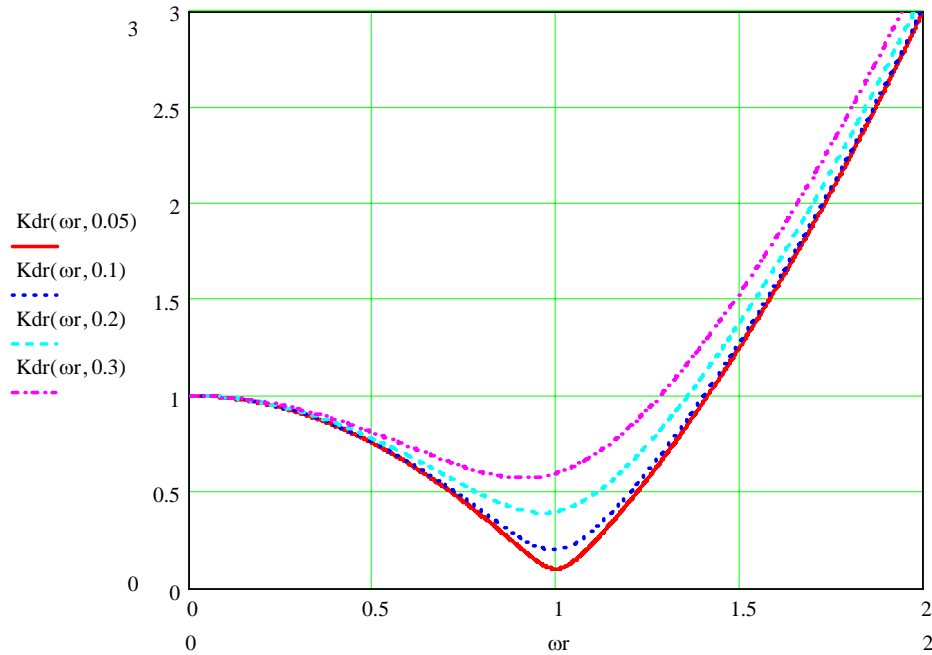


Figure 4.5: Variation of $|K_{dr}(\omega)|$ as a Function of Load Relative Frequency ωr , for Different Damping Ratios

Figure 4.6 shows the variation of phase angle $\phi(\omega)$ with the frequency ratio $\omega r = \omega/\omega_n$, for different damping ratios ξ . It can be seen that for static loads ($\omega=0$) the displacement is in phase with the force ($\phi=0$; the dynamic stiffness has only a real component), for resonant loads ($\omega=\omega_n$) the displacement lags the force by 90° ($\phi=\pi/2$, the dynamic stiffness has only an imaginary component), and for high frequency loads the displacement lags the load by 180° ($\phi=\pi$, the mass component of the dynamic stiffness is dominant).

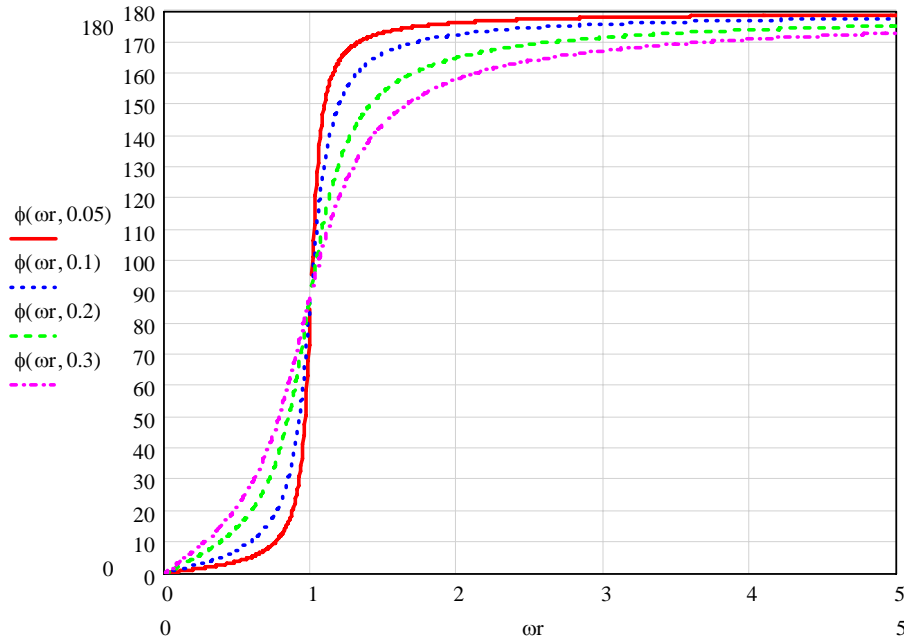


Figure 4.6 : Phase Angle ϕ a Function of Load Relative Frequency ωr , for Different Damping Ratios

The inverse of the dynamic stiffness is the *dynamic flexibility* $H(\omega)$ (equation 4.6), also known as *dynamic compliance*, *receptance*, *admittance*, and *Frequency Response Function* (FRF), this last designation being the most commonly used. One can give a physical meaning to $H(\omega)$, as the amplitude of the steady state displacement of a SDOF system when subjected to a complex unit harmonic force $F(t) = 1 e^{i\omega t}$.

$$H(\omega) = \frac{1}{Kd(\omega)} = \frac{1}{K - \omega^2 M + i \omega C}$$

$$H(\omega) = \frac{1}{|Kd(\omega)| e^{i\phi(\omega)}} = \frac{1}{\sqrt{(K - \omega^2 M)^2 + (\omega C)^2}} e^{-i\phi(\omega)} = \frac{1}{K \sqrt{\left[1 - \left(\frac{\omega}{\omega_n}\right)^2\right]^2 + \left[2\xi \left(\frac{\omega}{\omega_n}\right)\right]^2}} e^{-i\phi(\omega)} \quad (4.6)$$

The ratio between the dynamic flexibility and the static flexibility ($f = 1/K$) may be defined as the *relative dynamic flexibility* (or *dimensionless frequency response function*) $Hr(\omega)$, and is shown in equation 4.7.

$$Hr(\omega) = \frac{H(\omega)}{f} = \frac{H(\omega)}{\frac{1}{K}} = \frac{1}{\sqrt{\left[1 - \left(\frac{\omega}{\omega_n}\right)^2\right]^2 + \left[2\xi \left(\frac{\omega}{\omega_n}\right)\right]^2}} e^{-i\phi(\omega)} \quad (4.7)$$

Figure 4.7 shows the variation of the module of $Hr(\omega)$ with the frequency ratio $\omega r = \omega/\omega_n$; it can be seen that $|Hr(\omega)|$ is maximum near resonance ($\omega r = 1$).

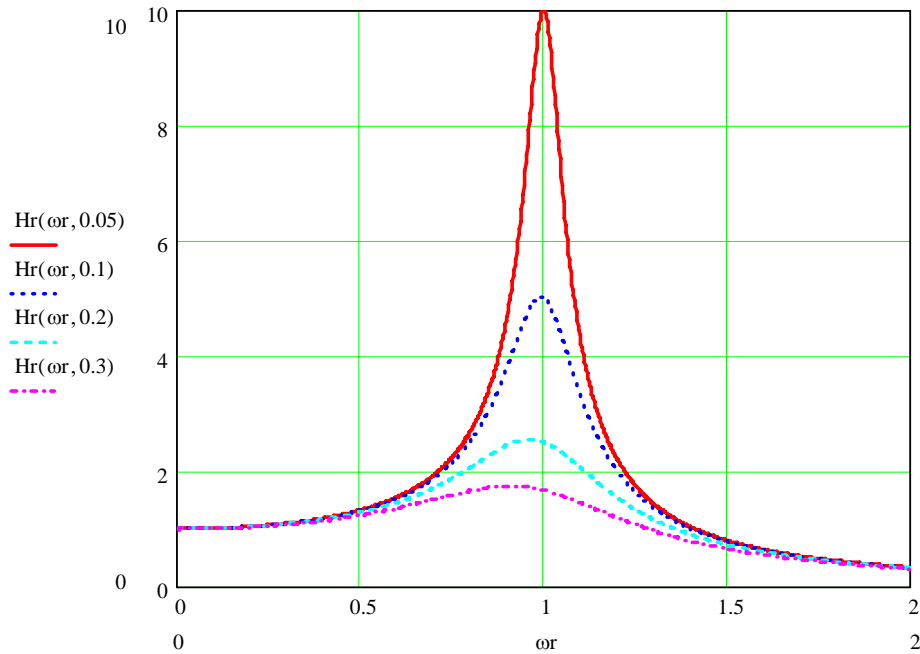


Figure 4.7: Variation of $|Hr(\omega)|$ as a Function of Load Relative Frequency ωr , for Different Damping Ratios

4.2 Novak's Dynamic Stiffness to Model Soil-Pile Interaction

Novak (1974) presented an approximate analytical expression of the dynamic stiffness and damping of piles based on linear elasticity, describing the dynamic soil reaction per unit length of pile by closed form formulas, as derived by Baranov in 1967. In Novak's study it is assumed that the soil is composed of a set of independent infinitesimally thin horizontal layers in plane strain state that extend to infinity and experience small displacements. The layers are considered to be composed of an homogeneous, isotropic, and linear-elastic material. The pile is assumed to be vertical, with circular cross section, and that the cross section shape and size remain unchanged and moves as a rigid body (a hypothesis that is consistent with the Navier-Bernoulli beam theory). The massless rigid circular disc that represents the pile cross section is considered to experience a harmonic vibration. No separation is allowed between the rigid cylinder and the soil medium.

This approach was later extended by Novak and his coworkers to viscoelastic materials with frequency independent material damping (hysteretic damping), as reported by Novak and Abloul-Ella (1978) and Novak et al. (1978). The damping is considered by means of the *Complex Shear Modulus* $G^* = G + i G' = G (1 + i D)$, where the parameter D (known as the *loss factor*) is defined in terms of the *loss angle* δ :

$$D = \tan \delta = \frac{G'}{G} \quad (4.8)$$

where:

D = loss factor

G = real part of the shear modulus

G' = imaginary part of the shear modulus

The complex horizontal stiffness of the soil associated with a unit length of the cylinder, “ ku ”, (or the dynamic soil reaction per unit length of pile to a unit horizontal harmonic displacement of the rigid disc) is given by the following equation:

$$ku = G \pi a_o^2 T \quad (4.9)$$

where:

$$T = - \frac{4K_1(b_o^*)K_1(a_o^*) + a_o^*K_1(b_o^*)K_0(a_o^*) + b_o^*K_0(b_o^*)K_1(a_o^*)}{b_o^*K_0(b_o^*)K_1(a_o^*) + a_o^*K_1(b_o^*)K_0(a_o^*) + b_o^*a_o^*K_0(b_o^*)K_0(a_o^*)} \quad (4.10)$$

in which:

K_n = modified Bessel function of the second kind of order n

$a_o = \frac{\omega r_o}{V_s}$ = dimensionless frequency

ω = vibration frequency in $\left[\frac{\text{rad}}{\text{sec}} \right]$

r_o = cylinder radius

$V_s = \sqrt{\frac{G}{\rho}}$ = shear wave velocity of the soil

ρ = mass density of the soil

$a_o^* = \frac{a_o}{\sqrt{1+iD}} i$ = complex dimensionless frequency

$b_o^* = \frac{a_o^*}{\eta}$

$\eta = \sqrt{\frac{2(1-\nu)}{1-2\nu}}$

ν = Poisson's ratio of the soil

(4.11)

Separating the real and imaginary parts of the function T , equation 4.9 can be rewritten in a condensed form as:

$$ku = G \left[S_{u1}(a_o, \nu, D) + i S_{u2}(a_o, \nu, D) \right] \quad (4.12)$$

in which S_{u1} and S_{u2} are real functions. The variations of these functions with a_o , ν , and D are shown in Figures 4.8 a and b.

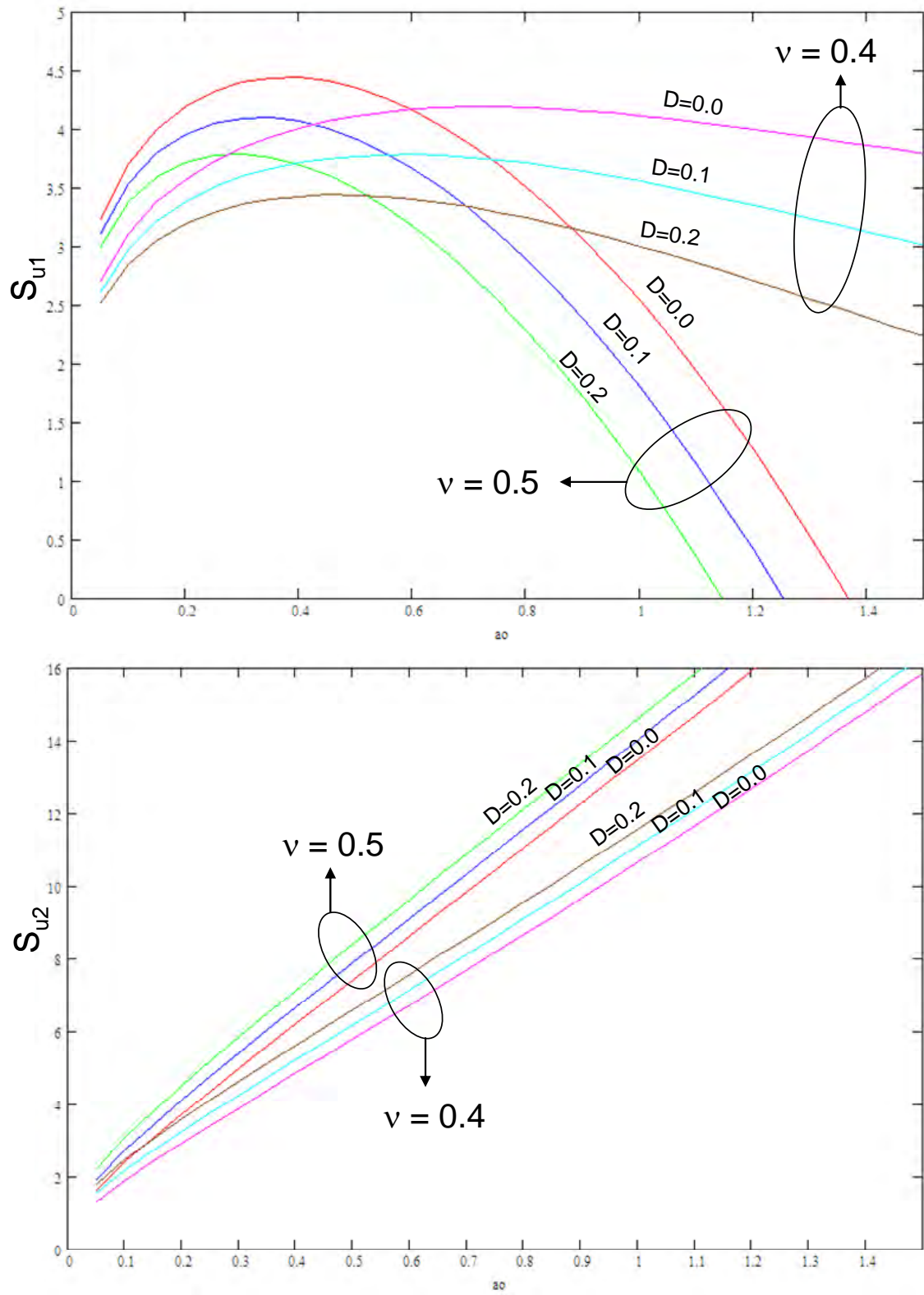


Figure 4.8: Horizontal Stiffness and Damping Parameters S_{u1} and S_{u2}

By analyzing this figure it can be appreciated that the imaginary part of the dynamic stiffness (S_{u2}), corresponding to the damping, has an almost linear variation, and that it increases (for the same frequency) as the hysteretic damping D increases. It also can be noted that the real part of the dynamic stiffness (S_{u1}), corresponding to the elastic and inertia contributions, has a parabolic type of variation, and decreases (for the same frequency) as the hysteretic damping D increases. An inspection of Figure 4.8 also allows to pinpoint that as the Poisson's ratio ν decreases the curve of the real part S_{u1} tends to flatten, and a decrease in the Poisson's ratio also lowers the slope of the imaginary part (decreasing the damping effect).

Novak (1974) and Novak and Aboul-Ella (1978) compared the dynamic stiffness of the pile head obtained with Novak's model with the results calculated with more rigorous approaches. An example of such comparisons is shown in Figure 4.9. It presents, for a case study of a pile fixed at the bottom, the real part (f_{u1}) and the imaginary part (f_{u2}) of the direct horizontal pile head stiffness (functions that relates the pile head horizontal force corresponding to a pile head horizontal displacement).

As stated by Novak (1974), the differences between the two solutions appear acceptable and diminish with increasing frequency. Novak's solution does not yield peaks attributed to the soil layer resonances; however, the sharpness of these peaks decreases and they even vanish with soil viscosity, so they are not considered important. Since the real part of the Novak's solution tends to zero as the frequency tends to zero (instead of yielding the static stiffness), Novak and Aboul-Ella (1978) recommended to extend the value of f_{u1} corresponding to $a_o = 0.3$ to the lower frequencies, as shown in Figure 4.9. Novak also recommended to use, for practical purposes, the value corresponding to $a_o = 0.3$ as the dynamic stiffness.

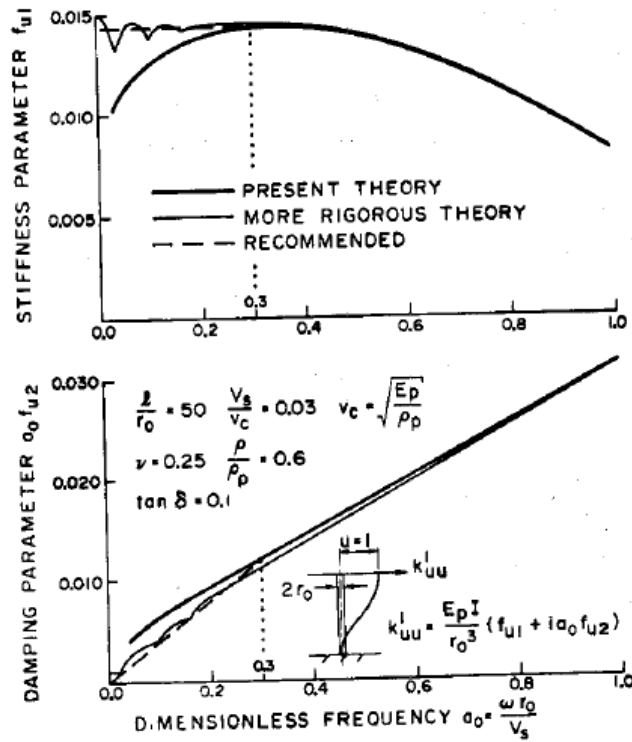


Figure 4.9: Comparison of Approximate (Novak) vs. More Rigorous Approach (Aboul-Ella and Novak, 1978)

Finally, considering the dynamic stiffness of a SDOF system presented in Figure 4.4, the similar trends presented by Novak's dynamic stiffness in Figure 4.9 (at least for high Poisson's ratio values) strongly suggest that an equivalent lumped model would be appropriate, avoiding the use of a complex expression for the dynamic stiffness that is also frequency dependent .

4.3 Equivalent Lumped Model

In order to obtain an equivalent lumped model it was decided to approximate the Novak's dynamic stiffness presented in section 4.2. To this end, the real part of Novak's solution will be approximated by a second degree polynomial with no linear term, and the

imaginary part of Novak's solution will be approximated by a straight line with no constant term.

In order to obtain the proposed approximation, the least square technique for curve fitting will be applied. The analysis will be performed for different Poisson's ratios.

Considering the fact that the maximum of the real part of Novak's dynamic stiffness is not located at zero frequency, and that the real part tends to zero as the frequency tends to zero, this maximum will be determined and extended as constant for the lower frequencies.

4.3.1 Lumped Coefficients Definition

By comparing equation 4.9, which describes the soil dynamic stiffness according to the Novak model, with equation 4.3, which describes the dynamic stiffness of a single degree of freedom system, a general form of the equivalent lumped model coefficients can be established.

It is proposed to obtain a polynomial approximation of the Novak's solution, taking the dimensionless frequency a_o as the independent variable. As stated before, the real part will be approximated by a constant term (corresponding to the static stiffness) and a quadratic term (corresponding to the mass), and the imaginary part will be represented by a linear term (corresponding to the viscous damping). Starting with equation 4.9:

$$ku = G \pi a_o^2 T(a_o, \nu, D)$$

and introducing a function f ,

$$f(a_o, \nu, D) = a_o^2 T(a_o, \nu, D)$$

the complex stiffness can be written as

$$ku = G \pi f(a_o, \nu, D) = G \pi \left\{ \text{Real}[f(a_o, \nu, D)] + i \text{Imag}[f(a_o, \nu, D)] \right\}$$

introducing the following approximations

$$\begin{aligned} \text{Real}[f(a_o, \nu, D)] &\approx \alpha_k - \alpha_m a_o^2 \\ \text{Imag}[f(a_o, \nu, D)] &\approx \alpha_c a_o \end{aligned}$$

the dynamic stiffness ku becomes

$$ku \approx G \pi (\alpha_k - \alpha_m a_o^2 + i \alpha_c a_o) \quad (4.13)$$

The coefficients α_i will be determined by the least square approximation of the function $f(a_o, \nu, D)$, for $i = k, m$ or c (the subscripts k, m and c correspond to the stiffness, mass, and damping coefficients, respectively). Comparing equation 4.13 with the dynamic stiffness of a SDOF system as expressed by equation 4.3, one can obtain:

$$\begin{aligned} ku &\approx G \pi (\alpha_k - \alpha_m a_o^2 + i \alpha_c a_o) = k_a - m_a \omega^2 + i c_a \omega \\ k_a &= G \pi \alpha_k \\ m_a \omega^2 &= G \pi \alpha_m a_o^2 = G \pi \alpha_m \frac{r_o^2 \omega^2}{\left(\frac{G}{\rho}\right)} = \rho \pi r_o^2 \alpha_m \omega^2 \\ c_a \omega &= G \pi \alpha_c a_o = G \pi \alpha_c \frac{r_o \omega}{V_s} = \frac{G \pi r_o}{V_s} \alpha_c \omega \end{aligned} \quad (4.14)$$

Solving for the stiffness coefficient k_a , the lumped mass m_a , and the lumped viscous damper coefficient c_a from equation 4.14, the equivalent lumped coefficients are:

$$\begin{aligned} k_a &= \pi G \alpha_k \\ m_a &= \pi r_o^2 \rho \alpha_m \\ c_a &= \pi r_o \frac{G}{V_s} \alpha_c = \pi r_o \rho V_s \alpha_c = \pi r_o \sqrt{G \rho} \alpha_c \end{aligned} \quad (4.15)$$

The viscous damping coefficient corresponds to the radiation damping. The material damping (hysteretic damping) is accounted by the parameter D , as defined previously.

These coefficients are defined per unit pile length. In order to obtain lumped coefficients to apply at each node of a pile discretized with beam elements, these values have to be multiplied by the tributary length for each node. Alternatively, the corresponding consistent matrices of a beam on elastic foundation, considering the beam element degree of freedom, should be obtained.

4.3.2 Determination of the Lumped Coefficients

As stated previously, the dynamic stiffness of the Novak's model will be approximated by polynomials using the least squares method. The basic equation of the method can be found in most textbook on applied numerical analysis (for instance, Gerald and Wheatley, 1994; Chapra and Canale, 1998).

Consider “ N ” known discrete data points (x, y) . It is desired to find an “ n ” degree polynomial that best fit these data points by minimizing the error between the known ordinates of the data points and the ordinates predicted by the following polynomial expression:

$$f(x) \approx d_o + d_1 x + d_2 x^2 + d_3 x^3 + \dots + d_n x^n$$

The polynomial coefficients d_i can be found by solving the following system of linear simultaneous equations:

$$\begin{bmatrix}
N & \sum_{i=1}^N x_i & \sum_{i=1}^N x_i^2 & \sum_{i=1}^N x_i^3 & \cdots & \sum_{i=1}^N x_i^n \\
\sum_{i=1}^N x_i & \sum_{i=1}^N x_i^2 & \sum_{i=1}^N x_i^3 & \sum_{i=1}^N x_i^4 & \cdots & \sum_{i=1}^N x_i^{n+1} \\
\sum_{i=1}^N x_i^2 & \sum_{i=1}^N x_i^3 & \sum_{i=1}^N x_i^4 & \sum_{i=1}^N x_i^5 & \cdots & \sum_{i=1}^N x_i^{n+2} \\
\vdots & \vdots & \vdots & \vdots & \vdots & \vdots \\
\sum_{i=1}^N x_i^n & \sum_{i=1}^N x_i^{n+1} & \sum_{i=1}^N x_i^{n+2} & \sum_{i=1}^N x_i^{n+3} & \cdots & \sum_{i=1}^N x_i^{n+n}
\end{bmatrix}
\begin{Bmatrix}
d_o \\
d_1 \\
d_2 \\
\vdots \\
d_n
\end{Bmatrix}
=
\begin{Bmatrix}
\sum_{i=1}^N y_i \\
\sum_{i=1}^N x_i y_i \\
\sum_{i=1}^N x_i^2 y_i \\
\vdots \\
\sum_{i=1}^N x_i^n y_i
\end{Bmatrix} \quad (4.16)$$

where x_i and y_i are, respectively, the abscise and ordinate of data point i .

The coefficients α_k and α_m are obtained from the real part of Novak's dynamic stiffness function $f(a_o, \nu, D)$ defined in the previous section. The application of the least square method leads to the following expressions:

$$\begin{aligned}
x &\equiv a_o \\
y &\equiv \text{Real}[f(a_o, \nu, D)] \\
y &\approx \alpha_k - \alpha_m a_o^2 \\
\begin{Bmatrix} \alpha_k \\ -\alpha_m \end{Bmatrix} &= \begin{bmatrix} N & \sum_{i=1}^N x_i^2 \\ \sum_{i=1}^N x_i^2 & \sum_{i=1}^N x_i^4 \end{bmatrix}^{-1} \begin{Bmatrix} \sum_{i=1}^N y_i \\ \sum_{i=1}^N x_i^2 y_i \end{Bmatrix}
\end{aligned} \quad (4.17)$$

The coefficient α_c is defined by using the imaginary part of Novak's dynamic stiffness function $f(a_o, \nu, D)$ defined in the previous section. Applying the least square method leads to the following expressions:

$$\begin{aligned}
x &\equiv a_o \\
y &\equiv \text{Imag}[f(a_o, \nu, D)] \\
y &\approx \alpha_c a_o \\
\alpha_c &= \frac{\sum_{i=1}^N x_i y_i}{\sum_{i=1}^N x_i^2}
\end{aligned} \tag{4.18}$$

The number of discrete points N adopted for the analysis was 30. The main objective was to obtain an adequate fitting of Novak's solution within the range of $0.3 < a_o < 3.0$. The lower range value correspond to the one suggested by Novak to be used for low frequencies; the upper range value was adopted as twice the upper value displayed in the charts presented by Novak, as a range where the model is expected to give adequate results.

Instead of using $a_o = 0.3$ in the lower frequency range, the maximum of the function was obtained (and adopted as the second data point). This value was then extended horizontally up to the intersection with the vertical axis, which was the point adopted as the first data point of the series.

Appendix D presents the listing of the MathCad worksheet prepared to perform the regression, for different Poisson's ratio values. As an example of the results of the analysis, Figure 4.10 presents the real part on Novak's dynamic stiffness function $f(a_o, \nu, D)$, in red, together with the data points used for the regression (in green), and the resulting polynomial approximation (in blue). These results are for the case of $\nu = 0.5$ (a value of 0.4999999 was adopted to avoid indetermination) and $D = 0.0$.

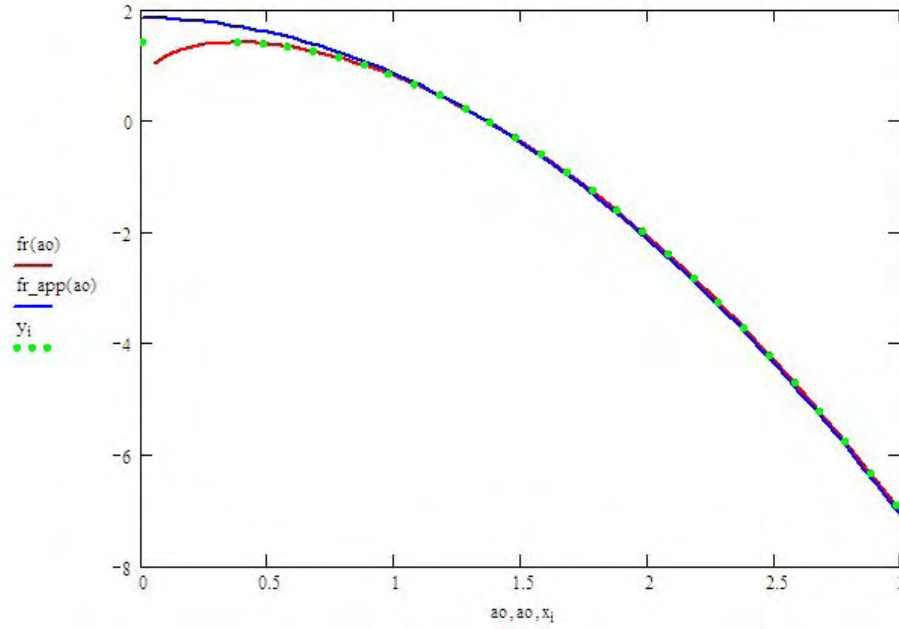


Figure 4.10: Real Part of $f(a_o, \nu, D)$ for $\nu = 0.5$ and $D = 0.0$ (red), Data Points (Green), and Polynomial Approximation (Blue)

Figure 4.11 presents the imaginary part on Novak's dynamic stiffness function $f(a_o, \nu, D)$ (in red) together with the data points used for the regression (in green), and the resulting polynomial approximation (in blue). The same values for ν and D were used.

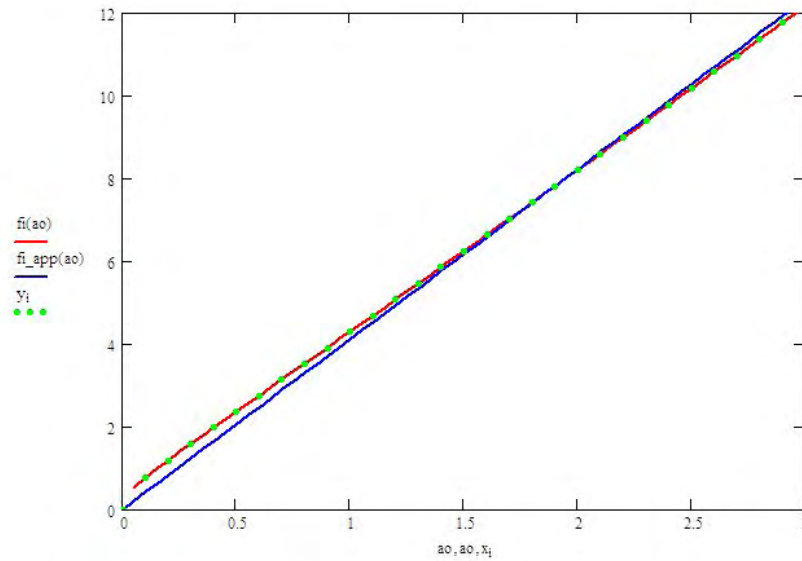


Figure 4.11: Imaginary Part of $f(a_o, \nu, D)$ for $\nu = 0.5$ and $D = 0.0$ (red), Data Points (Green), and Polynomial Approximation (Blue)

The resulting regression coefficients for this case are:

$$\begin{aligned}\alpha_k &= 1.721 \\ \alpha_m &= 0.965 \\ \alpha_c &= 4.107\end{aligned}\tag{4.19}$$

This analysis was performed for different soil Poisson's ratios ν . As the Poisson's ratio decreases, the real part on Novak's dynamic stiffness function $f(a_o, \nu, D)$, in red, starts to exhibit an inflection point after the maximum, and the function tends to increase for high frequencies, as shown in Figure 4.12. To show this effect, Figure 4.12 displays the real part on Novak dynamic stiffness function $f(a_o, \nu, D)$ (in red) together with the data points used for the regression (in green), and the resulting polynomial approximation (in blue) for the case of $\nu = 0.48$ and $D = 0.0$. As the Poisson's ratio continues decreasing, the curvature is reduced (the curve tends to get flatter, more horizontal), making the mass contribution less important. It also shows a tendency to move its maximum to the right.

In order to analyze these cases, it was decided to find the inflection point, and to extend the function along the tangent to this point to obtain the data points for higher frequencies, and not to include the rising portion of the function, as shown in Figure 4.13 for the case of $\nu = 0.47$ and $D = 0.0$.

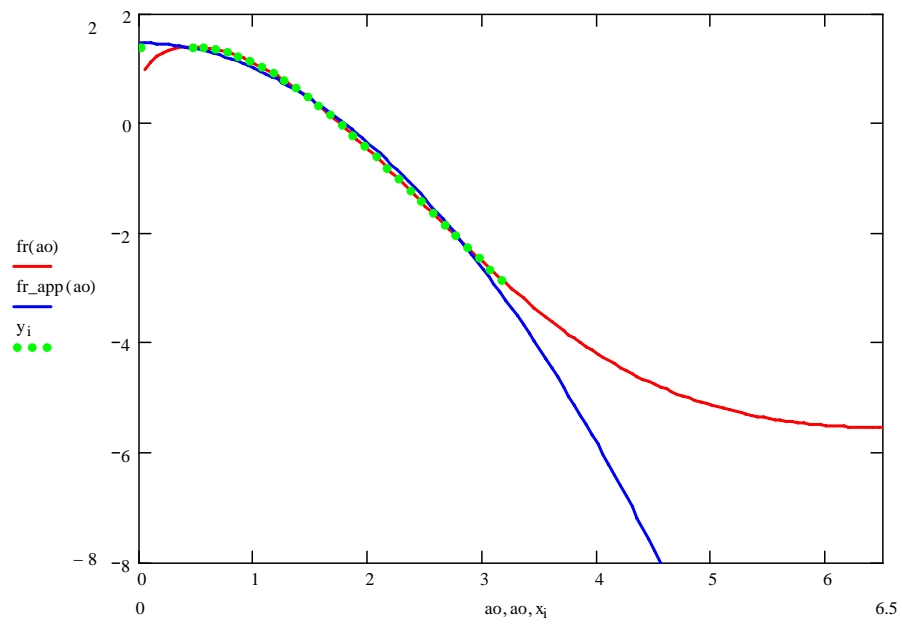


Figure 4.12: Real Part of $f(a_0, \nu, D)$ for $\nu = 0.48$ and $D = 0.0$ (red), Data Points (Green), and Polynomial Approximation (Blue)

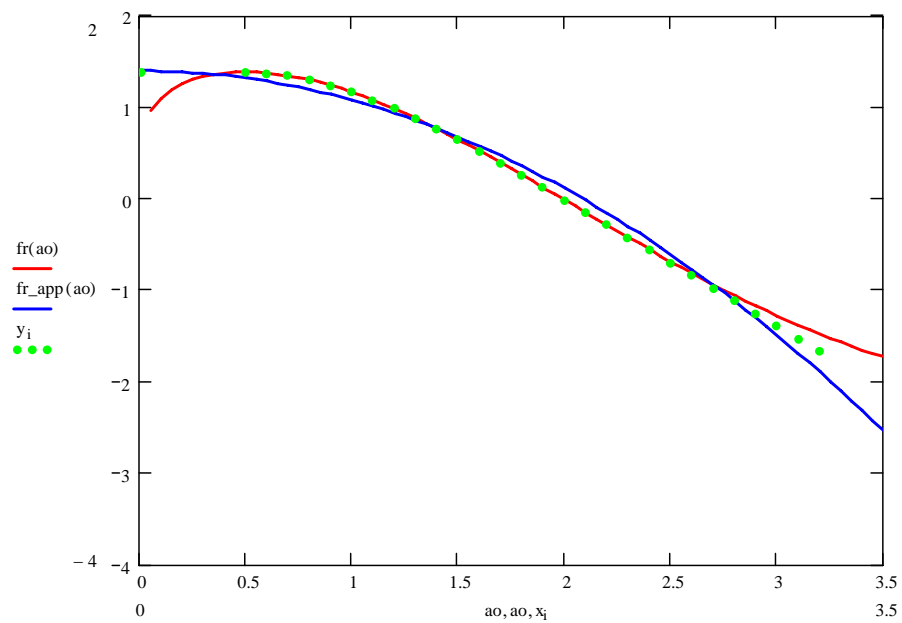


Figure 4.13: Real Part of $f(a_0, \nu, D)$ for $\nu = 0.47$ and $D = 0.0$ (red), Modified Data Points (Green), and Polynomial Approximation (Blue)

Figure 4.14 shows the variation of the regression coefficients α_k , α_m , and α_c with the Poisson's ratio ν , and Table 4.1 presents the numerical values obtained for them. It is recalled that the dynamic stiffness ku was approximated as follows:

$$ku \approx (G \pi \alpha_k) - (\rho \pi r_o^2 \alpha_m) \omega^2 + i(\pi r_o \rho V_s \alpha_c) \omega$$

Because the coefficient α_m becomes very small as the Poisson's ratio decreases, according to Novak's model, the contribution of the lumped soil mass to the system response tends to be less significant in this case. Indeed, its contribution is practically insignificant for Poisson's ratios smaller than 0.4. Figure 4.15 presents the variation of coefficient α_m alone, in order to better appreciate its behavior.

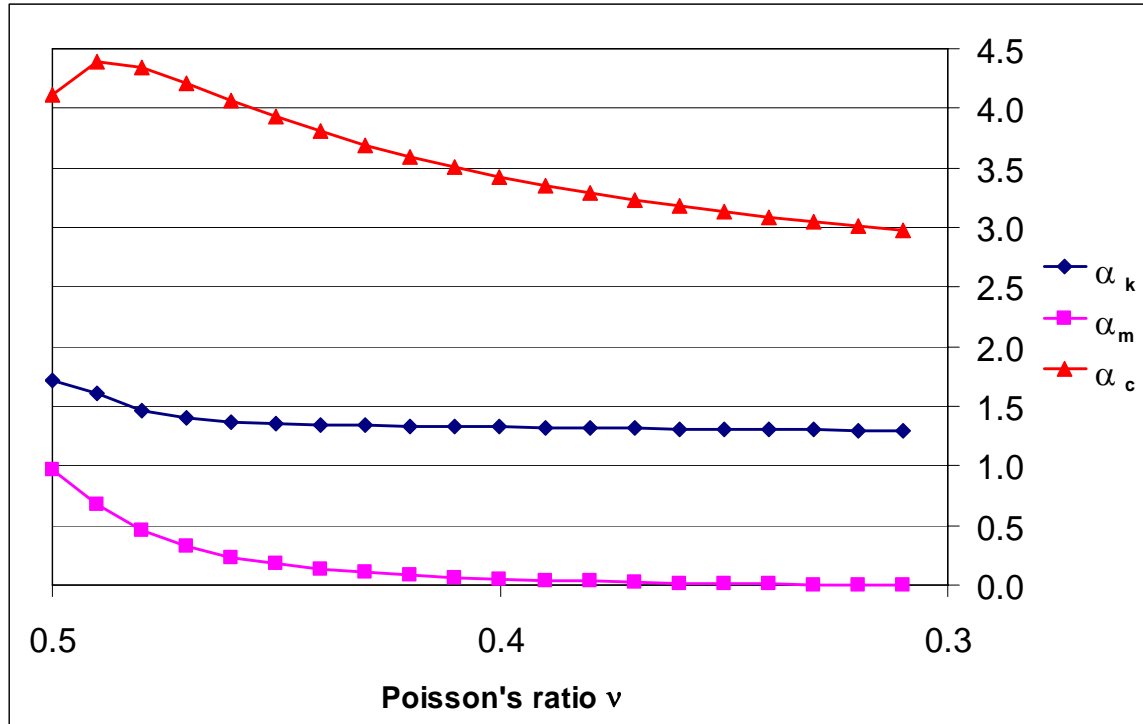
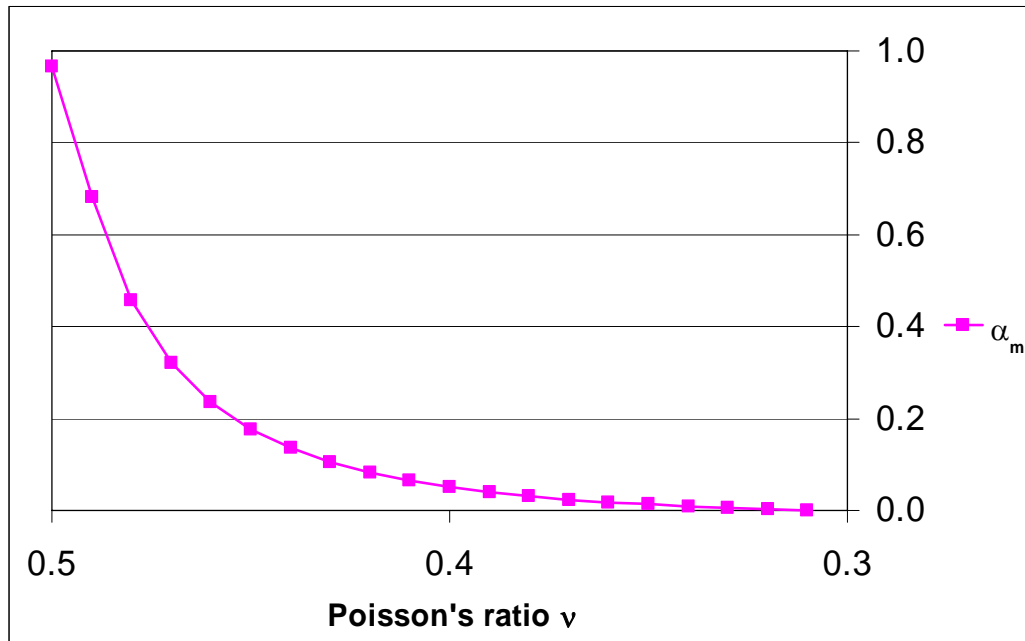


Figure 4.14: Variation of Regression Coefficients with Poisson's Ratio [0.3-0.5]

Table 4.1: Regression Coefficients α_k , α_m , and α_c for ν [0.5-0.31]

ν	α_k	α_m	α_c
0.50	1.72137	0.96533	4.10747
0.49	1.61062	0.68219	4.38920
0.48	1.46327	0.45715	4.33825
0.47	1.39946	0.32158	4.20948
0.46	1.36918	0.23482	4.06638
0.45	1.35437	0.17664	3.92941
0.44	1.34592	0.13555	3.80454
0.43	1.34015	0.10538	3.69268
0.42	1.33550	0.08258	3.59299
0.41	1.33130	0.06494	3.50411
0.40	1.32727	0.05106	3.42465
0.39	1.32329	0.03998	3.35334
0.38	1.31933	0.03104	3.28908
0.37	1.31540	0.02376	3.23091
0.36	1.31153	0.01780	3.17803
0.35	1.30775	0.01290	3.12978
0.34	1.30411	0.00886	3.08557
0.33	1.30067	0.00553	3.04493
0.32	1.29749	0.00280	3.00744
0.31	1.29479	0.00059	2.97274

Figure 4.15: Variation of Regression Coefficient α_m with Poisson's Ratio [0.3-0.5]

For values of Poisson's ratio of 0.30 and smaller, the real part of Novak's dynamic stiffness does not present a maximum. It was decided to approximate the function by a horizontal line. Since the real part of the function $f(a_o, \nu, D)$ was approximated by $\alpha_k - \alpha_m a_o^2$, this implies that the coefficient α_m must be zero. In turn, since the quadratic term gives the contribution of the mass to the dynamic stiffness, this implies that there will be no lumped mass contribution for small values of ν .

The first option was to select an horizontal line passing through the inflection point of the curve, as shown in Figure 4.16 for $\nu = 0.30$. However, for Poisson's ratios values less than 0.24 no inflection point was obtained, so it was opted to obtain the coefficient α_k as the mean value of the real part of the dynamic stiffness within the range of the dimensionless frequency between 1.0 and 3.0. In this way one avoids having to account for the steep variation in the initial range and it permits to have a good estimate within the range of interest of a_o . This procedure is equivalent to the least square method for a linear regression, keeping only the constant term. Figure 4.17 shows this approximation for $\nu = 0.30$.

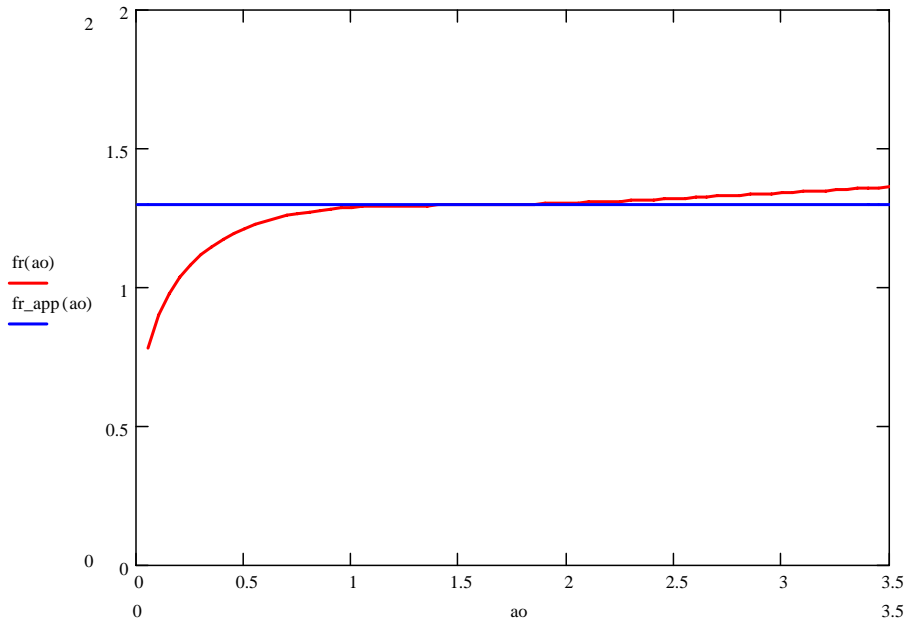


Figure 4.16: Real Part of $f(a_o, \nu, D)$ for $\nu = 0.30$ and $D = 0.0$ (red), and Horizontal Line Approximation (Blue) using Inflection Point

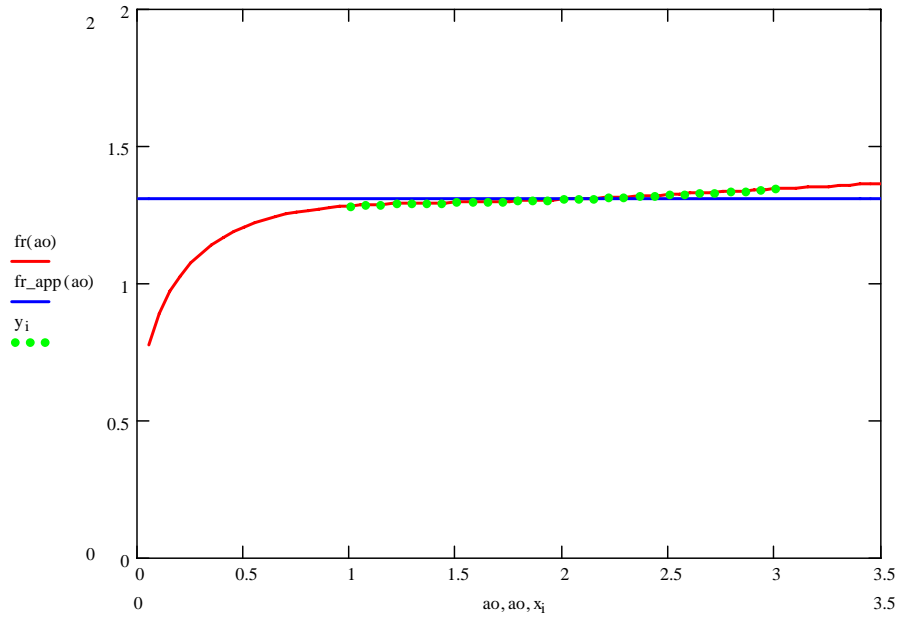


Figure 4.17: Real Part of $f(a_o, \nu, D)$ for $\nu = 0.30$ and $D = 0.0$ (red), Horizontal Line Approximation (Blue) using the Mean Value, and Selected Data Points (green)

Figure 4.18 shows the variation of the regression coefficients α_k , and α_c with the Poisson's ratio ν and Table 4.2 presents the results of this approximation for Poisson's ratios values ranging from 0.30 to 0.00.

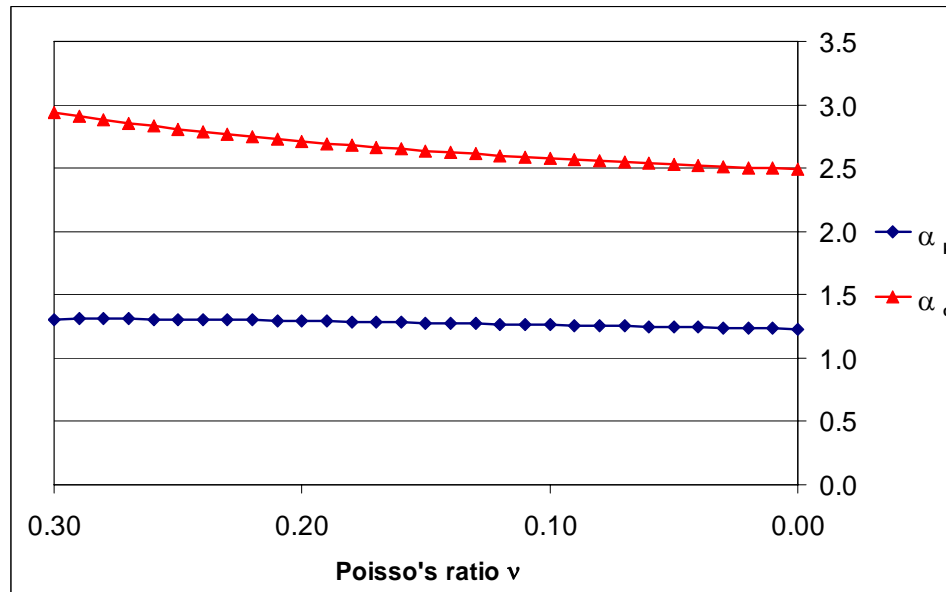


Figure 4.18: Variation of Regression Coefficients with Poisson's Ratio [0-0.3]

Table 4.2: Regression Coefficients α_k , α_m , and α_c for ν [0.3-0.0]

ν	α_k	α_m	α_c
0.30	1.30686	-	2.94054
0.29	1.30834	-	2.91058
0.28	1.30886	-	2.88262
0.27	1.30858	-	2.85647
0.26	1.30766	-	2.83197
0.25	1.30622	-	2.80895
0.24	1.30435	-	2.78729
0.23	1.30213	-	2.76687
0.22	1.29964	-	2.74757
0.21	1.29692	-	2.72932
0.20	1.29402	-	2.71203
0.19	1.29099	-	2.69562
0.18	1.28784	-	2.68003
0.17	1.28461	-	2.66519
0.16	1.28133	-	2.65106
0.15	1.27800	-	2.63758
0.14	1.27464	-	2.62470
0.13	1.27127	-	2.61240
0.12	1.26791	-	2.60062
0.11	1.26454	-	2.58934
0.10	1.26120	-	2.57852
0.09	1.25787	-	2.56814
0.08	1.25457	-	2.55817
0.07	1.25131	-	2.54859
0.06	1.24807	-	2.53937
0.05	1.24488	-	2.53049
0.04	1.24172	-	2.52194
0.03	1.23861	-	2.51370
0.02	1.23553	-	2.50574
0.01	1.23251	-	2.49806
0.00	1.22953	-	2.49064

4.3.3 Lumped Coefficients Analysis

Figure 4.19 presents a summary of the variation of the regression coefficients α_k , α_m , and α_c with the Poisson's ratio for whole range of ν values (between 0.0 and 0.5). Observing the figure, it becomes evident that the coefficient α_k , corresponding to the soil static stiffness contribution, remains practically constant for different ν values whereas the

coefficient α_m , corresponding to the soil mass contribution, decreases rapidly with the Poisson's ratio and for all practical purposes vanishes for values smaller than 0.30. The figure also shows that the coefficient α_c , corresponding to the radiation damping contribution, after an initial increase for ν below 0.5, experiences a significant reduction as the value of ν decreases, but nevertheless it keeps a non-negligible value for all the range of the Poisson's ratios.

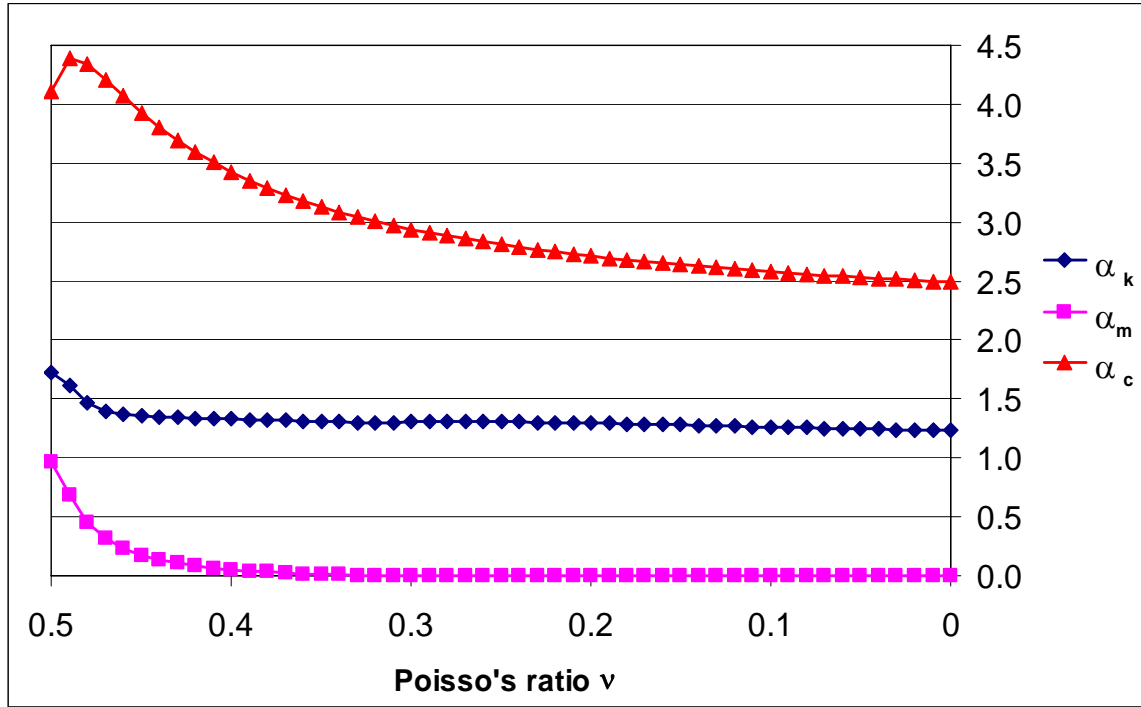


Figure 4.19: Variation of Regression Coefficients with Poisson's Ratio [0.5-0.0]

In order to analyze the type of dynamic response predicted by the model, the *critical damping coefficient* c_{cr} and the *damping ratio* ξ , considering that the rigid circular slice that represents the pile cross section is massless, will be obtained (Humar, 2002). It is well known that the critical damping coefficient of a single DOF oscillator is:

$$c_{cr} = 2\sqrt{k_a m_a}$$

Substituting k_a and m_a from equations 4.15 one obtains

$$c_{cr} = 2\sqrt{(\pi G \alpha_k)(\pi r_o^2 \rho \alpha_m)} = 2\pi r_o \rho \sqrt{\frac{G}{\rho} \alpha_k \alpha_m} \quad (4.20)$$

$$c_{cr} = 2\pi r_o \rho V_s \sqrt{\alpha_k \alpha_m}$$

By definition the viscous damping ratio is

$$\xi = \frac{c_a}{c_{cr}} = \frac{\pi r_o \rho V_s \alpha_c}{2\pi r_o \rho V_s \sqrt{\alpha_k \alpha_m}} \quad (4.21)$$

$$\xi = \frac{\alpha_c}{2\sqrt{\alpha_k \alpha_m}}$$

Table 4.3 presents the damping ratio ξ defined in equation 4.20 for values of the Poisson's ratios ranging from 0.50 to 0.30.

Table 4.3: Damping ratio ξ for ν [0.50-0.30]

ν	α_k	α_m	α_c	ξ
0.50	1.72137	0.96533	4.10747	1.5932
0.49	1.61062	0.68219	4.38920	2.0937
0.48	1.46327	0.45715	4.33825	2.6521
0.47	1.39946	0.32158	4.20948	3.1374
0.46	1.36918	0.23482	4.06638	3.5857
0.45	1.35437	0.17664	3.92941	4.0168
0.44	1.34592	0.13555	3.80454	4.4536
0.43	1.34015	0.10538	3.69268	4.9130
0.42	1.33550	0.08258	3.59299	5.4097
0.41	1.33130	0.06494	3.50411	5.9588
0.40	1.32727	0.05106	3.42465	6.5779
0.39	1.32329	0.03998	3.35334	7.2899
0.38	1.31933	0.03104	3.28908	8.1270
0.37	1.31540	0.02376	3.23091	9.1374
0.36	1.31153	0.01780	3.17803	10.3987
0.35	1.30775	0.01290	3.12978	12.0467
0.34	1.30411	0.00886	3.08557	14.3499
0.33	1.30067	0.00553	3.04493	17.9454
0.32	1.29749	0.00280	3.00744	24.9381
0.31	1.29479	0.00059	2.97274	53.6188
0.30	1.30686	0.00000	2.94054	∞

Since the damping ratio is always greater than 1, the model will predict an overdamped response. It is important to point out that if the model is applied to analyze a pile-soil system, this situation may vary due to the effect of the pile mass and stiffness.

It is instructive to evaluate the effect of the mass of a SDOF system on the system response as the damping ratio varies. To this end, the dimensionless frequency response function (presented in section 4.1) of a SDOF system will be evaluated, considering different mass values (M), and different damping ratios (ξ). For the analysis, the stiffness and mass properties of the original system will be first taken equal to 1, in order to obtain a natural frequency $\omega_n = 1$ rad/sec. Then, a mass one order of magnitude smaller than the original (i.e., $M = 0.1$) and one order of magnitude greater than the original (i.e., $M = 10$) are considered. Figures 20, 21 and 22 present the modulus of the FRF for $\xi = 0.2$, 1.5, and 10, respectively.

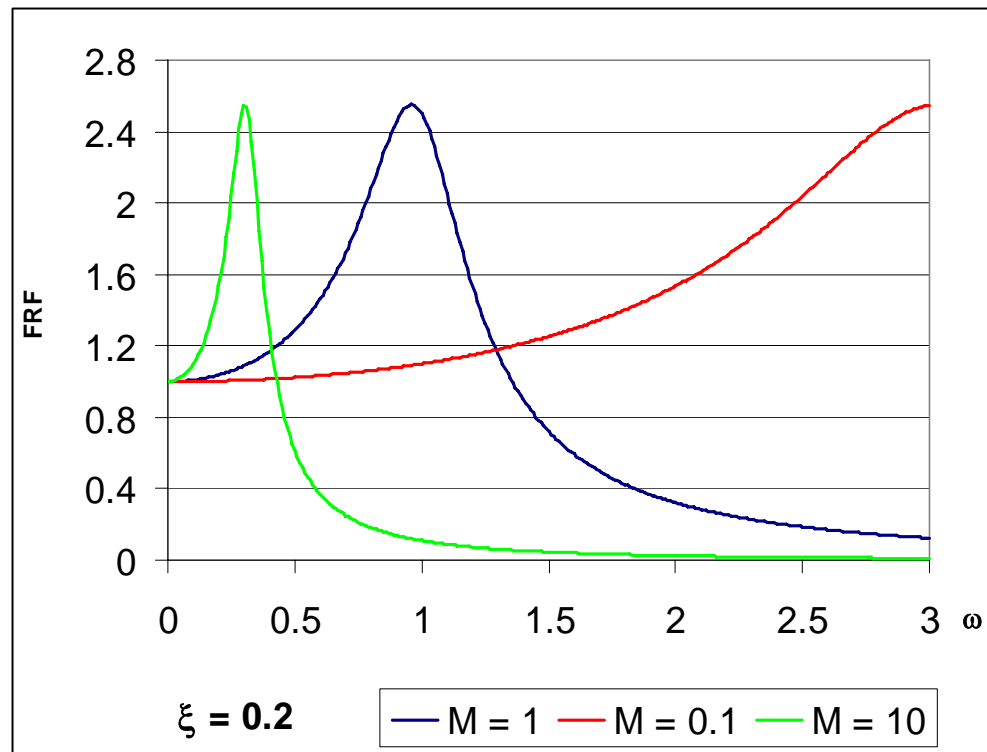


Figure 4.20: Dimensionless FRF for $\xi = 0.2$

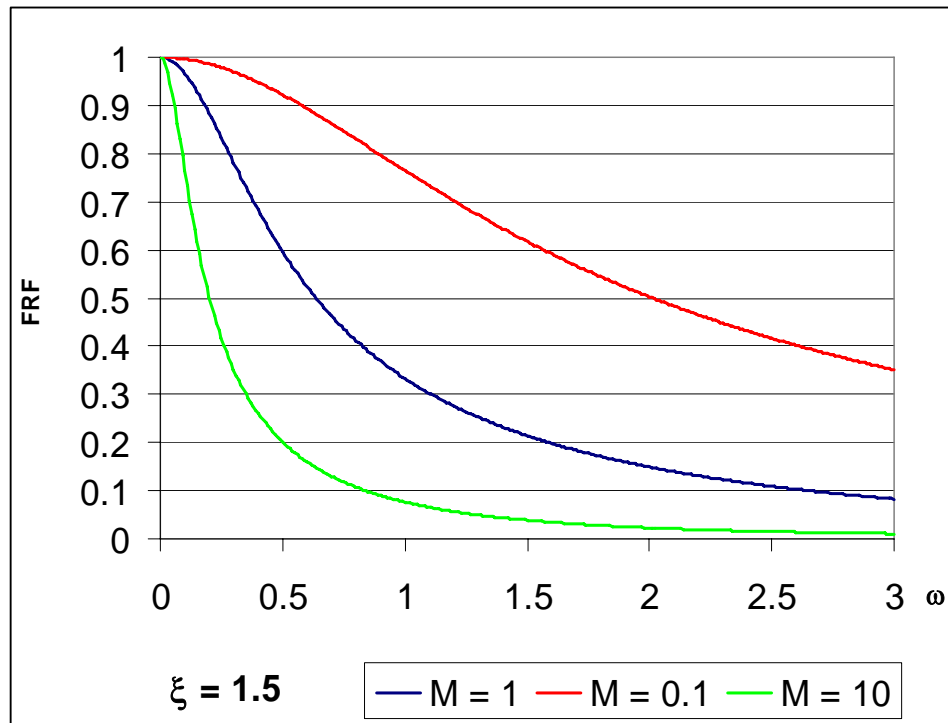


Figure 4.21: Dimensionless FRF for $\xi = 1.5$

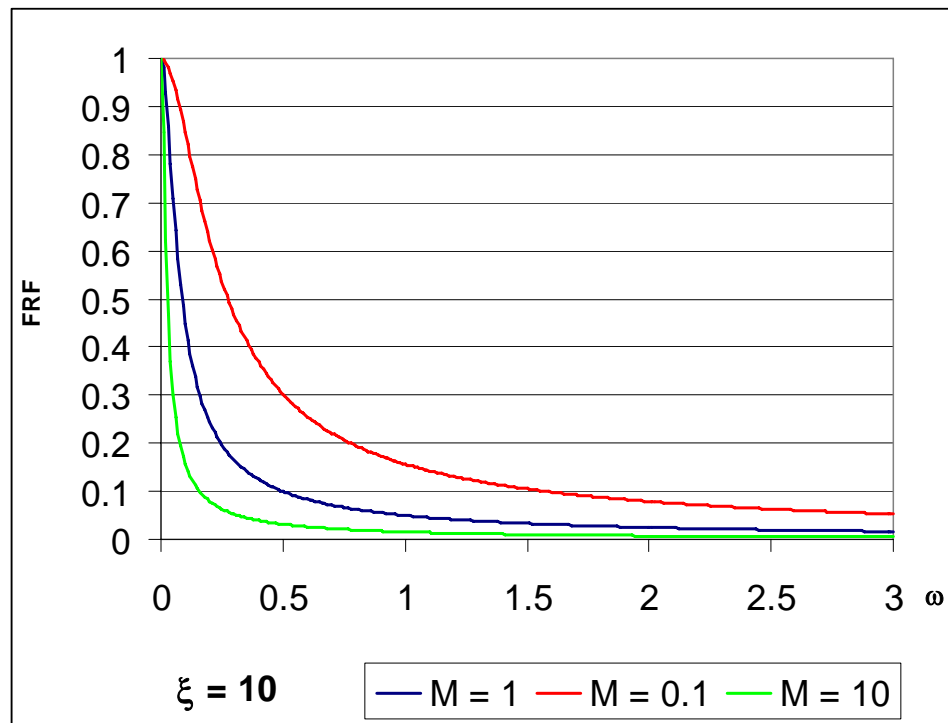


Figure 4.22: Dimensionless FRF for $\xi = 10.0$

It can be seen from Figure 4.20 that for systems with a relatively small damping ratios and for excitation frequencies $\omega < \sqrt{2}\omega_n$, the response experiences an amplification (peak) with respect to the static response ($\omega = 0$), and that the system mass plays an important role in establishing where the peak is located (for a constant stiffness). As the damping ratio becomes higher (specifically, $\xi > \sqrt{2}/2$), the FRF does not present a peak (there is no amplification for any excitation frequency), and the response of the systems with different masses becomes closer, making the effect of the mass less important in the system response. Figure 4.23 displays the response of systems with different masses and different damping ratios; this figure demonstrates that, in overdamped systems, an effect similar to the mass may be obtained with an appropriate damping.

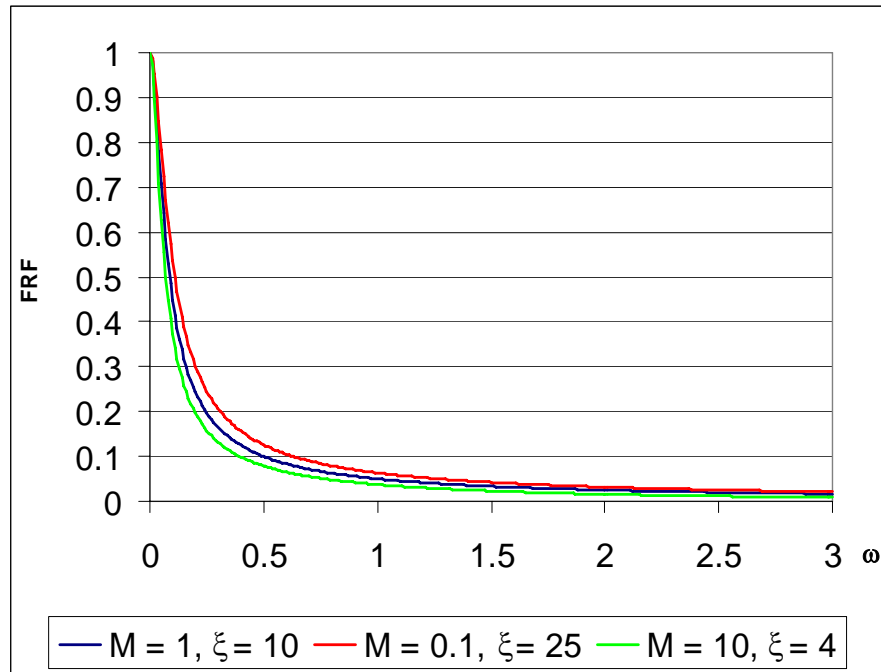


Figure 4.23: Dimensionless FRF for Different M and ξ

The fact that the radiation damping makes a soil deposit a highly dissipative medium may explain the reason why the model proposed by Novak, which was used as the basis of the present proposed lumped model developed in this chapter, does not yield an equivalent lumped mass for all Poisson's ratios:

This situation may be explained by the fact that, due to radiation damping, the soil response is overdamped; and overdamped SDOF systems behavior are basically controlled by damping and not by mass. The model also shows that the soil mass is important for high soil Poisson's ratios, as occurs in saturated soils (for $\nu = 0.5$ the soil mass contribution is in the same order of the pile mass contribution). However, the soil mass importance rapidly diminishes as the Poisson's ratio becomes smaller. This situation may be explained due to the fact that the larger the value of the Poisson's ratio ν , the larger the soil transverse deformation that will occur when the piles vibrates horizontally, so more soil mass is involved in the transmission of p-waves due to pile vibration, as presented in Figure 4.24: when $\nu = 0.0$ there are no transverse deformations, and the compressive waves propagate along one line of soil stress elements located along the direction of pile movement, but when ν increases, there are increasingly larger transverse deformations, so the compressive waves also affect the soil stress elements located perpendicular to the direction of pile movement.

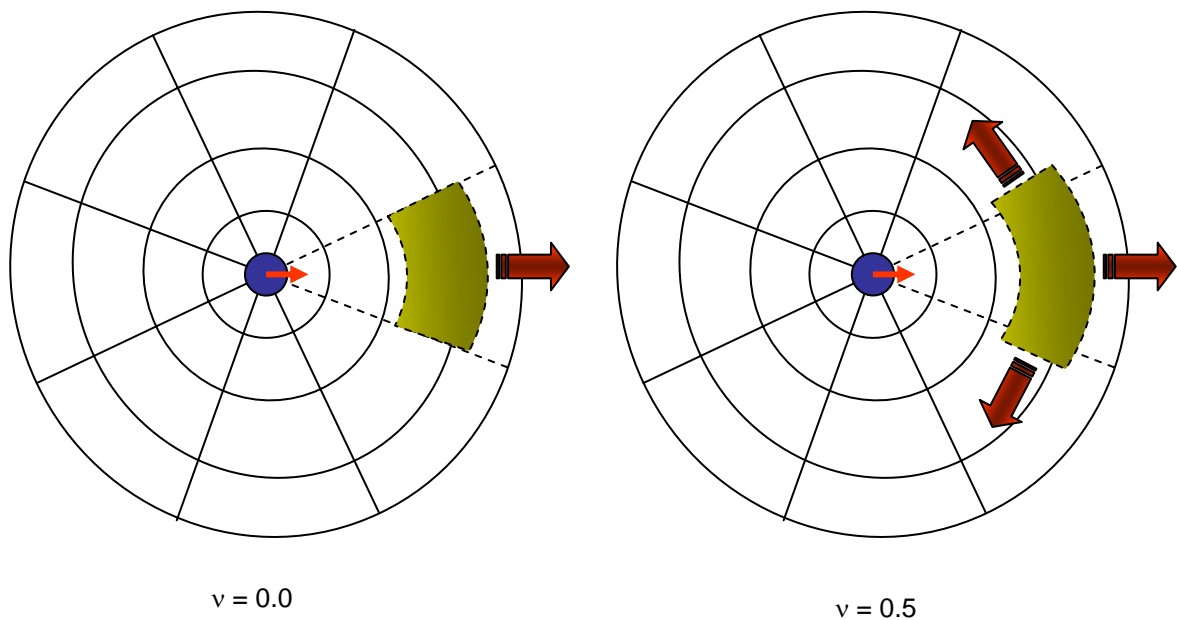


Figure 4.24: Effect of ν in the Propagation of P-Waves

4.4 Pile Element Matrices

This section briefly describes the implementation of the soil lumped model in the analysis of a single pile, using three types of one dimensional (1D) flexural beam elements.

4.4.1 Classical Beam Element with Lumped Soil

A classical beam element with its nodal degrees of freedom is shown in Figure 4.25. The corresponding element stiffness, lumped mass, and consistent mass matrices are presented in equations 4.21, 4.22 and 4.23 respectively (Chopra, 2001; Suarez, 2004).

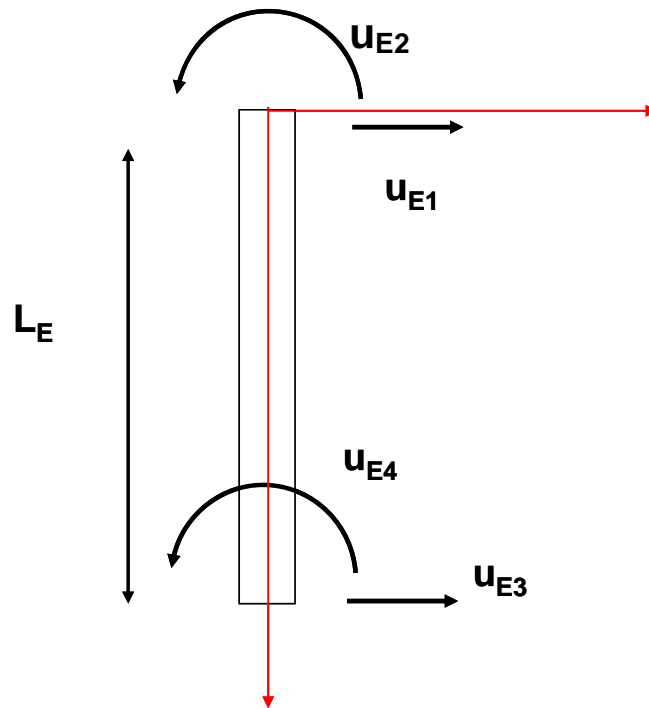


Figure 4.25: Pile Element DOF

$$[k_E] = \begin{bmatrix} \frac{12EI}{L_E^3} & \frac{6EI}{L_E^2} & -\frac{12EI}{L_E^3} & \frac{6EI}{L_E^2} \\ \frac{6EI}{L_E^2} & \frac{4EI}{L_E} & -\frac{6EI}{L_E^2} & \frac{2EI}{L_E} \\ -\frac{12EI}{L_E^3} & -\frac{6EI}{L_E^2} & \frac{12EI}{L_E^3} & -\frac{6EI}{L_E^2} \\ \frac{6EI}{L_E^2} & \frac{2EI}{L_E} & -\frac{6EI}{L_E^2} & \frac{4EI}{L_E} \end{bmatrix} \quad (4.22)$$

where:

$[k_E]$ = Pile element stiffness matrix

L_E = length of the pile element

E = modulus of elasticity of the pile element material

I = moment of inertia of the pile element cross section

$$[m_E] = \begin{bmatrix} \frac{M_P}{2} & 0 & 0 & 0 \\ 0 & 0 & 0 & 0 \\ 0 & 0 & \frac{M_P}{2} & 0 \\ 0 & 0 & 0 & 0 \end{bmatrix} \quad (4.23)$$

where:

$[m_E]$ = Pile element lumped mass matrix

$M_P = \rho A L_E$ = mass of the pile element

ρ = density of the pile element material

A = area of the pile element cross section

$$[m_E] = \frac{M_p}{420} \begin{bmatrix} 156 & 22L_E & 54 & -13L_E \\ 22L_E & 4L_E^2 & 13L_E & -3L_E^2 \\ 54 & 13L_E & 156 & -22L_E \\ -13L_E & -3L_E^2 & -22L_E & 4L_E^2 \end{bmatrix} \quad (4.24)$$

where:

$[m_E]$ = Pile element consistent mass matrix

$M_p = \rho A L_E$ = Pile element mass

The pile with a lumped mass-spring-dashpot at its ends (representing soil-pile interaction) is presented in Figure 4.26, together with the corresponding lumped parameters definition. The coefficients k_a , m_a , and c_a were obtained based on Novak's dynamic stiffness that represents the dynamic soil reaction per unit length of pile due to a unit horizontal harmonic displacement of a rigid disc (pile cross section). These coefficients must be multiplied by the tributary length of each pile element node, that is $L_E/2$, in order to obtain the nodal lumped parameters.

This approach of representing the soil-pile interaction has four main advantages:

- It can be easily implemented in any commercial structural analysis software (e.g. SAP2000, etc.).
- It is not difficult to incorporate possible soil non-linearities by varying the soil stiffness ka (i.e. using p-y curves).
- The required computational time is orders of magnitude smaller than the one required by a 3D FEM model.
- A simple model can be more easily understood and it is more likely to be accepted and adopted by the professional community.

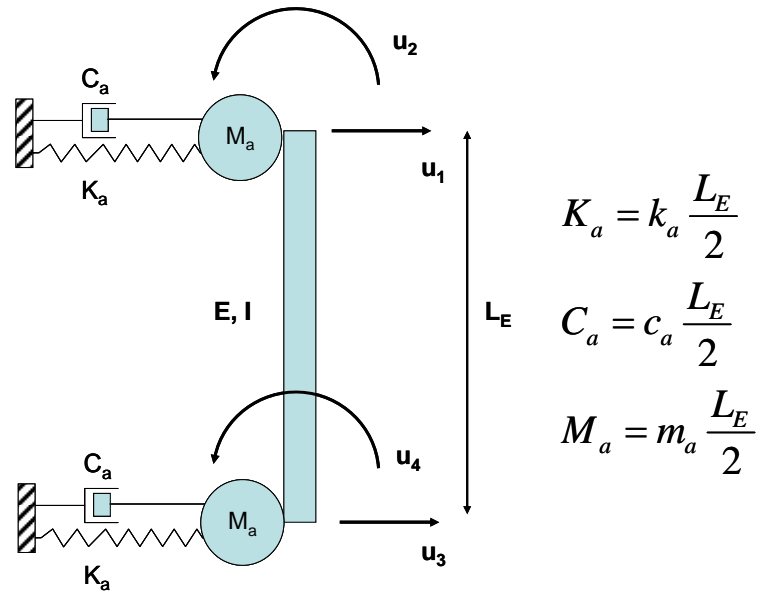


Figure 4.26: Pile Element with Lumped Soil Parameters

4.4.2 Classical Beam Element with Distributed Soil

Other possible approach to obtain a model of the pile that accounts for the soil contribution is to obtain a set of consistent stiffness, mass and damping matrices by applying an appropriate variational principle to the pile (beam) element with distributed soil parameters k_a , m_a , and c_a . The beam element is shown in Figure 4.27; note that the springs, dashpots and masses representing the soil are not lumped at its end nodes, but distributed along its length. Appendix E presents the derivation of these matrices; the results obtained are given in equations 4.24 through 4.26.

This approach is more elegant than the lumped model, but it has two drawbacks:

- It is not possible to implement in a commercial package, since the program should have this type of element matrices built in. Most commercial software use lumped mass matrices and only allow to add additional masses, dashpots and springs at discrete points.
- It is not evident how to incorporate nonlinear effects, since the soil stiffness is distributed (not lumped), and hence it is not associated to a particular displacement that may control this stiffness value.

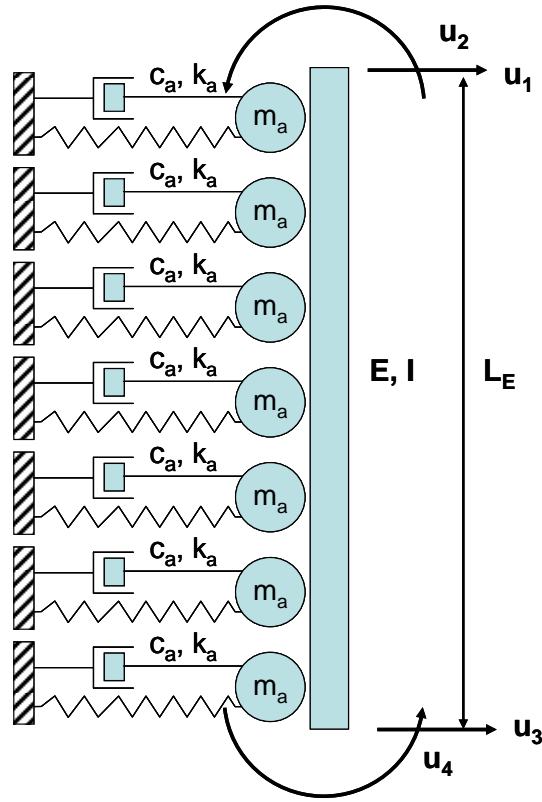


Figure 4.27: Pile Element with Distributed Soil Parameters

The stiffness matrix for the beam element with distributed soil stiffness is given by:

$$[k_E] = \begin{bmatrix} \frac{12EI}{L_E^3} & \frac{6EI}{L_E^2} & -\frac{12EI}{L_E^3} & \frac{6EI}{L_E^2} \\ \frac{6EI}{L_E^2} & \frac{4EI}{L_E} & -\frac{6EI}{L_E^2} & \frac{2EI}{L_E} \\ -\frac{12EI}{L_E^3} & -\frac{6EI}{L_E^2} & \frac{12EI}{L_E^3} & -\frac{6EI}{L_E^2} \\ \frac{6EI}{L_E^2} & \frac{2EI}{L_E} & -\frac{6EI}{L_E^2} & \frac{4EI}{L_E} \end{bmatrix} + \frac{K_S}{420} \begin{bmatrix} 156 & 22L_E & 54 & -13L_E \\ 22L_E & 4L_E^2 & 13L_E & -3L_E^2 \\ 54 & 13L_E & 156 & -22L_E \\ -13L_E & -3L_E^2 & -22L_E & 4L_E^2 \end{bmatrix} \quad (4.25)$$

where:

$[k_E]$ = Pile element stiffness matrix

L_E = length of the pile element

E = modulus of elasticity of the pile element material

I = moment of inertia of the pile element cross section

$K_S = k_a L_E$ = Total soil stiffness coefficient

The mass matrix for a beam element with distributed soil mass is given by:

$$[M_E] = \frac{M_P + M_S}{420} \begin{bmatrix} 156 & 22L_E & 54 & -13L_E \\ 22L_E & 4L_E^2 & 13L_E & -3L_E^2 \\ 54 & 13L_E & 156 & -22L_E \\ -13L_E & -3L_E^2 & -22L_E & 4L_E^2 \end{bmatrix} \quad (4.26)$$

where:

$[M_E]$ = Pile + soil element consistent mass matrix

$M_P = \rho A L_E$ = Total pile element mass

$M_S = m_a L_E$ = Total soil mass

ρ = density of the pile element material

A = area of the pile element cross section

ρA = mass per unit length of the pile element

m_a = mass per unit length of the soil

The damping matrix for a beam element with distributed soil damping is given by:

$$[c_E] = \frac{C_S}{420} \begin{bmatrix} 156 & 22L_E & 54 & -13L_E \\ 22L_E & 4L_E^2 & 13L_E & -3L_E^2 \\ 54 & 13L_E & 156 & -22L_E \\ -13L_E & -3L_E^2 & -22L_E & 4L_E^2 \end{bmatrix} \quad (4.27)$$

where:

$[c_E]$ = Pile + soil element consistent damping matrix

$C_s = c_a L_E$ = total soil damping

c_a = distributed damping coefficient of the soil

4.4.3 Refined Beam Element with Distributed Soil

Finally, a third approach to define a model to represent the pile and the soil contribution is presented. The refined beam element was proposed by Deschapelles (2003), and it has five degree of freedom (DOF): four corresponding to the classical beam element (nodal transverse displacements and rotations) plus one corresponding to the average transverse displacement along the beam length. This last displacement may be considered as a distributed or non nodal DOF. This element is displayed in Figure 4.28 with the distributed springs, dampers and masses.

The consistent stiffness, mass and damping matrices were obtained by applying the Principle of Virtual Work to the pile (beam) element with distributed soil parameters k_a , m_a , and c_a . The derivation is presented in Appendix E and the results are given in equations 4.27 through 4.28.

This approach is more elegant than the lumped model, and it has the advantage that the new DOF is directly associated with the distributed soil stiffness, so its value may be used to control the soil stiffness to perform a nonlinear analysis. Its major drawback is that it is not possible to implement it in a commercial structural analysis program, since no program has this type of element.

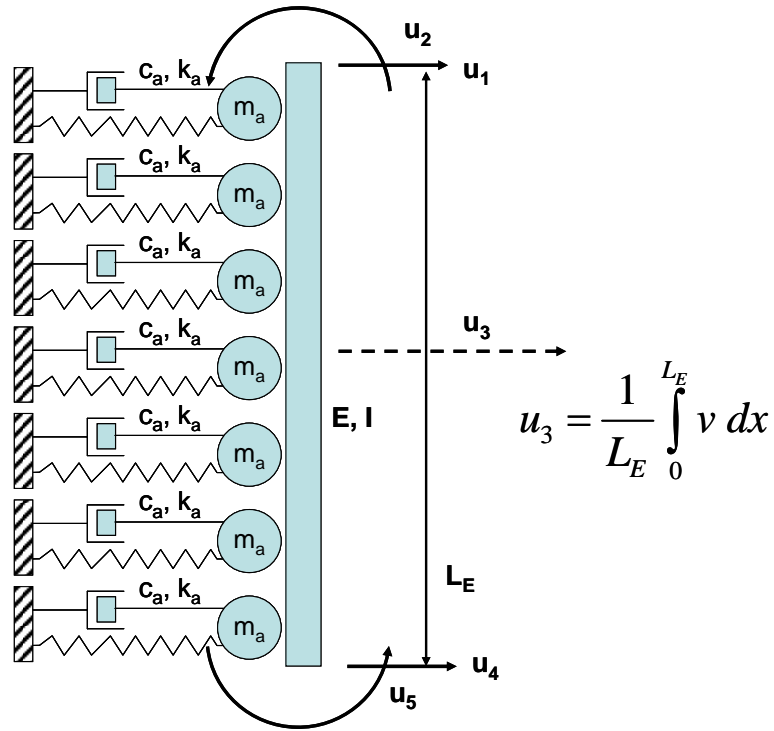


Figure 4.28: Refined Beam Element with Distributed Soil Parameters

The stiffness matrix for the refined beam element with distributed soil stiffness is given by:

$$[k_E] = \frac{3EI}{L_E} \begin{bmatrix} \frac{64}{L_E^2} & \frac{12}{L_E} & -\frac{120}{L_E^2} & \frac{56}{L_E^2} & -\frac{8}{L_E} \\ \frac{12}{L_E} & 3 & -\frac{20}{L_E} & \frac{8}{L_E} & -1 \\ -\frac{120}{L_E^2} & -\frac{20}{L_E} & \frac{240}{L_E^2} & -\frac{120}{L_E^2} & \frac{20}{L_E} \\ \frac{56}{L_E^2} & \frac{8}{L_E} & -\frac{120}{L_E^2} & \frac{64}{L_E^2} & -\frac{12}{L_E} \\ -\frac{8}{L_E} & -1 & \frac{20}{L_E} & -\frac{12}{L_E} & 3 \end{bmatrix} + \frac{K_s}{1260} \begin{bmatrix} 288 & 21L_E & -270 & -18 & 6L_E \\ 21L_E & 2L_E^2 & -15L_E & -6L_E & L_E^2 \\ -270 & -15L_E & 1800 & -270 & 15L_E \\ -18 & -6L_E & -270 & 288 & -21L_E \\ 6L_E & L_E^2 & 15L_E & -21L_E & 2L_E^2 \end{bmatrix} \quad (4.28)$$

where $[k_E]$ is the stiffness matrix of the pile plus soil element, and the other parameters are the same as those previously defined for equation 4.24.

The mass matrix for a refined beam element with distributed soil mass is given by:

$$[M_E] = \frac{M_P + M_S}{1260} \begin{bmatrix} 288 & 21L_E & -270 & -18 & 6L_E \\ 21L_E & 2L_E^2 & -15L_E & -6L_E & L_E^2 \\ -270 & -15L_E & 1800 & -270 & 15L_E \\ -18 & -6L_E & -270 & 288 & -21L_E \\ 6L_E & L_E^2 & 15L_E & -21L_E & 2L_E^2 \end{bmatrix} \quad (4.29)$$

where $[M_E]$ is the pile plus soil element consistent mass matrix, and the remaining parameters were defined before for the mass matrix in equation 4.25.

The damping matrix for a refined beam element with distributed soil damping is given by:

$$[c_E] = \frac{C_s}{1260} \begin{bmatrix} 288 & 21L_E & -270 & -18 & 6L_E \\ 21L_E & 2L_E^2 & -15L_E & -6L_E & L_E^2 \\ -270 & -15L_E & 1800 & -270 & 15L_E \\ -18 & -6L_E & -270 & 288 & -21L_E \\ 6L_E & L_E^2 & 15L_E & -21L_E & 2L_E^2 \end{bmatrix} \quad (4.30)$$

where $[c_E]$ is the pile plus soil element consistent damping matrix. The definition of C_s was given after equation 4.26.

5 Proposed Lumped Model Validation/Verification

The objective of this chapter is to present a series of validations of the proposed lumped model. First, a comparison between the *Dynamic Stiffness* of the equivalent lumped *Single Degree of Freedom System* is compared to Novak's solution for plane strain, to determine the accuracy of the approximation (within a selected dimensionless frequency range). Then, a comparison of a pile system response, given by the pile top dynamic flexibility, analyzing the system with the lumped model and Novak's model is performed, in order to assess the adequacy of the lumped system to model pile-soil response. This is followed by a comparison between a 3D FEM model and a 1D lumped model response. Then a comparison between experimental and analytical results using the lumped model is carried out, in order to assess the lumped model capability of predicting experimental results. The effect of the Poisson's ratio in a 3D FEM model response is obtained next, in order to evaluate if there is a similar impact than the one obtained for the lumped mass of the approximate model. Lastly, the stiffness and the damping coefficients of the approximate model are compared to the corresponding values presented in the literature for other approaches.

5.1 Lumped Dynamic Stiffness Approximation of Novak Continuum Model for Plane Strain

As the lumped model was obtained through a polynomial least square regression of Novak's model, the accuracy of the obtained approximate polynomial function is evaluated by means of the coefficient of determination R^2 (*R-squared*). The R^2 value is a number between 0 and 1 that reveals how closely the estimated values for the polynomial regression match the actual data (Zwillinger and Kokoska, 2000; Chapra and Canale, 1998). The approximation is most reliable when its R^2 value is 1 or near 1. R^2 is computed as the ratio between the variance S_E^2 of the predicted data (as a measure of its statistical dispersion, indicating how its values are spread around the expected value,

which is the mean value) and the variance S_T^2 of the sample (actual) data. Equation 5.1 shows the reference formula:

$$R^2 = \frac{S_E^2}{S_T^2} \quad (5.1)$$

The R^2 coefficient can also be calculated in terms of the Estimated Sum of Squares and the Total Sum of Squares:

$$R^2 = \frac{ESS}{TSS} = 1 - \frac{RSS}{TSS} \quad (5.2)$$

where:

$$S_E^2 = \frac{\sum_{i=1}^N (\hat{y}_i - \bar{y})^2}{N-1} = \frac{ESS}{N-1} = \text{Explained (or Estimated) Variance}$$

$$S_T^2 = \frac{\sum_{i=1}^N (y_i - \bar{y})^2}{N-1} = \frac{TSS}{N-1} = \text{Total (Sample) Variance}$$

$$ESS = \sum_{i=1}^N (\hat{y}_i - \bar{y})^2 = \text{Explained (or Estimated) Sum of Squares}$$

$$TSS = \sum_{i=1}^N (y_i - \bar{y})^2 = \text{Total Sum of Squares}$$

$$RSS = \sum_{i=1}^N (y_i - \hat{y}_i)^2 = \text{Residual Sum of Squares (or Sum of the Squared Errors)}$$

N = number of data points

y_i = data value

\hat{y}_i = estimated value

$$\bar{y} = \frac{\sum_{i=1}^N y_i}{N} = \text{mean value of data points}$$

A value of $R^2 = 1$ implies that the predicted data with the regression equation has the same variance (respect to the sample mean) than the sample data. In this sense, one can interpret that the R^2 coefficient is intended to give quantification of how better is to approximate the ordinates by the polynomial equation instead of using the mean value as an approximation, in which case $R^2 = 0$.

Appendix D presents the MathCad worksheet prepared to compute the R^2 coefficient for the different regressions performed, both for the real part and the imaginary part of the dynamic stiffness. The results are summarized in Table 5.1 and presented graphically in Figure 5.1 for the range of values of ν where a parabolic regression was applicable for the real part ($0.31 \leq \nu \leq 0.50$).

Table 5.1: Coefficient of Determination for Different Poisson's Ratios [0.31-0.50]

ν	R^2 Real	R^2 Imaginary	ν	R^2 Real	R^2 Imaginary
0.50	0.999	0.997	0.40	0.981	0.999
0.49	0.999	0.994	0.39	0.981	0.999
0.48	0.995	0.993	0.38	0.981	0.999
0.47	0.990	0.994	0.37	0.981	0.999
0.46	0.987	0.995	0.36	0.981	0.999
0.45	0.984	0.997	0.35	0.982	0.999
0.44	0.983	0.997	0.34	0.982	0.998
0.43	0.982	0.998	0.33	0.982	0.998
0.42	0.981	0.998	0.32	0.983	0.998
0.41	0.981	0.999	0.31	0.984	0.998

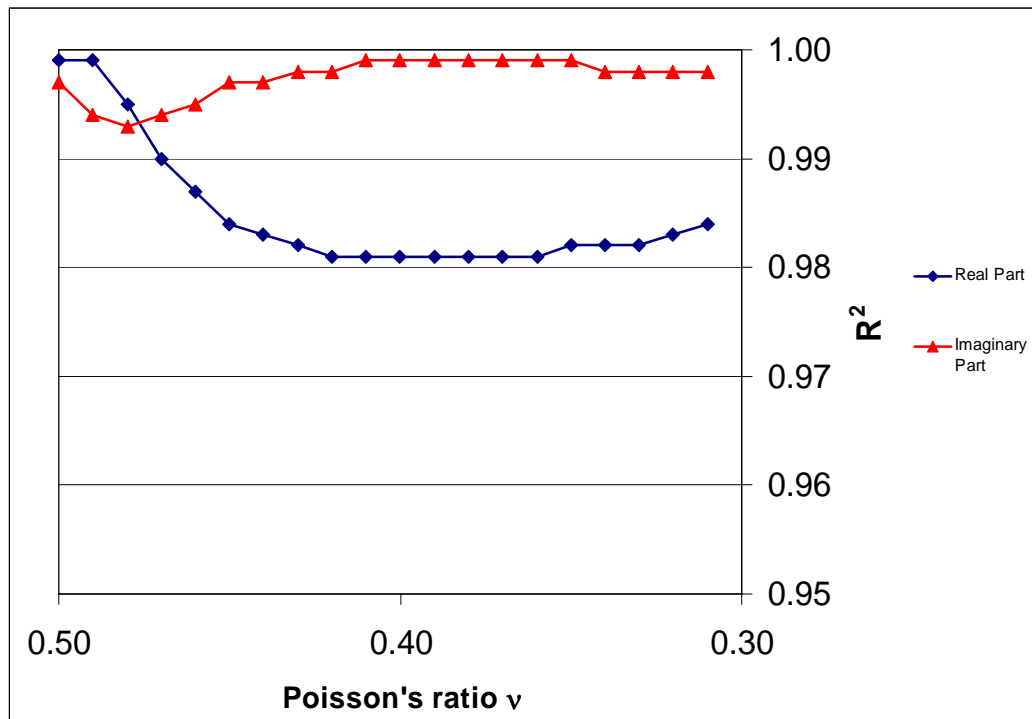


Figure 5.1: Coefficient of Determination for Different Poisson's Ratios

The results demonstrate that the proposed polynomial approximations yield very good estimates of the selected data points.

In the cases when the real part of Novak's Dynamic Stiffness does not present a maximum ($\nu \leq 0.3$) and is approximated by an horizontal line, the least squares solutions gives a constant value as the mean value of the ordinate data points. In this case, the coefficient of determination is meaningless, and its value is zero ($ESS=0$ and $RSS=TSS$). For these cases, the *coefficient of variation* CV in percentage (also known as the relative standard deviation) will be used to determine the fitness of the approximation: the closer CV is to zero, the better the mean value (used as the approximation) represents the whole data (since the values are less disperse around the mean). The CV is defined as:

$$CV = \frac{s}{\bar{y}} \times 100 \quad (5.3)$$

where:

$$\bar{y} = \frac{\sum_{i=1}^N y_i}{N} = \text{sample mean value}$$

$$s = \sqrt{\frac{(y_i - \bar{y})^2}{N-1}} = \text{sample standard deviation}$$

$$N = \text{number of data points}$$

The results are summarized in Table 5.2 and presented graphically in Figures 5.2 and 5.3 for the range of ν values where a horizontal approximation was applicable for the real part ($0.00 \leq \nu \leq 0.30$). For the imaginary part the R^2 coefficient was computed. The results demonstrate that the proposed approximations result in very good estimates of the selected data points.

Table 5.2: Coefficient of Determination and Coefficient of Variation for Different Poisson's Ratios [0.31-0.50]

ν	CV % Real	R^2 Imaginary
0.30	1.186	0.998
0.29	1.368	0.998
0.28	1.527	0.998
0.27	1.664	0.998
0.26	1.783	0.998
0.25	1.885	0.998
0.24	1.974	0.998
0.23	2.051	0.998
0.22	2.118	0.997
0.21	2.176	0.997
0.20	2.227	0.997
0.19	2.271	0.997
0.18	2.310	0.997
0.17	2.344	0.997
0.16	2.374	0.997
0.15	2.401	0.997

ν	CV % Real	R^2 Imaginary
0.15	2.401	0.997
0.14	2.424	0.997
0.13	2.445	0.997
0.12	2.463	0.997
0.11	2.479	0.997
0.10	2.493	0.997
0.09	2.505	0.997
0.08	2.516	0.997
0.07	2.526	0.997
0.06	2.535	0.997
0.05	2.542	0.997
0.04	2.548	0.997
0.03	2.554	0.997
0.02	2.559	0.997
0.01	2.563	0.997
0.00	2.567	0.997

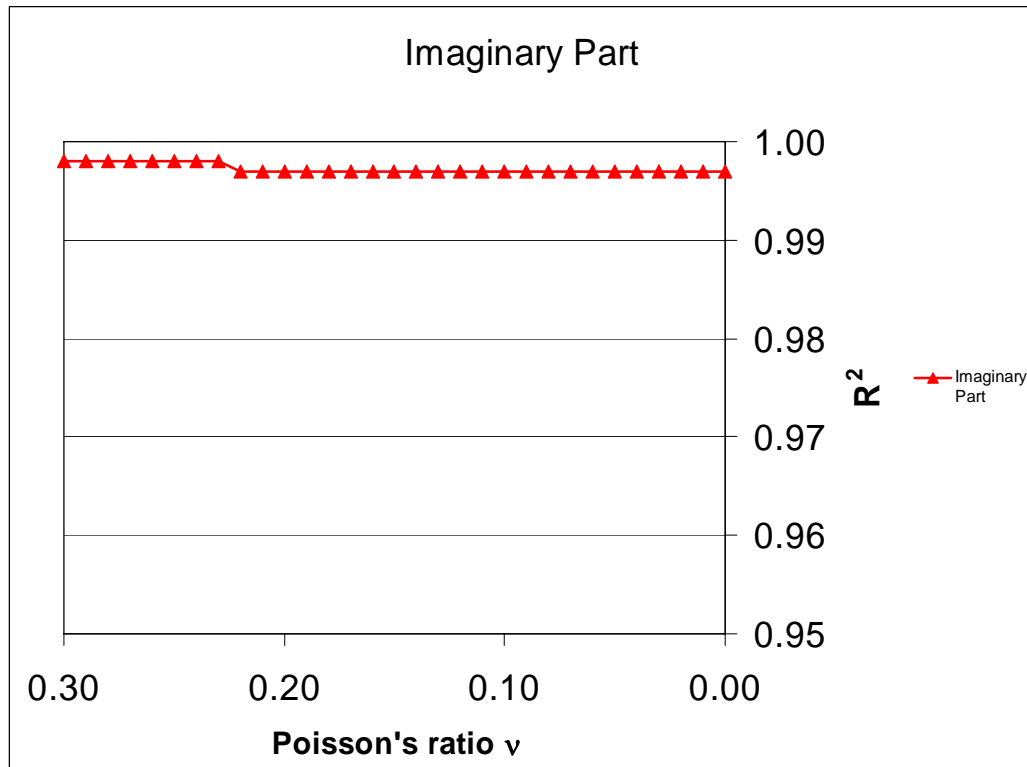


Figure 5.2: Coefficient of Determination of the Imaginary Part for Different Poisson's Ratios

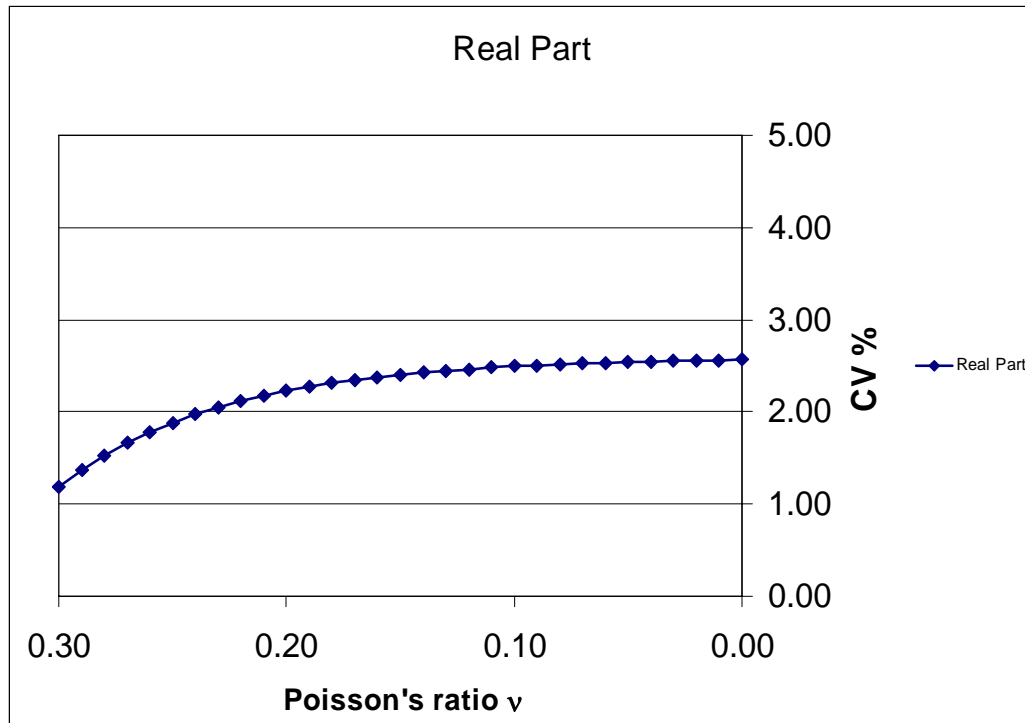


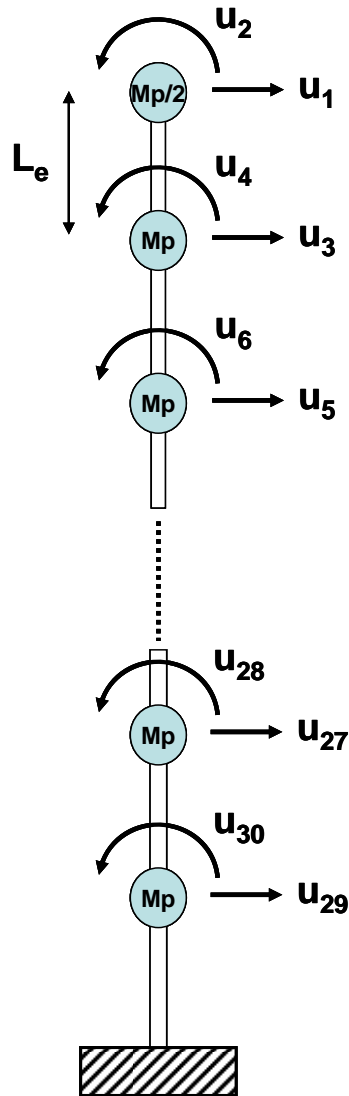
Figure 5.3: Coefficient of Variation of the Real Part for Different Poisson's Ratios

5.2 Pile with Lumped Model vs Pile with Novak Model

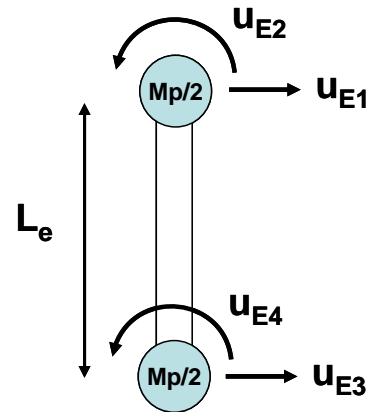
A case study will be developed to compare the predicted pile-soil response using the proposed lumped model, and using Novak's plane strain model, as presented in Chapter 4. A RC circular pile, with a 1ft radius, a length of 30 ft, a Young's elastic modulus of 3600 ksi and a specific weight of 150 pcf is placed in a sand stratum. The soil has an elastic modulus of 12 ksi, a specific weight of 110 pcf, and a Poisson's ratio of 0.4.

The Poisson's ratio was initially taken as 0.4 in order to analyze a case where the soil mass has a contribution. Later, the analysis will be extended to cover different Poisson's ratios values, in order to generalize the findings of the comparison.

Regarding the analytical model to be used, the pile will be discretized with 15 beam (flexural) elements. The pile analytical model (with the corresponding nodal degrees of freedom), and the pile element stiffness and mass matrices are presented in Figure 5.4.



Pile Analytical Model



$$[k_E] = \begin{bmatrix} \frac{12EI}{L_E^3} & \frac{6EI}{L_E^2} & -\frac{12EI}{L_E^3} & \frac{6EI}{L_E^2} \\ \frac{6EI}{L_E^2} & \frac{4EI}{L_E} & -\frac{6EI}{L_E^2} & \frac{2EI}{L_E} \\ -\frac{12EI}{L_E^3} & -\frac{6EI}{L_E^2} & \frac{12EI}{L_E^3} & -\frac{6EI}{L_E^2} \\ \frac{6EI}{L_E^2} & \frac{2EI}{L_E} & -\frac{6EI}{L_E^2} & \frac{4EI}{L_E} \end{bmatrix}$$

$[k_E]$ = Pile element stiffness matrix

$$[m_E] = \begin{bmatrix} \frac{M_P}{2} & 0 & 0 & 0 \\ 0 & 0 & 0 & 0 \\ 0 & 0 & \frac{M_P}{2} & 0 \\ 0 & 0 & 0 & 0 \end{bmatrix}$$

$[m_E]$ = Pile element lumped mass matrix

L_E = Pile element length

E = Pile element material modulus of elasticity

I = Pile element cross section moment of inertia

$M_P = \rho A L_E$ = Pile element mass

ρ = Pile element material density

A = Pile element cross section area

Pile Element Analytical Model, Stiffness Matrix and Mass Matrix

Figure 5.4: Pile Analytical Model and Element Matrices

The system response to be evaluated is the pile head dynamic flexibility, or frequency response function (FRF). Appendix F (sections F.1, F.2 and F.3) presents the programs developed in Matlab in order to perform the analyses. First, the FRF of the pile without the soil was obtained, in order to appreciate the isolated pile response. The result obtained was also compared to the FRF obtained with the commercial package SAP2000, in order to verify the Matlab program. Figure 5.5 presents the comparison. The FRF presents a series of peaks, as expected for a system with multiple degrees of freedoms and without damping. The results obtained with the program developed agree very well with those obtained with SAP2000 (in SAP2000 analysis, a default material damping of 0.05 of the system stiffness matrix was used, so the peaks are smoother).

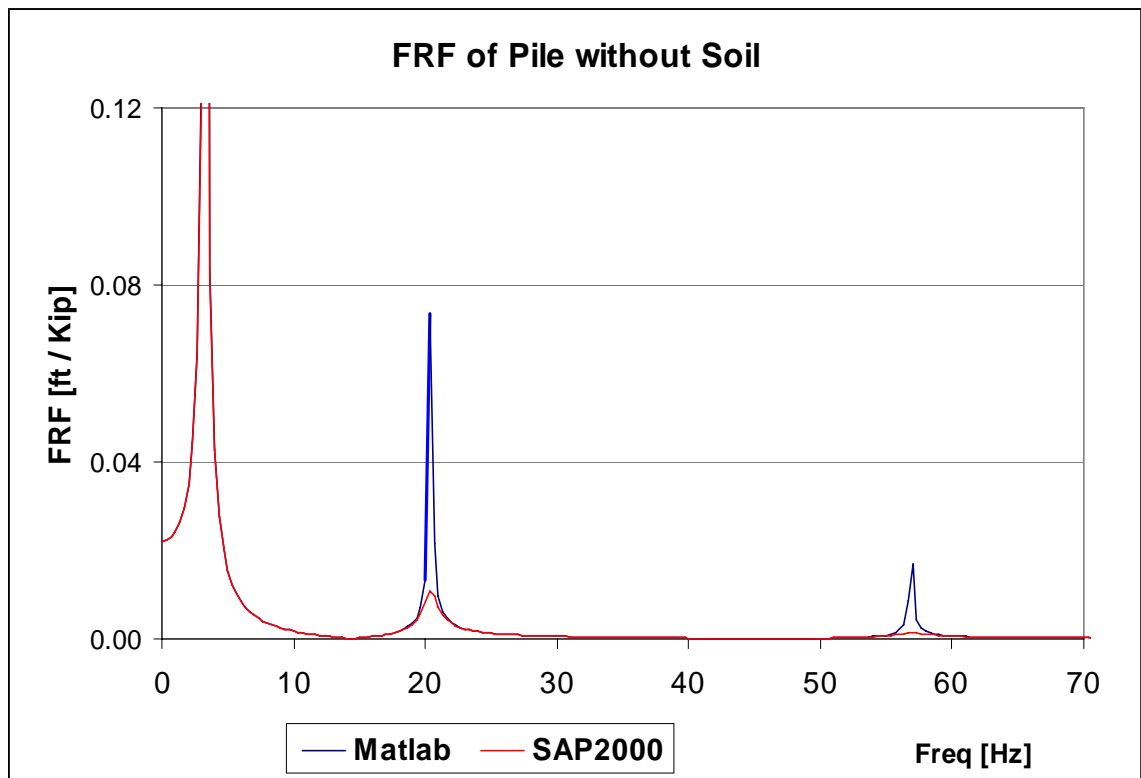
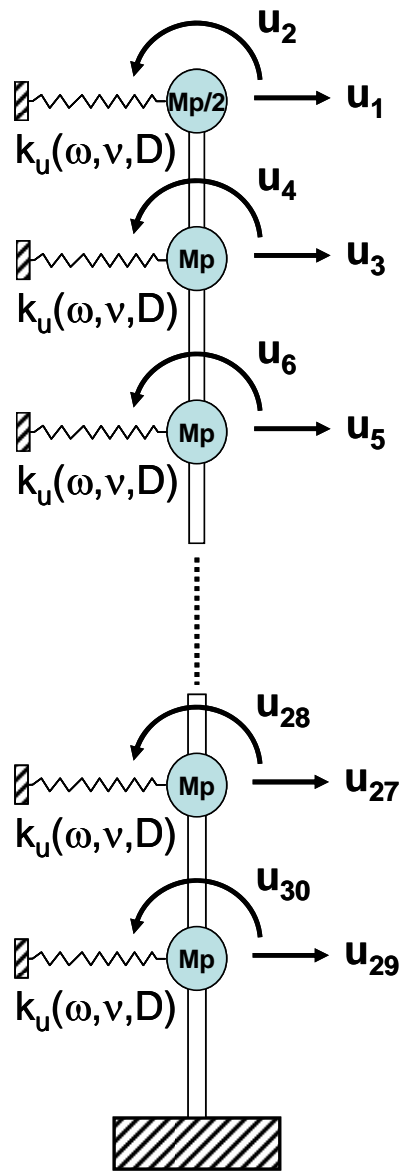
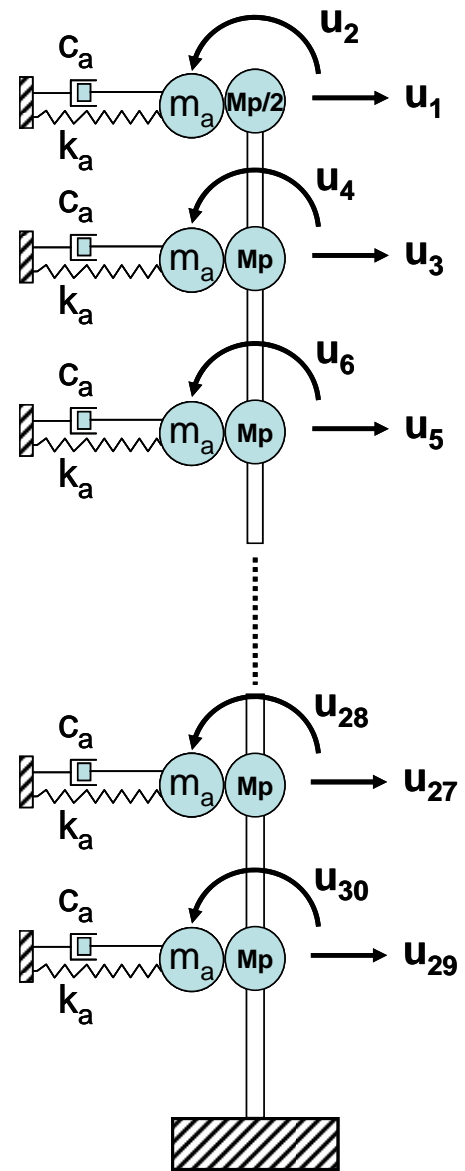


Figure 5.5: FRF of Pile without Soil Contribution

Next an analysis including the soil contribution was conducted. Both the Novak's plane strain model and the equivalent lumped model presented in Chapter 4 were used. Figure 5.6 shows the analytical models for the two approaches.



Pile Analytical
Model with Novak
Dynamic Stiffness



Pile Analytical
Model with Lumped
 k, m and c coefficients

Figure 5.6: Soil-Pile Analytical Models

Figure 5.7 presents the modulus of the FRF obtained using Novak's dynamic stiffness; Figure 5.8 presents the similar response calculated with the equivalent lumped model. Figure 5.9 presents both responses together for comparison purposes.

A good agreement in the predicted system responses can be observed. This indicates that the lumped model is able to produce accurate results for this pile-soil system and similar cases.

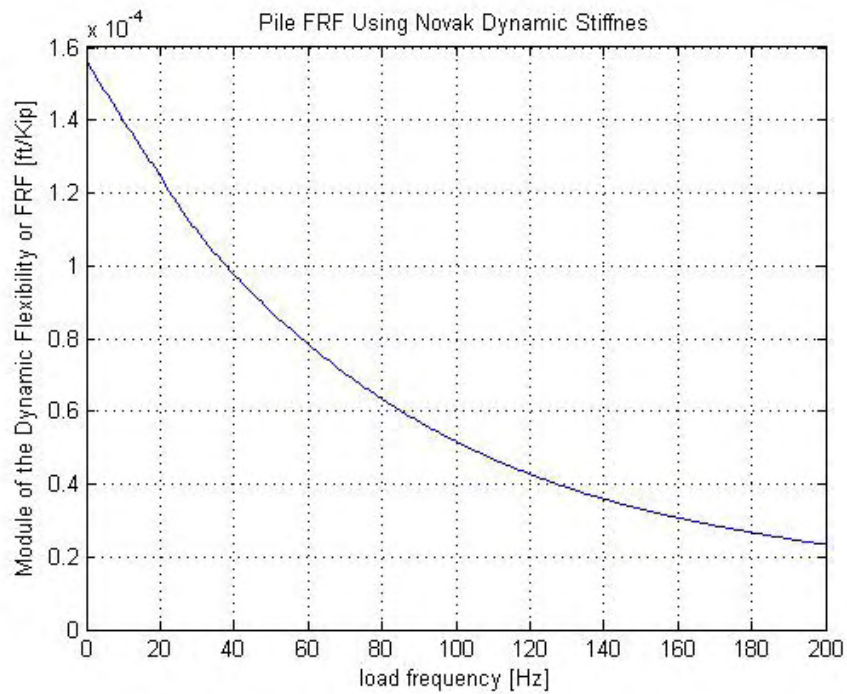


Figure 5.7: Pile-Soil System FRF Using Novak Model

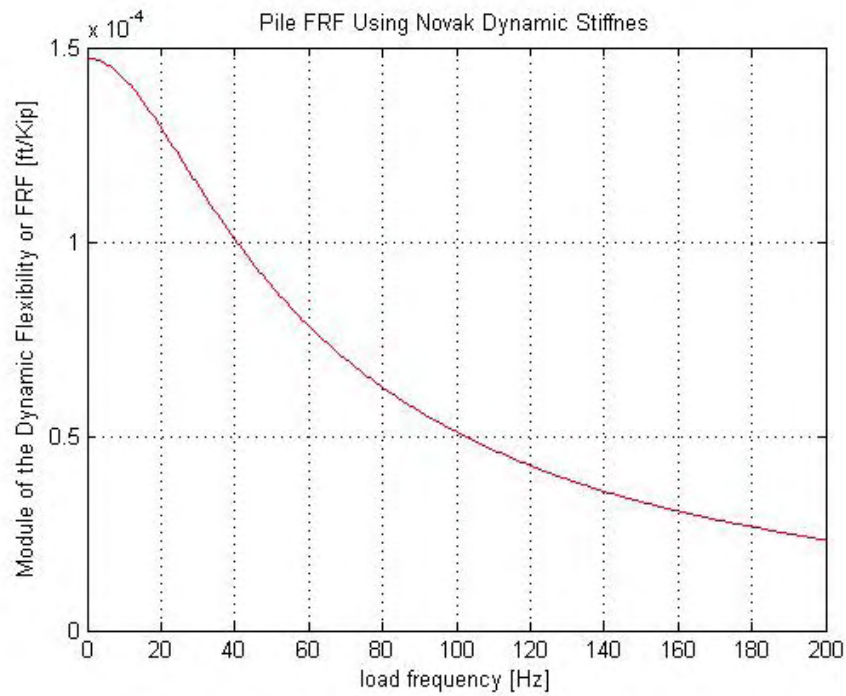


Figure 5.8: Pile-Soil System FRF Using Lumped Model

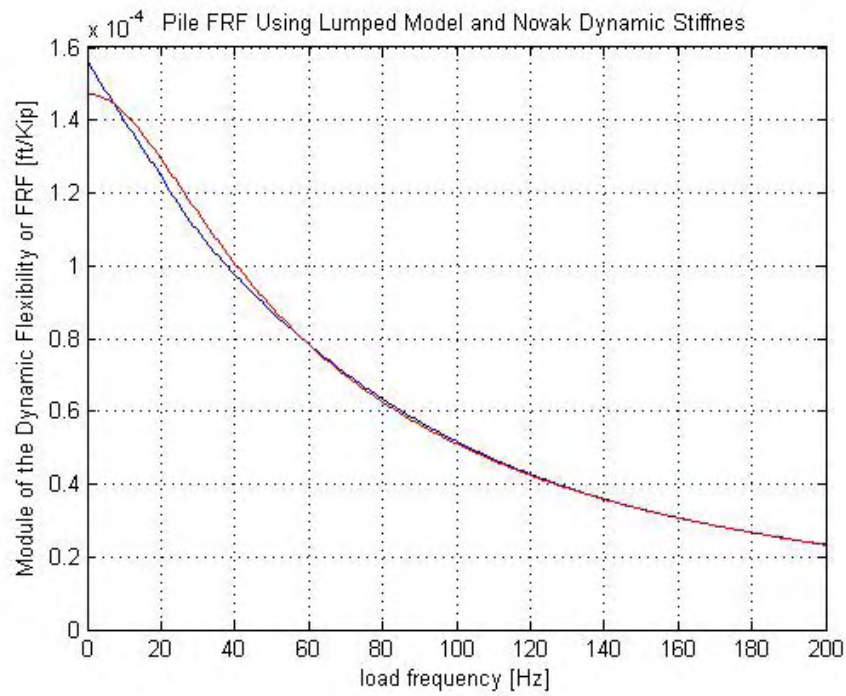


Figure 5.9: Comparison between Lumped FRF (red) and Novak FRF (blue)

It also can be seen that the pile responds as an overdamped system, since there are no peaks in its FRF. Figure 5.5 showed the system response disregarding soil contribution, and Figure 5.10 presents the two responses, those that account and neglect the soil contribution. A different vertical scale was used in order to better appreciate the effect of the soil contribution. It is clear that for this case the soil has a great impact in the system response: the magnitude of the static displacement is dramatically reduced, and the peaks of the FRF are eliminated.

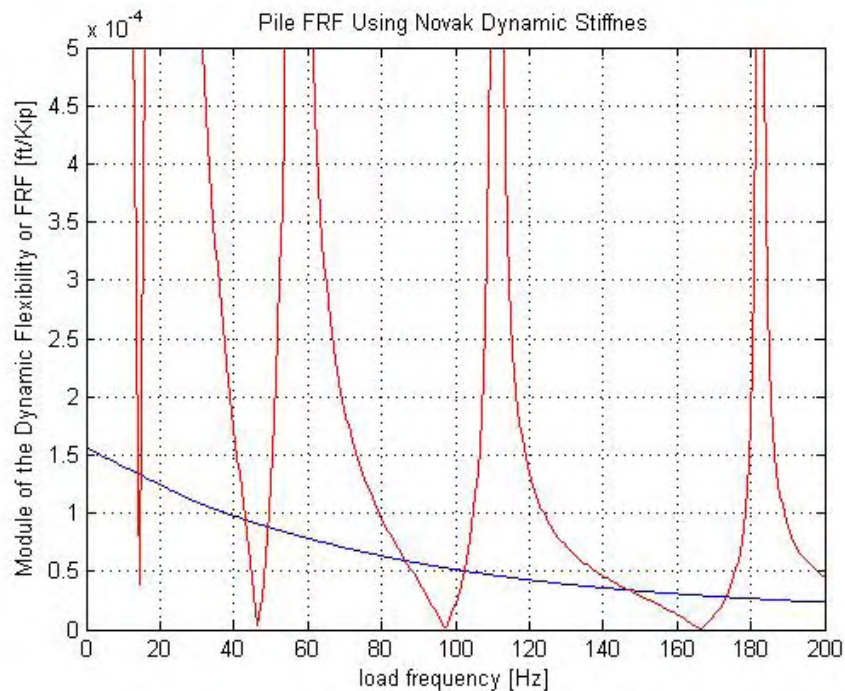


Figure 5.10: FRF with and Without Soil Contribution

In order to extend the conclusions regarding the adequacy of the lumped model, a series of numerical tests are conducted next over a range of soil Poisson's ratio and pile radius.

5.2.1 Lumped vs Novak Model for Different Soil Poisson's Ratios

Figures 5.11, 5.12, and 5.13 display the response (dynamic flexibility) of both models for different soil Poisson's ratios, ranging from 0.2 to 0.5, and maintaining fixed the rest of the parameters of the case study.

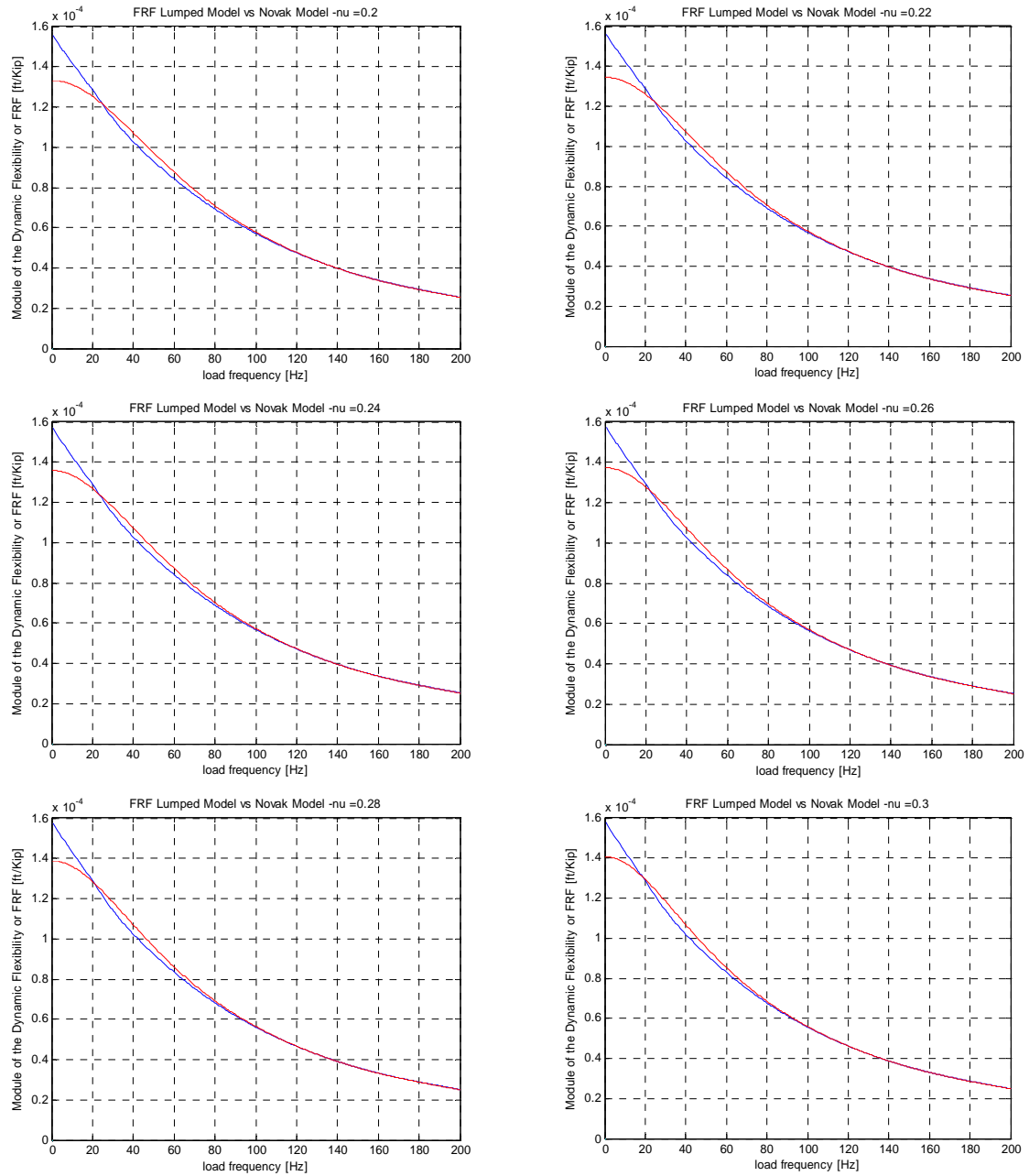


Figure 5.11: Comparison Between Lumped FRF (red) and Novak FRF (blue) for Different Soil Poisson's Ratios $[0.20 \leq \nu \leq 0.30]$

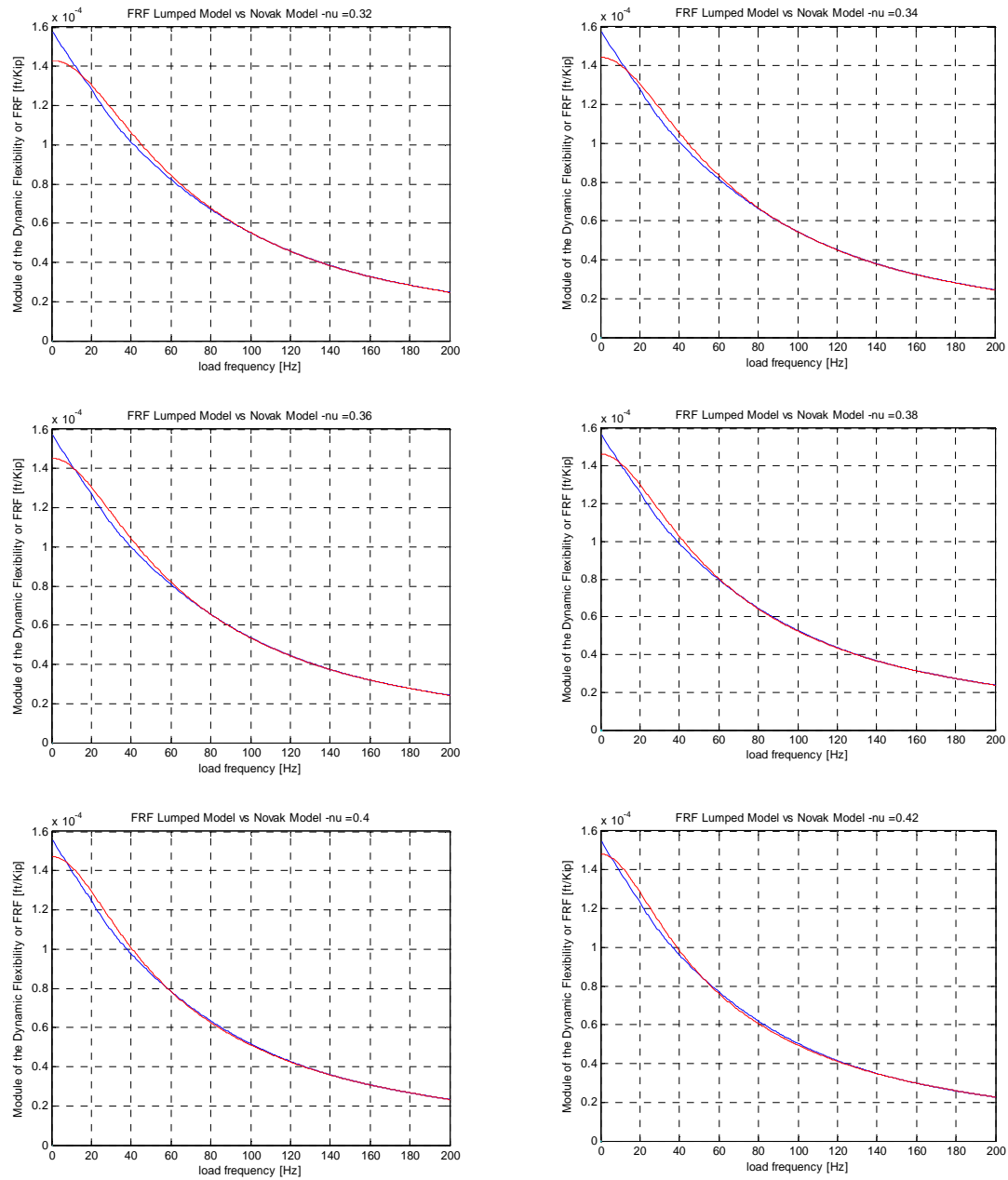


Figure 5.12: Comparison Between Lumped FRF (red) and Novak FRF (blue) for Different Soil Poisson's Ratios [$0.32 \leq \nu \leq 0.42$]

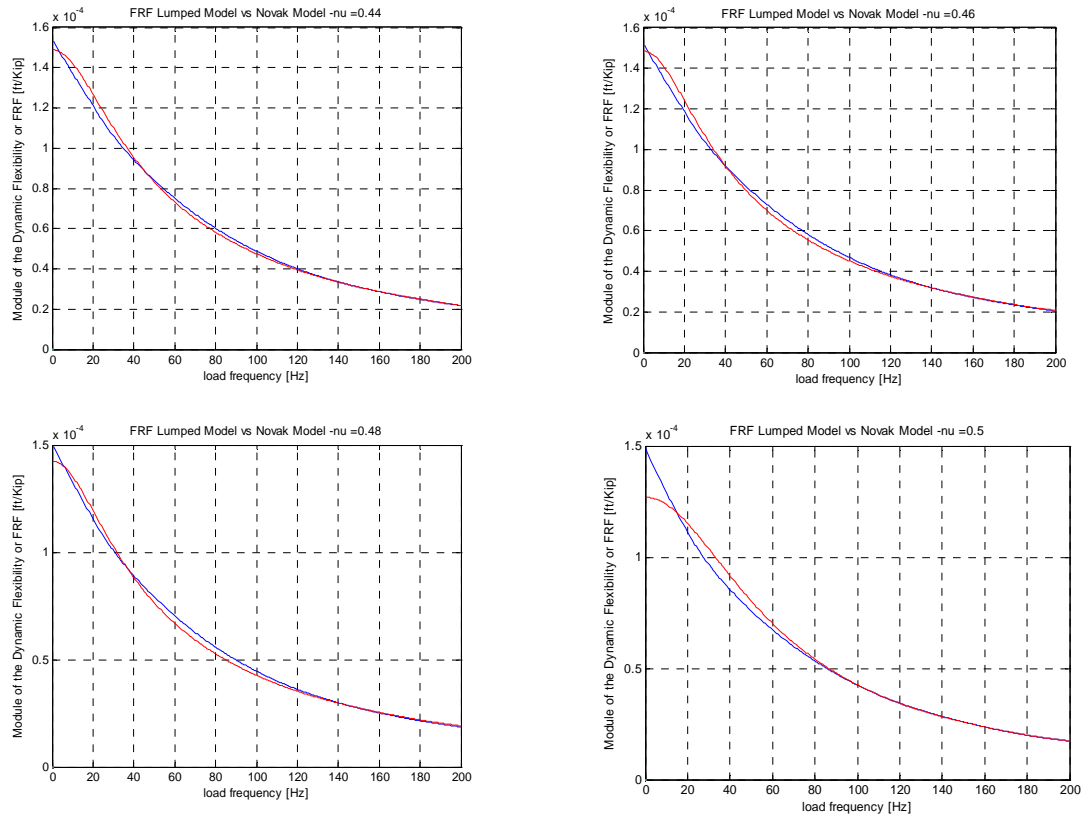


Figure 5.13: Comparison Between Lumped FRF (red) and Novak FRF (blue) for Different Soil Poisson's Ratio $[0.44 \leq \nu \leq 0.50]$

Appendix F, section F.4, contains the Matlab program written to perform the comparison.

These figures demonstrate that there is a very good agreement between both dynamic flexibilities for all the 16 cases evaluated.

5.2.2 Lumped vs Novak Model for Different Pile Radius

Figures 5.14 and 5.15 show the response of both models for piles with increasing radius, ranging from 1ft to 10 ft, while maintaining fixed the rest of the data of the case study. The programs used for this purpose are included in Appendix F, section F.5. These figures verify that the agreement between both frequency response functions is excellent for all the cases evaluated.

It can also be seen that as the pile diameter becomes larger (thus increasing the pile stiffness), the FRF starts to present peaks. This situation will be analyzed in more detail in Chapter 6.

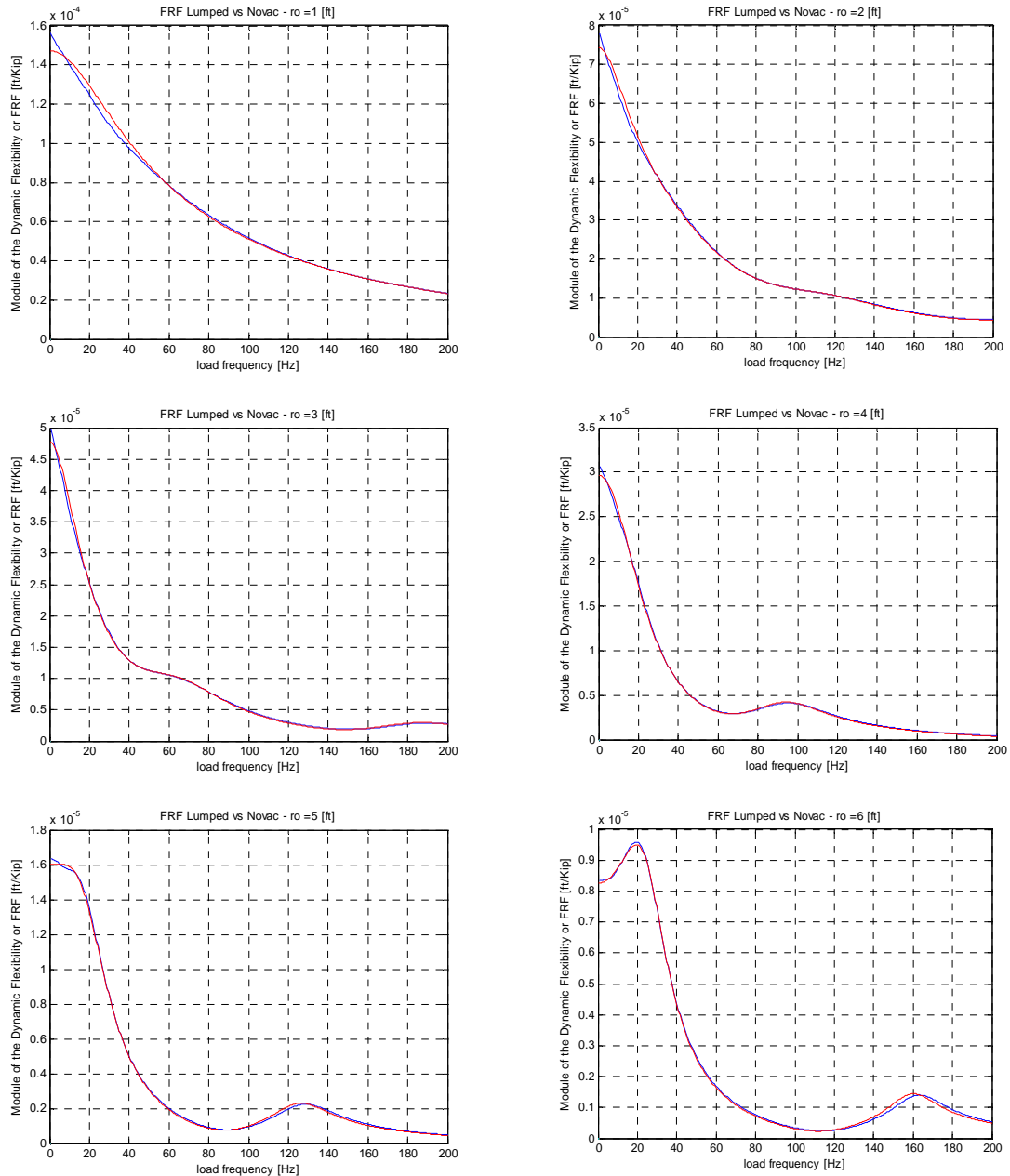


Figure 5.14: Comparison Between Lumped FRF (red) and Novak FRF (blue) for Different Pile Radius [$1.0 \text{ ft} \leq r_o \leq 6.0 \text{ ft}$]

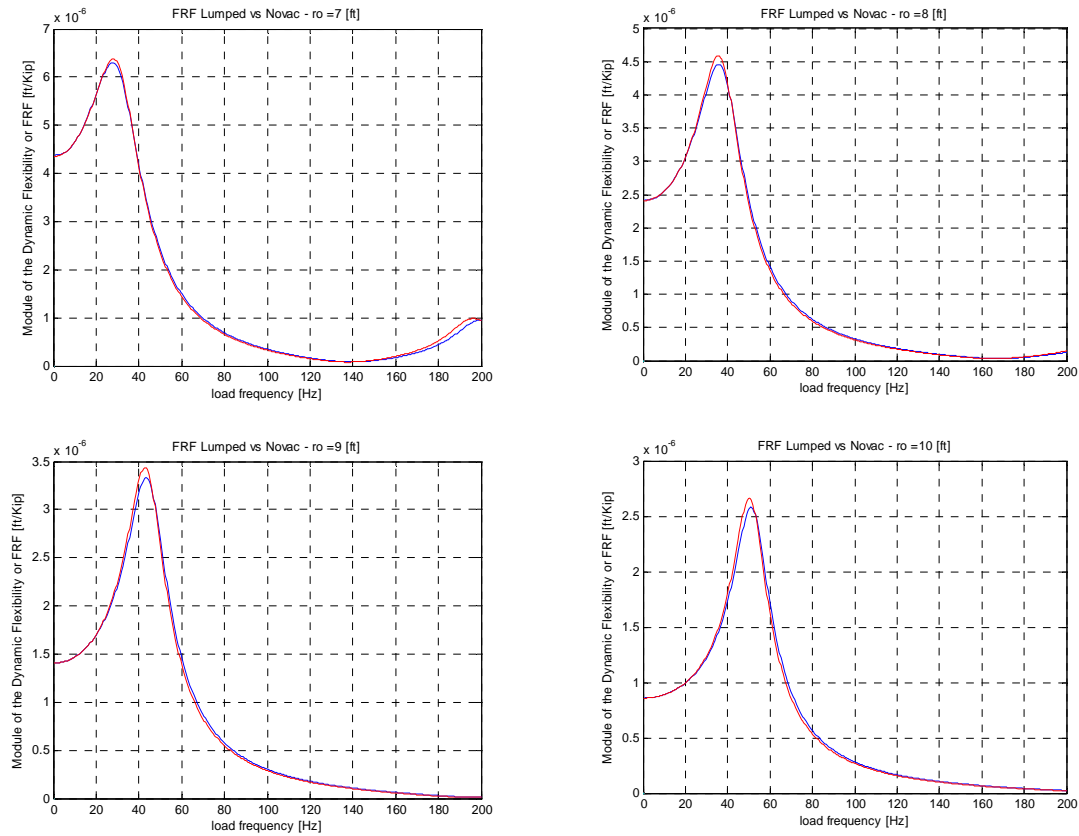


Figure 5.15: Comparison Between Lumped FRF (red) and Novak FRF (blue) for Different Pile Radius [$7.0 \text{ ft} \leq r_o \leq 10.0 \text{ ft}$]

5.2.3 Lumped vs Novak Model for Different Soil Modulus of Elasticity

Figures 5.16 and 5.17 show the modulus of the FRF calculated with both models for different soil modulus of elasticity E . The rest of the data of the case study described at the beginning of section 5.2 were not varied. The corresponding program developed for this study is listed in Appendix F, section F.6. The range for the adopted values of E was chosen to represent the usual values of Young's modulus for different soil types cited in the literature (Barkan, 1962; Bowles, 1996; Cernica, 1995; Coduto, 2001; Das, 1999; and Poulos and Davis, 1980). The range of rounded values for E is from 10 to 150 MPa ($\approx 1,500$ to 25,000 psi, $\approx 200,000$ to 3,800,000 psf).

The figures demonstrate that there is a very good match between both dynamic flexibility functions for all the cases evaluated.

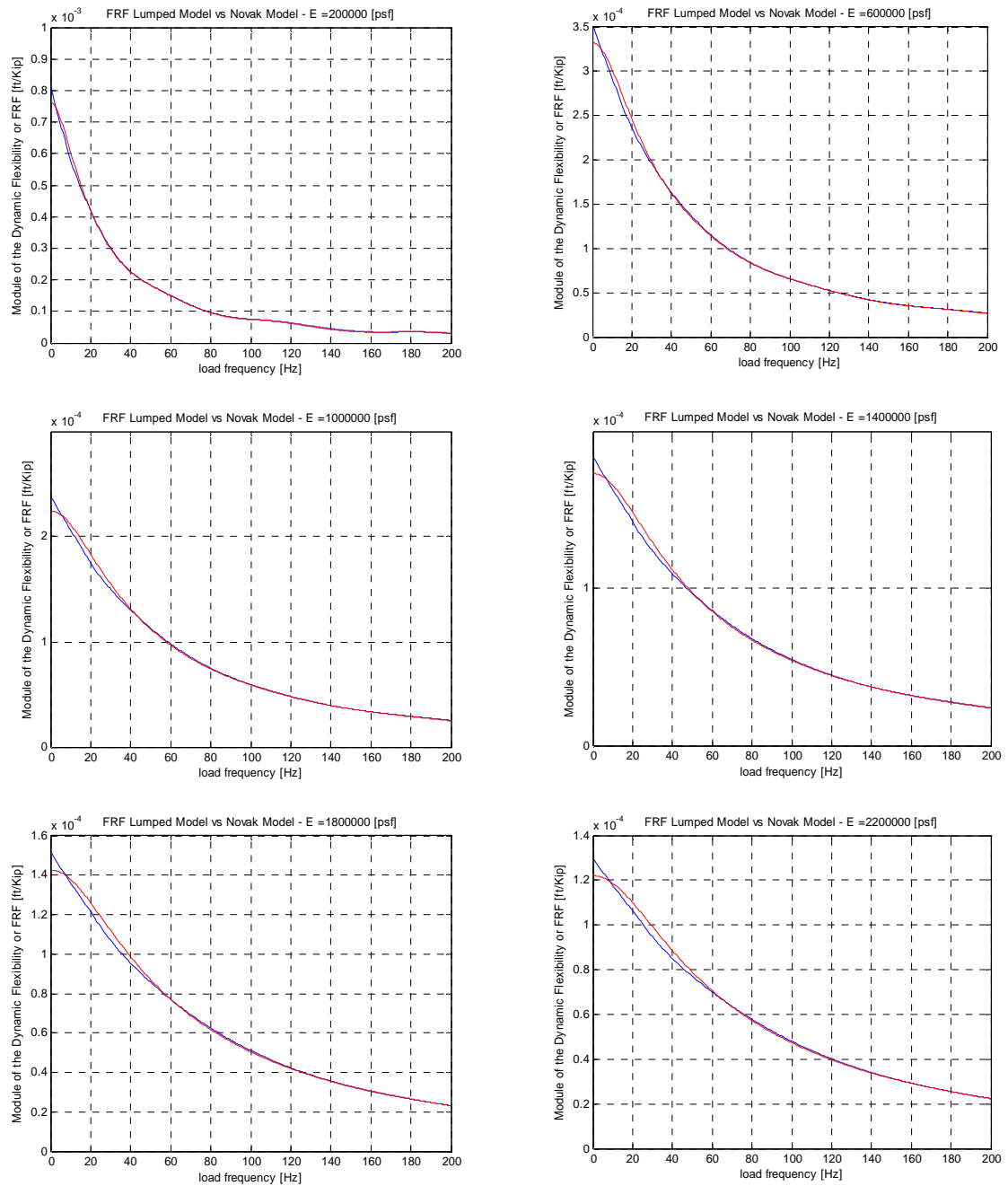


Figure 5.16: Comparison between Lumped FRF (red) and Novak FRF (blue) for Different Soil Elastic Modulus [$200 \text{ ksf} \leq E \leq 2200 \text{ ksf}$]

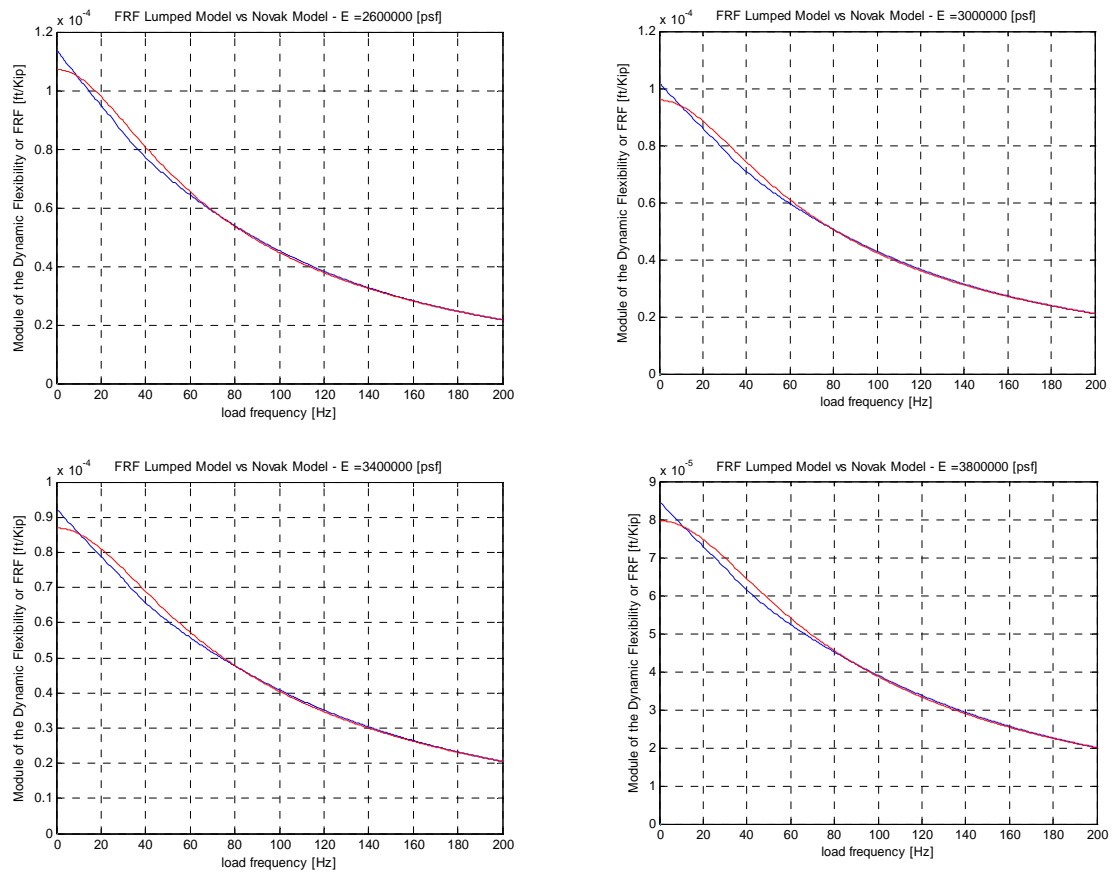


Figure 5.17: Comparison between Lumped FRF (red) and Novak FRF (blue) for Different Soil Elastic Modulus [$2600 \text{ ksf} \leq E \leq 3800 \text{ ksf}$]

5.3 1D Stiffness Method Model vs. 3D FEM Model

The case study presented in section 5.2 will be used to compare the results obtained from a 3D FE analysis and those obtained with a 1D Stiffness Method analysis (i.e. beam on elastic foundation model).

Both analyses were performed using the computer program SAP2000, in a PC with a Pentium IV processor, 3.2 Ghz of speed, 512 MB of RAM, and 143 GB of hard drive (101 GB free). This is considered, at the present moment, a robust PC for any small to midsize engineering firm (either a Structural or a Geotechnical Engineering firm).

First the 1D model using beam (frame) elements for the pile and the proposed lumped model for the soil was implemented. In order to verify the model implementation in SAP2000 (i.e definition and assignment of the link elements required to model the spring-dashpot soil elements), the results obtained with this program were compared to those obtained with routines developed in Matlab. Appendix F, section F.7, presents some of the details of the modeling process and the examples used to verify the SAP2000 results.

Figure 5.18 presents the 1D model created in SAP2000. Figure 5.19 presents the comparison of the results obtained with SAP2000 and the Matlab program: a perfect agreement between both analysis tools can be verified. This validates the selection and implementation of the link elements used in SAP2000 to model the spring-dashpot soil element. The lumped soil masses are directly assigned to the pile nodes in the SAP2000 model.

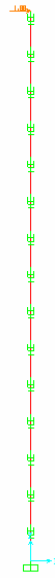


Figure 5.18: 1D Model Implemented in SAP2000

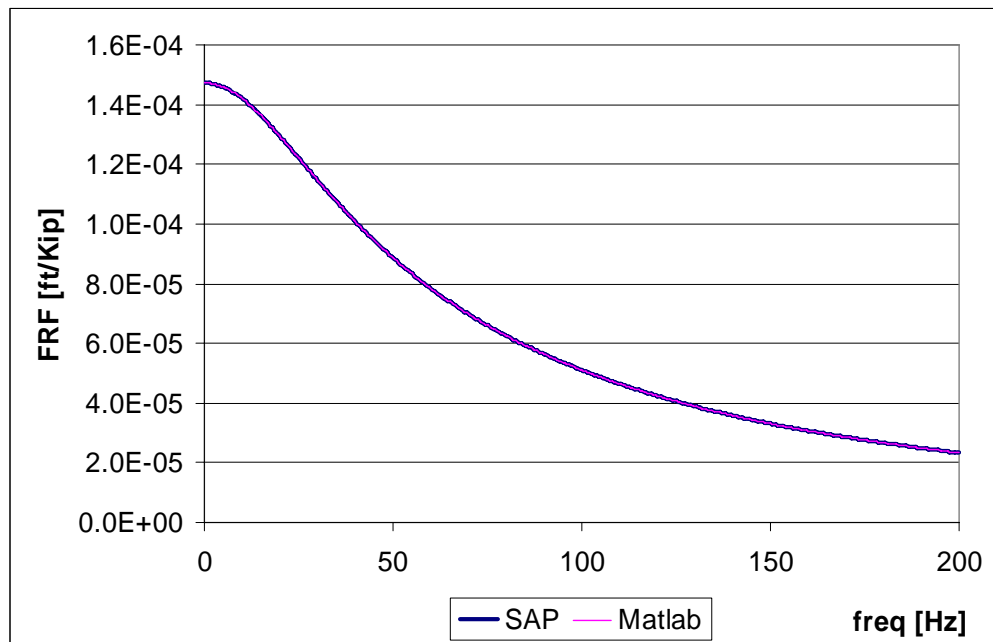


Figure 5.19: FRF of Pile Head using the 1D Model

Next a 3D FE Model was implemented in SAP2000, with a similar layout than the model presented in Chapter 3, section 3.6. Figure 5.20 shows the results of this analysis, along

with a comparison with the results obtained with the previously described 1D analysis. Figure 5.21 presents the modulus of the FRF computed with the 3D FE model and similar results obtained with the 1D model but now with a reduced damping coefficient C_a . The value adopted here for α_c is 1, instead of the value obtained from the regression analysis and used to generate Figure 5.20.

It can be seen from Figure 5.20 that the 1D model is stiffer (it has less static displacement, i.e. for zero frequency) and more damped (there are no peaks in its FRF). When a reduced damping coefficient is used for the 1D model in Figure 5.21, the first peaks of the FRFs predicted by both models are closely located. Assuming that the 3D model gives a more accurate response, this may suggest that the definition of an appropriate value for the damping coefficient is a potential research topic to extend the present project.

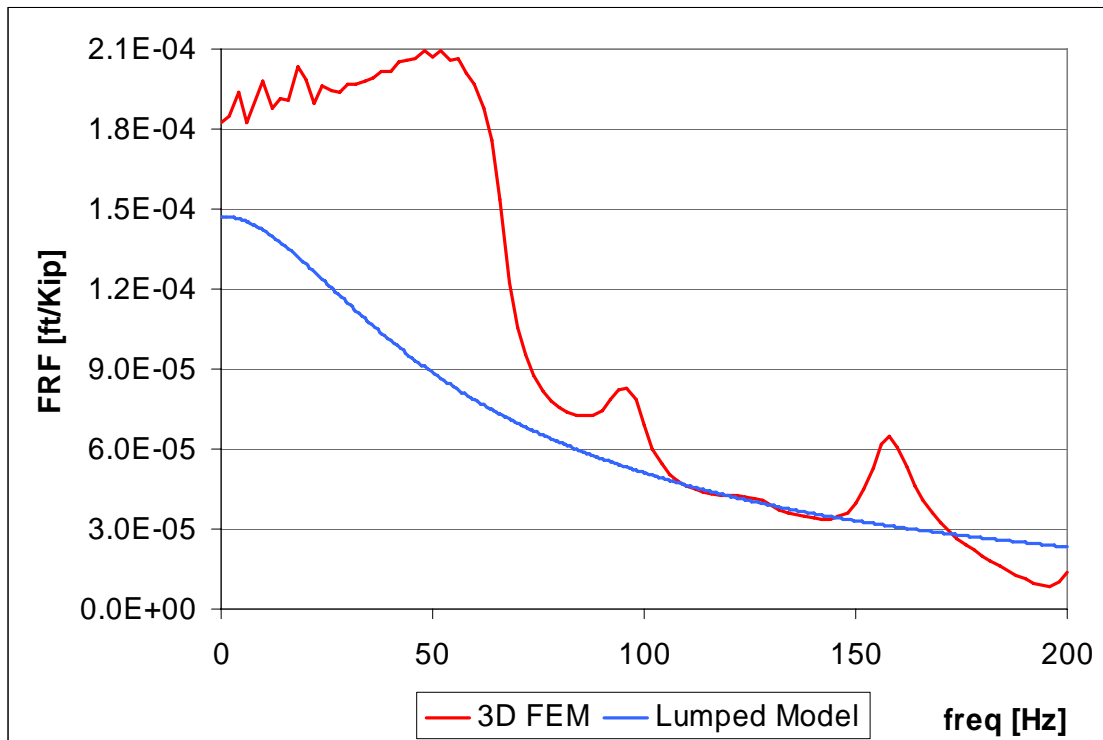


Figure 5.20: FRF of Pile Head: 3D vs. 1D Models

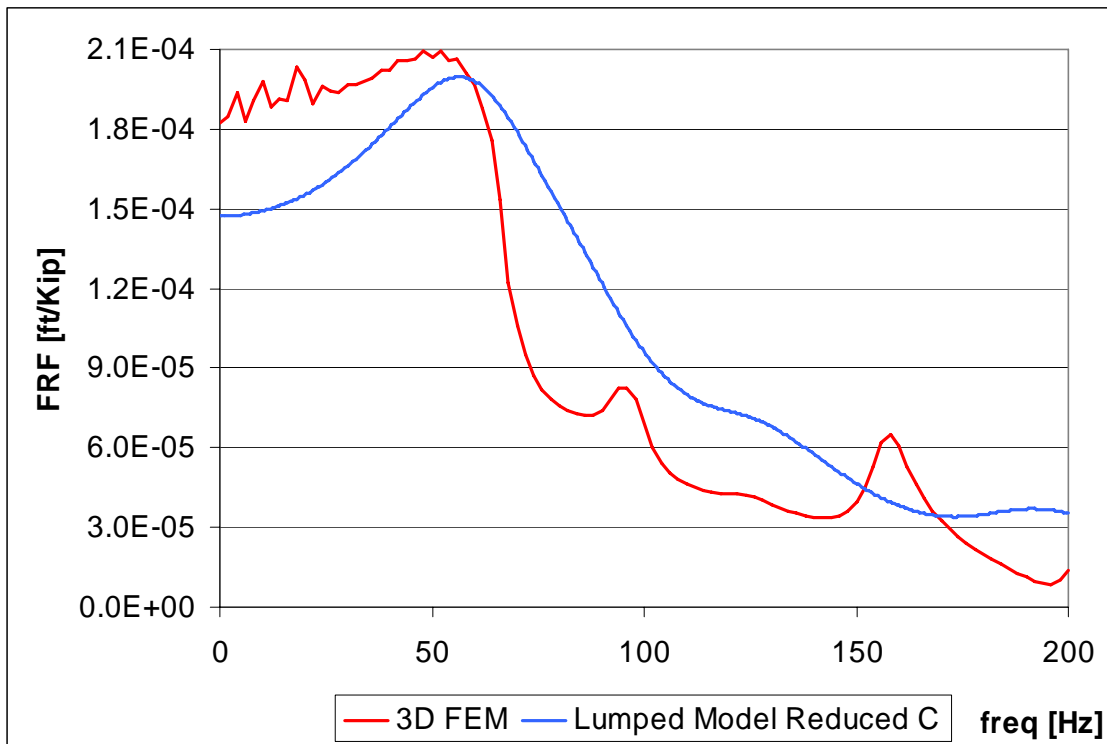


Figure 5.21: FRF of Pile Head: 3D vs. 1D Models with Reduced Damping

When performing the 3D analysis, and due to the size of the problem, to obtain the dynamic flexibility of the pile top for each frequency analyzed took more than 20 minutes with the computer system described at the beginning of section 5.3. For 100 frequency increments, the analysis lasted about 38 hours. The 1D analysis performed with 200 frequency increments took just less than 15 seconds.

The enormous difference in processing time (the 1D analysis is more than 9000 times faster than the 3D analysis), in conjunction with the reasonably predictions of the response provided by the 1D analysis for common engineering practice purposes, make the 1D analysis a valuable analysis tool.

5.4 Modeling of Experimental Pile Test with Lumped Soil Model

The ability of the lumped model to predict experimentally obtained results will be evaluated in this section. To this end the results of the dynamic tests reported by De Napoli (2006) and De Napoli and Prato (2006) will be used. The experiment consisted in applying an impulsive lateral load of small amplitude to the top of a series of piles. To apply the excitation, a pendulum mounted with a load cell was used, and an accelerometer was used to register the top pile movement, as shown in Figure 5.22.



Figure 5.22: Load Cell Fixed to the Pendulum and Accelerometer Fixed to Pile Top (De Napoli and Prato, 2006)

From the dynamic response of the pile top to the impulsive force, the dynamic stiffness of the pile head is obtained for small strains.

Figure 5.23 presents the layout of the piles tested, consisting of five piles: three piles are 30 cm and two are 35 cm in diameter, with lengths of 3 m and 5 m for the first and second group respectively. The piles were drilled on a loessic soil deposit approximately 7 years before the reported tests. The shorter piles were initially tested under static axial

compression up to failure, while the longer ones were used as tension piles to provide the reaction for the compression tests shortly after construction.

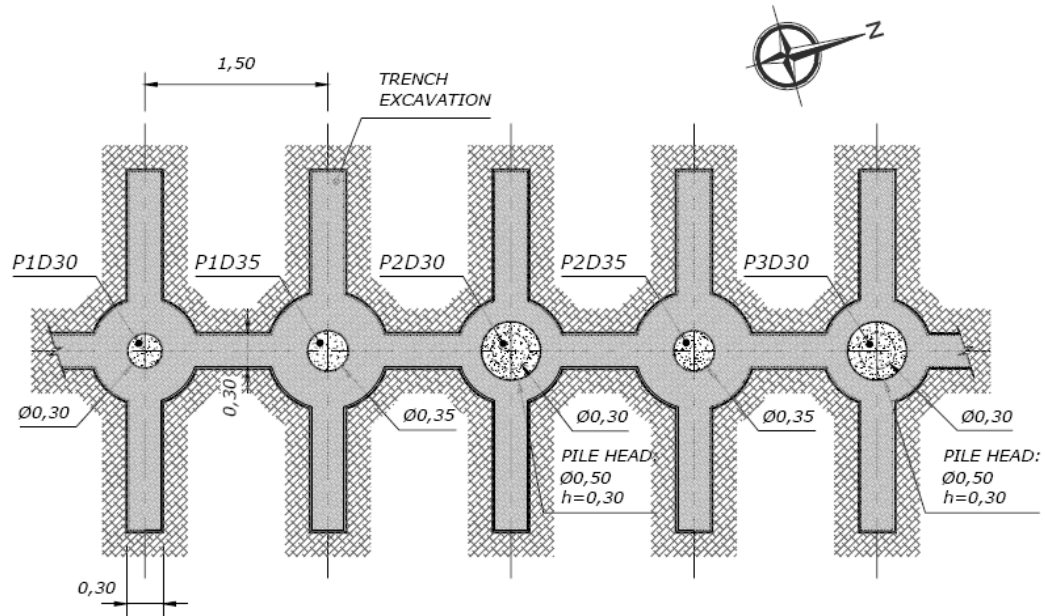


Figure 5.23: Tested Pile Group Layout (De Napoli and Prato, 2006)

De Napoli and Prato reported a good agreement with the results obtained using Novak's plane strain model for the soil (De Napoli and Prato, 2006). Therefore it was decided to compare the reported experimental results for the dynamic stiffness of pile P3D30 head (see Figure 5.23) to the results obtained with the proposed lumped model. Appendix F, section F.8, contains the Matlab program developed for this task.

The pile has a modulus of elasticity $E_p = 31,000$ MPa, a density $\rho_p = 2.4$ tn/m³, and a Poisson's ratio of $\nu_p = 0.18$. The pile cap has a 0.5 m diameter and a length of 0.3 m. The soil was removed along this depth, leaving the remainder 2.7 m pile length surrounded by the soil. The soil has a density $\rho_s = 1.55$ tn/m³, a Poisson's ratio $\nu_s = 0.31$, and an average modulus of elasticity at the surface $E_{so} = 288$ MPa.

The experimental results obtained by De Napoli and Prato for the real and imaginary part of the pile head dynamic stiffness are presented in Figure 5.24, and the predicted results

using the proposed lumped model are shown in Figure 5.25. By comparing viz-a-viz the figures it can be concluded that there is a reasonable agreement with the experimental results. The response predicted by the proposed analytical model resulted slightly stiffer and, to some extent, more damped.

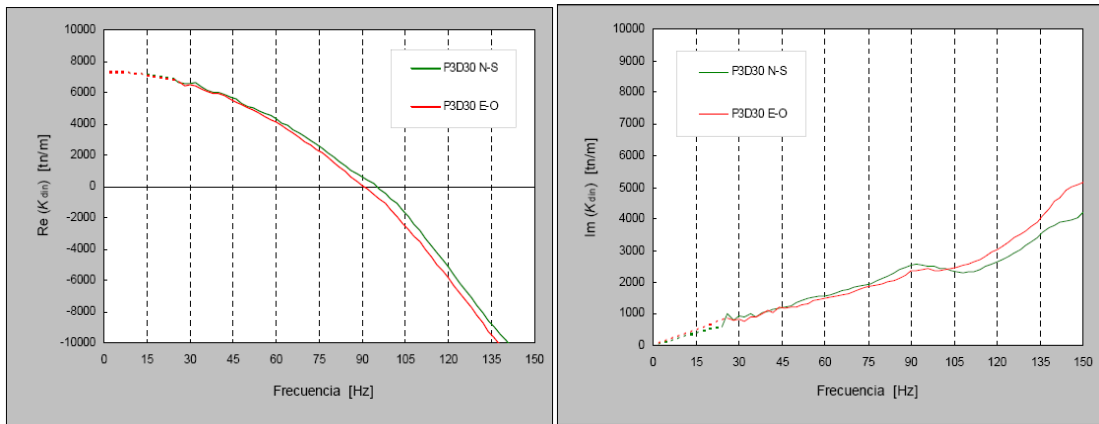


Figure 5.24: Real and Imaginary Components of the Dynamic Stiffness. Pile P3D30. Directions N-S and E-W (E-O) (De Napoli, 2006)

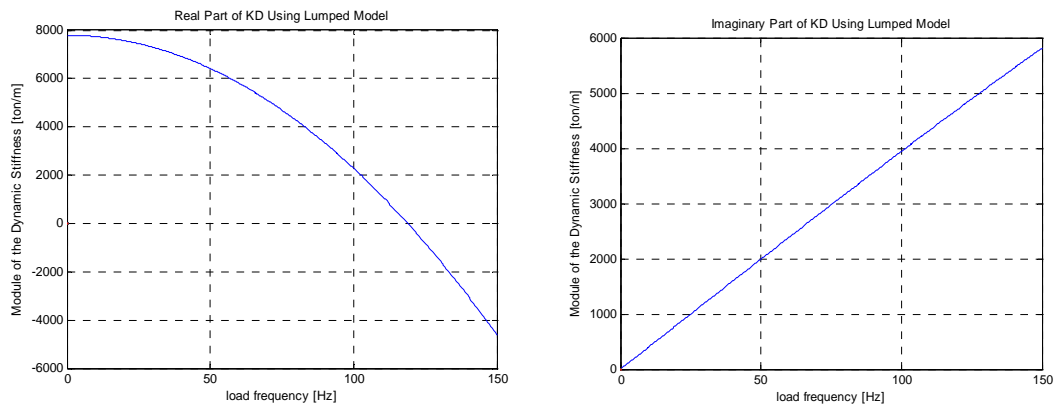


Figure 5.25: Real and Imaginary Components of the Dynamic Stiffness Obtained Numerically with the Lumped Model

5.5 The Effect of Poisson's Ratio in the 3D FE System Response

In order to evaluate if the 3D FE model presents a significant change in response as the Poisson's ratio ν increases, similar to the one obtained for the α_k , α_c , and α_m coefficients of the proposed approximated model, the FRF for the pile top was obtained for several values of soil Poisson's ratio ν , in the range of $0.0 \leq \nu \leq 0.495$. The same parameters used in section 3.6 for the soil and the pile were adopted for this analysis.

The results for the FRF corresponding to each ν value are presented in Figure 5.26. Figure 5.27 presents the variation of the static flexibility $F = FRF(\omega=0)$ of the pile top with the Poisson's ratio, and Figure 5.28 the corresponding variation of the static stiffness of the pile top $K = 1/F$. One can observe in these figures that as the Poisson's ratio increases from 0 to 0.3 the static stiffness K decreases (the FRF for $\omega = 0$, or static flexibility, increases), and the corresponding peaks of the FR functions move to the left, being this one the expected response for a system when K decreases and the mass remains constant. It also can be noted that for values of ν larger than 0.3, as ν increases the static stiffness increases, and tends to a large value as ν approaches 0.5.

The increase in stiffness as the Poisson's ratio approaches 0.5 is explained by considering the 3D stress strain relationships for normal stresses and longitudinal strains, presented in equations 5.4. It is evident that the denominator tends to infinity as ν tends to 0.5, indicating that the system becomes stiffer as ν becomes closer to 0.5.

$$\begin{aligned}\sigma_x &= \frac{E}{(1+\nu)(1-2\nu)} \left[\varepsilon_x (1-\nu) + \nu \varepsilon_y + \nu \varepsilon_z \right] = \frac{E\nu}{(1+\nu)(1-2\nu)} \left[\varepsilon_x + \varepsilon_y + \varepsilon_z \right] + 2G\varepsilon_x \\ \sigma_y &= \frac{E}{(1+\nu)(1-2\nu)} \left[\nu \varepsilon_x + (1-\nu)\varepsilon_y + \nu \varepsilon_z \right] = \frac{E\nu}{(1+\nu)(1-2\nu)} \left[\varepsilon_x + \varepsilon_y + \varepsilon_z \right] + 2G\varepsilon_y \quad (5.4) \\ \sigma_z &= \frac{E}{(1+\nu)(1-2\nu)} \left[\nu \varepsilon_x + \nu \varepsilon_y + (1-\nu)\varepsilon_z \right] = \frac{E\nu}{(1+\nu)(1-2\nu)} \left[\varepsilon_x + \varepsilon_y + \varepsilon_z \right] + 2G\varepsilon_z\end{aligned}$$

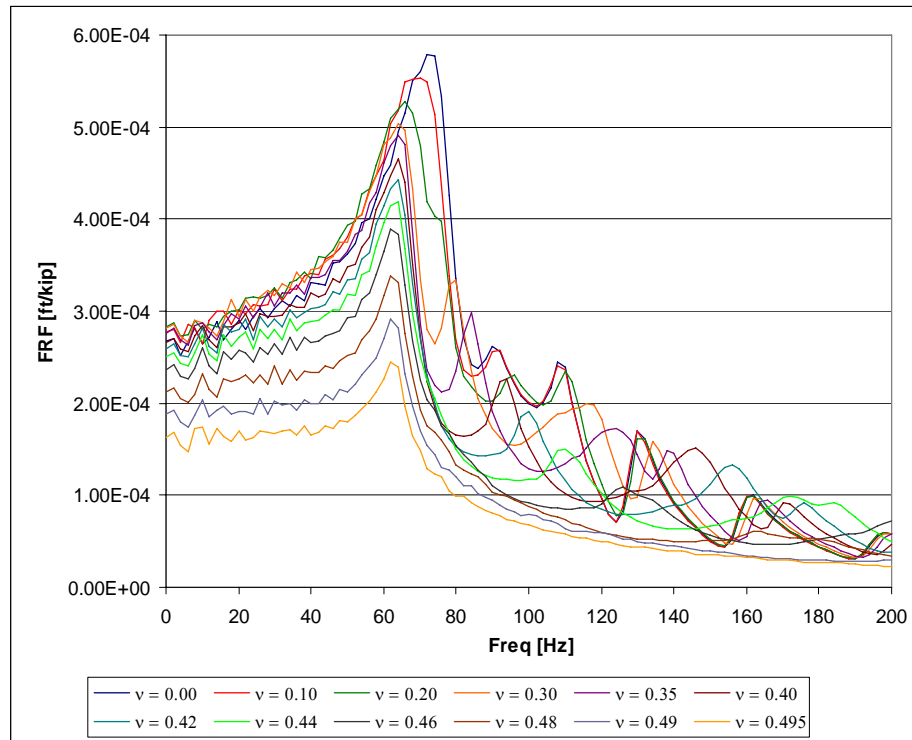


Figure 5.26: 3D FE Model FRF for Different Poisson's Ratios

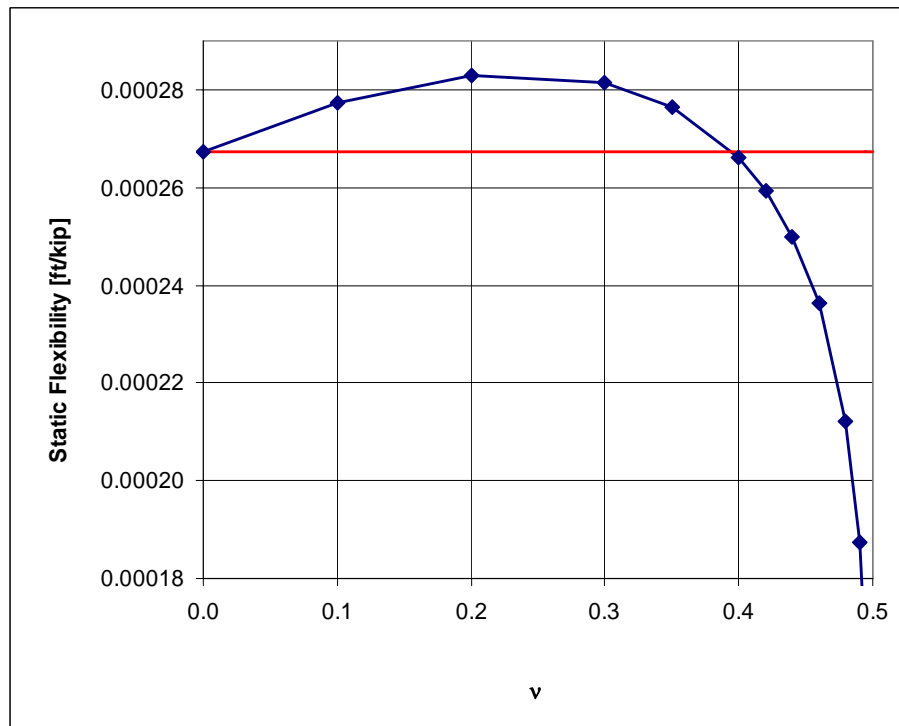


Figure 5.27: 3D FE Model Static Flexibility for Different Poisson's Ratios

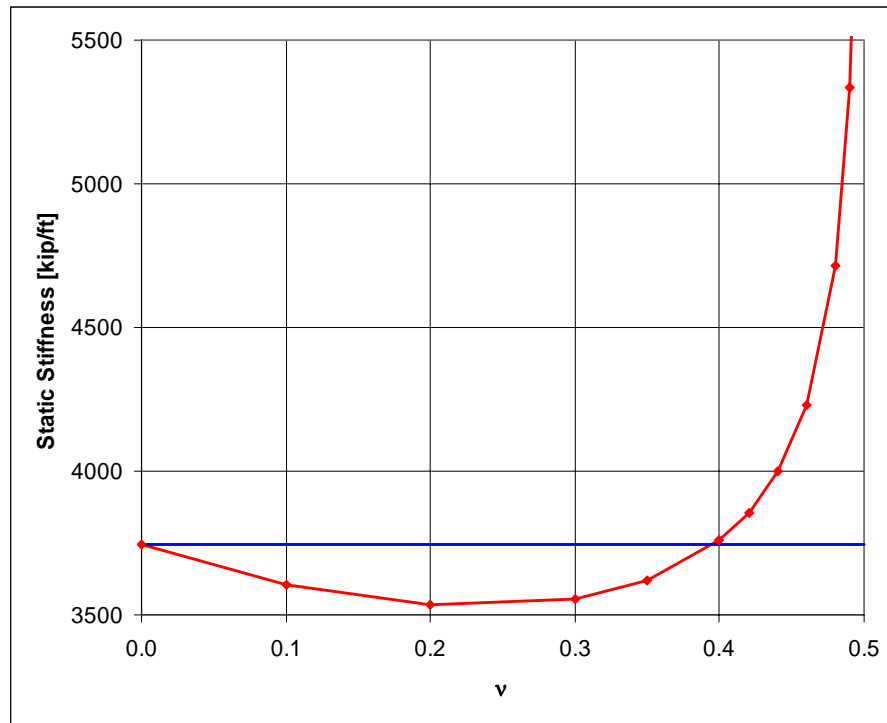


Figure 5.28: 3D FE Model Static Stiffness for Different Poisson's Ratios

By analyzing Figure 5.26 it can be noted that the Poisson's ratio has a significant impact in the system response, given through the FRF of pile top. One can also appreciate the locations of the peaks of the different FRF do not significantly vary for Poisson's ratios larger than 0.3. Considering that the stiffness K increases and knowing that the FRF peak occurs near the natural frequency, the mass M of an equivalent SDOF system should also increase as ν tends to 0.5 in order to obtain this type of behavior. The effect of the Poisson's ratio on the 3D FE model discussed before may contribute to explain the behavior of the α_m coefficient of the proposed simplified model, which has non zero values for high Poisson's ratios, indicating that the model requires an added mass for these cases.

5.6 Comparison to other Models

The equations obtained for the stiffness k_a and the damping coefficient c_a in the proposed approximated model of Novak's continuous solution will be compared to the corresponding coefficients found in the literature. In order to have a valid comparison, the models selected have to be based in the soil elastic properties (elastic modulus E , and Poisson's ratio ν) and soil density, and have to be frequency independent. The mass contribution is not compared, since this effect was not addressed in the literature.

5.6.1 Damping Coefficient

As reported by Wang et al (1998) and Gazetas and Dobry (1984a), Berger and coworkers proposed a 1-D model, assuming that the horizontal moving pile cross section only generates 1 dimensional P-waves traveling in the direction of the shaking, and 1 dimensional SH-waves traveling in the direction perpendicular to the shaking, as shown in Figure 5.29.

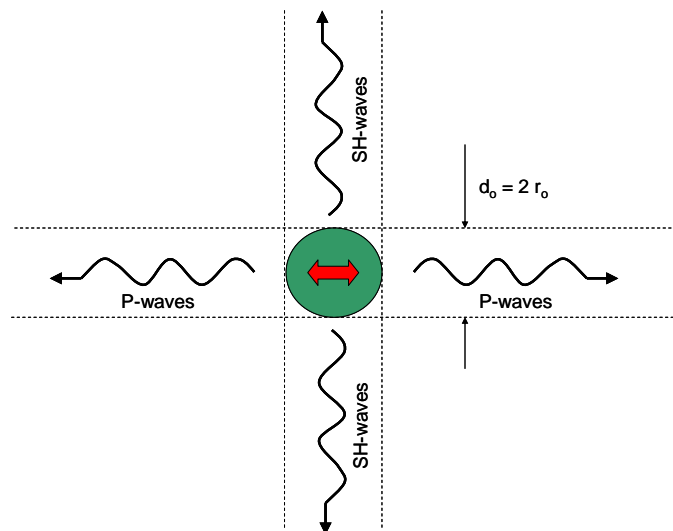


Figure 5.29: 1-D Radiation Damping Model

Based on these assumptions, the radiation damping coefficient results:

$$C_B = 2 d_o \rho (V_S + V_P) = 4 r_o \rho V_S \left(1 + \frac{V_P}{V_S} \right) \quad (5.5)$$

where:

- d_o = diameter of the pile cross section
- r_o = radius of the pile cross section
- ρ = soil mass density
- V_S = shear-wave velocity in the soil medium
- V_P = P-wave velocity in the soil medium

Considering that the P-Wave and the SH-wave velocities in a 2D or 3D continuous are given by:

$$\begin{aligned} V_P &= \sqrt{\frac{E}{\rho} \frac{(1-\nu)}{(1+\nu)(1-2\nu)}} \\ V_S &= \sqrt{\frac{G}{\rho}} = \sqrt{\frac{E}{\rho} \frac{1}{2(1+\nu)}} \end{aligned} \quad (5.6)$$

where:

- E = elastic modulus of the soil
- G = shear (rigidity) modulus of the soil
- ν = Poisson's ratio of the soil

the ratio between P-wave and S-wave velocities results:

$$\frac{V_P}{V_S} = \sqrt{\frac{2(1-\nu)}{(1-2\nu)}} \quad (5.7)$$

and the radiation damping coefficient becomes:

$$C_B = 4 r_o \rho V_S \left(1 + \sqrt{\frac{2(1-\nu)}{(1-2\nu)}} \right) \quad (5.8)$$

The ratio between the radiation damping coefficient obtained in the present study and the one proposed by Berger and coworkers is given by:

$$C_{rel} = \frac{C_a}{C_B} = \frac{\pi r_o \rho V_s \alpha_c}{4 r_o \rho V_s \left(1 + \sqrt{\frac{2(1-\nu)}{(1-2\nu)}} \right)} = \frac{\pi \alpha_c}{4 \left(1 + \sqrt{\frac{2(1-\nu)}{(1-2\nu)}} \right)} \quad (5.9)$$

This ratio is represented in Figure 5.30 for different Poisson's ratios. Appendix F, section F.9, contains the MathCad worksheet developed to perform this comparison.

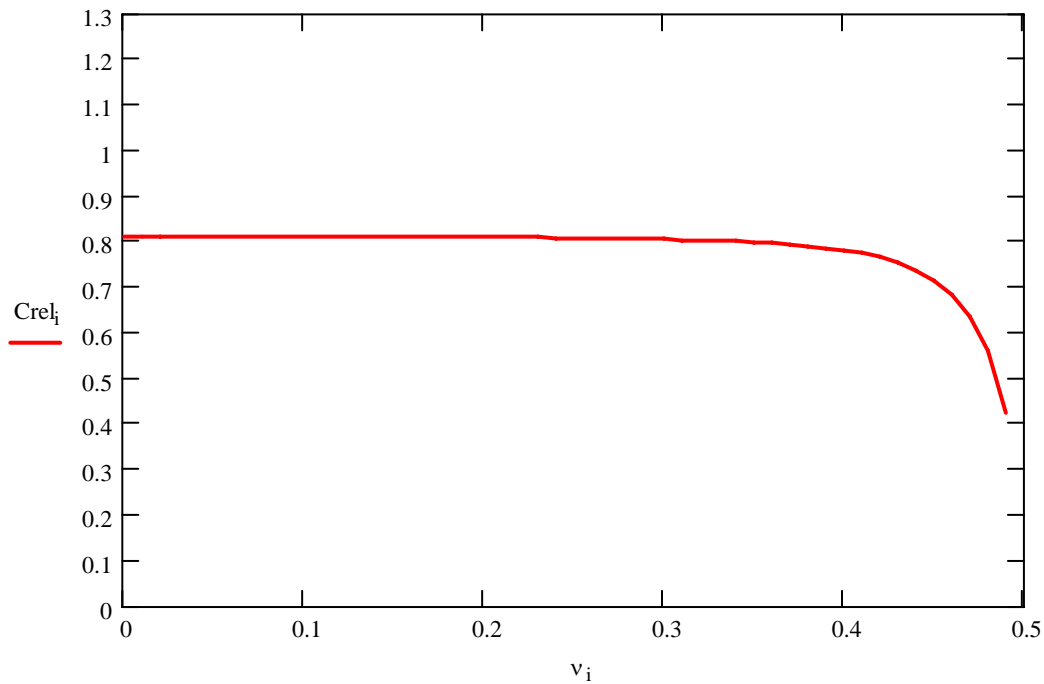


Figure 5.30: Ratio between Damping Coefficients C_a and C_B for Different Poisson's Ratio of the Soil

As shown in the figure, the proposed model estimates a damping coefficient of around 80% of the one proposed by Berger and coworkers for a wide range of Poisson's ratios; for values of ν above 0.4 the difference significantly increases since C_B tends to infinity as ν approaches 0.5. This is a drawback of Berger model, and several authors propose to accept Berger's basic expression, but using a velocity $V < V_P$ instead of V_P : Wang et al. (1998) proposed to adopt V_S instead of V_P ; Gazetas and Dobry (1984a) presented three alternatives, one of them is to adopt the P-wave velocity corresponding to the compression-extension wave propagation in an elastic rod $V_p = \sqrt{E/\rho}$. Adopting this last

approach, the resulting V_P/V_S ratio and the corresponding ratio between the radiation damping coefficients C_a/C_B are:

$$\begin{aligned}
 V_P &= \sqrt{\frac{E}{\rho}} \\
 V_S &= \sqrt{\frac{G}{\rho}} = \sqrt{\frac{E}{\rho} \frac{1}{2(1+\nu)}} \\
 \frac{V_P}{V_S} &= \sqrt{2(1+\nu)} \\
 C_{rel} &= \frac{C_a}{C_B} = \frac{\pi r_o \rho V_s \alpha_c}{4 r_o \rho V_s (1 + \sqrt{2(1+\nu)})} = \frac{\pi \alpha_c}{4(1 + \sqrt{2(1+\nu)})}
 \end{aligned} \tag{5.10}$$

This ratio is represented in Figure 5.31 for different Poisson's ratios; it can be seen that both models predict similar radiation damping coefficients for all Poisson's ratio values.

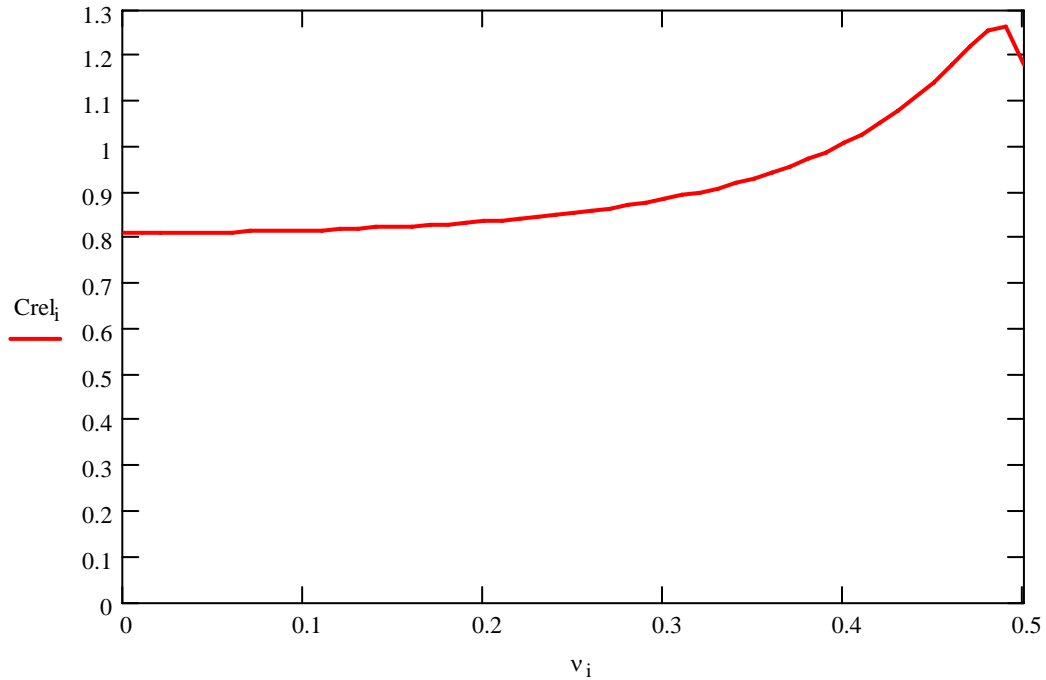


Figure 5.31: Ratio between Damping Coefficients C_a and Modified C_B for Different Poisson's Ratio of the Soil

5.6.2 Stiffness Coefficient

The coefficient of subgrade reaction for beams resting on isotropic elastic medium presented by Vesić (1961) was used for the analysis of piles under lateral loads (e.g. Poulos and Davis, 1980; Wang et al., 1998). This coefficient, representing the static stiffness of the soil per unit beam length, is given in the following equation:

$$k = 0.65 \sqrt[12]{\frac{E_s d_o^4}{E_B I_B}} \frac{E_s}{(1 - \nu_s^2)} \quad (5.11)$$

where:

E_s = modulus of elasticity of the soil

ν_s = Poisson's ratio of the soil

E_B = modulus of elasticity of the beam

I_B = moment of inertia of the beam cross section

d_o = diameter (width) of the beam cross section

Considering that this coefficient has been obtained for a beam resting on the surface of an infinite half space, and that the pile is completely surrounded by the soil, the corresponding horizontal subgrade reaction modulus for the pile will be obtained as twice the coefficient proposed by Vesić. It is important to mention than to take the subgrade reaction modulus as two times the Vesić modulus is a recommended practice for buried pipes (Klar et al., 2004). For piles with solid circular cross section the final expression becomes:

$$k_h = 2 \left[0.65 \sqrt[12]{\frac{E_s 64}{E_p \pi}} \frac{E_s}{(1 - \nu_s^2)} \right] \quad (5.12)$$

where:

E_s = modulus of elasticity of the pile

The results obtained for the static stiffness of the proposed approximated model k_a will be compared to Vesić solution, by computing the ratio $k_a/k_h = k_{rel}$. The same parameters used in section 5.2 for the pile and the soil will be adopted here:

$$E_p = 518400 \text{ [ksf]}$$

$$E_s = 1728 \text{ [ksf]}$$

$$\nu_s = 0.4$$

Figure 5.32 presents k_{rel} for different modulus of elasticity of the soil deposit in the range of 200 to 3800 [ksf], while keeping all the other parameters unchanged; Figure 5.33 presents k_{rel} for different Poisson's ratios of the soil deposit, while keeping all the other parameters unchanged; and Figures 5.34 and F.35 present k_{rel} for different modulus of elasticity of the soil deposit in the range of 200 to 3800 [ksf], three values of the modulus of elasticity of the pile (100E3, 1000E3, and 10000E3 [ksf]), while keeping constant the Poisson's ratio. Appendix F, section F.10, contains the MathCad worksheets developed to obtain these results.

It can be appreciated that the proposed model predicts, in general, a higher stiffness than Vesic's model, but in the same order of magnitude.

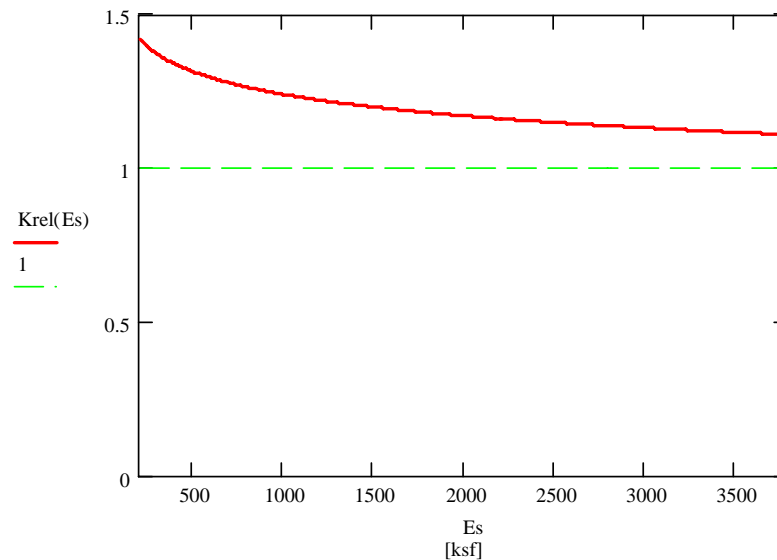


Figure 5.32: Relative Stiffness k_a/k_h for Different Modulus of Elasticity of the Soil

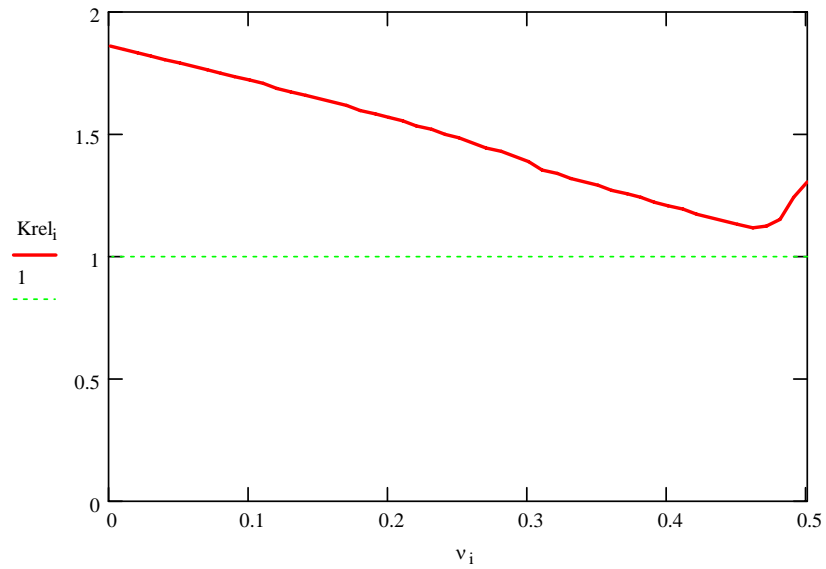


Figure 5.33: Relative Stiffness k_a/k_h for Different Poisson's Ratio of the Soil

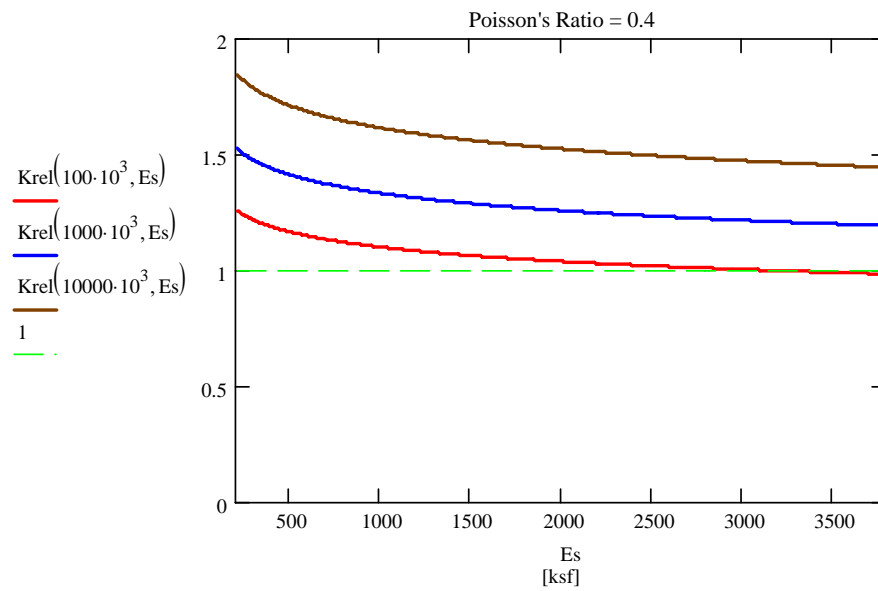


Figure 5.34: Relative Stiffness k_a/k_h for Different Modulus of Elasticity of the Soil and the Pile for Soil Poisson's Ratio $\nu = 0.4$

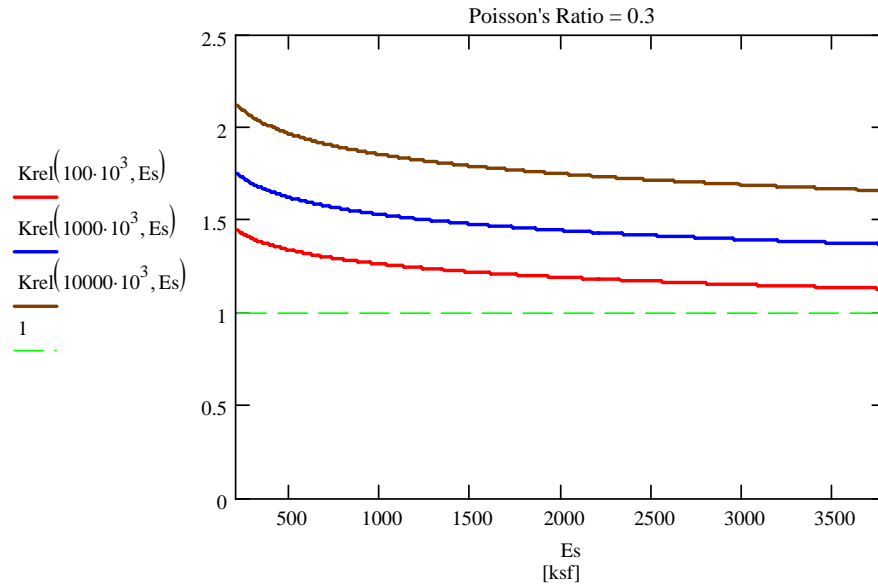


Figure 5.35: Relative Stiffness k_a/k_h for Different Modulus of Elasticity of the Soil and the Pile for Soil Poisson's Ratio $\nu = 0.3$

5.7 Final Comments

The proposed lumped model gives results (for the damping and stiffness coefficients) in the same order of magnitude of other available models, situations that strengthen its reliability. The model has also proven to be a reliable approximation of Novak's continuum model, a reasonable approximation of more rigorous approaches (i.e., FEM), and a good predictor of laboratory tests. These situations lead to the conclusion that the analysis of the model may lead to reasonable conclusions.

6 Applications of the Proposed Lumped Model

The objective of this chapter is to present a series of applications and case studies using the proposed lumped model, whose development and verification were presented in Chapter 4 and Chapter 5, respectively.

6.1 Effect of the Pile Stiffness on the System Response

In order to evaluate the effect of the pile stiffness on the system response, a series of analysis with different increasing pile radius are performed. The same case study described in section 5.2 will be used here. Figures 6.1 and 6.2 present the pile FRF and the pile-soil FRF for different pile radius, in a range of 1 ft to 10 ft. The Matlab program developed to perform this analysis is presented in Appendix G.

As mentioned in section 5.2, it can be noticed that the larger the pile diameter, the stiffer the pile, and the FRF starts to exhibit peaks. This is due to the fact that as the pile radius increases, the response starts to be controlled by the stiffness and mass properties of the pile itself rather than those of the soil. This situation becomes evident since the static displacement and the location of the FRF peaks do not appreciably change from those obtained by considering the pile alone. The effect of the soil in these cases of large diameter pile is basically to reduce and smooth the peaks of the FRF, due to the radiation damping.

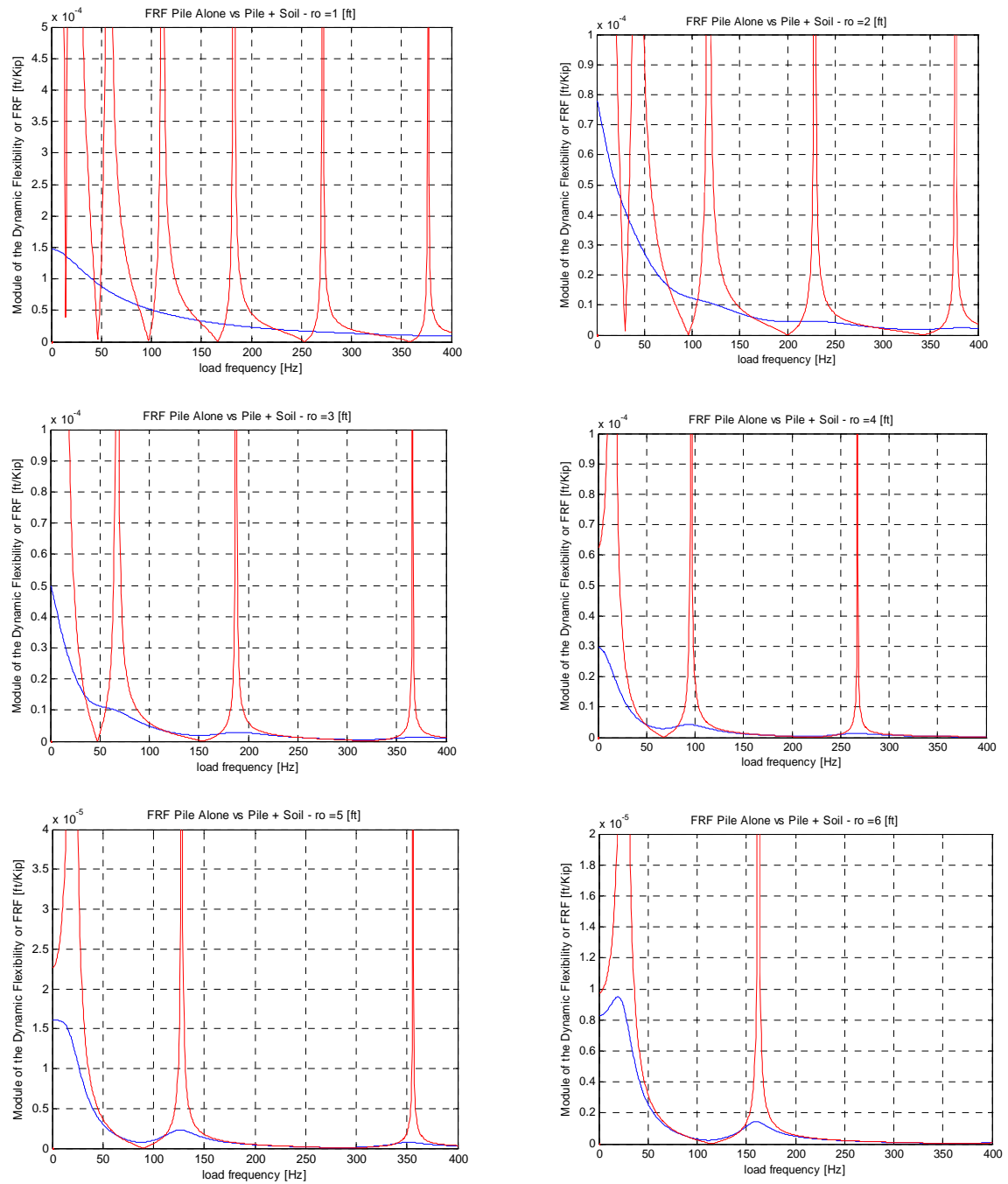


Figure 6.1: Comparison between Pile Alone FRF (red) and Pile with Soil FRF (blue) for Different Pile Radius

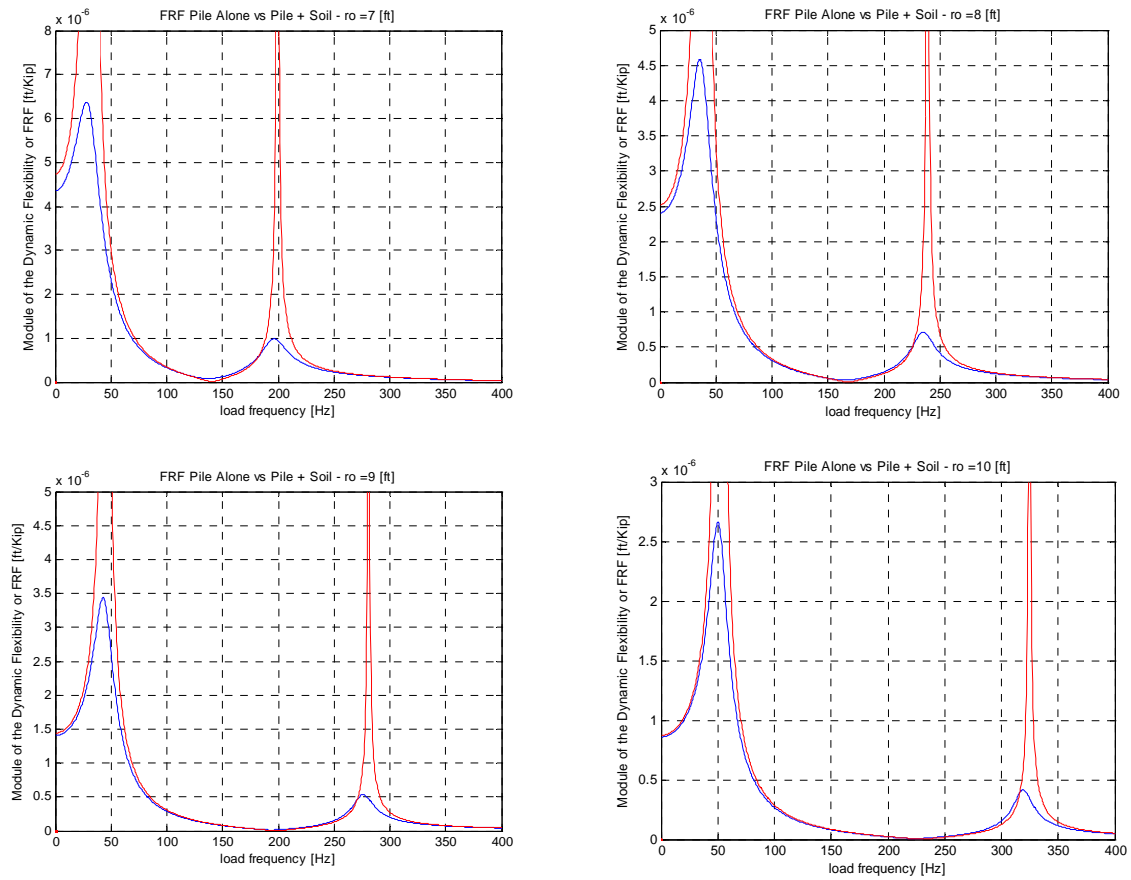


Figure 6.2: Comparison between Pile Alone FRF (red) and Pile with Soil FRF (blue) for Different Pile Radius

6.2 Effect of the Radiation Damping on the System Response

The effect of the radiation damping on the response of the pile-soil system is evaluated in this section. The FRF of the pile head for the case study presented in section 5.2 was obtained for different intensities of the radiation damping, expressed as a fraction of the lumped model damping coefficient c_a . Figure 6.3 presents the results for six different damping values: 0.0, 0.2 c_a , 0.4 c_a , 0.6 c_a , 0.8 c_a , and 1.0 c_a . Appendix H presents the Matlab program developed to compute this response.

As expected, the effect of the damping was to smoothen the peaks of the FRF, and even to eliminate them for large values of damping. Figure 6.3 also shows that the value of the damping coefficient is critical to the system response. For the case study in section 5.2, the value of the damping coefficient obtained as a regression from Novak's plain strain model leads an overdamped system, with a monotonically decreasing FRF module. As presented in sections 5.3 and 5.4, the differences in the FRFs between a 3D FE model and the 1D FE model, and between experimental and predicted results, suggest that the appropriate value of the damping coefficient is a potential research topic to extend the present project. In this way the lumped model will be able to give more accurate predictions of the system response.

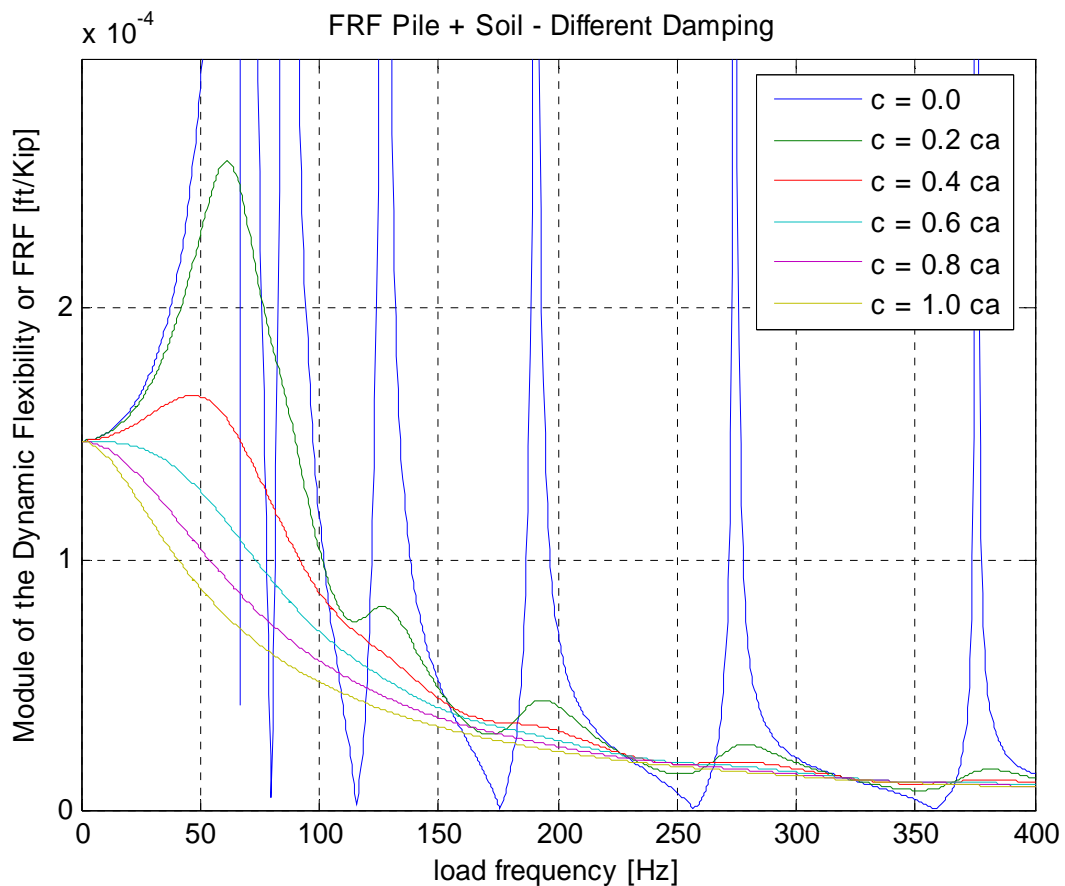


Figure 6.3: Effect of Different Damping Coefficient Value on the System FRF

6.3 Analysis of the Mass Effect on a 3D FE Model System Response

Section 3.6 presented the analysis of a case study by means of a 3D FE model. The response obtained considering and ignoring the soil mass contribution, originally presented in Figure 3.14, is reproduced here in Figure 6.4.

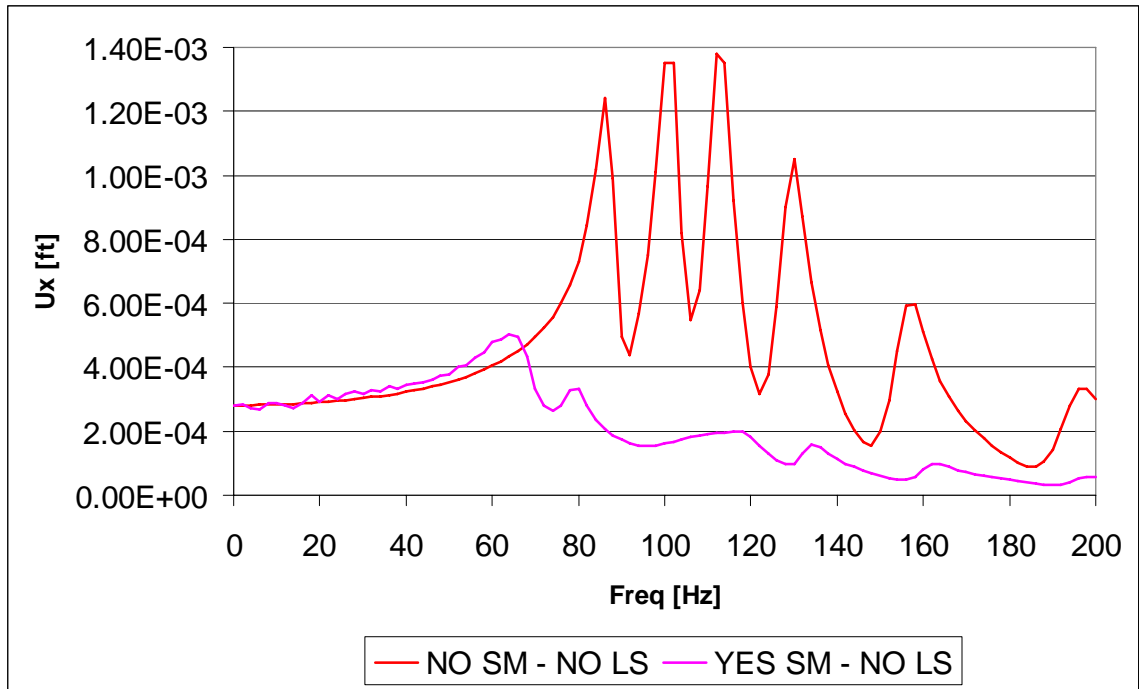


Figure 6.4: FRF for the 3D Model with and without Soil Mass, and no Lateral Supports

This analysis was performed without dashpots in the cutoff boundaries, and considering a material damping represented by a complex elastic modulus equal to $E (1 + 5/100 i)$, where E is the (small strain) soil elastic modulus. As discussed in section 3.6.4, Figure 6.4 indicates that, for this case study, the general effect of including the soil mass in the 3D FE analysis was to produce a damped like response (as compared to the response without soil mass). It is evident that the FRF peaks were smothered and there was a shift in their location to the left (at least in the first two peaks).

The objective of the study presented in the following sections is to evaluate if this type of response may be achieved with a 1D analysis, by representing the soil not as a single spring and a lumped mass added to the pile mass, but as a series of springs with lumped masses at the connecting nodes, to simulate the spatial distribution of the soil mass.

A series of analysis will be performed. First, the effect of the mass distribution will be analyzed for a single spring, by replacing the spring by a set of series and parallel springs. Then, the effect will be evaluated for a pile-soil interaction, where the spring is replaced by a series of springs. The programs developed to carry out these studies are presented in Appendix I.

6.3.1 Effect of the Mass Distribution on a System of Springs in Series

The first example analyzed consists of a single degree of freedom (SDOF) system (that may represent a single soil layer in plane strain). The SDOF has a spring of stiffness constant “ K ” equal to 1000, mass “ m ” equal to 10, and an added mass “ m_a ” equal to 50, all in consistent units. The effect of the added mass directly assigned to the mass node, and distributed among different series spring nodes is evaluated, as schematized in Figure 6.5. The single spring is replaced by “ n ” springs in series, of stiffness constant equal to “ nK ”, in order to obtain the same static stiffness than the single spring, where “ n ” was taken equal to 10.

The results of the analysis of these systems, in terms of the dynamic flexibility or frequency response function “FRF” (steady state horizontal displacement of the mass “ m ” due to unit horizontal harmonic load applied at this point) are presented in Figure 6.6, where:

- “ m, K ” corresponds to the single spring without added mass
- “ $m+m_a, K$ ” corresponds to the single spring with added mass
- “ $m+m_a, n K$ ” corresponds to the equivalent series spring, with the added mass distributed among the spring nodes.

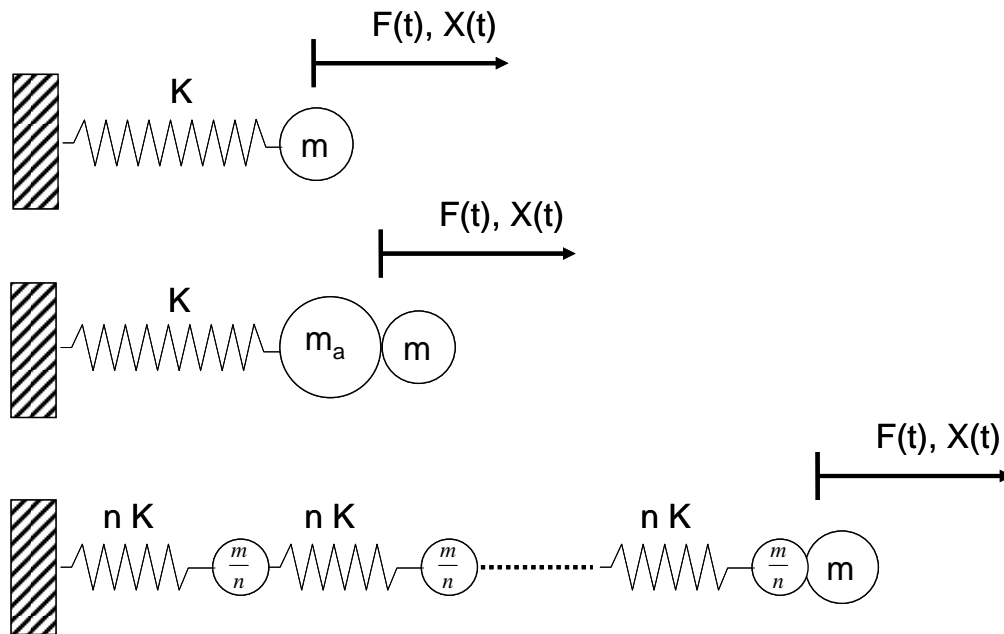


Figure 6.5: Models used to Analyze the Effect of the Added Mass in a System of Springs in Series

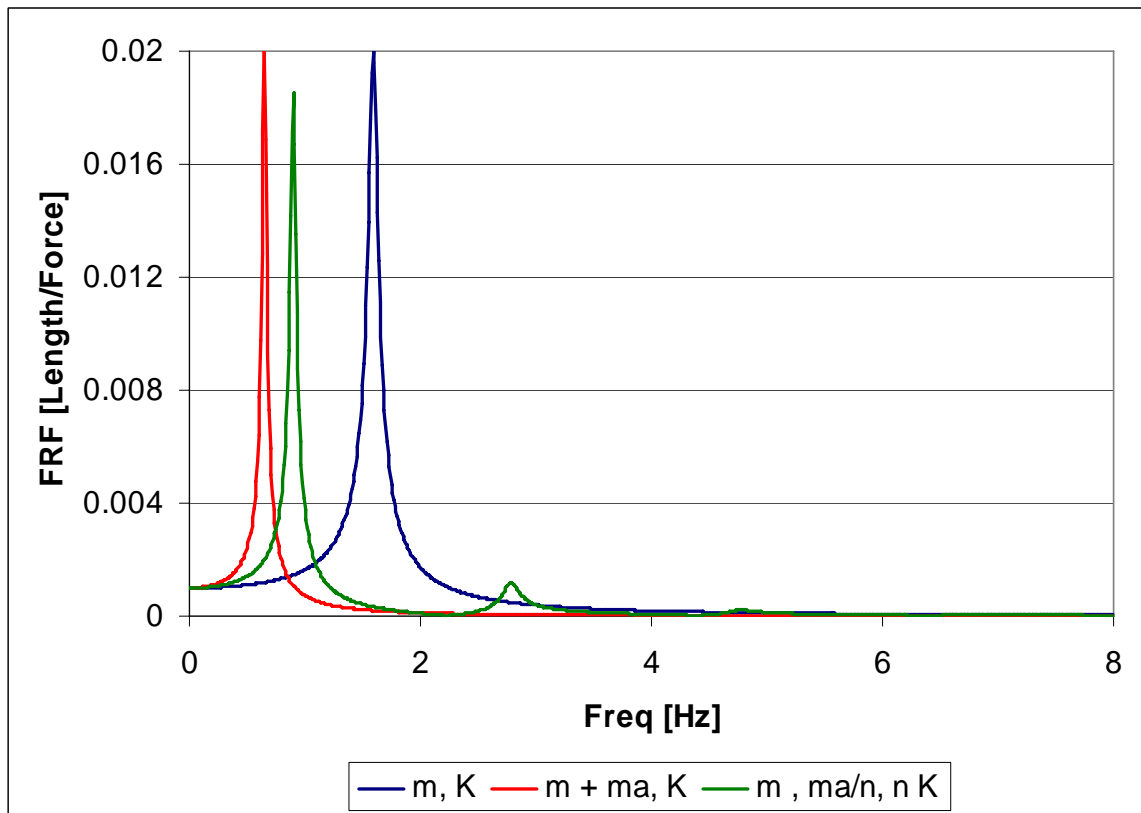


Figure 6.6: Effect of the Mass Distribution in a System of Springs in Series

These results indicate that the effect of the added mass, as expected, is to produce a shift of the natural frequency to the left (lower natural frequency). The effect of the added mass distribution along a series of springs is to increase this natural frequency, and give rise to new peaks of the FRF (corresponding to the higher natural frequencies that appear due to the multiple DOF of the system), but this model does not produce an effect equivalent to a damper, as found in a 3D FEM analysis due to the 3D mass distribution.

6.3.2 Effect of the Mass Distribution on a MDOF System

The second example analyzed consists of a SDOF system having a spring stiffness constant “ K ” equal to 1000, mass “ m ” equal to 10, and an added mass “ m_a ” equal to 50. The effect of the added mass directly assigned to the mass node, and distributed among different parallel spring nodes is evaluated, as schematized in Figure 6.7, where the single spring is replaced by “ n ” springs in series, on both sides of the mass “ m ”, of stiffness constant equal to “ $n K / 2$ ”, and a variable number of springs in parallel (np), with stiffness constant equal to “ $n K / 2 (np+1)$ ”, in order to obtain the same static stiffness than the single spring, where “ n ” was taken equal to 2 and np was varied from 1 to 6.

The results of the analysis of these systems, in terms of the dynamic flexibility or frequency response function “FRF” (steady state horizontal displacement of the mass “ m ” due to unit horizontal harmonic load applied at this point) are presented in Figure 6.8, where:

- “No m_a ” corresponds to the single spring without added mass
- “ m_a ” corresponds to the single spring with the added mass
- “ m_a i P ” corresponds to the series of 2 springs to each side of mass “ m ”, and “ i ” parallel (P) springs (as depicted in Figure 6.7), with the added mass “ m_a ” distributed among spring nodes.

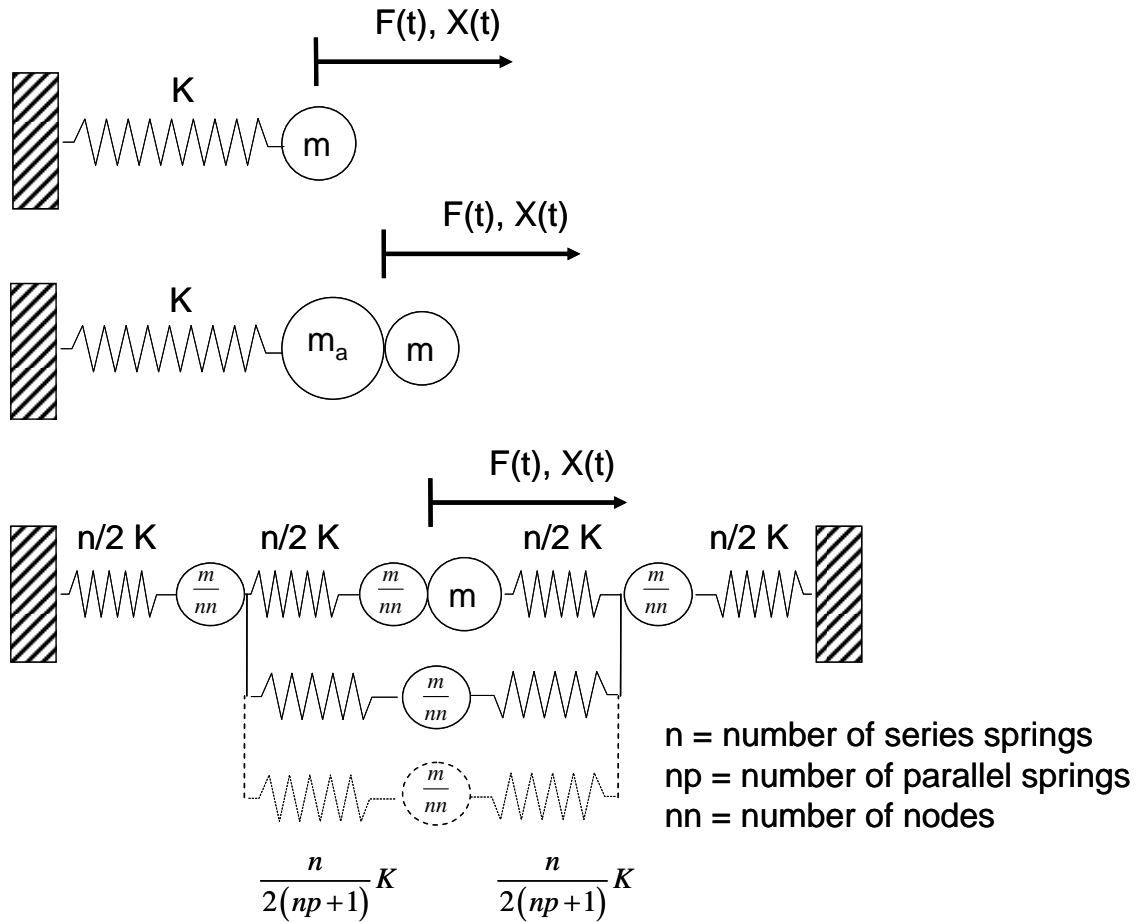


Figure 6.7: Models used to Analyze the Effect of the Added Mass in a System of Springs in Parallel

The results indicate that the addition of parallel springs produce an effect similar to damping, since the first peak of the FRF is reduced. This may be explained by the fact that the parallel springs provide alternate paths so the waves (energy) that are generated due to the vibration of mass “ m ” may travel in the system without returning to this point, producing a phenomenon similar to the radiation damping, which may be called *propagation damping*. The figure also shows that second peak of the FRF, corresponding to the system without added mass (mass “ m ” alone) is accentuated.

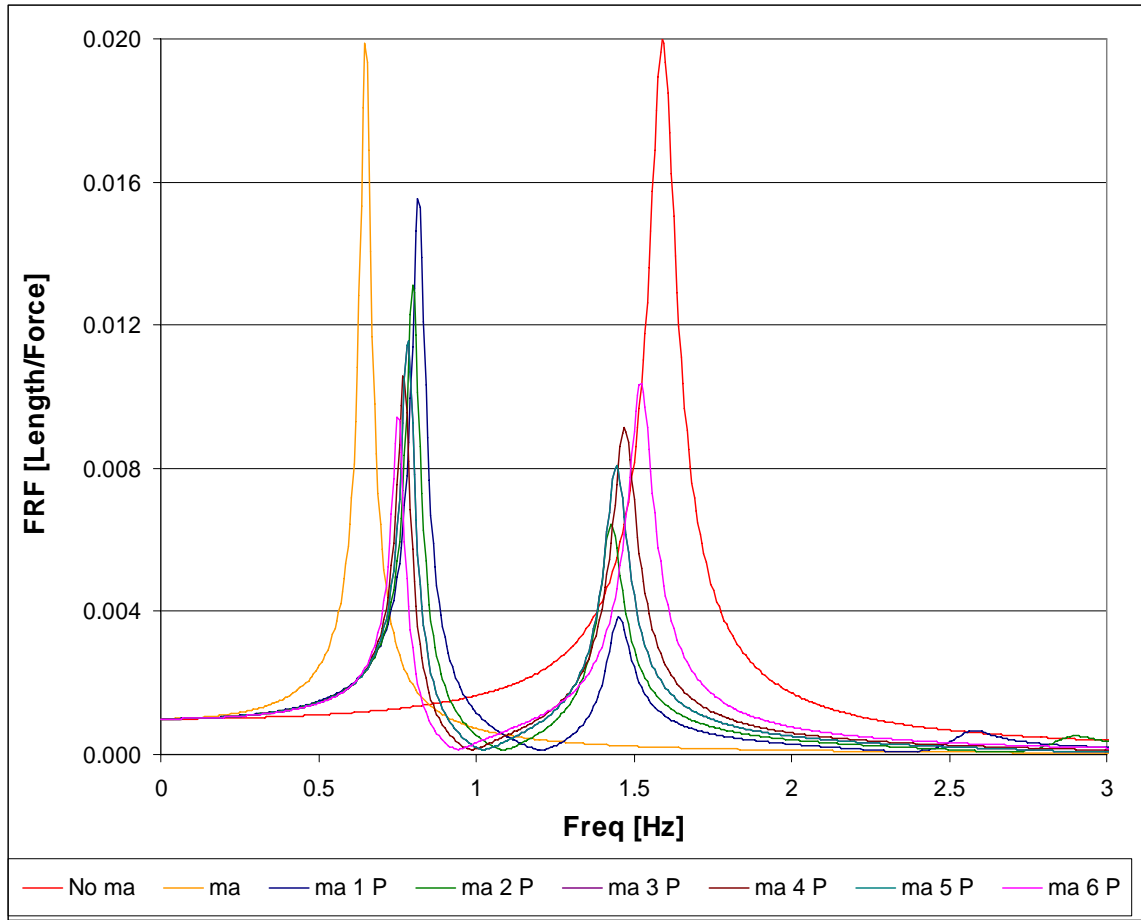


Figure 6.8: Effect of the Mass Distribution in a System of Springs in Parallel

6.3.3 Effect of the Mass Distribution on a Pile-Soil System

Finally, a pile-soil system will be analyzed, in which the contribution of the soil will be accounted for as a set of several parallel layers each represented by a spring and a mass. The effect of considering a single spring with the lumped parameters proposed in Chapter 4 (Figure 6.9 top), versus considering the soil layer as a series of springs with distributed added soil mass (Figure 6.9 bottom) will be evaluated first. Next the soil layers will be represented as a set of parallel springs with the added mass distributed on the spring nodes (similar to the scheme presented in Figure 6.7). The different spring layouts will have an equivalent condensed stiffness equal to the one obtained in Chapter 4 in the

proposed lumped model, and the soil mass to be distributed among spring nodes will be taken from the 3D FE analysis with partial soil mass presented in section 6.3. The case of adding this mass with a single spring is also considered.

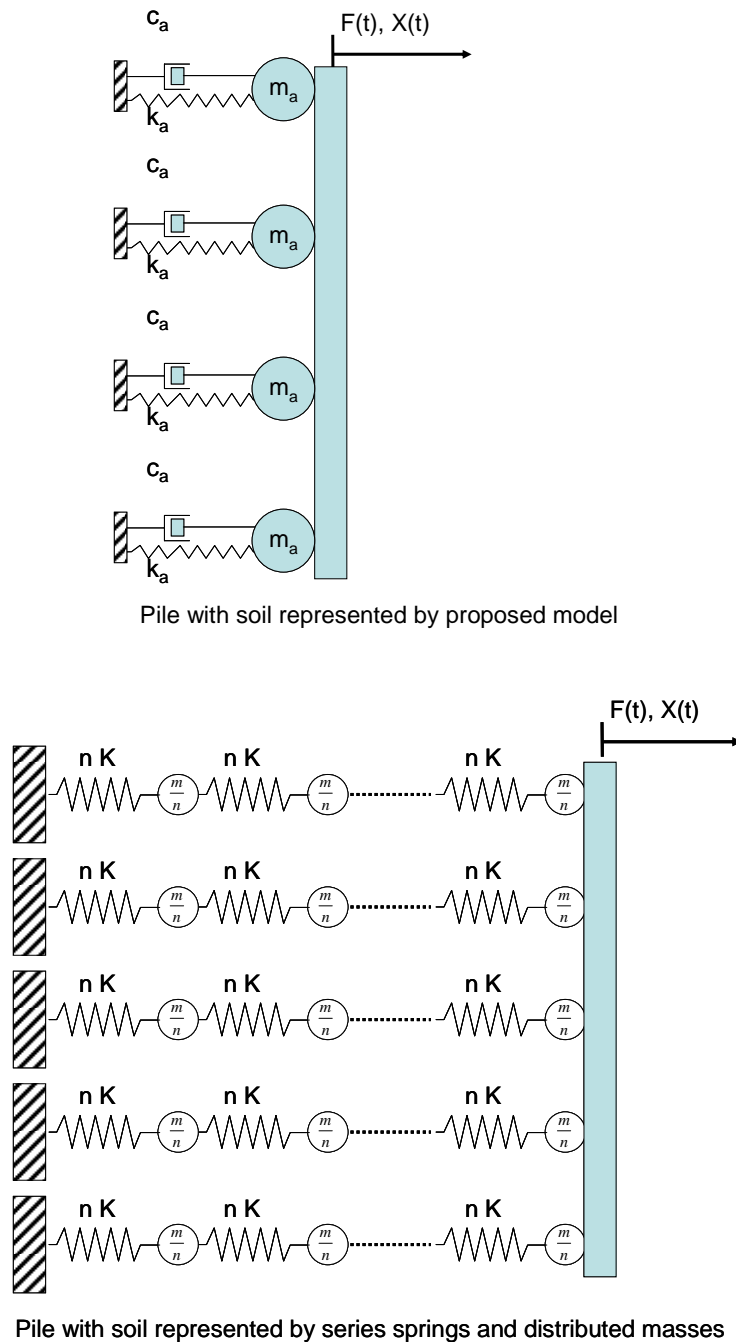


Figure 6.9: Piles Models to be Analyzed

The same set of data used in Section 5.3 to present a comparison between a 3D FE analysis and the proposed lumped model will be used. The number of series and parallel springs was taken equal to twenty; the results obtained were similar to the ones obtained with ten springs. A complex elastic modulus $E (1+0.05i)$ was assigned to the pile and soil.

Figure 6.10 presents the results of the analysis of the pile alone, i.e. without the soil contribution. Figure 6.11 presents the results for the pile with the soil contribution and an added soil mass about 40 times the pile mass. Figure 6.12 presents similar results for an added soil mass of about 100 times the pile mass. The following nomenclature applies for Figures 6.11 and 6.12:

- PLM = Pile with the soil represented by the proposed lumped model developed in Chapter 4 (as a reference response).
- SS DM = Pile with the soil represented by springs in series and an added mass distributed among the spring nodes.
- PS DM = Pile with the soil represented by a set of parallel springs and an added mass distributed among the spring nodes.
- 1S LM = Pile with the soil represented by single springs and added masses lumped at each pile node.
- 1S = Pile with the soil represented by single springs and no added masses.

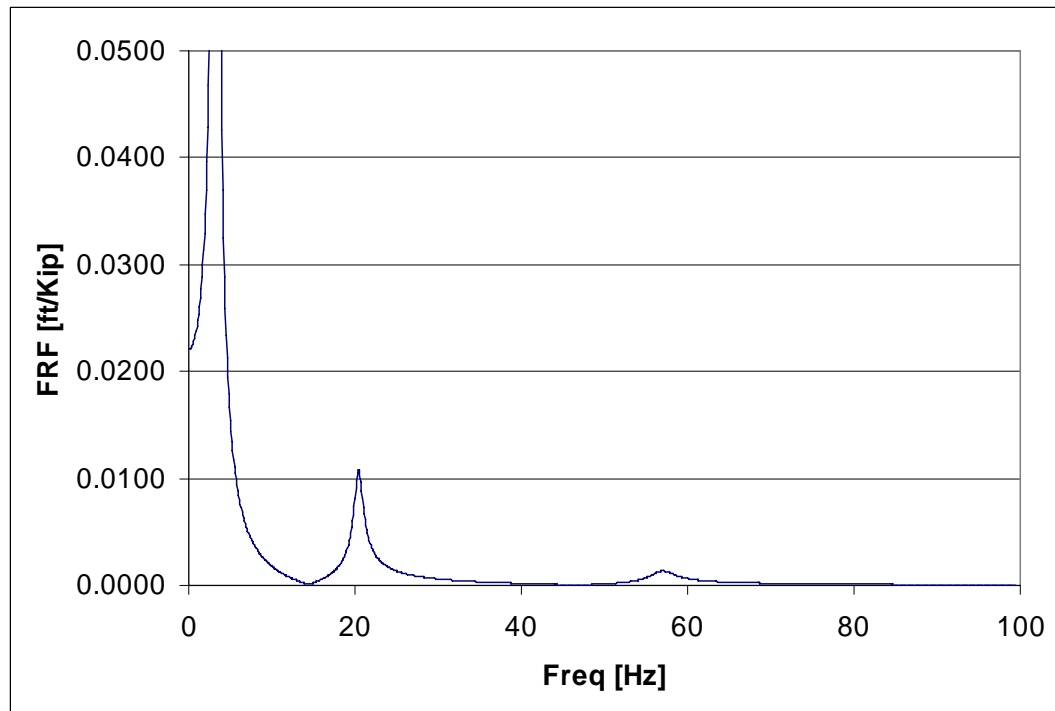


Figure 6.10: FRF of the Pile without Soil Contribution

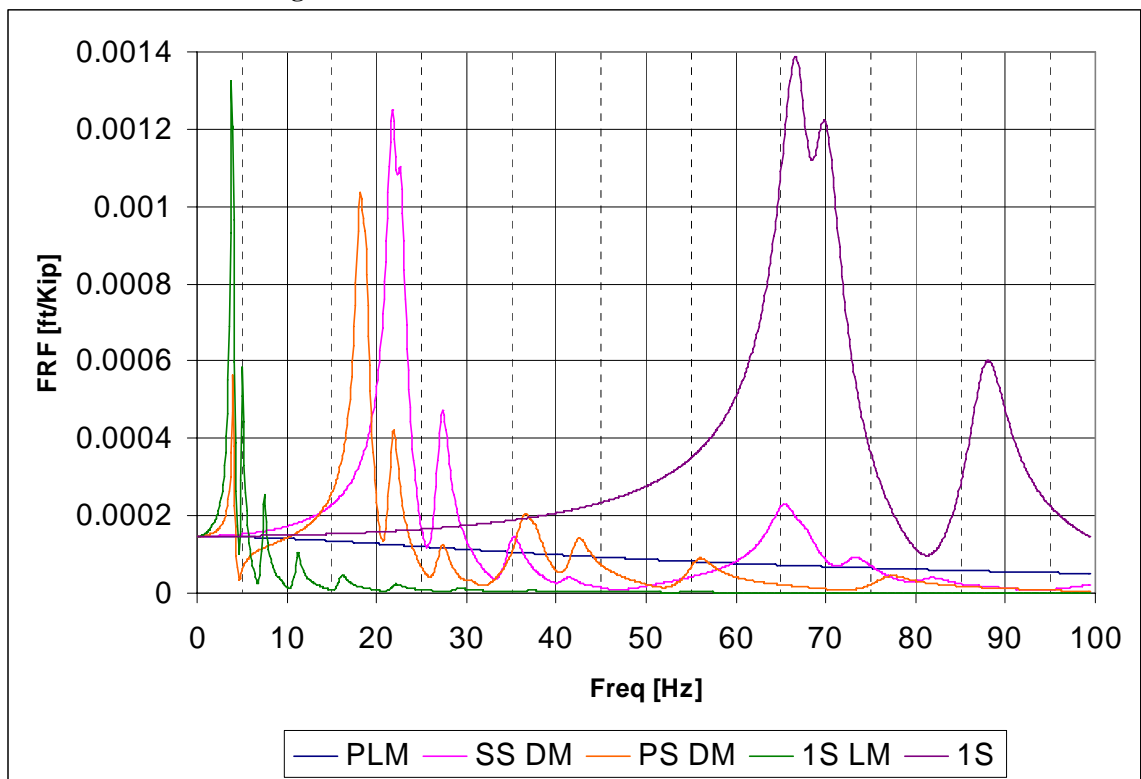


Figure 6.11: FRF of the Pile with Soil Contribution. $Ma \approx 10$ Mp

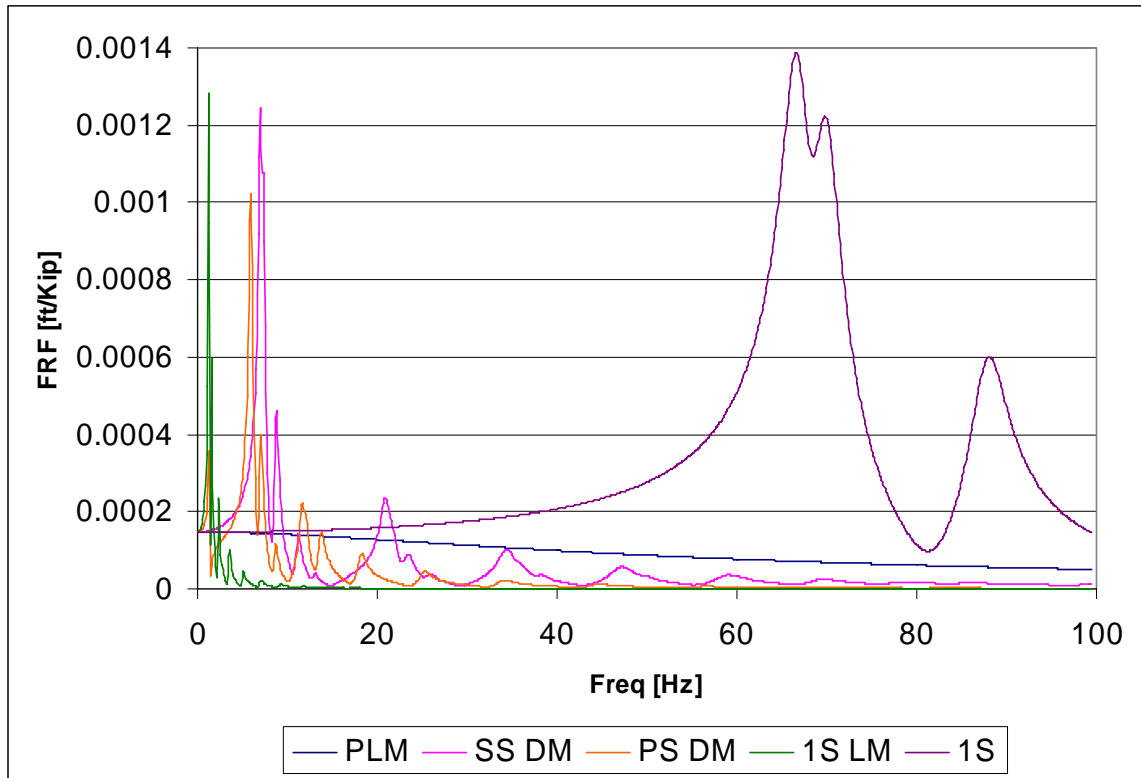


Figure 6.12: FRF of the Pile with Soil Contribution. $M_a \approx 100$ Mp

The analysis of Figures 6.10, 6.11 and 6.12 reveals that the effect of the soil stiffness is to drastically reduce the system response and increase the value of the natural frequencies (the peaks of the FRF are shifted to the right). The added mass produces a reduction of the natural frequencies (the peaks of the FRF are shifted to the left; in a region similar to the pile alone for this case study), a narrowing of the FRF peaks, and a reduction of the FRF peak values (more pronounced at high frequencies), giving a damped-like response, more evident for the set of parallel springs. But this damped-like response is not as drastic as in the 3D FEM model, probably due to the fact that the soil was modeled as a set of unconnected layers, lacking the real 3D nature of wave propagation (and hence, piles response attenuation).

6.3.4 Discussion of the Results – FE Model Propagation Damping

It is well known that the *radiation damping* represents the energy carried away by the elastic waves generated at the pile-soil interface radiated to infinity and hence not returning to the interface. The damping-like response observed in the 3D FE model may be the result of the waves generated at the soil-pile interface that travel within the soil mass, without returning to the pile. In a numerical model the waves keep traveling within the soil mass after reflecting in the model edges. Therefore, they create an effect that may be called *propagation damping*. To have this type of response, the model should have alternate paths that allow the waves to propagate within the system without returning to the interface, as provided by the parallel springs presented in Section 6.3.2 for a one layer system. The analysis presented in Section 6.3.3 reveals that it is not possible to obtain this type of response with a relative simple layout of springs and a distributed soil mass along spring nodes, so the simplified pile-soil model where the soil is replaced by an equivalent spring-mass-dashpot element should always include the dashpot to account for this phenomenon.

In order to gain a deeper understanding of the characteristics of the wave propagation phenomenon when using a FE model, three simple cases are analyzed next:

6.3.4.1 2D FE Model Subjected to an Impulsive Force

The FE model presented in section 3.5 was used for the analysis. The impulsive rectangular force displayed in Figure 6.13 was applied at the pile top, and a time history analysis was performed. The response at a number of points located along the same horizontal line, shown in Figure 6.14, was obtained by neglecting and considering the soil mass in the whole FE model. As expected, when the soil mass was neglected there is no wave propagation: the motion of all points starts at instant $t = 0$, and they move in a synchronous way. This can be explained by considering that when the soil mass density approaches zero, the wave velocity tends to infinity. The displacement-time traces are

presented in Figure 6.15 for node number 495 (located at the soil-pile interface) and node number 30 (located at the lateral edge of the soil deposit). Note that although the amplitudes are different, the time variations are quite similar.

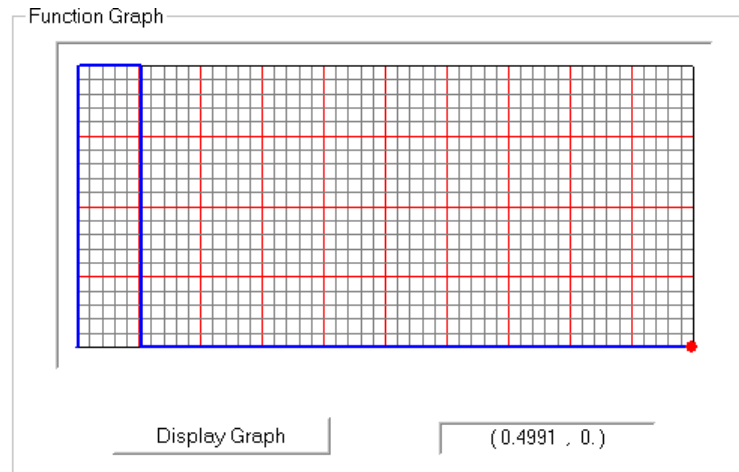


Figure 6.13: Impulsive Ramp Function

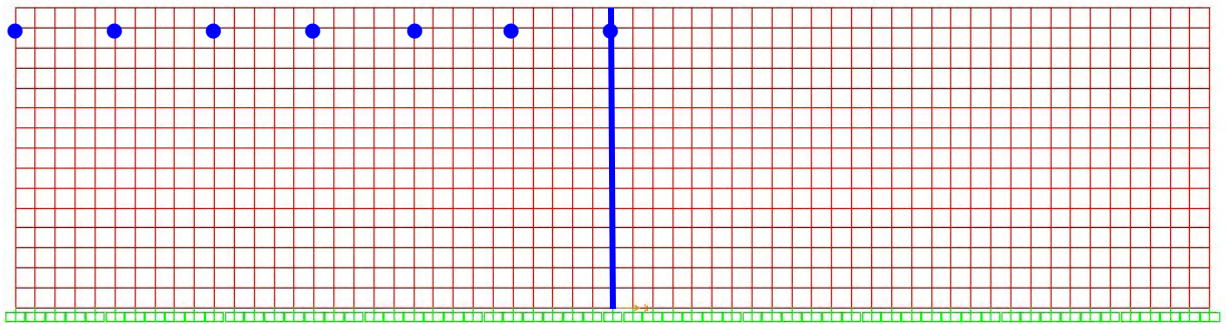


Figure 6.14: Points for Response Calculation

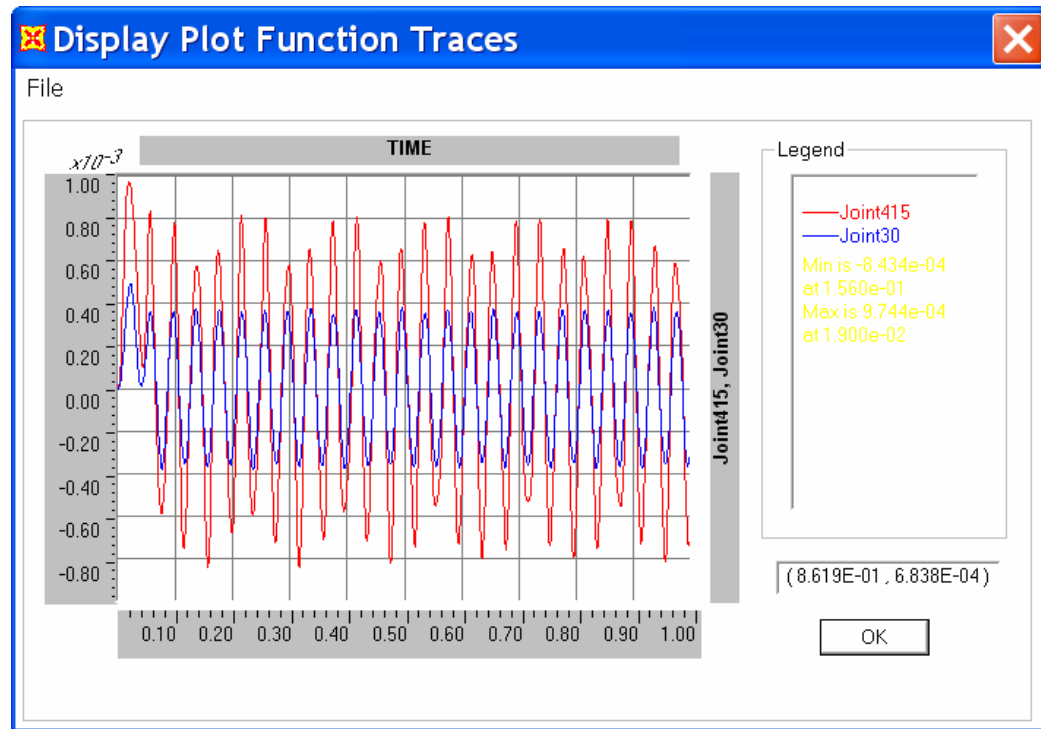


Figure 6.15: Displacement Time Histories of two Nodes when the Soil Mass is Neglected

Figure 6.16 presents the same response when the soil mass is included in the analysis. This figure clearly shows that the response at the node away from the force (joint number 30) starts after time zero. As shown later, this effect is larger for those points located farther away from the interface. Considering the soil properties ($E = 1900$ ksf and $\gamma = 0.11$ kcf), one can obtain that the p-wave velocity is around 475.8 ft/sec. Considering that the distance from the pile to the edge is 60 ft, it should take about 0.08 sec for the wave to reach the edge, which is approximately the same time lapse that is observed in Figure 6.16.

Figure 6.17 presents the results for all the points along the horizontal line (the higher the node number, the closer the node is to the soil-pile interface). By observing the lag in the response between consecutive points located further away from the soil pile interface, one can notice the time required for the perturbation (wave front) to propagate.

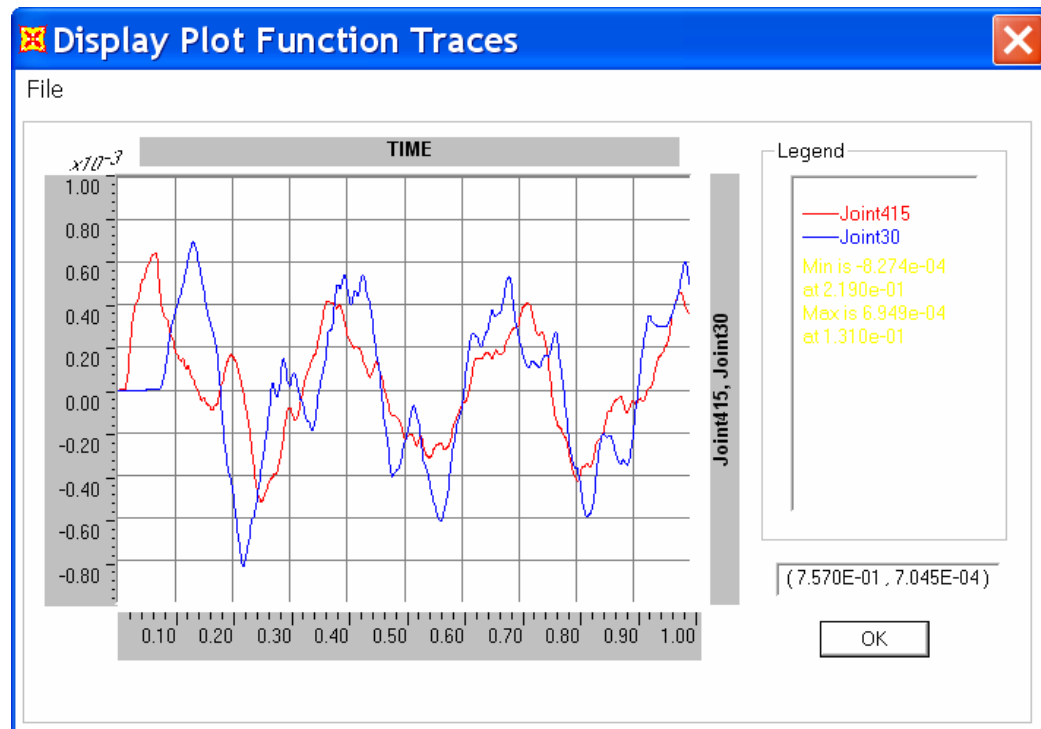


Figure 6.16: Response of First and Last Point when Soil Mass is Considered

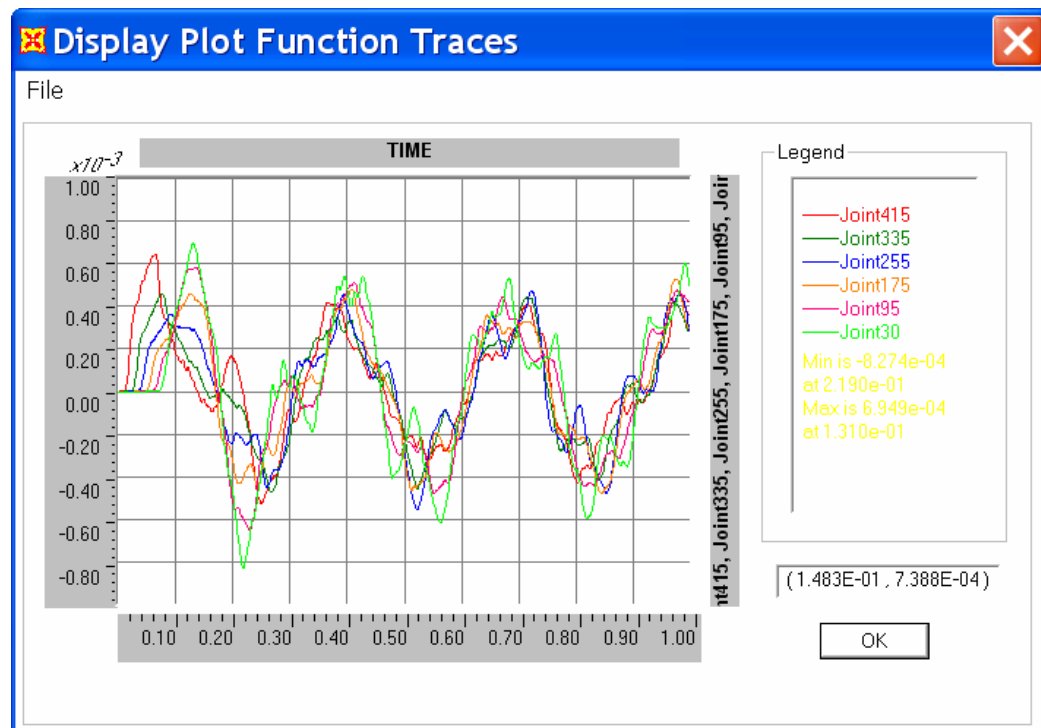


Figure 6.17: Response for all Points when Soil Mass is Considered

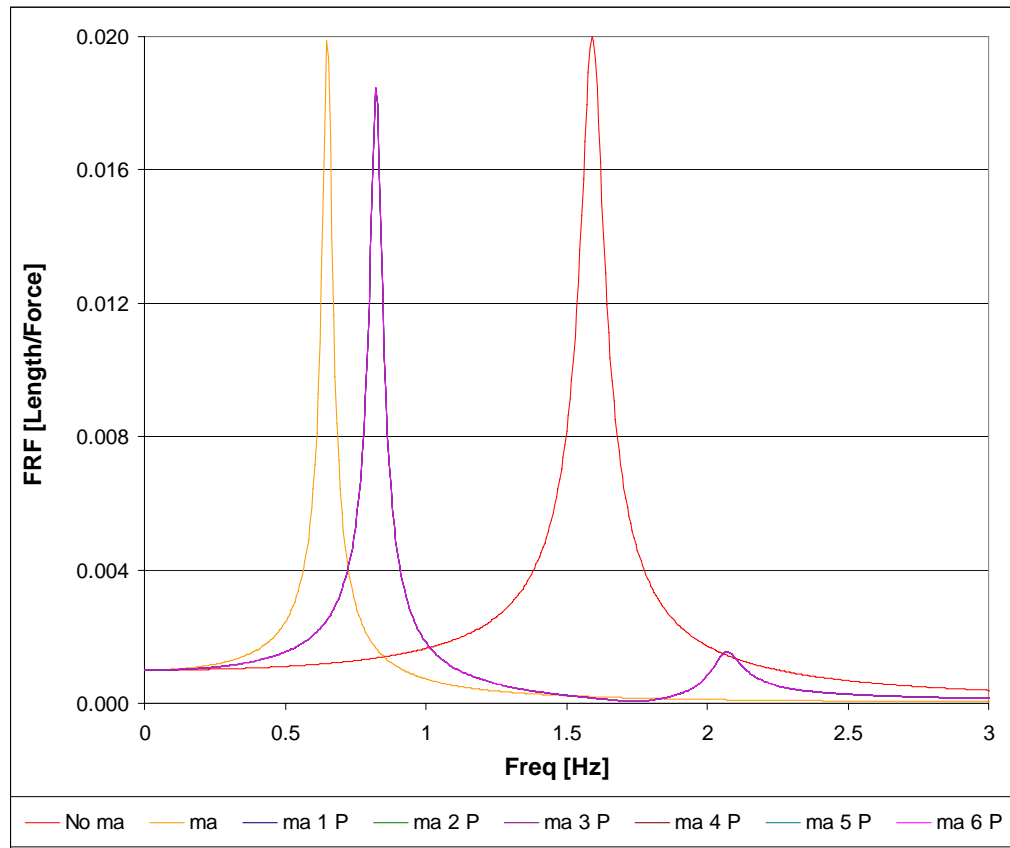


Figure 6.19: FRF for the System with Parallel Springs with no Added Masses

6.3.4.3 Effect of the Mass in a 3D Truss

In order to verify if a damped type response may be obtained with bar elements, a 3D truss model was developed in SAP2000. Figure 6.20 shows a isometric view of the 3D truss. The objective is to study the 3D nature of soil wave propagation in a non-solid medium. The FRF of the pile head was obtained by considering the bars without mass and with mass. The mass of the pile (vertical element) was always considered. A hysteretic damping of 5% was adopted by assigning a constant damping matrix equal to 0.05 times the stiffness matrix (equivalent to adopt a complex elastic modulus equal to $E(1+0.05i)$)

Figure 6.21 shows the FRFs of the pile top; the two curves results show that considering the mass of the bars has an effect similar to that provoked by damping. This is in agreement with the results obtained in the 3D FE model.

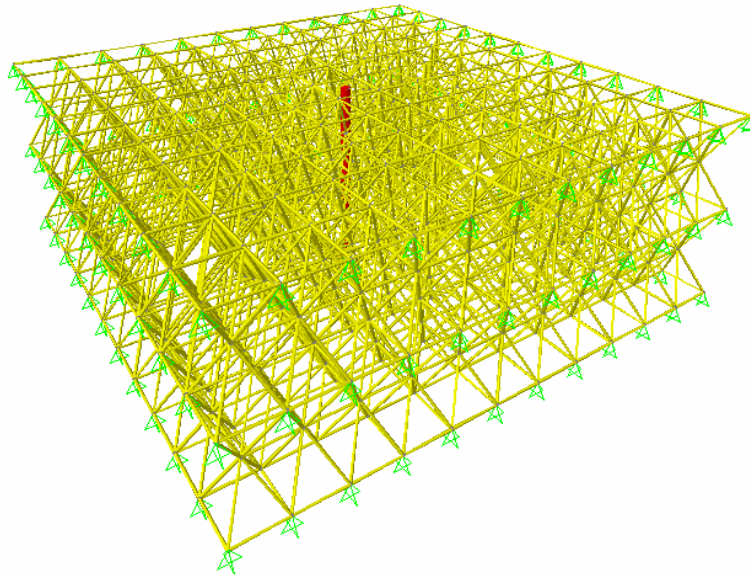


Figure 6.20: 3D Truss Model View

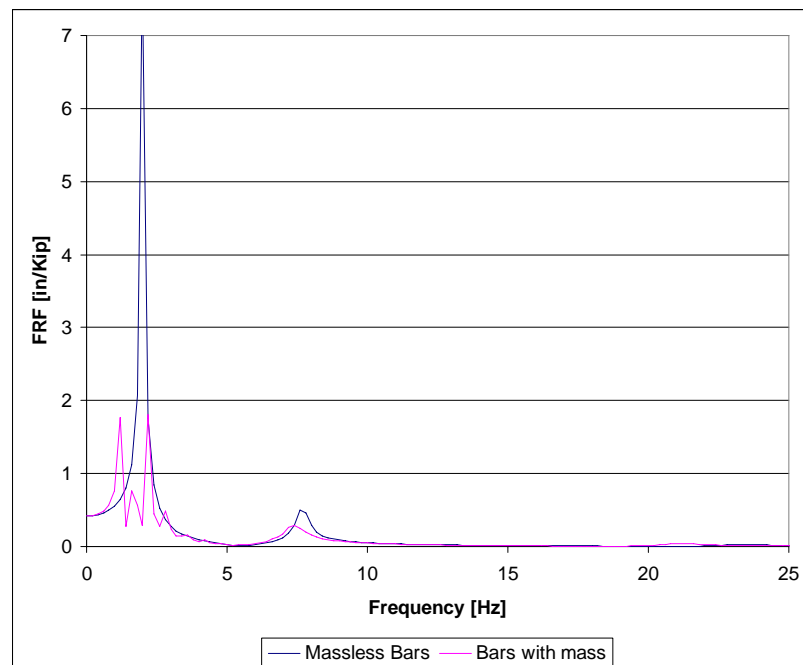


Figure 6.21: FRF of Pile Top in the 3D Truss Model

7 Conclusions and Recommendations

The objective of this chapter is to present the general conclusions of the research project together with a brief summary of the work undertaken, and recommendations for possible research topics that may complement the present project and contribute with valuable information for the academic and professional community in topics related to the response of piles under dynamic horizontal excitations.

7.1 Summary and Conclusions

The following is a listing of the most relevant conclusions of the present research project:

- 2D FEM and 3D FEM were used to evaluate the impact of considering and neglecting the mass of the soil in the dynamic response of a single pile. The effects of the cutoff boundary conditions were also evaluated. The dynamic flexibility of the pile top (or frequency response function, FRF), defined as the horizontal displacement due to a unitary horizontal harmonic load in the pile top, was selected as the system dynamic response to be evaluated. The analyses, results, and their interpretation were presented in Chapter 3. Following is a summary of the most relevant findings and conclusions for this part of the project:
 - The differences found by adopting free, fixed, or flexible cut-off boundaries were not very significant, suggesting that the model size (i.e. the soil island) was taken large enough so the soil half space is adequately represented.
 - The assignment of dashpots in the cutoff boundaries, added in order to represent the radiation damping, had an important effect only at low frequencies. They produce a smoothening of the FRF peaks (thus lowering the system displacement response) and eliminating some peaks (probably associated with the rebounding of waves in the cutoff boundaries), and producing a shift in the peaks location.

- The inclusion of the soil mass in the FE models produces a significant qualitative and quantitative change in the system behavior. As expected, the presence of the soil mass reduces the natural frequencies (the frequencies where the peaks of the FRF occur). It also was observed that, for the 3D analysis, the general effect of the mass was quite similar to adding damping in the system: the FRF peaks were smoothened and there was a shift in their locations to the left.
 - A model with partial soil mass assignment captures the general behavior of the system with full soil mass, leading to the conclusion that a partial soil mass assignment may result in reasonable good estimates of the overall pile dynamic response.
 - A 2D FE analysis may be appropriate to analyze sheet piles or wall foundations on closely spaced piles. This type of model allows one to draw general conclusions of the pile-soil behavior, and to gain insight in the system response and parameters affecting its behavior. However, a 3D FE analysis should be used to obtain more specific and accurate conclusions about the pile-soil dynamic interaction problem.
 - The large amount of time required by the pre-processing, analysis, and post-processing of 3D FE models strongly suggests that simplified analyses, such as the Winkler approach, are still recommendable for professional practice despite the increase in power of current computers.
- A simplified lumped model, consistent with the Winkler hypothesis, was obtained by performing a regression analysis of the continuous (plane strain) model developed by Novak. This development is presented in Chapter 4. In the proposed approach, the pile-soil interaction is taken into account through three frequency independent elements: a spring with stiffness k_a , a mass with value m_a , and a dashpot with coefficient c_a . The spring-mass-dashpot coefficients k_a , m_a , and c_a that represent the soil can be obtained by means of simple equations presented again next for easy reference. These equations include three parameters α_k , α_m ,

and α_c that depend on the soil Poisson's ratio. The values of these three parameters were presented in Table 4.1.

$$\begin{aligned} k_a &= \pi G \alpha_k \\ m_a &= \pi r_o^2 \rho \alpha_m \\ c_a &= \pi r_o \frac{G}{V_s} \alpha_c = \pi r_o \rho V_s \alpha_c = \pi r_o \sqrt{G \rho} \alpha_c \end{aligned} \quad (7.1)$$

where:

r_o = pile radius

G = soil shear modulus

ρ = soil mass density

ν = soil Poisson's ratio

$V_s = \sqrt{\frac{G}{\rho}}$ = shear wave velocity in the soil

$\alpha_k, \alpha_m, \alpha_c$ = parameters function of ν

The three coefficients k_a , m_a , and c_a in equation 7.1 are defined per unit pile length. In order to implement them in the 1D Finite Element Model, they should be multiplied by the node tributary length (half element length for the top node and the element length for the internal nodes).

Figure 7.1 presents the general view of the analytical model to be implemented for a pile subdivided in “ n ” elements, when the pile rests on rigid bedrock. Instead of using spring-mass-dashpot elements lumped at the pile nodes, consistent pile stiffness, mass and damping matrices may be used, as presented in Section 4.4 for the classical beam element with four degrees of freedom (DOF) and the refined beam element with five DOF proposed by Deschappelles (2003).

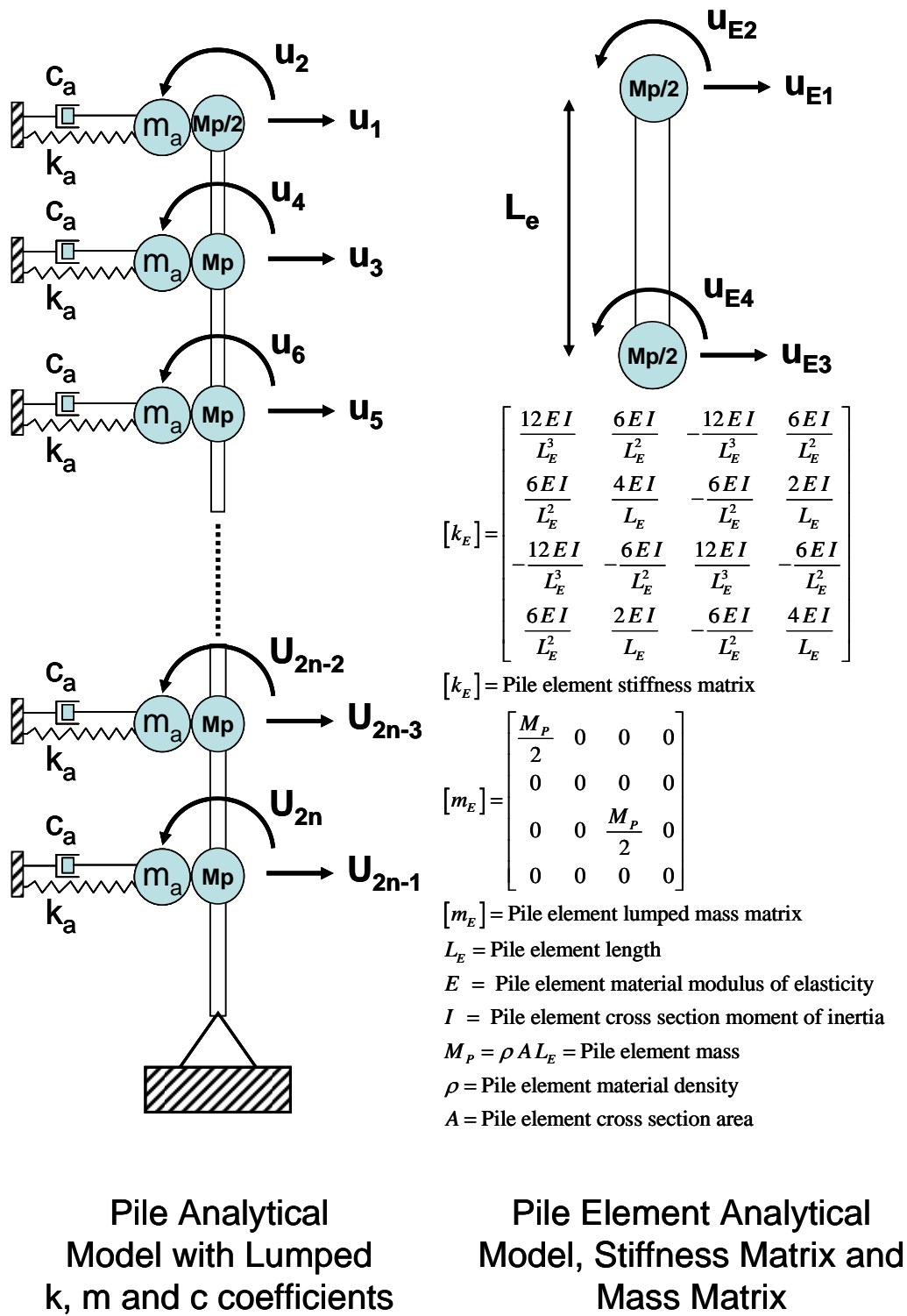


Figure 7.1: Analytical Model for the Proposed Lumped Soil Representation

- The proposed lumped model has been proven to be a reliable approximation of Novak's continuous, frequency dependent solution, as it was verified in Chapter 5 for an isolated layer and for a pile-soil system.
- The proposed lumped model was used to demonstrate that a lumped soil mass is not required for small soil Poisson's ratios ($\nu \leq 0.3$). This situation may be explained by the fact that, due to radiation damping, the soil response is overdamped; and overdamped SDOF systems behavior are basically controlled by damping and not by mass, as shown in section 4.3.1.

It is important to note that, as shown in equation 7.1, the damping coefficient c_a depends on the soil density, among other parameters. Therefore, the soil inertial properties are basically taken into account by the radiation damping coefficient for Poisson's ratios lower than 0.4.

The model also shows that the soil mass is important for high soil Poisson's ratios, as occurs in saturated soils (for $\nu = 0.5$ the soil mass contribution is in the same order of the pile mass contribution). However, the soil mass importance rapidly diminishes as the Poisson's ratio becomes smaller. This situation may be explained due to the fact that the larger the value of the Poisson's ratio ν , the larger the soil transverse deformation that will occur when the piles vibrates horizontally, so more soil mass is involved in the transmission of p-waves due to pile vibration. The increase in the static stiffness for high Poisson's ratios (parameter α_k) could also explain the increase in the lumped soil mass (parameter α_m), by considering a SDOF system where the natural frequency does not change (as explained in section 5.5).

- The frequency independent concentrated spring-mass-dashpot element proposed is available in most of the commercial analysis packages, making the model simple to implement by the professional community.

- This type of model could serve as the basis to develop simplified Soil Structure Interaction Specifications for structures on pile foundations, similar to those for structures on spread footings currently contained in the NEHRP Recommended Provisions for Seismic Regulations for New Buildings and Other Structures (Building Seismic Safety Council, 2003).
- Having independent expressions for the stiffness coefficient (ka), the dashpot coefficient (ca), and the mass (ma), instead of a complex equation for the dynamic stiffness, allows one to perform different “what if” analyses, and evaluate the impact of the variation of each coefficient in the system response (examples of this study were presented in Chapter 6). These analyses may contribute to a better understanding of the factors affecting the system response. They can also help calibrate the parameters to be adopted for a particular analysis or to be included in future recommended provisions.
- Considering that the *radiation damping* represents the energy, or elastic waves, generated at the pile-soil interface, that is radiated away to infinity (i.e. does not return to the interface), the damped-like response observed in the 3D FEM model when the soil mass is considered (Section 3.6) may be the result of the waves generated at the soil-pile interface that travel within the soil mass, without returning to the pile, generating an effect that may be called *propagation damping*. As demonstrated in section 6.3.2 for a one layer system, to have this type of response the model should have alternate paths that allow the waves to propagate within the system without returning to the interface, as provided by the parallel springs. It was not possible to obtain this type of response with a relative simple layout of springs and a distributed soil mass along spring nodes. The simplified pile-soil model (where the soil is replaced by an equivalent spring-mass-dashpot element) should always include the dashpot to account for this phenomenon.

- The model could be extended to perform nonlinear dynamic analysis of pile-soil system, by replacing the spring constant k_a by a nonlinear static soil response, such as the one provided by the p-y method. In this case, the implementation of a hysteretic soil model to account for damping due to plastic effects (e.g. use of Masing Rules) is recommended.

7.2 Recommendations

The following recommended research topics emerge as a possible complement continuation of the present project; other suggested topics can provide useful information to the academic and professional community:

- Develop other lumped models based on the curve-fitting of other continuum mechanics theories and rigorous approaches (e.g. Tajimi, 1969; Kausel, 1974; Kaynia, 1982). These new models will allow to compare different solutions, and to verify the findings regarding the influence of the soil mass in the dynamic response of the pile-soil system.
- Study the effect of radiation damping, by comparing different models and different analyses, in order to establish the most appropriate lumped damping coefficient (as suggested by the analyses presented in Sections 5.3, 5.4 and 6.2).
- Study the effect of the pile cross section size and shape in the dynamic system response by performing 3D FEM analyses, modeling the soil and the pile with solid 3D elements, and applying the appropriate constraints to pile nodes in order to simulate rigid cross section behavior.
- Study the applicability of the proposed simplified model to battered piles.

- Extend the analysis to pile groups.
- Develop state-of-the-art reports of dynamic soil-pile interaction topics, with theoretical fundamentals and detailed practical applications and examples. Two topics are considered relevant to the professional and the academic community: a) recommended procedures for the 3D Finite Element analysis of soil-pile interaction problems, and b) available continuum mechanics models for soil-pile interaction problems.
- Perform a study of the constitutive equations of the p-y method, in order to compare its initial slope to the coefficient k_a presented previously, and develop the appropriate conclusions and recommendations.
- Implement the proposed model in a graphically oriented program, with adequate pre-processing and post-processing capabilities, and a wide variety of dynamic analyzes available. This program may serve as a tool for research, teaching and professional use.
- Perform a comparison of the seismic analysis response of an isolated pile by modeling the pile-soil system with the proposed simplified model and with a 3D FE model.

8 References

8.1 Books

Barkan D.D. 1962. “*Dynamics of Bases and Foundations*”, McGraw-Hill Companies, New York.

Bowles J. E. 1974. “*Analytical and Computer Methods in Foundation Engineering*”. McGraw-Hill Companies, New York.

Bowles J. E. 1996. “*Foundation Analysis and Design*”. McGraw-Hill Companies, New York.

Cernica J. N. 1995. “*Geotechnical Engineering – Soil Mechanics*”, John Wiley & Sons, New York.

Chapra S. C. and Canale R. P. 1998. “*Numerical Methods for Engineers with Programming and Software Applications*”, WCB/McGraw-Hill, Boston.

Chopra A. K. 2001. “*Dynamic of Structures – Theory and Applications to Earthquake Engineering*”, Prentice-Hall, Englewood Cliffs, NJ.

Coduto D. P. 2001. “*Foundation Design – Principles and Practives*”, Prentice-Hall, Englewood Cliffs, NJ.

Das B. M. 1999. “*Principles of Foundation Engineering*”, PWS Publishing, Pacific Grove, CA

Fleming W. G. K., Weltman A. J., Randolph M. F., and Elson W. K. 1992. “*Piling Engineering*”, Blackie & Son, Glasgow, and Halsted Press (imprint of John Wiley & Sons), New York.

Gerald C. F., and Wheatley P. O. 1994. “*Applied Numerical Analysis*”, Addison-Wesley Publishing Company, Reading, Massachusetts.

Humar J. L. 2002. “*Dynamic of Structures*”, A.A. Balkema Publishers, Lisse, The Netherlands

Poulos H. G., and Davis E. H. 1974. “*Elastic Solutions for Soil and Rock Mechanics*”. John Wiley & Sons, New York.

Poulos H. G., and Davis E. H. 1980. “*Pile Foundation Analysis and Design*”. John Wiley & Sons, New York.

Reese L. C. and Van Impe W. F. 2001. “*Single Piles and Pile Groups under Lateral Loading*”, A.A. Balkema Publishers.

Scott R. F. 1981. “*Foundation Analysis*”, Prentice-Hall, Englewood Cliffs, NJ.

Suarez L. 2003. “*Dinámica de Suelos*”, Universidad de Puerto Rico, Recinto Universitario de Mayagüez, PR.

Suárez L. E. 2004. “*Dinámica Estructural*”, Universidad de Puerto Rico, Recinto Universitario de Mayagüez, PR.

Ugural A. C., Fenster S. K. 1995. “*Advanced Strength and Applied Elasticity*”, Prentice-Hall, Englewood Cliffs, NJ.

Wolf J. P. 1985. “*Dynamic Soil-Structure Interaction*”, Prentice-Hall, Englewood Cliffs, NJ.

Zeevaert L. 1980. “*Interacción Suelo-Estructura de Cimentaciones Superficiales y Profundas, Sujetas a Cargas Estáticas y Sísmicas*”, Editorial Limusa, México D.F.

Zeevaert L. 1983. “*Foundation Engineering for Difficult Subsoil Conditions*”, Van Nostrand Reinhold Co., New York.

Zwillinger D. and Kokoska S. 2000. “*CRC Standard Probability and Statistics Tables and Formulae*”, CHAPMAN & HALL/CRC, Boca Raton.

8.2 Class Notes

Battini J. C. 2006. “*Structural Dynamics*”, Royal Institute of Technology (KTH), Stockholm, Sweden, <http://www2.mech.kth.se/~jean/dynamics.html>

Deschapelles, B. 2003. “*Nonlinear Analysis of Soil-Structure Interaction*”, Polytechnic University of Puerto Rico, San Juan, PR.

8.3 Technical Manuals, Guides and Reports

Arduino P. 2005. “*Semi-Infinite Domain Characterization Using OpenSees*”, www online article, <http://www.ce.washington.edu/%7Egeotech/opensees/>

Bently Nevada 2000. “*Understanding and Using Dynamic Stiffness*”, ORBIT magazine, 44-54.

Building Seismic Safety Council, 2003. “*NEHRP (National Earthquake Hazards Reduction Program) Recommended Provisions for Seismic Regulations for New Buildings and Other Structures (FEMA 450)*”, National Institute of the Building Sciences, Washington, D.C.

Computers and Structures Inc. 2004. “*CSI Analysis Reference Manual for SAP 2000*”, CSI, Berkeley, California.

Federal Highway Administration 1997 (revised 1998). “*Design and Construction of Driven Pile Foundations. Workshop Manual – Volume I*”, Publication No. FHWA HI 97-013. Washington, D.C., FHWA

Federal Highway Administration 1998. “*Geotechnical Earthquake Engineering Reference Manual*”, Publication No. FHWA HI 99-012. Washington, D.C., FHWA

International Conference of Building Officials (ICBO) 1997. “*Uniform Building Code*” (UBC)

Itasca Consulting Group, Inc. 1996. “*FLAC3D version 2.0. Fast Lagrangian Analysis of Continua in Three Dimensions*”, Minneapolis, Minnesota.

Lam I., and Martin G. R. 1986. “*Seismic Design of Highway Bridge Foundations—Design Procedures and Guidelines*”, Report FHWA/RD-86/102. Washington, D.C., FHWA

Mosher, R. L. and Dawkins, W. P. 2000. “*Theoretical Manual for Pile Foundations*”, U.S. Army Corps of Engineers, *Computer-Aided Structural Engineering Project*, Publication ERDC/ITL TR-00-5, Washington, DC.

Naval Facilities Engineering Command 1986. “*Foundations and Earth Structures*”, Publication DESIGN MANUAL 7.02 (DM 7.02), Alexandria, Virginia

U.S. Army Corps of Engineers 1991. “*Design of Pile Foundations*”, Engineering and Design, Publication EM 1110-2-2906, Washington, DC.

U.S. Army Corps of Engineers 1998. “*Design of Deep Foundations*”, Technical Instructions, Publication TI 818-02, Washington, DC.

8.4 Research Reports and Thesis

Brown D. A., O'Neil M. W., Hoit M., McVay M., El Naggar M. H., and Chakraborty S. 2001. "*Static and Dynamic Lateral Loading of Pile Groups*", National Cooperative Highway Research Program, NCHRP Report 461, Transportation Research Board – National Research Council, National Academy Press, Washington, D.C.

De Napoli V. E. 2006. "*Análisis Numérico y Experimental de Pilotes Excavados de Hormigón Armado Cargados Lateralmente*", Tesis, Facultad de Ciencias Exactas, Físicas y Naturales, Universidad Nacional de Córdoba, Argentina.

Idriss I. M., and Sun J. I. 1992. "*User's Manual for SHAKE91, A Computer Program for Conducting Equivalent Linear Seismic Response Analysis of Horizontally Layered Soil Deposits*", Center for Geotechnical Modeling, Department of Civil & Environmental Engineering, University of California at Davis.

Kausel E. 1974. "*Forced Vibrations of Circular Foundations on Layered Media*", Research Report R74-11, Department of Civil Engineering, University of California at Berkeley.

Kaynia A. M. 1982. "*Dynamic Stiffness and Seismic Response of Pile Groups*", Publication No. R82-03, Massachusetts Institute of Technology, Cambridge.

Klar A. 2003. "*Model Studies of Seismic Behavior of Piles in Sand*", Research Thesis, Israel Institute of Technology.

Klar A., Vorster T. E. B., Soga K., and Mair R. J. 2004. "*Soil - Pipe – Tunnel Interaction: Comparison between Winkler and Elastic Continuum Solutions*", Technical Report CUED/D-SOILS/TR 332, University of Cambridge, United Kingdom.

Lysmer J. 1979. "*Finite Element Analysis of Soil-Structure Interaction*", Appendix to "*Analysis for Soil-Structure Interaction Effects for Nuclear Power Plants*", Report by the Ad Hoc Group on Soil-Structure Interaction, Nuclear Structures and Materials Committee of the Structural Division of ASCE

PoLam I., Kapuskar M., and Chaudhuri D. 1998. "*Modeling of Pile Footings and Drilled Shafts for Seismic Design*", Technical Report MCEER-98-0018. Multidisciplinary Center for Earthquake Engineering Research, State University of New York at Buffalo.

Schnabel, P. B., Lysmer, J., and Seed, H. B. 1972. "*SHAKE: A Computer Program for Earthquake Response Analysis of Horizontally Layered Sites*", Report No. UCB/EERC72/12, Earthquake Engineering Research Center, University of California, Berkeley.

Wallace J. W., Fox P. J., Stewart J. P. 2001. “*Cyclic Large Deflection Testing of Shaft Bridges*”, California DOT, University of California, Los Angeles.

8.5 Papers

Aristizábal-Ochoa J. D. 2003. “*Estructuras de Vigas Sobre Suelos Elásticos de Rigidez Variable*”, Revista Internacional de Desastres Naturales, Accidentes e Infraestructura Civil, Vol. 3(2), Universidad de Puerto Rico, Recinto Universitario de Mayagüez, Puerto Rico, 157-174.

Ashour M., Norris G., and Pilling P. 1998. “*Lateral Loading of a Pile in Layered Soil Using the Strain Wedge Model*”, Journal of Geotechnical and Geoenvironmental Engineering, ASCE, Vol. 124(4), 303-315.

Ashour M., and Norris G. 2000. “*Modeling Lateral Soil-Pile Response Based on Soil-Pile Interaction*”, Journal of Geotechnical and Geoenvironmental Engineering, ASCE, Vol. 126(5), 420-428.

Badoni D., and Makris N. 1996. “*Nonlinear Response of Single Piles under Lateral Inertial and Seismic Loads*”, Soil Dynamics and Earthquake Engineering, Vol. 15, 29-43.

Baguelin F. and Frank R. 1979. “*Theoretical Studies of Piles Using the Finite Element Method*”, Proceedings of the Conf. Num. Methods in Offshore Piling, London, Institute of Civil Engineers.

Banerjee P. K. and Davies T. G. 1978. “*The Behavior of Axially and Laterally Loaded Single Piles Embedded in Non-Homogeneous Soils*”, Géotechnique, Vol. 28 (3).

Basile F. 2002. “*Integrated Form of Singular Mindlin’s Solution*”, Proceedings of the 10th ACME Conference, Swansea, Wales, UK, 191-194.

Basile F. 2003. “*Analysis and design of pile groups*”, extract from “*Numerical Analysis and Modelling in Geomechanics*”, Spon press (eds J. W. Bull), London, 2003, Chapter 10, 278-315.

Ben Jamma S. and Shiojiri H. 2000. “*A Method for Three Dimensional Interaction Analysis of Pile-Soil System in Time Domain*”, Transactions of the Japan Society for Computational Engineering and Science, Paper No.20000013.

Bentley K.J., and El Naggar M.H. 2000. “*Numerical Analysis of Kinematic Response of Single Piles*”, Canadian Geotechnical Journal, Vol. 37, 1368-1382.

Berger E., Mahin S.A., and Pyke R. 1977. “*Simplified Method for Evaluating Soil-Pile Structure Interaction Effects*”, Proceedings of the 9th Offshore Technology Conference, Houston, Texas, 589-598.

Broms B. B. 1964a. *Lateral resistance of Piles in Cohesive Soils*”, Journal of the Soil Mechanics and Foundations Division, ASCE, Vol 90(2), 27-63.

Broms B. B. 1964b. “*Lateral resistance of Piles in Cohesionless Soils*”, Journal of the Soil Mechanics and Foundations Division, ASCE, Vol 90(3), 123-156.

Broms B. B. 1965. “*Design of Laterally Loaded Piles*”, Journal of the Soil Mechanics and Foundations Division, ASCE, Vol 91(3), 79-99.

Davis E. H. and Booker J. R. 1971. “*The Bearing Capacity of Strip Footings from the Standpoint of Plasticity Theory*”, Proc. of the 1st Australian-New Zealand Conf. on Geomechanics, Melbourne, Australia, Vol. 1.

De Napoli V. E. and Prato C. A. 2006. “*Small Amplitude Dynamic Tests for Prediction of Nonlinear Response of Drilled Piles to Lateral Loads*”, Proceedings of the 23rd Southeastern Conference on Theoretical and Applied Mechanics, Mayagüez, Puerto Rico.

Desai C. S. and Appel G. C. 1976. “*3-D Analysis of Laterally Loaded Structures*”, Proceedings of the 2nd Int. Conf. Num. Methods in Geomechanics, Blacksburg, Virginia, ASCE, Vol. 1.

Douglas D. J. and Davis E. H. 1964. “*The Movements of Buried Footings Due to Moment and Horizontal Load and the Movement of Anchor Plates*”, Géotechnique, Vol. 14.

El Naggar M. H. and Novak M. 1995. “*Nonlinear Lateral Interaction in Pile Dynamics*”, Soil Dynamics and Earthquake Engineering, Vol. 14, Elsevier Science Limited, 141-157.

El Naggar M. H. and Novak M. 1996. “*Nonlinear Analysis for Dynamic Lateral Pile Response*”, Soil Dynamics and Earthquake Engineering, Vol. 15, Elsevier Science Limited, 233-244.

El Naggar M. H. and Bentley K. J. 2000. “*Dynamic Analysis for Laterally Loaded Piles and Dynamic p-y Curves*”, Canadian Geotechnical Journal, Vol. 37, 1166-1113.

Gazetas G., and Dobry R. 1984a. “*Horizontal Response of Piles in Layered Soils*”, Journal of Geotechnical Engineering, ASCE, Vol. 110 (1), pp. 20-40.

Gazetas G., and Dobry R. 1984b. “*Simple Radiation Damping Model for Piles and Footings*”, Journal of Engineering Mechanics, ASCE, Vol. 110 (6), 937-956.

Hetyenyi M. 1946. *"Beams on Elastic Foundations"*, University of Michigan Press, Ann Arbor, Michigan.

Hsiung Y. 2003. *"Theoretical Elastic-Plastic Solution for Laterally Loaded Piles"*, Journal of Geotechnical and Geoenvironmental Engineering, ASCE, Vol 129 (6), 475-480.

Hutchinson T. C., Chai Y. H., Boulanger R.W., Idriss I. M. 2004. *"Inelastic Seismic Response of Extended Pile-Shaft-Supported Bridge Structures"*, Earthquake Spectra, EERI, Vol. 20 (4), 1057-1080.

Kagawa T., and Kraft L.M. 1980a. *"Lateral Load-Deflection Relationship of Piles Subjected to Dynamic Loadings"*, Soil and Foundation, Japanese Society of Soil Mechanics and Foundation Engineering, Vol. 20(4), 19-35.

Kagawa T., and Kraft L.M. 1980b. *"Seismic p - y Responses of Flexible Piles"*, Journal of the Geotechnical Engineering Division, ASCE, Vol. 106 (8), 899-919.

Kagawa T., and Kraft L.M. 1981. *"Lateral Piles Response During Earthquakes"*, Journal of the Geotechnical Engineering Division, ASCE, Vol. 107 (12), 1713-1731.

Kagawa T. 1992. *"Modeling Soil Reaction to Laterally Loaded Piles"*, Transportation Research Record No 1336 – Foundations Engineering: Seismic Design, Drilled Shafts and other Issues, Transportation Research Board, Washington, 81-89.

Kim B. T., Kim N., Lee W. J., and Kim Y. S. 2004. *"Experimental Load-Transfer Curves of Laterally Loaded Piles in Nak-Dong River Sand"*, Journal of Geotechnical and Geoenvironmental Engineering, ASCE, Vol. 130 (4), 416-425.

Klar A. and Frydman S. 2002. *"Three-Dimensional Analysis of Lateral Pile Response using Two-Dimensional Explicit Numerical Scheme"*, Journal of Geotechnical and Geoenvironmental Engineering, ASCE, Vol. 128 (9), 775-784

Luco J. E. 2004. *"Approximate External Boundaries for Truncated Models of Unbounded Media"*, Proceedings Third of the UJNR Workshop on Soil-Structure Interaction, March 29-30, 2004, Menlo Park, California.

Lysmer J. and Kuhlemeyer R. L. 1969. *"Finite Dynamic Model for Infinite Media"*, Journal of the Engineering Mechanics Division, ASCE, Vol. 95, 859-877.

Maheshwari B. K., Truman K. Z., El Naggar M. H., and Gould P. L. 2004. *"Three-Dimensional Finite Element Nonlinear Dynamic Analysis of Pile Groups for Lateral Transient and Seismic Excitations"*, Canadian Geotechnical Journal, Vol. 41, 118-133.

- Matlock H. and Reese L. C. 1960. "*Generalized Solutions for Laterally Loaded Piles*", Journal of the Soil Mechanics and Foundations Division, ASCE, Vol. 86 (5), 63-91.
- Matlock H. 1970. "*Correlations for Design of Laterally Loaded Piles in Soft Clay*", Proceedings of the 2nd Offshore Tech. Conference, Houston, Texas, Vol. 1.
- Matlock H., Foo S., Bryant L. L. 1978. "*Simulation of Lateral Pile Behavior*", Proceedings of the Earthquake Engineering and Soil Dynamics Div., ASCE.
- Mengi Y. and Tanrikulu A. K. 1993. "*Absorbing Boundary Conditions in Soil-Structure Interaction Analyses*", Developments in Dynamic Soil-Structure Interaction, P Güllkan and R. W. Clough (eds.), NATO ASI Series, Kluwer Academic Publishers, Netherlands, 111-146.
- Mostafa Y. E. and El Naggar M. H. 2002. "*Dynamic Analysis of Laterally Loaded Pile Groups in Sand and Clay*", Canadian Geotechnical Journal, Vol 39, 1358-1383.
- Ng C. W. W., and Zhang L. M. 2001. "*Three-Dimensional Analysis of Performance of Laterally Loaded Sleeved Piles in Sloping Ground*", Journal of Geotechnical and Geoenvironmental Engineering, Vol. 127 (6), 499-509.
- Nogami T., and Konagai K. 1988. "*Time Domain Flexural Response of Dynamically Loaded Single Piles*", Journal of Engineering Mechanics, ASCE, Vol. 114(9), 1512-1525.
- Nogami, T., and Novak M. 1980. "*Coefficients of Soil Reaction to Pile Vibration*", Journal of Geotechnical Engineering, ASCE, Vol. 106(5), 565-570.
- Nogami T., Otani J., Konagai K., and Chen H.L. 1992. "*Nonlinear Soil-Pile Interaction Model for Dynamic Lateral Motion*", Journal of Geotechnical Engineering, ASCE, Vol. 118(1), 89-106.
- Novak M. 1974. "*Dynamic Stiffness and Damping of Piles*", Canadian Geotechnical Journal, Vol 11, NRC Research Press, 574-598.
- Novak M., Nogami T., and Aboul-Ella F. 1978. "*Dynamic Soil Reaction for Plane Strain Case*", Journal Engineering Mechanics, ASCE Vol. 104(4), 953-995.
- Palmer L. A. and Thompson J. B. 1948. "*The Earth Pressure and Deflection Along Embedded Lengths of Piles Subjected to Lateral Thrusts*", Proceedings of the 2nd International Conference in Soil Mechanics and F.E., Rotterdam, Vol. 5.
- Penzien J., Scheffy C., and Parmelee R. (1964) "*Seismic Analysis of Bridges on Long Piles*", Journal Engineering Mechanics Division., ASCE Vol. 90(3), pp. 223-254.

- Poulos H. G. 1971. “*Behavior of Laterally Loaded Piles: I – Single Piles*”, Journal of the Soil Mechanics and Foundation Division, ASCE, Vol. 97 (SM5), 711-731.
- Poulos H. G. 1972. “*Behavior of Laterally Loaded Piles: III – Socketed Piles*”, Journal of the Soil Mechanics and Foundation Division, ASCE, Vol 98 (SM4), 733-751.
- Reese L. C. and Matlock H. 1956. “*Non-Dimensional Solutions for Laterally Loaded Piles with Soil Modulus Assumed Proportional to Depth*” Proc. 8th Texas Conf. S.M. and F.E., Spec. Pub. 29, Bureau of Eng. Res., Univ. of Texas, Austin.
- Reese L. C. 1977. “*Laterally Loaded Piles: Program Documentation*”, Journal of the Geotechnical Engineering Division, ASCE, Vol 103.
- Shen W. Y., and Teh C. I. 2004. “*Analysis of Laterally Loaded Piles in Soil with Stiffness Increasing with Depth*”, Journal of Geotechnical and Geoenvironmental Engineering, ASCE, Vol 130 (8), 878-882.
- Spillers W. R., and Stoll R. D. 1964. “*Lateral Response of Piles*”, Journal of the Soil Mechanics and Foundation Division, ASCE, Vol. 90 (6), 1-9.
- Tajimi, H. 1969. “*Dynamic Analysis of a Structure Embedded in an Elastic Stratum*”, Proceedings of the 4th World Conf. Earthquake Engineering, Santiago, Chile, Vol. 3, 53-69.
- Wang S., Kutter B. L., Chacko M. J., Wilson D. W., Boulanger R. W., and Abghari A. 1998. “*Nonlinear Soil-Pile Structure Interaction*”, Earthquake Spectra, EERI, Vol. 14 (2), 377-396.
- Wu G. and Finn W. D. L. 1997a. “*Dynamic Elastic Analysis of Pile Foundations Using Finite Element Method in the Frequency Domain*”, Canadian Geotechnical Journal, National Research Council Canada, Vol. 34, 34-43.
- Wu G. and Finn W. D. L. 1997b. “*Dynamic Nonlinear Analysis of Pile Foundations Using Finite Element Method in the Time Domain*”, Canadian Geotechnical Journal, National Research Council Canada, Vol. 34, 44-52.
- Yang Z. and Jeremic B. (2002). “*Numerical Analysis of Pile Behavior under Lateral Loads in Layered Elastic-Plastic Soils*”, International Journal for Numerical and Analytical Methods in Geomechanics, Vol 26, 1385–1406.
- Vesić A. B. 1961. “*Bending of Beams Resting on Isotropic Elastic Solid*”, Journal of the Engineering Mechanics Division, ASCE, Vol 87 (2), 35-53.

APENDICES

A Soil Deposit and Pile Natural Frequencies

This appendix presents the computation of the soil deposit natural frequencies and wave lengths, as presented by Suarez (2003), and the appropriated FEM element size, following the recommendations by Lysmer (2979).

The computations of the pile natural frequencies and mode shapes are also presented. The reference equations were taken fro Humar (2002).

A.1 Soil Deposit Natural Frequencies, Wave Length, and FEM Element Size

The computations of the appropriate finite element size so the finite element model is able to transmit up to the fourth soil deposit natural frequency (for vertical propagating shear waves) is presented in Figure A.1. The computations are performed in MathCad software package.

Problem Data

$$\begin{aligned}
 E &:= 12 && [\text{Ksi}] \\
 \gamma &:= 110 && [\text{pcf}] \\
 \nu &:= 0.3 \\
 g &:= 32.2 && [\text{ft/sec}^2] \\
 h &:= 30 && [\text{ft}]
 \end{aligned}$$

Computations

$$\begin{aligned}
 G &:= \frac{E}{2 \cdot (1 + \nu)} \cdot 144 \cdot 1000 && [\text{psf}] && G = 6.646 \times 10^5 \\
 \rho &:= \frac{\gamma}{g} && && \rho = 3.416 \\
 V_s &:= \sqrt{\frac{G}{\rho}} && [\text{ft/sec}] && V_s = 441.079 \\
 r &:= 4 \\
 \omega_{\max} &:= \frac{\pi}{2} \cdot (2 \cdot r - 1) \cdot \frac{V_s}{h} && [\text{rad/sec}] && \omega_{\max} = 161.664 \\
 f_{\max} &:= \frac{\omega_{\max}}{2 \cdot \pi} && [\text{herz}] && f_{\max} = 25.73 \\
 \lambda_s &:= \frac{V_s}{f_{\max}} && [\text{ft}] && \lambda_s = 17.143 \\
 &&&&& \frac{\lambda_s}{8} = 2.143
 \end{aligned}$$

Figure A.1: Maximum Element Size for 4th Natural Frequency

Figure A.2 presents the computations required to determine the maximum appropriate element size if it is desired that the finite element model is able to transmit a maximum frequency equal to the eighth soil deposit natural frequency.

Problem Data

$$E := 12 \quad [\text{Ksi}]$$

$$\gamma := 110 \quad [\text{pcf}]$$

$$\nu := 0.3$$

$$g := 32.2 \quad [\text{ft/sec}^2]$$

$$h := 30 \quad [\text{ft}]$$

Computations

$$G := \frac{E}{2 \cdot (1 + \nu)} \cdot 144 \cdot 1000 \quad [\text{psf}] \quad G = 6.646 \times 10^5$$

$$\rho := \frac{\gamma}{g} \quad \rho = 3.416$$

$$V_s := \sqrt{\frac{G}{\rho}} \quad [\text{ft/sec}] \quad V_s = 441.079$$

$$r := 8$$

$$\omega_{\max} := \frac{\pi}{2} \cdot (2 \cdot r - 1) \cdot \frac{V_s}{h} \quad [\text{rad/sec}] \quad \omega_{\max} = 346.423$$

$$f_{\max} := \frac{\omega_{\max}}{2 \cdot \pi} \quad [\text{herz}] \quad f_{\max} = 55.135$$

$$\lambda_s := \frac{V_s}{f_{\max}} \quad [\text{ft}] \quad \lambda_s = 8$$

$$\frac{\lambda_s}{8} = 1$$

Figure A.2: Maximum Element Size for 8th Natural Frequency

A.2 Pile Natural Frequencies and Modal Shape

Following is a listing of the MathCad worksheet developed to compute the pile natural frequencies and modal shape. The pile is considered as a cantilever beam, and the reference equations were taken from Humar (2002).

Pile Natural Frequencies

Problem Data

$$E := 518400 \quad [\text{ksf}]$$

$$\gamma := 0.150 \quad [\text{kcf}]$$

$$\nu := 0.2$$

$$g := 32.2 \quad [\text{ft/sec}^2]$$

$$L := 30 \quad [\text{ft}]$$

$$r := 1 \quad [\text{ft}]$$

Computations

$$A := r^2$$

$$A = 1$$

$$I := \frac{r^4}{12}$$

$$I = 0.083$$

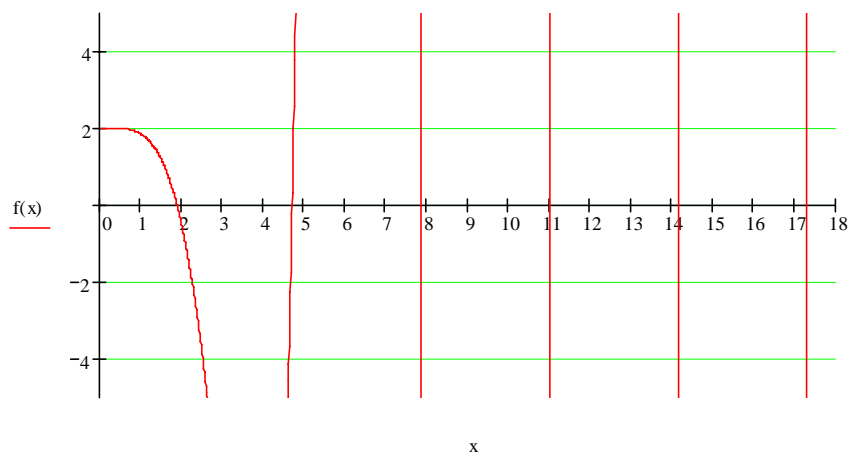
$$\rho := \frac{\gamma}{g}$$

$$\rho = 4.658 \times 10^{-3}$$

$$m := A \cdot \rho$$

$$m = 4.658 \times 10^{-3}$$

$$f(x) := 1 + \cosh(x) \cdot \cos(x) \quad \text{characteristic equation} \quad x := 0, 0.01..20$$



$$\underline{\underline{x}} := 1$$

First Mode

Given

$$1 + \cosh(x) \cdot \cos(x) = 0$$

$$x1 := \text{Find}(x)$$

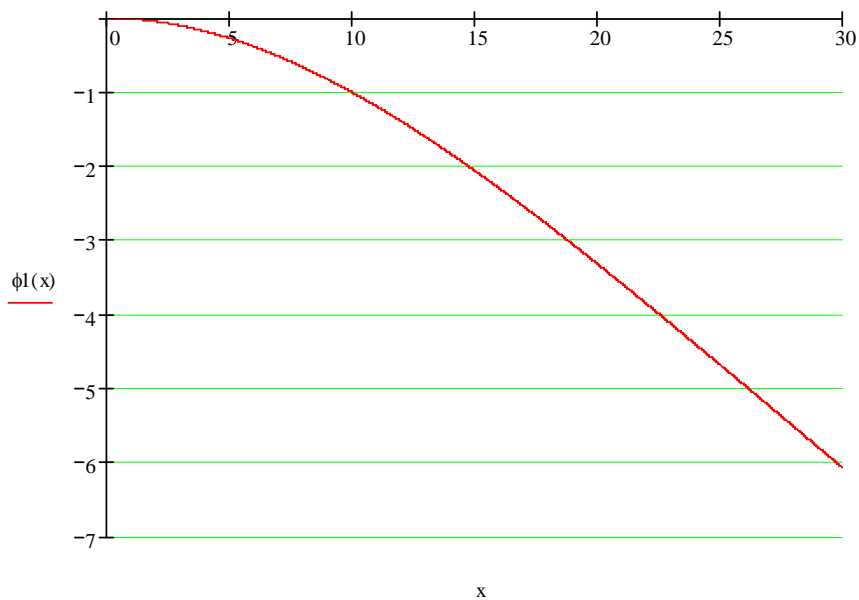
$$x1 = 1.875$$

$$\omega_1 := x1^2 \cdot \sqrt{\frac{EI}{m \cdot L^4}} \quad [\text{rad/sec}] \quad \omega_1 = 11.897$$

$$f1 := \frac{\omega_1}{2 \cdot \pi} \quad [\text{herz}] \quad f1 = 1.893$$

$$\phi I(x) := 1 \cdot \left[(\sin(x1) - \sinh(x1)) \cdot \left(\sin\left(\frac{x1}{L} \cdot x\right) - \sinh\left(\frac{x1}{L} \cdot x\right) \right) + (\cos(x1) + \cosh(x1)) \cdot \left(\cos\left(\frac{x1}{L} \cdot x\right) - \cosh\left(\frac{x1}{L} \cdot x\right) \right) \right]$$

$$\underline{\underline{x}} := 0, 0.01..L$$



$\underline{\underline{x}} := 5$

Second Mode

Given

$1 + \cosh(x) \cdot \cos(x) = 0$

$x2 := \text{Find}(x)$

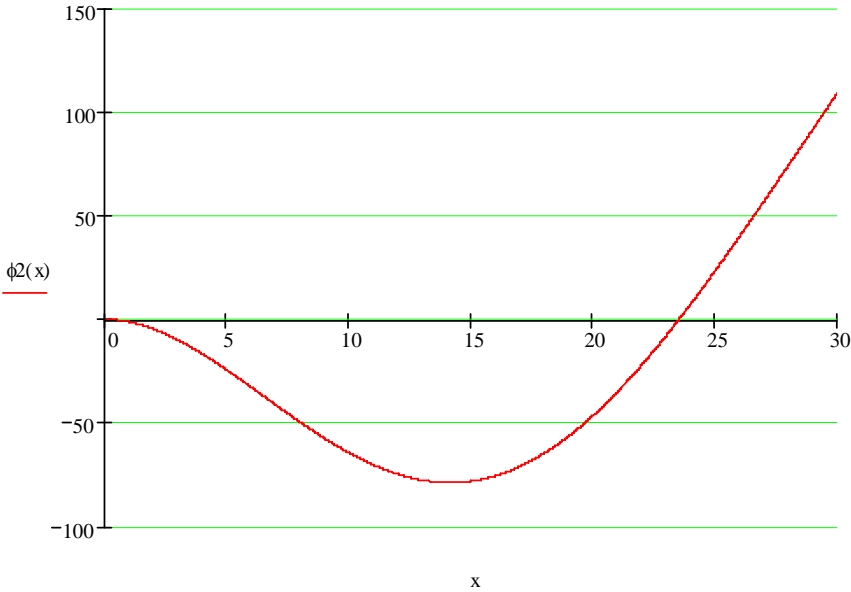
$x2 = 4.694$

$\omega2 := x2^2 \cdot \sqrt{\frac{EI}{m \cdot L^4}}$ [rad/sec] $\omega2 = 74.556$

$f2 := \frac{\omega2}{2 \cdot \pi}$ [herz] $f2 = 11.866$

$\phi2(x) := 1 \cdot \left[(\sin(x2) - \sinh(x2)) \cdot \left(\sin\left(\frac{x2}{L} \cdot x\right) - \sinh\left(\frac{x2}{L} \cdot x\right) \right) + (\cos(x2) + \cosh(x2)) \cdot \left(\cos\left(\frac{x2}{L} \cdot x\right) - \cosh\left(\frac{x2}{L} \cdot x\right) \right) \right]$

$\underline{\underline{x}} := 0, 0.01..L$



Third Mode

$$x_3 := 8$$

Given

$$1 + \cosh(x) \cdot \cos(x) = 0$$

$$x_3 := \text{Find}(x)$$

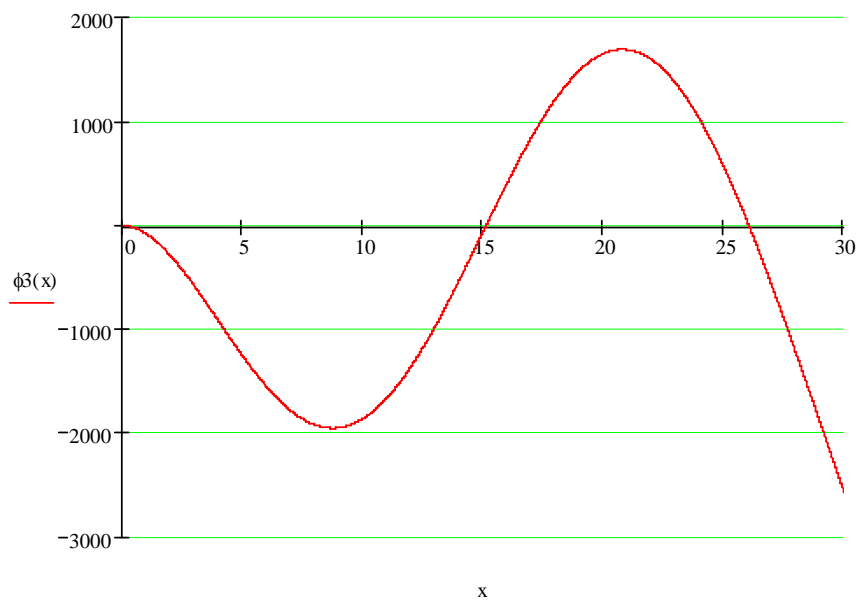
$$x_3 = 7.855$$

$$\omega_3 := x_3^2 \cdot \sqrt{\frac{E \cdot I}{m \cdot L^4}} \quad [\text{rad/sec}] \quad \omega_3 = 208.76$$

$$f_3 := \frac{\omega_3}{2 \cdot \pi} \quad [\text{herz}] \quad f_3 = 33.225$$

$$\phi_3(x) := 1 \cdot \left[(\sin(x_3) - \sinh(x_3)) \cdot \left(\sin\left(\frac{x_3}{L} \cdot x\right) - \sinh\left(\frac{x_3}{L} \cdot x\right) \right) + (\cos(x_3) + \cosh(x_3)) \cdot \left(\cos\left(\frac{x_3}{L} \cdot x\right) - \cosh\left(\frac{x_3}{L} \cdot x\right) \right) \right]$$

$$x := 0, 0.01 \dots L$$



$$\underline{\underline{x}} := 11$$

Fourth Mode

Given

$$1 + \cosh(x) \cdot \cos(x) = 0$$

$$x4 := \text{Find}(x)$$

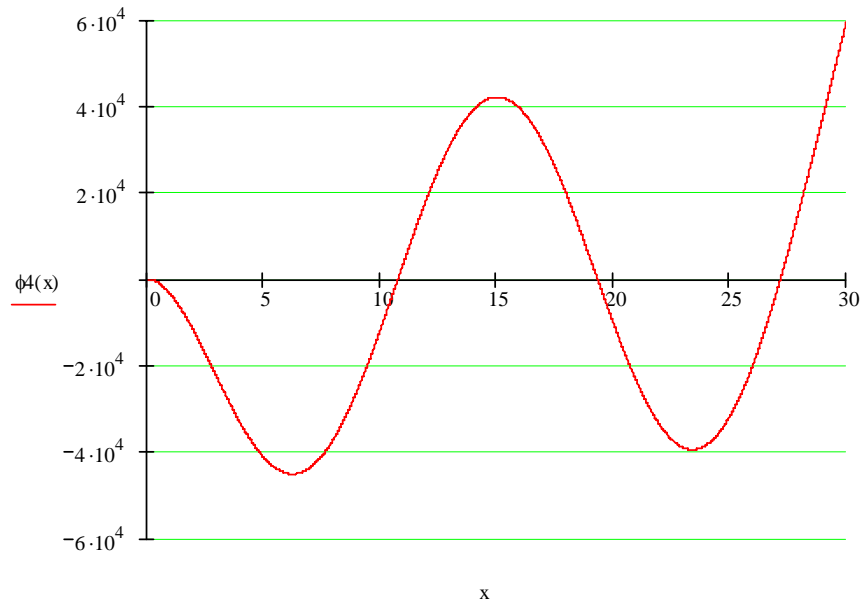
$$x4 = 10.996$$

$$\omega 4 := x4^2 \cdot \sqrt{\frac{E \cdot I}{m \cdot L^4}} \quad [\text{rad/sec}] \quad \omega 4 = 409.086$$

$$f4 := \frac{\omega 4}{2 \cdot \pi} \quad [\text{herz}] \quad f4 = 65.108$$

$$\phi 4(x) := 1 \cdot \left[(\sin(x4) - \sinh(x4)) \cdot \left(\sin\left(\frac{x4}{L} \cdot x\right) - \sinh\left(\frac{x4}{L} \cdot x\right) \right) + (\cos(x4) + \cosh(x4)) \cdot \left(\cos\left(\frac{x4}{L} \cdot x\right) - \cosh\left(\frac{x4}{L} \cdot x\right) \right) \right]$$

$$\underline{\underline{x}} := 0, 0.01 \dots L$$



$$x_5 := 14.13$$

$$f(x) = 4.909 \times 10^3$$

Fifth Mode

Given

$$1 + \cosh(x) \cdot \cos(x) = 0$$

$$x_5 := \text{Find}(x)$$

$$x_5 = 14.137$$

$$\omega_5 := x_5^2 \cdot \sqrt{\frac{E \cdot I}{m \cdot L^4}}$$

[rad/sec]

$$\omega_5 = 676.249$$

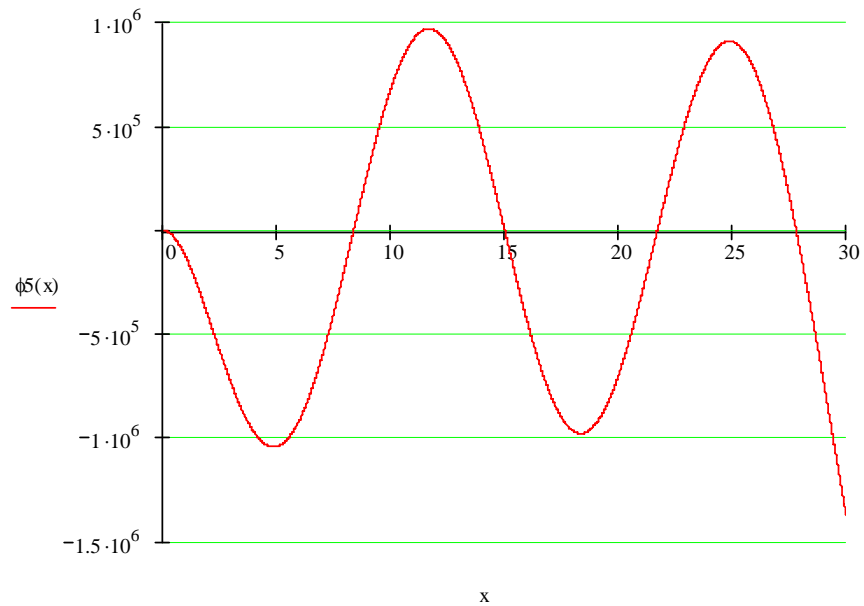
$$f_5 := \frac{\omega_5}{2 \cdot \pi}$$

[herz]

$$f_5 = 107.628$$

$$\phi_5(x) := 1 \cdot \left[(\sin(x_5) - \sinh(x_5)) \cdot \left(\sin\left(\frac{x_5}{L} \cdot x\right) - \sinh\left(\frac{x_5}{L} \cdot x\right) \right) + (\cos(x_5) + \cosh(x_5)) \cdot \left(\cos\left(\frac{x_5}{L} \cdot x\right) - \cosh\left(\frac{x_5}{L} \cdot x\right) \right) \right]$$

$$x := 0, 0.01 \dots L$$



$$x_6 := 17.28$$

$$f(x) = 1.982 \times 10^4$$

Sixth Mode

Given

$$1 + \cosh(x) \cdot \cos(x) = 0$$

$$x_6 := \text{Find}(x)$$

$$x_6 = 17.279$$

$$\omega_6 := x_6^2 \cdot \sqrt{\frac{E \cdot I}{m \cdot L^4}}$$

[rad/sec]

$$\omega_6 = 1.01 \times 10^3$$

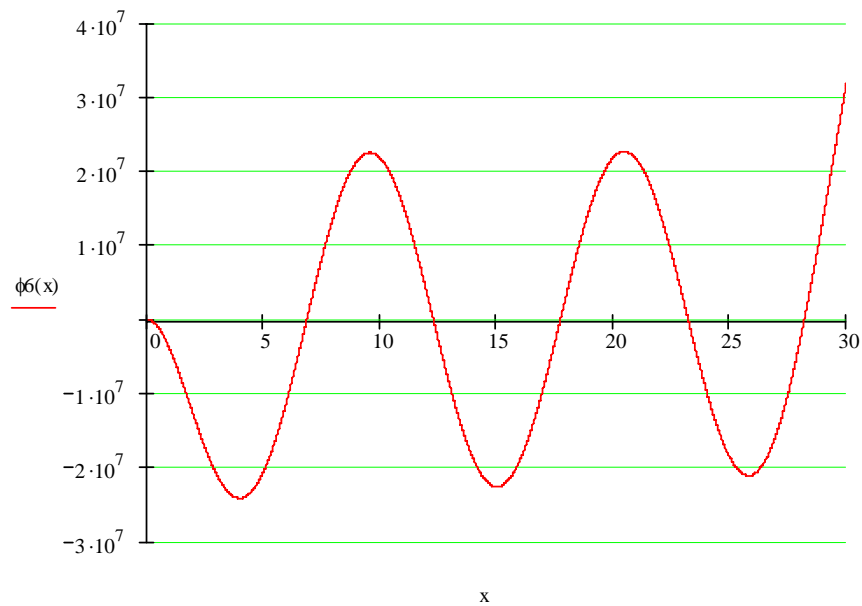
$$f_6 := \frac{\omega_6}{2 \cdot \pi}$$

[herz]

$$f_6 = 160.778$$

$$\phi_6(x) := 1 \cdot \left[(\sin(x_6) - \sinh(x_6)) \cdot \left(\sin\left(\frac{x_6}{L} \cdot x\right) - \sinh\left(\frac{x_6}{L} \cdot x\right) \right) + (\cos(x_6) + \cosh(x_6)) \cdot \left(\cos\left(\frac{x_6}{L} \cdot x\right) - \cosh\left(\frac{x_6}{L} \cdot x\right) \right) \right]$$

$$x := 0, 0.01 \dots L$$



B FEM Analysis in SAP

This appendix briefly describes the model generation and analysis performed to obtain the Frequency Response Function (FRF) of the pile head horizontal displacement with the SAP2000 computer package (CSI, 2004). The results of this analysis are presented in Chapter 3.

B.1 Analysis Type

The analysis performed is identified as *Steady State Analysis* in SAP2000. A steady-state analysis case solves for the response of the structure due to cyclic (harmonic, sinusoidal) loading at one or more frequencies of interest (a range of frequencies of interest may be specified).

B.2 Step by Step Model Generation

This section describes the steps required to generate the 2D Finite Element Model used. When it is considered relevant to help to demonstrate the model generation process, a brief explanation of the step and/or a snapshot of the SAP2000 window is displayed.

1) Define the Model Geometry (FEM Mesh)

The wall template (plane stress elements) was selected to develop the soil model, as shown in Figure B.1. Once this template is selected, a dialog box is displayed in order to enter the parameters that define the FEM mesh. The resulting model is displayed in Figure B.2. Frame elements are then added to model the pile, as shown in Figure B.3

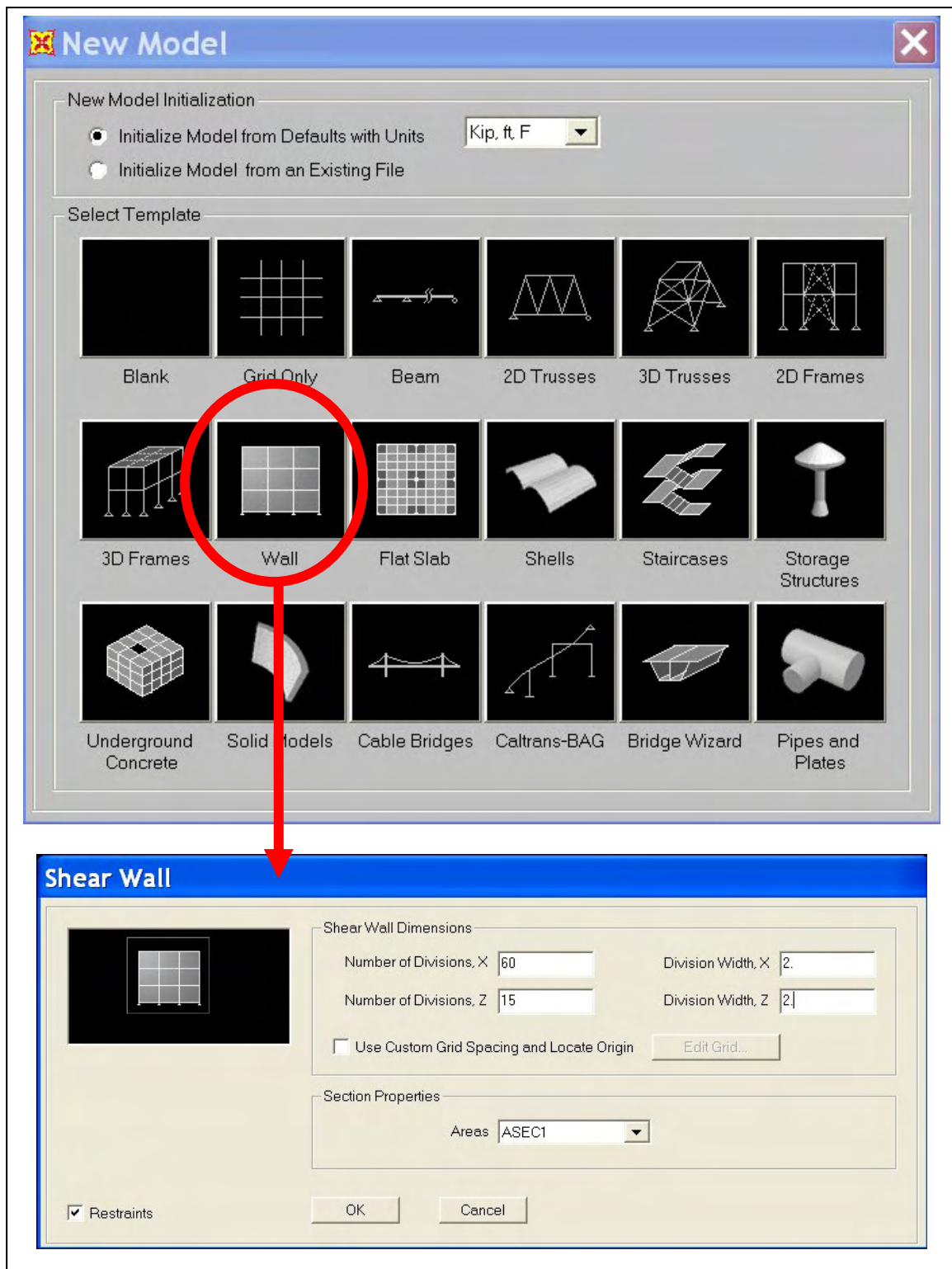


Figure B.1: Template Selection and Mesh Parameters

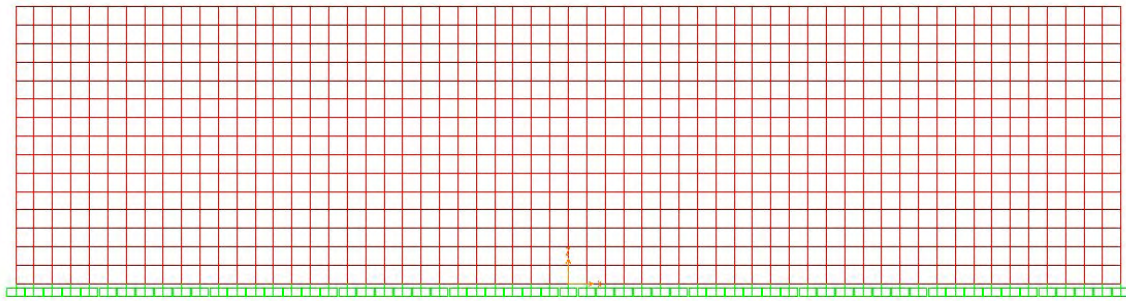


Figure B.2: Soil Mesh

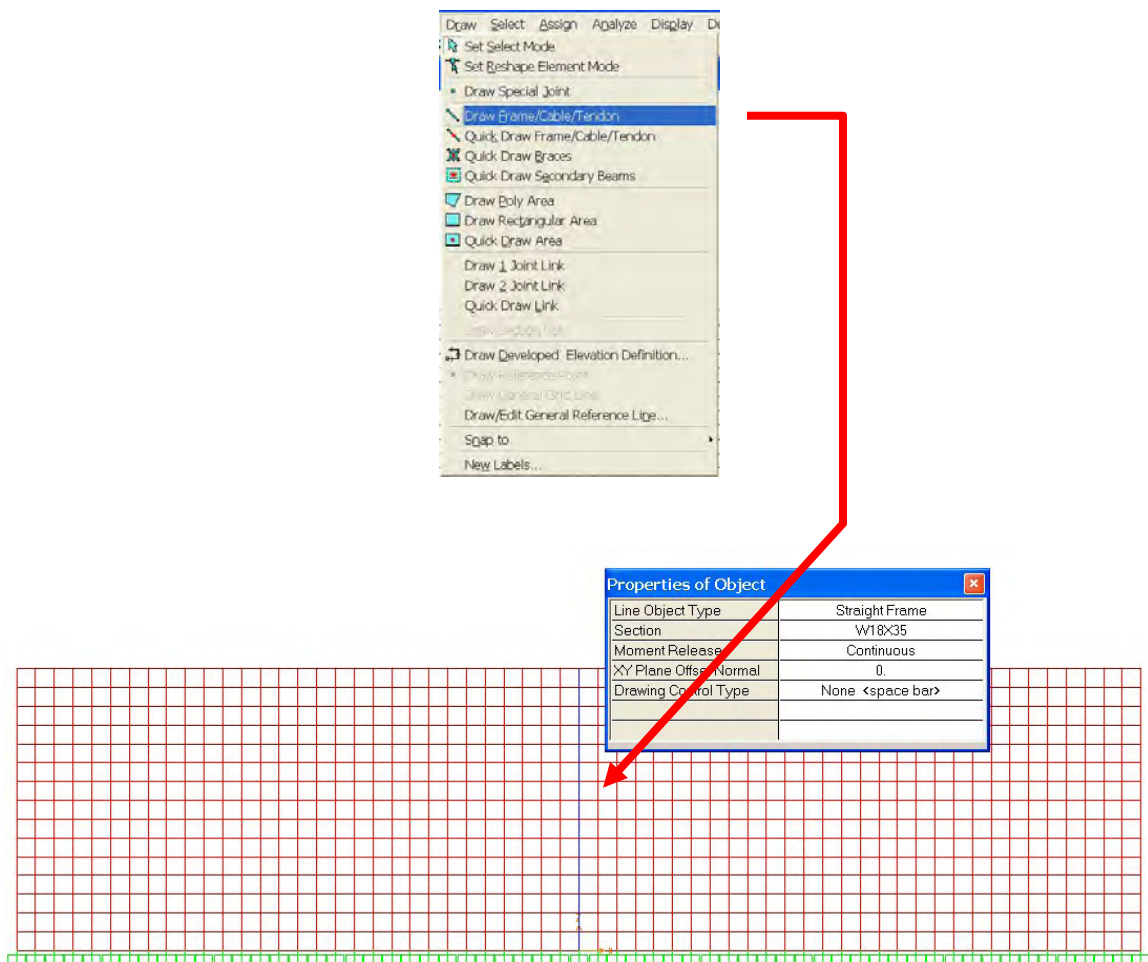


Figure B.3: Soil Mesh (Area Elements) and Pile (Frame Elements)

2) Define the *Material Properties* for soil and concrete, using equivalent elastic modulus and Poisson's ratio.

- 3) Define the *Frame Section* for the pile (1ft x 1ft square cross section), and the *Area Section* for the soil (1 ft thickness, plane stress).
- 4) Assign the previously defined elements sections to the soil and the pile elements.
- 5) Define a *Load Case* that will be used to assign a unit load applied to the pile head (top). In this project, this load was named *Unit*. Figure B.4 shows this definition:

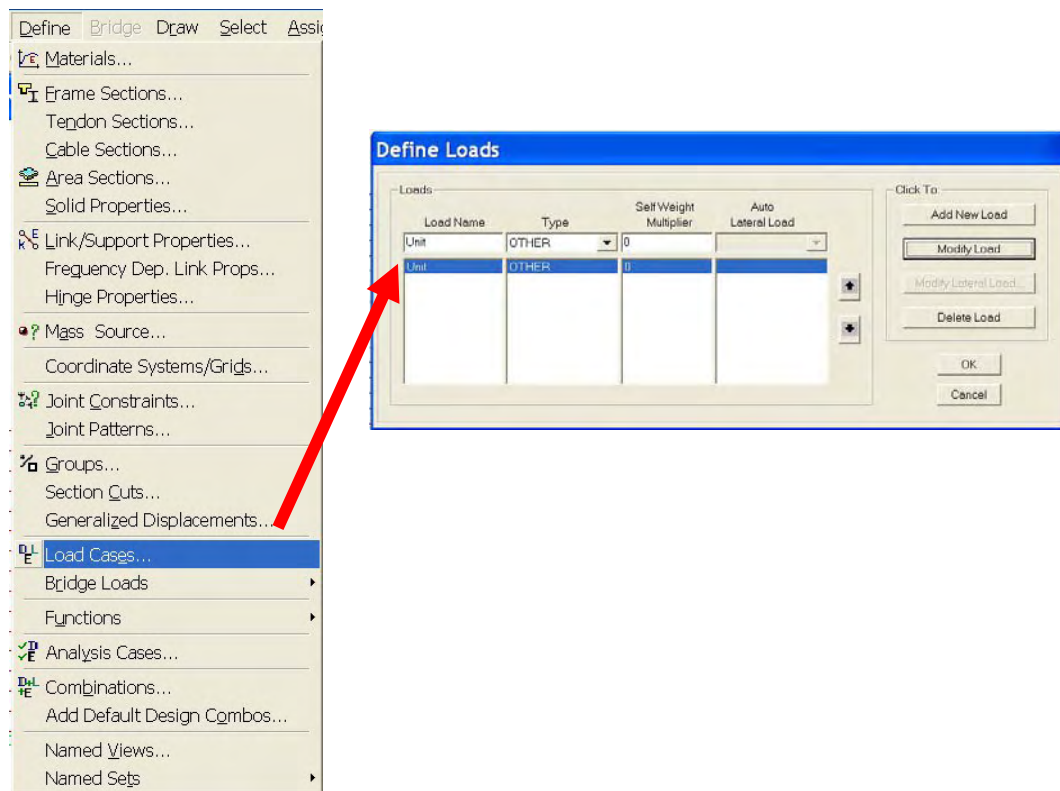


Figure B.4: Load Case Definition

- 6) Define the *Analysis Case* that will be performed. A *Steady State Analysis* is selected, and named FRF (Frequency Response Function). It is specified that this analysis will be performed with a load and that this load is defined in the *Unit* load case. The range of frequencies for which the response will be obtained and the number of frequency steps to

be used are also specified, as displayed in Figure B.5. The Function UNIFSS is a multiplying unit function used as default, that may be modified when certain frequencies are required to be eliminated (Function = 0) or highlighted (Function > 1), or when a force with a frequency dependant magnitude value is present.

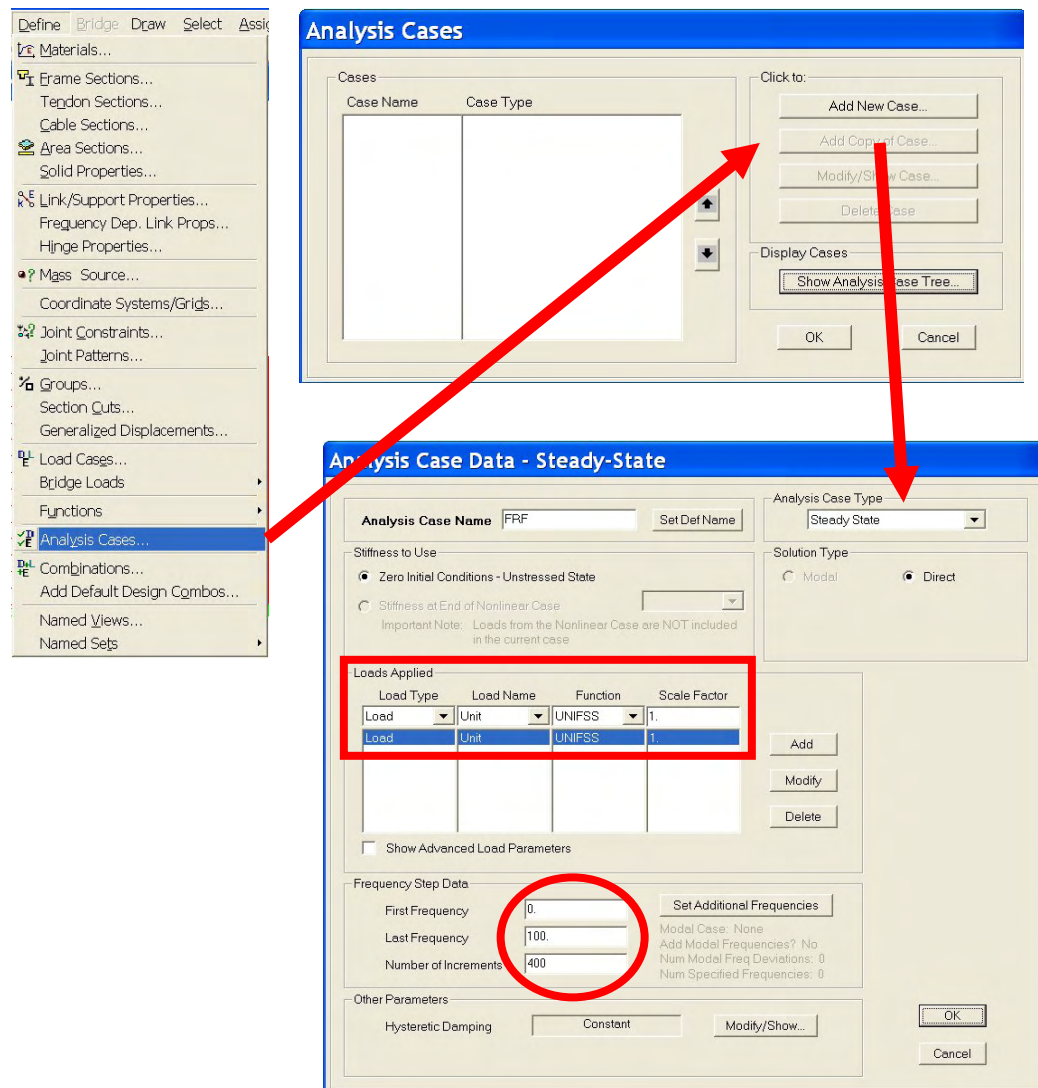


Figure B.5: Analysis Case Definition

- 7) Assign a unit horizontal load to the pile head (top), in the *Unit* load case.
- 8) Apply the appropriate out-of-plane *Restraints*, since this is a 2D (plane) analysis

9) Perform the *Analysis*.

10) Review the results. In the *Display Menu Option*, select the *Show Plot Functions* command. In the dialog box that is displayed, select the *Define Plot Functions* command button, as shown in Figure B.6.

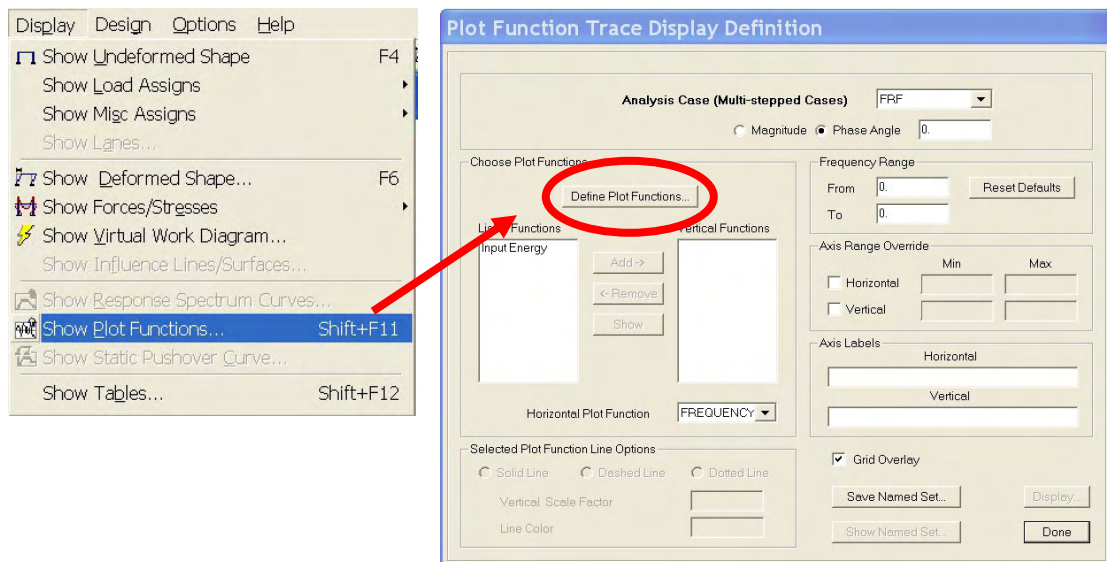


Figure B.6: Setting the Parameters to be Plotted - a

The user is asked to select the variable to be plotted as a function of the frequency. For this study the horizontal displacement of the pile top was selected, as shown in Figure B.7.

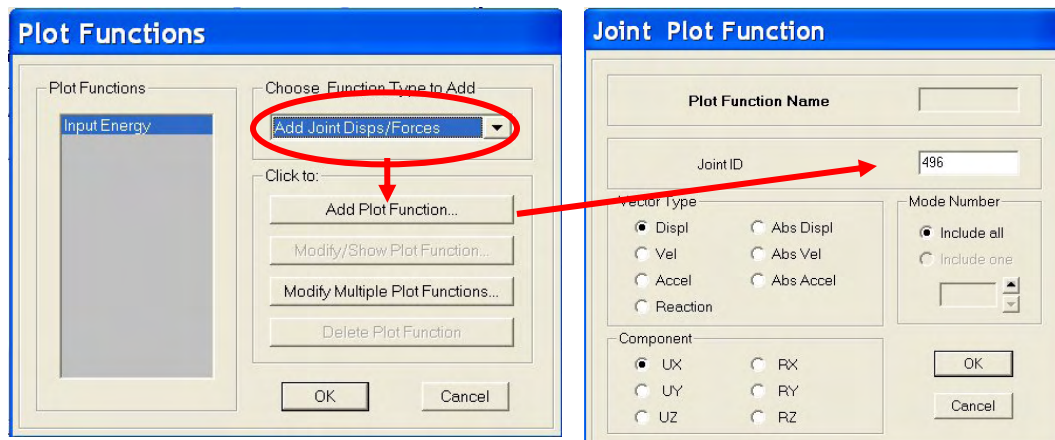


Figure B.7: Setting the Parameters to be Plotted - b

After defining the variable to be plotted, the two dialog boxes are closed, and the selected variable is added to the plot to be displayed, as shown in Figure B.8, the *Magnitude* option button is selected, and the *Display* command button is pressed to display the Frequency Response Function. The results for the present 2D soil model, considering the soil massless, are displayed in Figure B.9

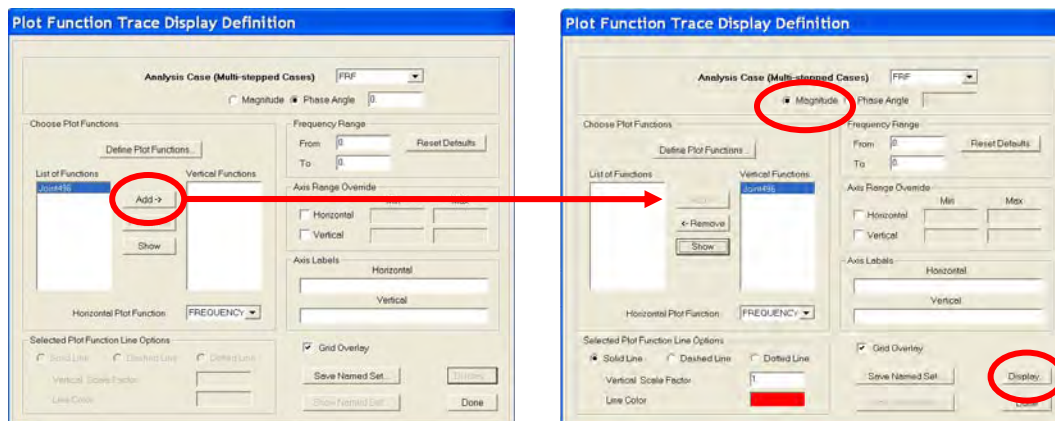


Figure B.8: Setting the Parameters to be Plotted - c

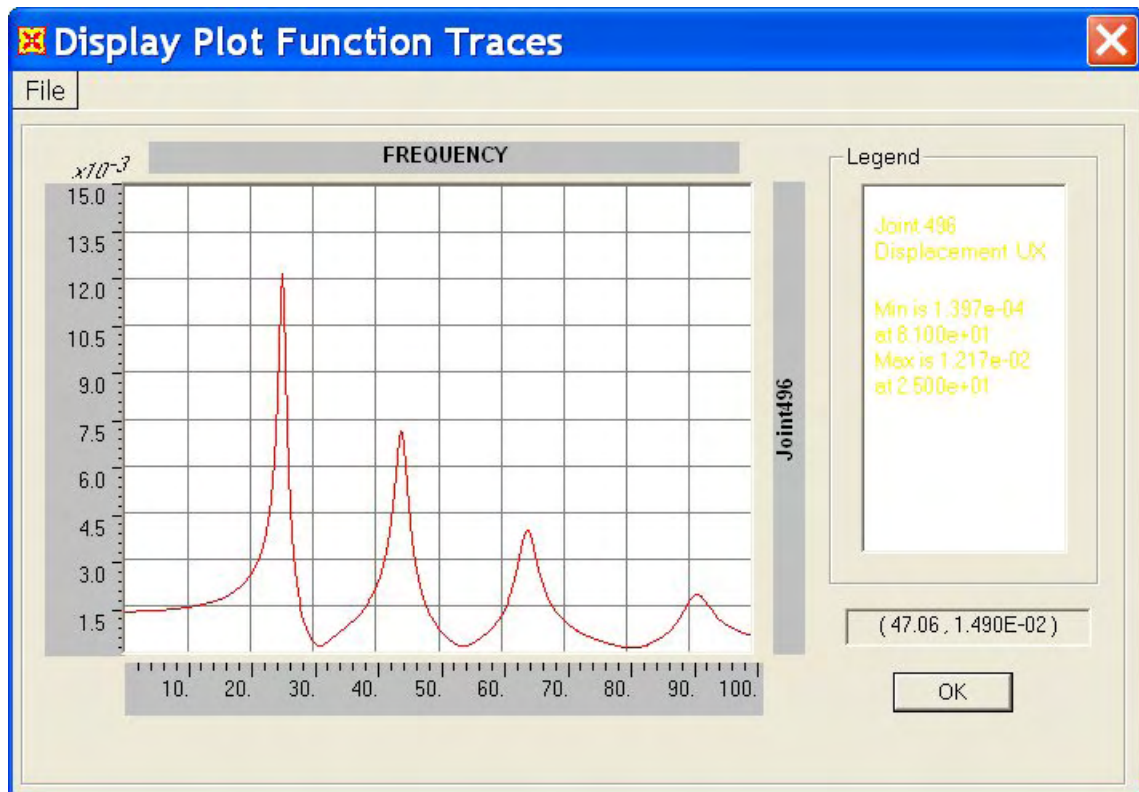


Figure B.9: Frequency Response Function

These results may be exported to a file, by selecting the command *Print Tables to File*, within the *File* menu on the top left of the plot window.

C FEM Boundary Spring Constants

The computations of the appropriate spring constant for the boundaries of the FEM model to simulate the unbounded media nature of the soil deposit are presented. These computations are based on the recommendations given by Luco (2004).

Luco obtained expressions for the average distributed spring constant to be applied in the boundaries of a rectangular soil island or truncated region of dimensions $2a_x \times 2a_y \times a_z$, as depicted in Figure C.1, carved out of the half space. In the present problem $a_x = 60$ ft, $a_y = 30$ ft, and $a_z = 30$ ft.

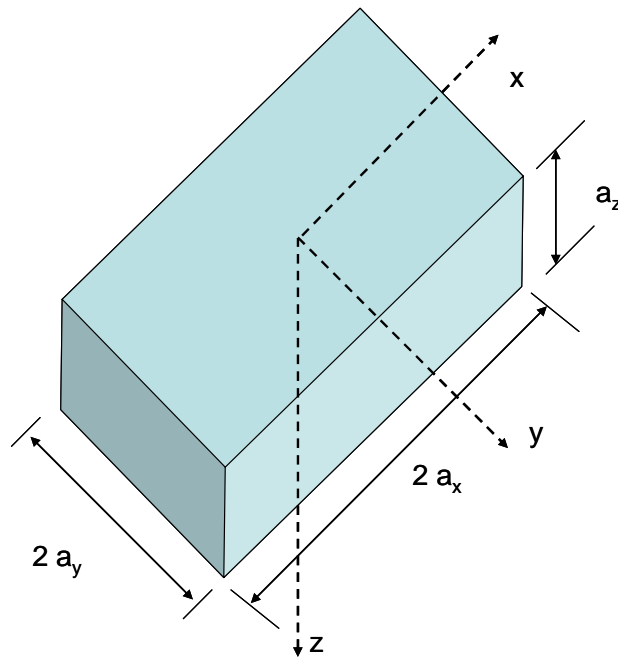


Figure C.1: Rectangular Soil Island Dimensions

Luco proposed that the average distributed springs constants to be applied at the region boundaries are obtained from the following equation:

$$k_{ij} = \frac{G}{a_i} \beta_{ij}$$

Where:

k = distributed spring constant

i = x, y, or z = plane in which the spring is applied

j = x, y, or z = direction in which spring acts

a_i = dimension in the i direction

β_{ij} = coefficient that depends on soil Poisson's ratio and block dimensions

These coefficients have to be multiplied by the *influence area* “A” of each node of the FEM boundary in order to obtain a concentrated spring coefficient, resulting in: $K_{ij} = k_{ij} A$, where the capital letter represents nodal concentrated values. Being the FE model mesh 2'x2', an internal node will have an influence area of $A = 4 \text{ ft}^2$, and edge node of $A = 2 \text{ ft}^2$, and a corner node of $A = 1 \text{ ft}^2$.

The computations are performed in MathCad software package, as displayed in Figure C.2 and C.3 for the boundary located in the longitudinal direction, at $x = 60 \text{ ft}$. This plane is named “x”, since its normal is x axis; so all the stiffness coefficients will be designated as k_{xj} , where j = x, y and z indicates the direction of the spring.

Problem Data

$$E := 12 \quad [\text{Ksi}]$$

$$\nu := 0.3$$

$$a_x := 60 \quad [\text{ft}]$$

$$a_y := 30 \quad [\text{ft}]$$

$$a_z := 30 \quad [\text{ft}]$$

Computations

$$G := \frac{E}{2 \cdot (1 + \nu)} \cdot 144 \cdot 1000 \quad [\text{psf}] \quad G = 6.646 \times 10^5$$

$$\beta_{xx} := 2 \cdot a_x^2 \cdot \frac{\int_{-a_y}^{a_y} \int_0^{a_z} \left[(1 - 2 \cdot \nu) + 3 \cdot \left(\frac{a_x}{\sqrt{a_x^2 + y^2 + z^2}} \right)^2 \right] \cdot \left(\sqrt{a_x^2 + y^2 + z^2} \right)^{-3} dz dy}{\int_{-a_y}^{a_y} \int_0^{a_z} \left[(3 - 4 \cdot \nu) + \left(\frac{a_x}{\sqrt{a_x^2 + y^2 + z^2}} \right)^2 \right] \cdot \left(\sqrt{a_x^2 + y^2 + z^2} \right)^{-1} dz dy} \quad \beta_{xx} = 1.965$$

$$\beta_{xy} := 2 \cdot a_x^2 \cdot \frac{\int_{-a_y}^{a_y} \int_0^{a_z} \left[(1 - 2 \cdot \nu) + 3 \cdot \left(\frac{y}{\sqrt{a_x^2 + y^2 + z^2}} \right)^2 \right] \cdot \left(\sqrt{a_x^2 + y^2 + z^2} \right)^{-3} dz dy}{\int_{-a_y}^{a_y} \int_0^{a_z} \left[(3 - 4 \cdot \nu) + \left(\frac{y}{\sqrt{a_x^2 + y^2 + z^2}} \right)^2 \right] \cdot \left(\sqrt{a_x^2 + y^2 + z^2} \right)^{-1} dz dy} \quad \beta_{xy} = 0.547$$

$$\beta_{xz} := 2 \cdot a_x^2 \cdot \frac{\int_{-a_y}^{a_y} \int_0^{a_z} \left[(1 - 2 \cdot \nu) + 3 \cdot \left(\frac{z}{\sqrt{a_x^2 + y^2 + z^2}} \right)^2 \right] \cdot \left(\sqrt{a_x^2 + y^2 + z^2} \right)^{-3} dz dy}{\int_{-a_y}^{a_y} \int_0^{a_z} \left[(3 - 4 \cdot \nu) + \left(\frac{z}{\sqrt{a_x^2 + y^2 + z^2}} \right)^2 \right] \cdot \left(\sqrt{a_x^2 + y^2 + z^2} \right)^{-1} dz dy} \quad \beta_{xz} = 0.547$$

Figure C.2: Computation of Coefficients β for x plane

$k_{xx} := \frac{G}{a_x} \cdot \beta_{xx}$	$k_{xx} = 2.177 \times 10^4$	[pcf]
$K_{xx_int} := k_{xx} \cdot 4$	$K_{xx_int} = 8.708 \times 10^4$	[lb/ft]
$K_{xx_ext} := k_{xx} \cdot 2$	$K_{xx_ext} = 4.354 \times 10^4$	[lb/ft]
$k_{xy} := \frac{G}{a_x} \cdot \beta_{xy}$	$k_{xy} = 6.064 \times 10^3$	[pcf]
$K_{xy_int} := k_{xy} \cdot 4$	$K_{xy_int} = 2.426 \times 10^4$	[lb/ft]
$K_{xy_ext} := k_{xy} \cdot 2$	$K_{xy_ext} = 1.213 \times 10^4$	[lb/ft]
$k_{xz} := \frac{G}{a_x} \cdot \beta_{xz}$	$k_{xz} = 6.064 \times 10^3$	[pcf]
$K_{xz_int} := k_{xz} \cdot 4$	$K_{xz_int} = 2.426 \times 10^4$	[lb/ft]
$K_{xz_ext} := k_{xz} \cdot 2$	$K_{xz_ext} = 1.213 \times 10^4$	[lb/ft]

Figure C.3: Computation of Coefficients k and K for x plane

D Lumped Equivalent Coefficients for Novak Model

The computations of the appropriate spring, mass and damping coefficients to approximate Novak dynamic stiffness by a lumped SDOF system is presented. The *least square method* to perform a *polynomial fitting* of the data points was implemented.

The following pages present a listing of the MathCad worksheet developed to this end, with the computations performed for a soil hysteretic damping ration of $D = 0.0$, and a soil Poisson's ratio $\nu = 0.5$, $\nu = 0.45$ and $\nu = 0.35$, and $\nu = 0.30$ as examples of the performed analysis.

The worksheet also presents the computation of coefficient of determination R^2 (R-squared), obtained in order to determine how well does the regression equation truly represent the set of data used (points of the Novak plane strain model in the range of dimensionless frequency $0 < \omega < 3$). The reference equations used to obtain R^2 are:

$$R^2 = 1 - \frac{RSS}{TSS}$$

$$RSS = \sum_{i=1}^N (y_i - \hat{y}_i)^2 = \text{Residual Sum of Squares}$$

$$TSS = \sum_{i=1}^N (y_i - \bar{y})^2 = \text{Total Som of Squares}$$

$$y_i = \text{data value}$$

$$\hat{y}_i = \text{estimated value}$$

$$N = \text{number of data points}$$

$$\bar{y} = \frac{\sum_{i=1}^N y_i}{N} = \text{mean value of data points}$$

In the cases when the real part of Novak Dynamic Stiffness is approximated by an horizontal line, the least squares solutions gives the constant value as the mean value of

the ordinate data points. In this case, the coefficient of determination is meaningless, and its results is zero, since it is intended to give a quantification of how better is to approximate the ordinates by the polynomial equation instead of using the mean value. For these cases, the *coefficient of variation CV*, in percentage (also known as the relative standard deviation) will be used to determine the adequacy of the approximation: the closer CV is to zero, the better the mean value represents the whole data. CV is defined as:

$$CV = \frac{s}{\bar{y}} \times 100$$

$$\bar{y} = \frac{\sum_{i=1}^N y_i}{N} = \text{sample mean value}$$

$$s = \sqrt{\frac{(y_i - \bar{y})^2}{N-1}} = \text{sample standard deviation}$$

N = number of data points

D.1 Case of $D = 0.0$ and $\nu = 0.5$

Novak Dinamic Stiffness (Novak et al, 1978)

Pile and Soil Data

$$\nu := 0.4999999$$

soil Poisson's ratio

$$D := 0$$

soil hysteretic damping ratio = G'/G

Computations

$$\eta := \sqrt{\frac{2 \cdot (1 - \nu)}{1 - 2 \cdot \nu}} \quad \eta = 2.236 \times 10^3$$

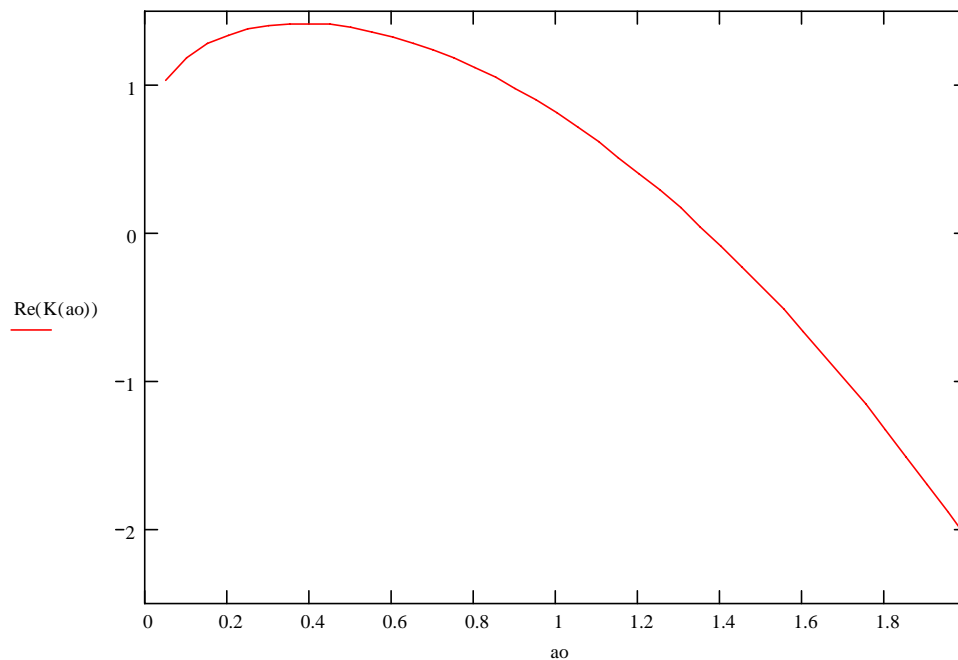
$$ao'(ao) := \frac{aoi}{\sqrt{1 + Di}}$$

$$bo'(ao) := \frac{aoi}{\eta \cdot \sqrt{1 + Di}}$$

$$T(ao) := \frac{4 \cdot K1(bo'(ao)) \cdot K1(ao'(ao)) + ao'(ao) \cdot K1(bo'(ao)) \cdot K0(ao'(ao)) + bo'(ao) \cdot K0(bo'(ao)) \cdot K1(ao'(ao))}{bo'(ao) \cdot K0(bo'(ao)) \cdot K1(ao'(ao)) + ao'(ao) \cdot K1(bo'(ao)) \cdot K0(ao'(ao)) + bo'(ao) \cdot ao'(ao) \cdot K0(bo'(ao)) \cdot K0(ao'(ao))}$$

$$K(ao) := -1 \cdot ao^2 \cdot T(ao)$$

$$ao := 0, 0.05..2$$



Real Part Maximum Determination

$$\text{fr}(\text{ao}) := \text{Re}(K(\text{ao}))$$

$$\text{ao} := 0.3$$

Given

$$\text{ao} \geq 0.0$$

$$\text{maxRe} := \text{Maximize}(\text{fr}, \text{ao}) \quad \text{maxRe} = 0.378$$

Real Part Curve Fitting by Least-Squares Approximation

$$N := 29$$

$$x_1 := 0.0$$

$$y_1 := \text{fr}(\text{maxRe})$$

$$i := 2..N$$

$$x_i := \text{maxRe} + 0.1 \cdot (i - 2)$$

$$y_i := \text{fr}(x_i)$$

$$\begin{pmatrix} \alpha K \\ \alpha M \end{pmatrix} := \begin{bmatrix} N & \sum_{i=1}^N (x_i)^2 \\ \sum_{i=1}^N (x_i)^2 & \sum_{i=1}^N (x_i)^4 \end{bmatrix}^{-1} \cdot \begin{bmatrix} \sum_{i=1}^N y_i \\ \sum_{i=1}^N [(x_i)^2 \cdot y_i] \end{bmatrix}$$

$$\alpha M := -\alpha M$$

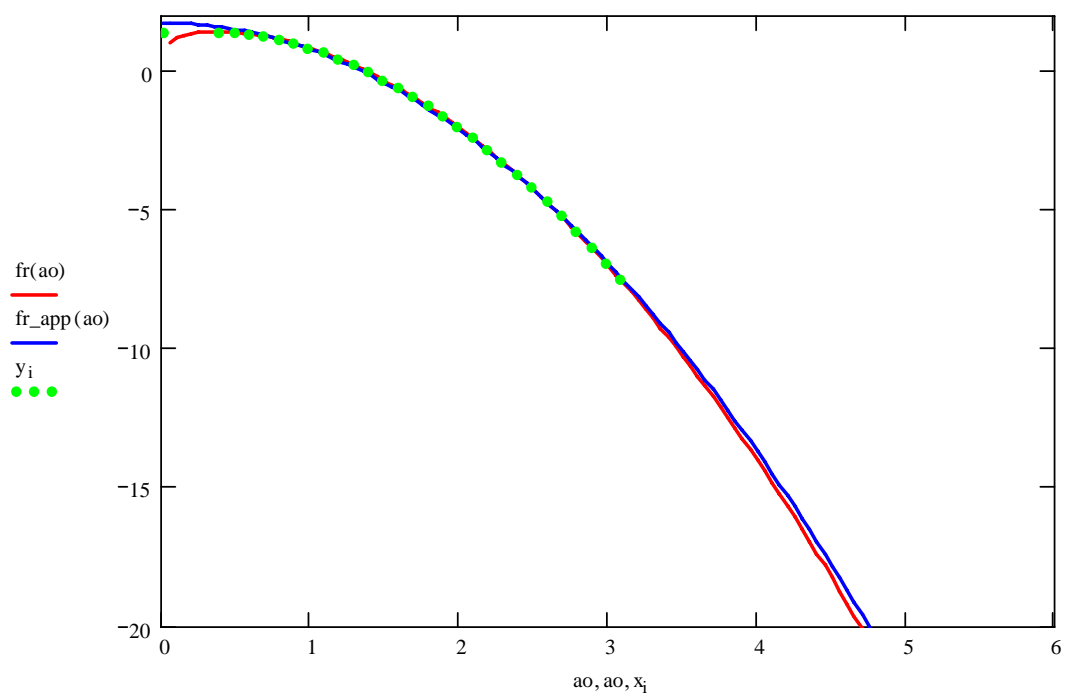
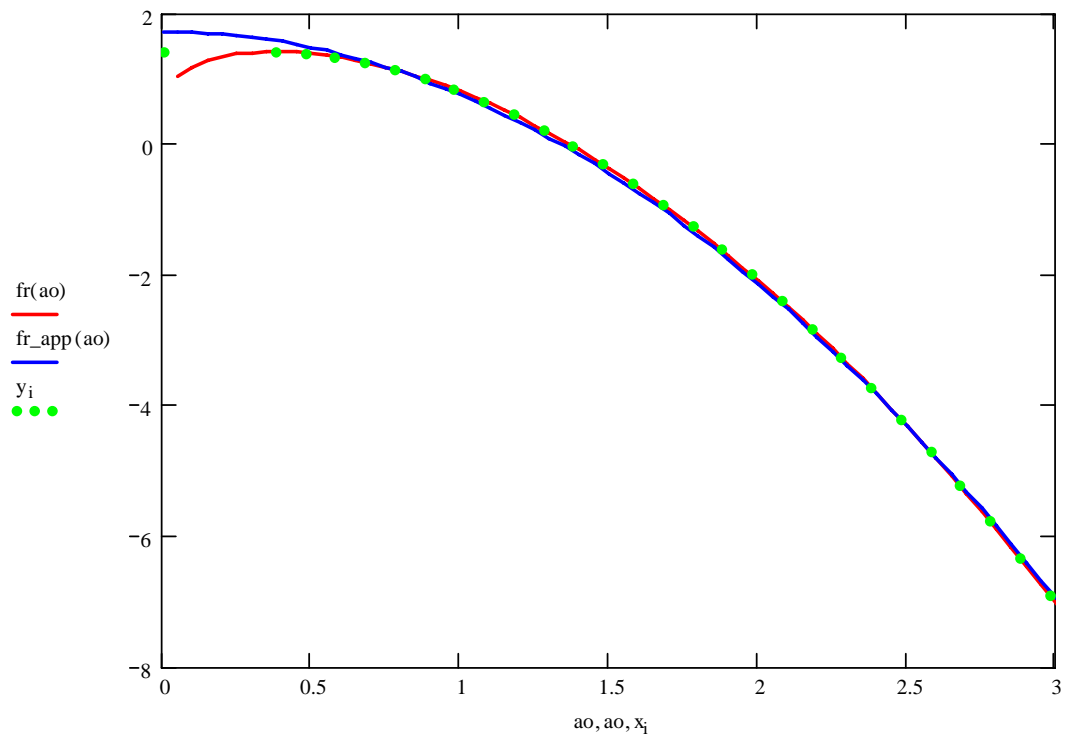
$$\alpha K = 1.7213669$$

$$\alpha M = 0.9653314$$

$$\text{fr_app}(\text{ao}) := \alpha K - \alpha M \cdot \text{ao}^2$$

$i := 1..N$

$ao := 0, 0.05..5.5$



Coefficient of Determination for the Real Part

$$y_m := \frac{\sum_{j=1}^N y_j}{N}$$

$$i := 1..N$$

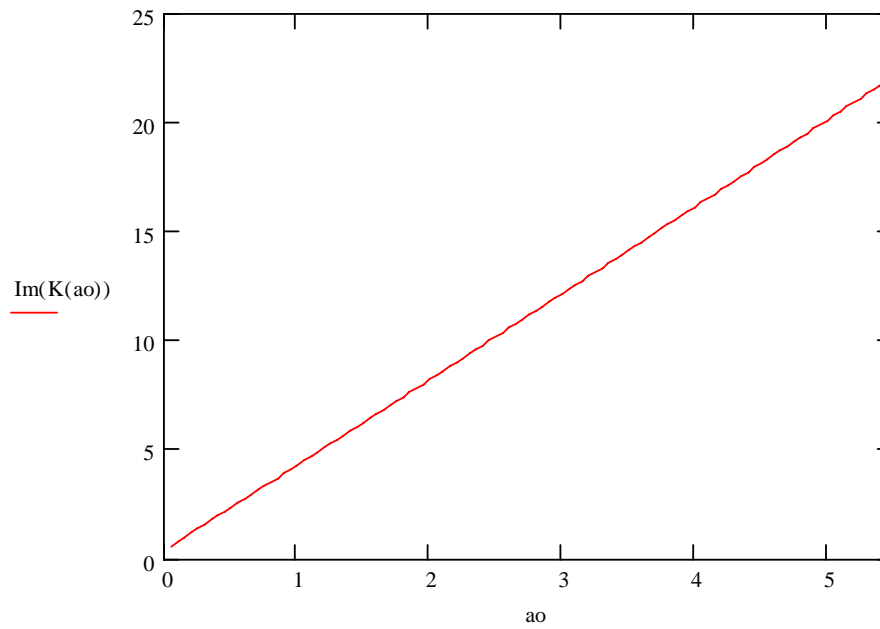
$$ya_i := \text{fr_app}(x_i)$$

$$\text{RSS} := \sum_{j=1}^N (y_j - ya_j)^2$$

$$\text{TSS} := \sum_{j=1}^N (y_j - y_m)^2$$

$$R^2 := 1 - \frac{\text{RSS}}{\text{TSS}}$$

$$R^2 = 0.999$$



Imaginary Part Curve Fitting by Least-Squares Approximation

$$f_i(ao) := \text{Im}(K(ao))$$

$$N := 30$$

$$x_1 := 0.0$$

$$y_1 := 0$$

$$i := 2..N$$

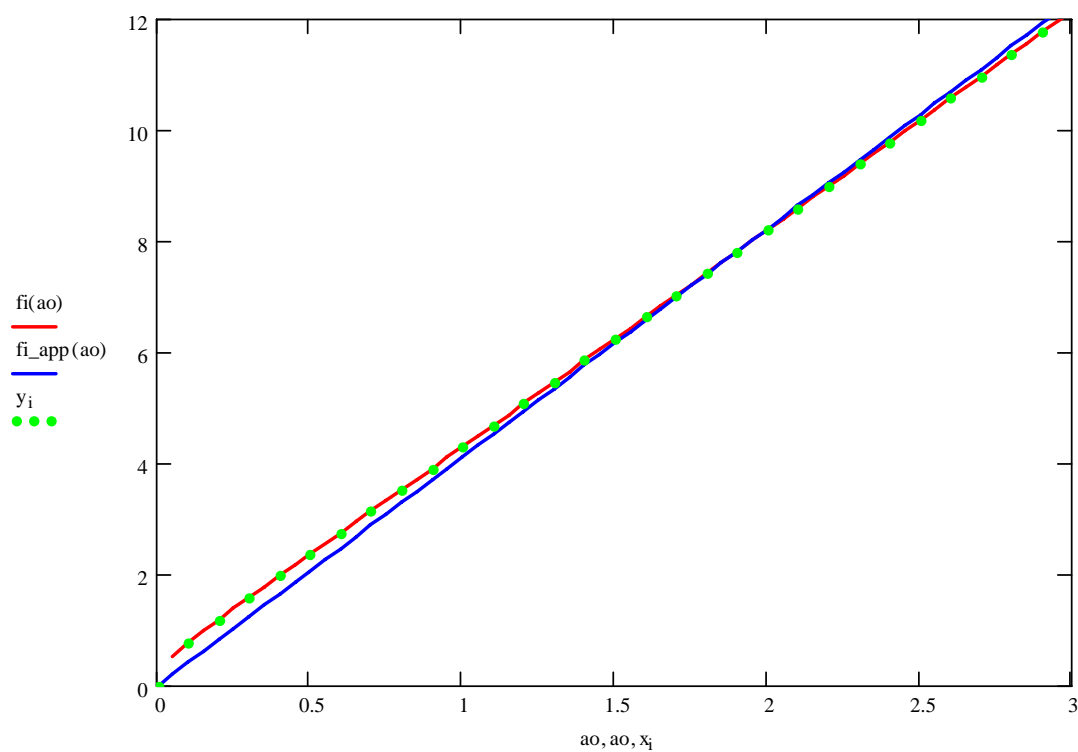
$$x_i := 0.1 \cdot (i - 1)$$

$$y_i := f_i(x_i)$$

$$\alpha C := \frac{\sum_{i=1}^N (x_i \cdot y_i)}{\sum_{i=1}^N (x_i)^2}$$

$$\alpha C = 4.1074708$$

$$f_{i_app}(ao) := \alpha C \cdot ao$$

$i := 1..N$
 $ao := 0, 0.05..6.9$


Coefficient of Determination for the Imaginary Part

$$y_m := \frac{\sum_{j=1}^N y_j}{N}$$

$$i := 1..N$$

$$y_{a_i} := \text{fi_app}(x_i)$$

$$\text{RSS} := \sum_{j=1}^N (y_j - y_{a_j})^2$$

$$\text{TSS} := \sum_{j=1}^N (y_j - y_m)^2$$

$$R^2 := 1 - \frac{\text{RSS}}{\text{TSS}}$$

$$R^2 = 0.997$$

D.2 Case of $D = 0.0$ and $\nu = 0.45$

Novak Dynamic Stiffness (Novak et al, 1978)

Pile and Soil Data

$$\nu := 0.45$$

soil Poisson's ratio

$$D := 0$$

soil hysteretic damping ratio = G'/G

Computations

$$\eta := \sqrt{\frac{2 \cdot (1 - \nu)}{1 - 2 \cdot \nu}} \quad \eta = 3.317$$

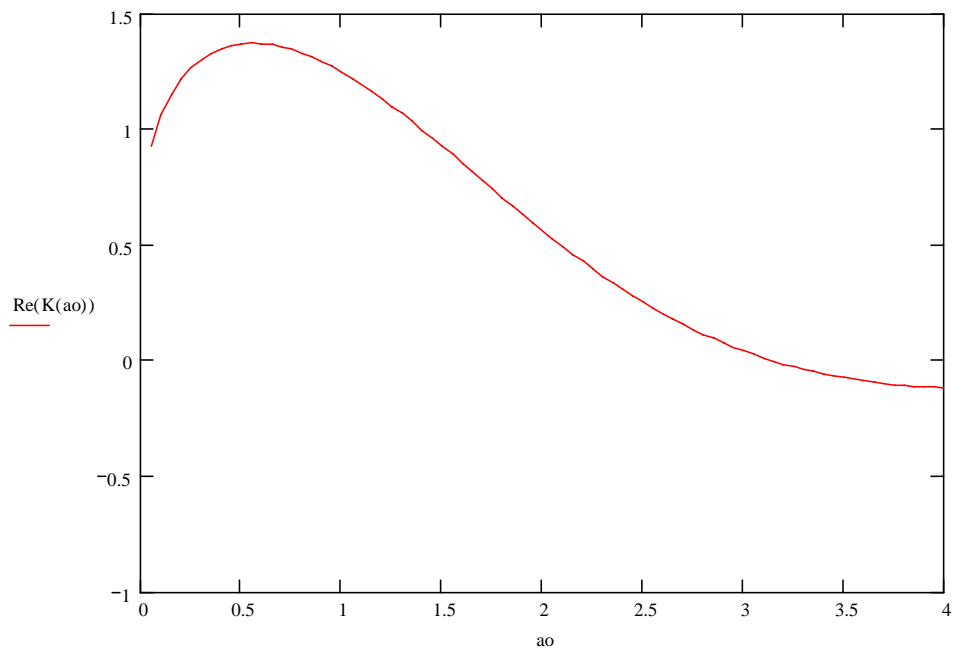
$$ao'(ao) := \frac{aoi}{\sqrt{1 + Di}}$$

$$bo'(ao) := \frac{aoi}{\eta \cdot \sqrt{1 + Di}}$$

$$T(ao) := \frac{4 \cdot K1(bo'(ao)) \cdot K1(ao'(ao)) + ao'(ao) \cdot K1(bo'(ao)) \cdot K0(ao'(ao)) + bo'(ao) \cdot K0(bo'(ao)) \cdot K1(ao'(ao))}{bo'(ao) \cdot K0(bo'(ao)) \cdot K1(ao'(ao)) + ao'(ao) \cdot K1(bo'(ao)) \cdot K0(ao'(ao)) + bo'(ao) \cdot ao'(ao) \cdot K0(bo'(ao)) \cdot K0(ao'(ao))}$$

$$K(ao) := -1 \cdot ao^2 \cdot T(ao)$$

$$ao := 0, 0.05..4$$



Real Part Maximum Determination

$$\text{fr}(\text{ao}) := \text{Re}(K(\text{ao}))$$

$$\text{ao} := 0.3$$

Given

$$\text{ao} \geq 0.0$$

$$\text{maxRe} := \text{Maximize}(\text{fr}, \text{ao}) \quad \text{maxRe} = 0.558$$

Real Part Inflection Point Determination

$$\text{gr}(\text{ao}) := \frac{d}{d\text{ao}} \text{fr}(\text{ao})$$

$$\text{ao} := 1.1 \cdot \text{maxRe}$$

Given

$$\text{ao} \geq 0.0$$

$$\text{minRe}' := \text{Minimize}(\text{gr}, \text{ao}) \quad \text{minRe}' = 1.671$$

Real Part Curve Fitting by Least-Squares Approximation

$$N := 29$$

$$x_1 := 0.0$$

$$y_1 := \text{fr}(\text{maxRe})$$

$$i := 2..N$$

$$x_i := \text{maxRe} + 0.1 \cdot (i - 2)$$

$$y_i := \text{if} \left[x_i < \text{minRe}', \text{fr}(x_i), \text{fr}(\text{minRe}') + \text{gr}(\text{minRe}') \cdot (x_i - \text{minRe}') \right]$$

$$\begin{pmatrix} \alpha K \\ \alpha M \end{pmatrix} := \begin{bmatrix} N & \sum_{i=1}^N (x_i)^2 \\ \sum_{i=1}^N (x_i)^2 & \sum_{i=1}^N (x_i)^4 \end{bmatrix}^{-1} \begin{bmatrix} \sum_{i=1}^N y_i \\ \sum_{i=1}^N [(x_i)^2 \cdot y_i] \end{bmatrix}$$

$$\alpha M := -\alpha M$$

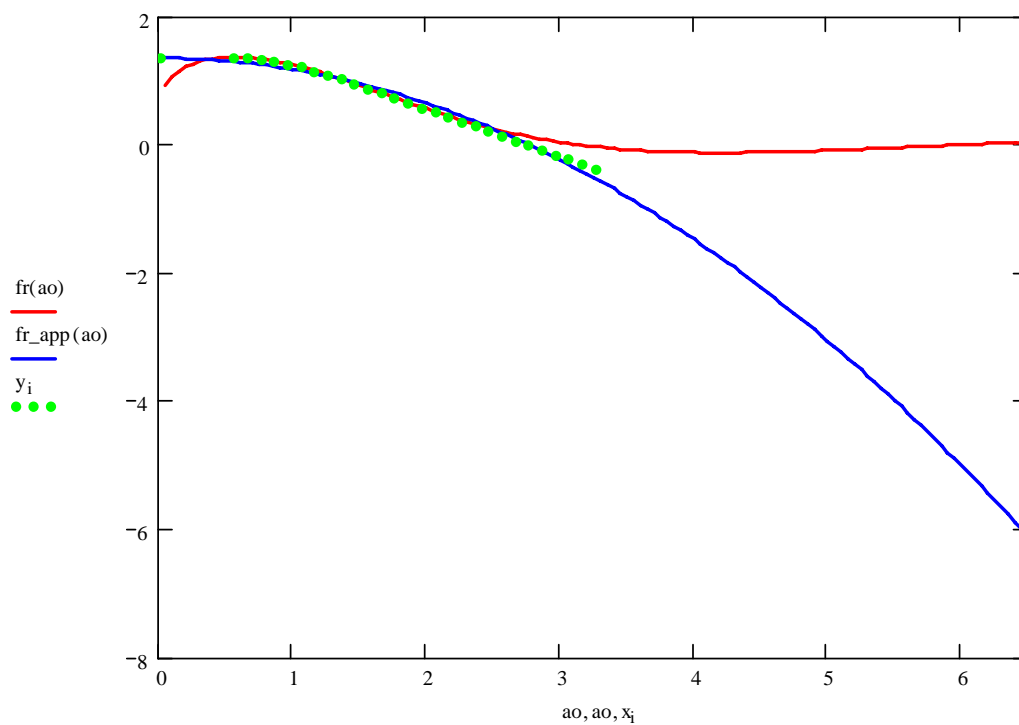
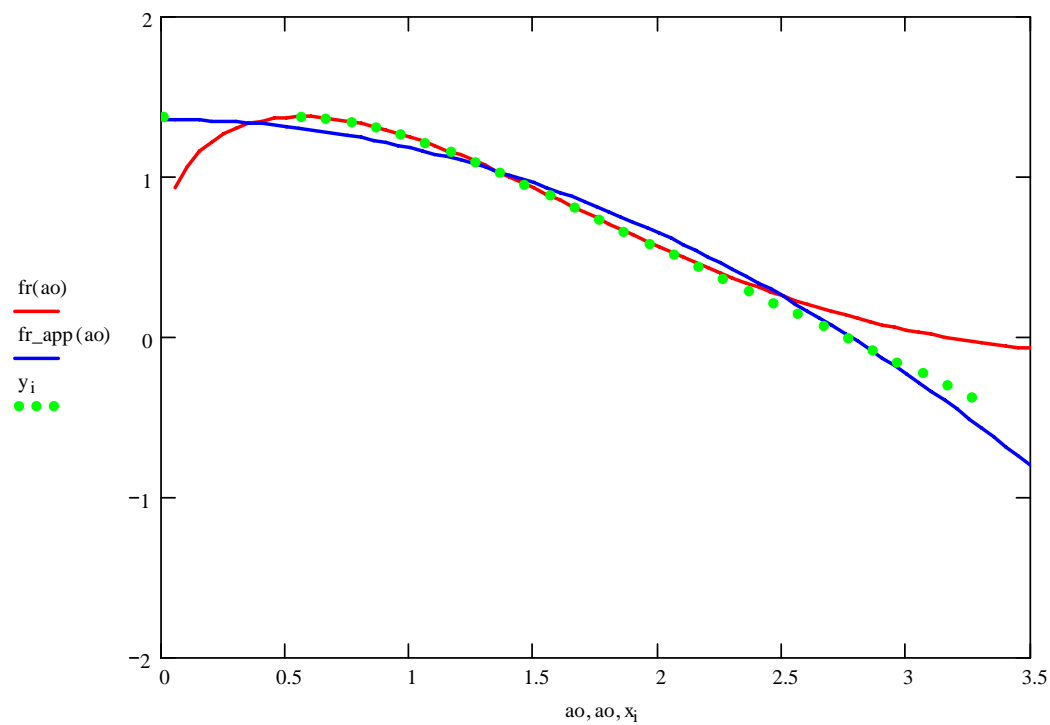
$$\alpha K = 1.3543719$$

$$\alpha M = 0.1766402$$

$$\text{fr_app}(\text{ao}) := \alpha K - \alpha M \cdot \text{ao}^2$$

i := 1..N

ao := 0, 0.05.. 6.5



Coefficient of Determination for the Real Part

$$y_m := \frac{\sum_{j=1}^N y_j}{N}$$

$$i := 1..N$$

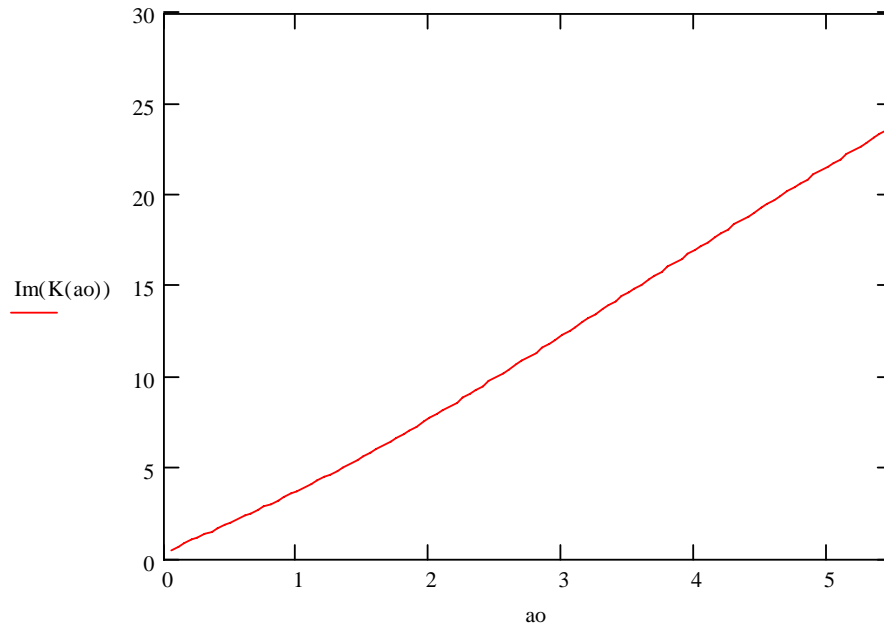
$$ya_i := \text{fr_app}(x_i)$$

$$\text{RSS} := \sum_{j=1}^N (y_j - ya_j)^2$$

$$\text{TSS} := \sum_{j=1}^N (y_j - y_m)^2$$

$$R^2 := 1 - \frac{\text{RSS}}{\text{TSS}}$$

$$R^2 = 0.984$$



Imaginary Part Curve Fitting by Least-Squares Approximation

$$f_i(ao) := \text{Im}(K(ao))$$

$$N := 30$$

$$x_1 := 0.0$$

$$y_1 := 0$$

$$i := 2..N$$

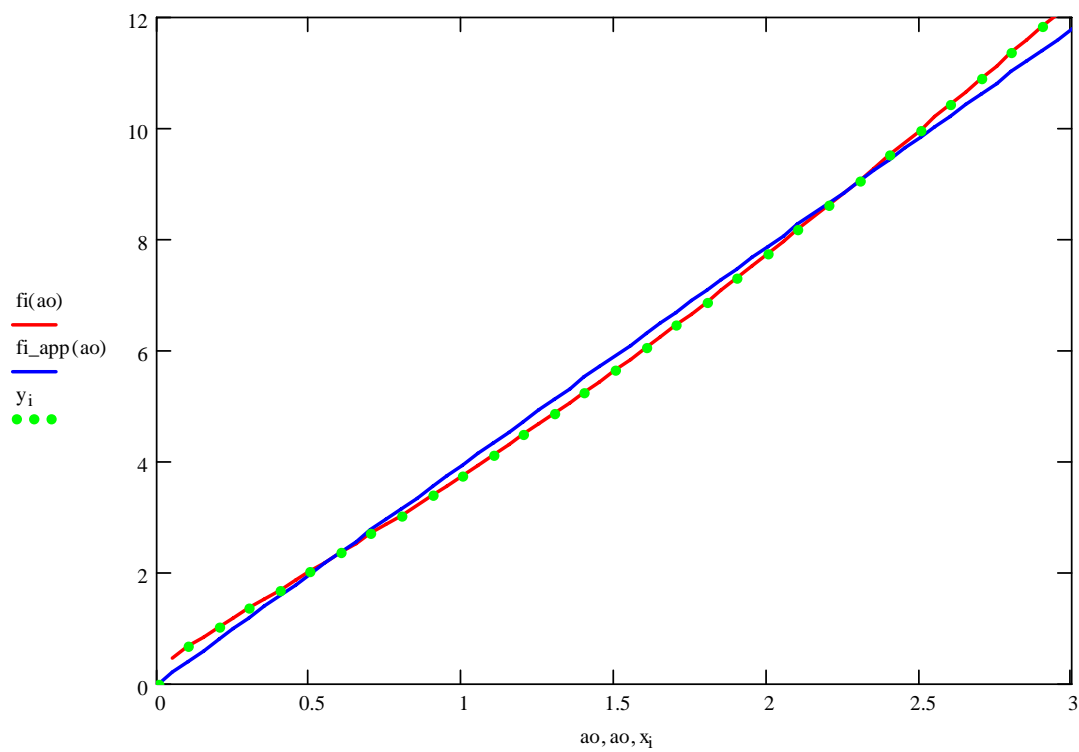
$$x_i := 0.1 \cdot (i - 1)$$

$$y_i := f_i(x_i)$$

$$\alpha C := \frac{\sum_{i=1}^N (x_i \cdot y_i)}{\sum_{i=1}^N (x_i)^2}$$

$$\alpha C = 3.9294084$$

$$f_{i_app}(ao) := \alpha C \cdot ao$$

$i := 1..N$
 $ao := 0, 0.05..6.9$


Coefficient of Determination for the Imaginary Part

$$y_m := \frac{\sum_{j=1}^N y_j}{N}$$

$$i := 1..N$$

$$y_{a_i} := \text{fi_app}(x_i)$$

$$\text{RSS} := \sum_{j=1}^N (y_j - y_{a_j})^2$$

$$\text{TSS} := \sum_{j=1}^N (y_j - y_m)^2$$

$$R^2 := 1 - \frac{\text{RSS}}{\text{TSS}}$$

$$R^2 = 0.997$$

D.3 Case of $D = 0.0$ and $\nu = 0.35$

Novak Dinamic Stiffness (Novak et al, 1978)

Pile and Soil Data

$$\nu := 0.35$$

soil Poisson's ratio

$$D := 0$$

soil hysteretic damping ratio = G'/G

Computations

$$\eta := \sqrt{\frac{2 \cdot (1 - \nu)}{1 - 2 \cdot \nu}} \quad \eta = 2.082$$

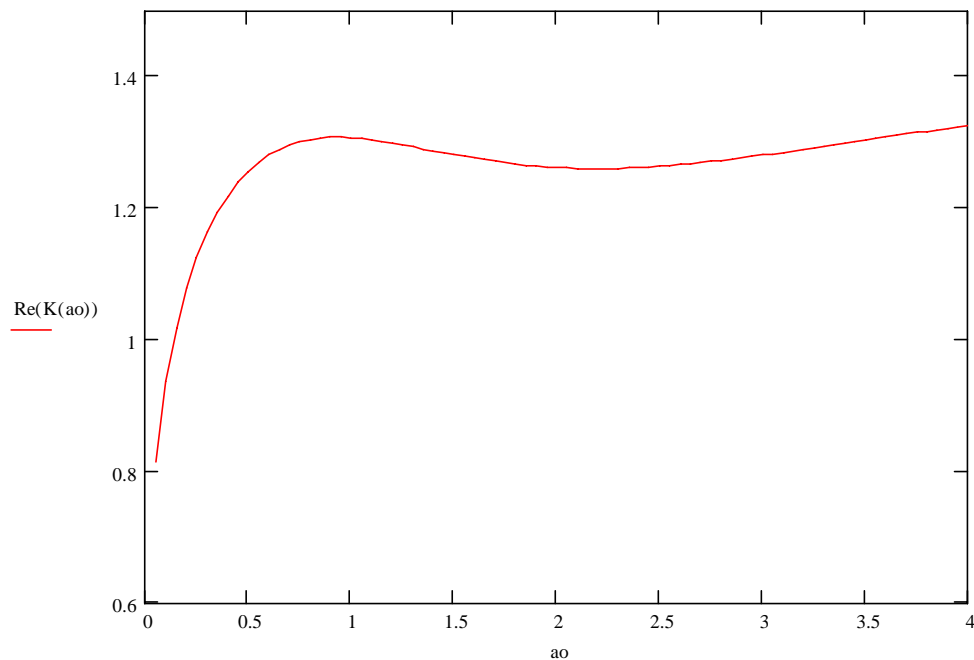
$$ao'(ao) := \frac{aoi}{\sqrt{1 + Di}}$$

$$bo'(ao) := \frac{aoi}{\eta \cdot \sqrt{1 + Di}}$$

$$T(ao) := \frac{4 \cdot K1(bo'(ao)) \cdot K1(ao'(ao)) + ao'(ao) \cdot K1(bo'(ao)) \cdot K0(ao'(ao)) + bo'(ao) \cdot K0(bo'(ao)) \cdot K1(ao'(ao))}{bo'(ao) \cdot K0(bo'(ao)) \cdot K1(ao'(ao)) + ao'(ao) \cdot K1(bo'(ao)) \cdot K0(ao'(ao)) + bo'(ao) \cdot ao'(ao) \cdot K0(bo'(ao)) \cdot K0(ao'(ao))}$$

$$K(ao) := -1 \cdot ao^2 \cdot T(ao)$$

$$ao := 0, 0.05..4$$



Real Part Maximum Determination

$$\text{fr}(\text{ao}) := \text{Re}(K(\text{ao}))$$

$$\text{ao} := 0.3$$

Given

$$\text{ao} \geq 0.0$$

$$\text{maxRe} := \text{Maximize}(\text{fr}, \text{ao}) \quad \text{maxRe} = 0.933$$

Real Part Inflection Point Determination

$$\text{gr}(\text{ao}) := \frac{d}{d\text{ao}} \text{fr}(\text{ao})$$

$$\text{ao} := 1.1 \cdot \text{maxRe}$$

Given

$$\text{ao} \geq 0.0$$

$$\text{minRe}' := \text{Minimize}(\text{gr}, \text{ao}) \quad \text{minRe}' = 1.37$$

Real Part Curve Fitting by Least-Squares Approximation

$$N := 29$$

$$x_1 := 0.0$$

$$y_1 := \text{fr}(\text{maxRe})$$

$$i := 2..N$$

$$x_i := \text{maxRe} + 0.1 \cdot (i - 2)$$

$$y_i := \text{if} \left[x_i < \text{minRe}', \text{fr}(x_i), \text{fr}(\text{minRe}') + \text{gr}(\text{minRe}') \cdot (x_i - \text{minRe}') \right]$$

$$\begin{pmatrix} \alpha K \\ \alpha M \end{pmatrix} := \begin{bmatrix} N & \sum_{i=1}^N (x_i)^2 \\ \sum_{i=1}^N (x_i)^2 & \sum_{i=1}^N (x_i)^4 \end{bmatrix}^{-1} \begin{bmatrix} \sum_{i=1}^N y_i \\ \sum_{i=1}^N [(x_i)^2 \cdot y_i] \end{bmatrix}$$

$$\alpha M := -\alpha M$$

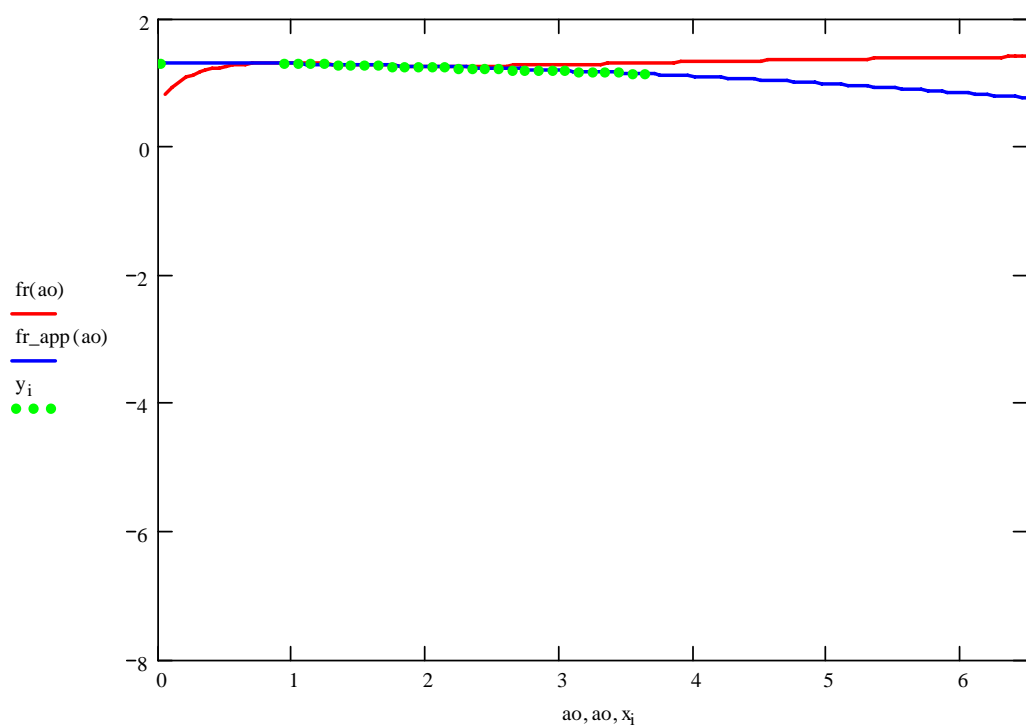
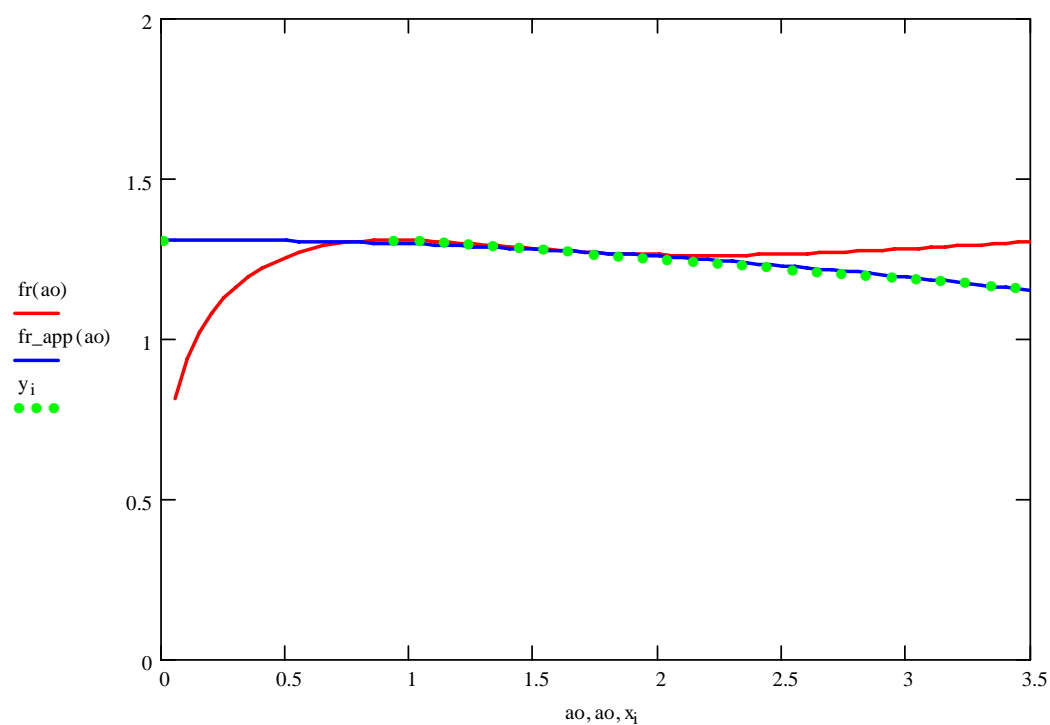
$$\alpha K = 1.3077538$$

$$\alpha M = 0.0129035$$

$$\text{fr_app}(\text{ao}) := \alpha K - \alpha M \cdot \text{ao}^2$$

i := 1..N

ao := 0, 0.05.. 6.5



Coefficient of Determination for the Real Part

$$y_m := \frac{\sum_{j=1}^N y_j}{N}$$

$$i := 1..N$$

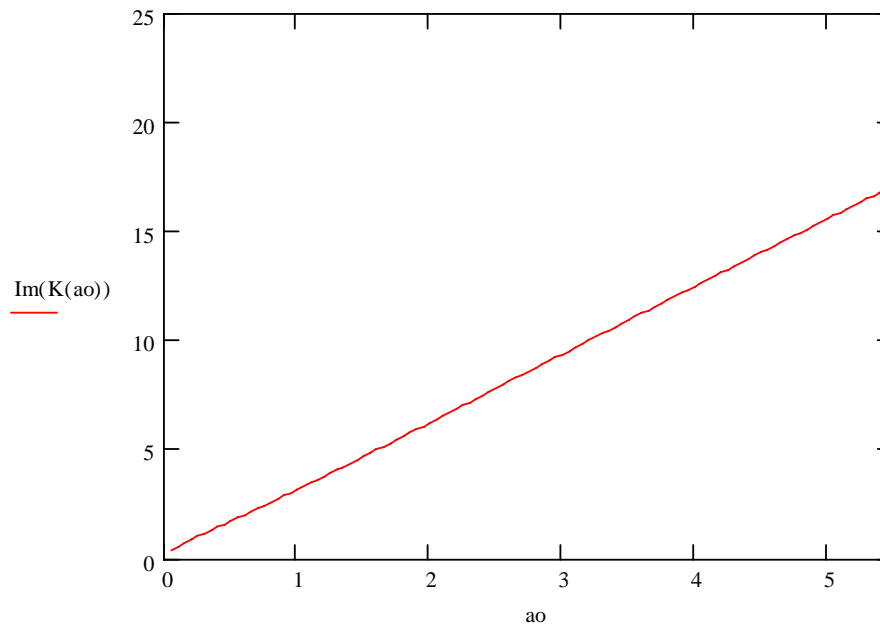
$$ya_i := \text{fr_app}(x_i)$$

$$\text{RSS} := \sum_{j=1}^N (y_j - ya_j)^2$$

$$\text{TSS} := \sum_{j=1}^N (y_j - y_m)^2$$

$$R^2 := 1 - \frac{\text{RSS}}{\text{TSS}}$$

$$R^2 = 0.982$$



Imaginary Part Curve Fitting by Least-Squares Approximation

$$f_i(ao) := \text{Im}(K(ao))$$

$$N := 30$$

$$x_1 := 0.0$$

$$y_1 := 0$$

$$i := 2..N$$

$$x_i := 0.1 \cdot (i - 1)$$

$$y_i := f_i(x_i)$$

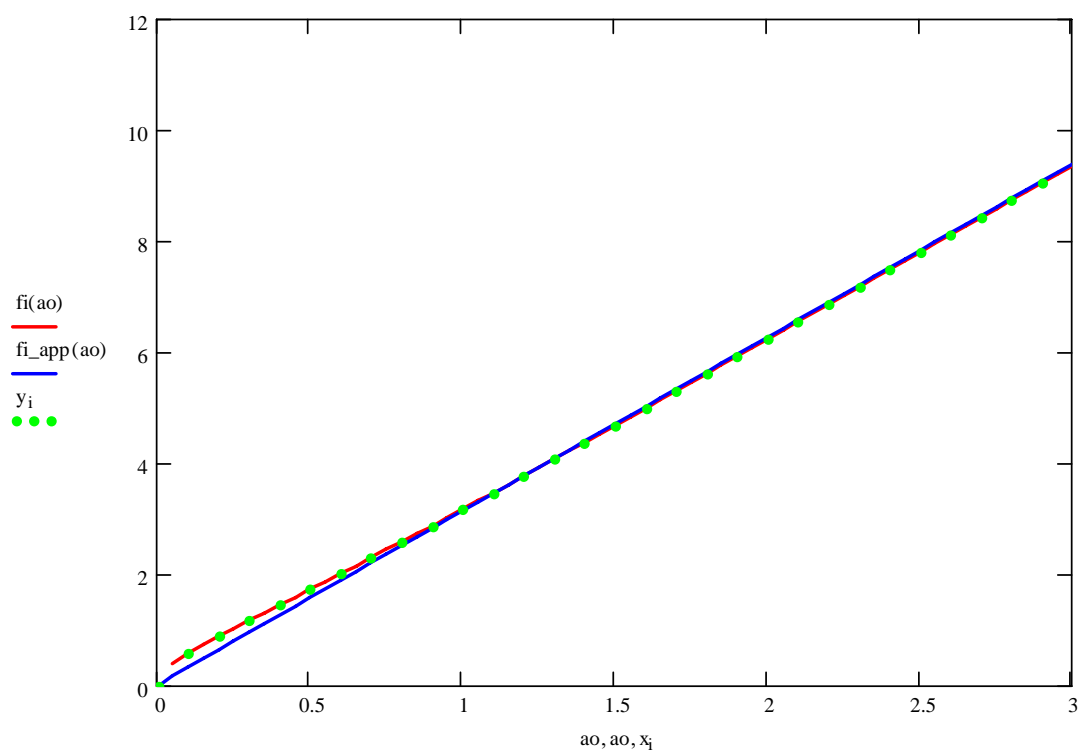
$$\alpha C := \frac{\sum_{i=1}^N (x_i \cdot y_i)}{\sum_{i=1}^N (x_i)^2}$$

$$\alpha C = 3.1297789$$

$$f_{i_app}(ao) := \alpha C \cdot ao$$

$i := 1..N$

$ao := 0, 0.05..6.9$



Coefficient of Determination for the Imaginary Part

$$y_m := \frac{\sum_{j=1}^N y_j}{N}$$

$$i := 1..N$$

$$y_{a_i} := \text{fi_app}(x_i)$$

$$\text{RSS} := \sum_{j=1}^N (y_j - y_{a_j})^2$$

$$\text{TSS} := \sum_{j=1}^N (y_j - y_m)^2$$

$$R^2 := 1 - \frac{\text{RSS}}{\text{TSS}}$$

$$R^2 = 0.999$$

D.4 Case of $D = 0.0$ and $\nu = 0.3$

Novak Dinamic Stiffness (Novak et al, 1978)

Pile and Soil Data

$$\nu := 0.30$$

soil Poisson's ratio

$$D := 0$$

soil hysteretic damping ratio = G'/G

Computations

$$\eta := \sqrt{\frac{2 \cdot (1 - \nu)}{1 - 2 \cdot \nu}} \quad \eta = 1.871$$

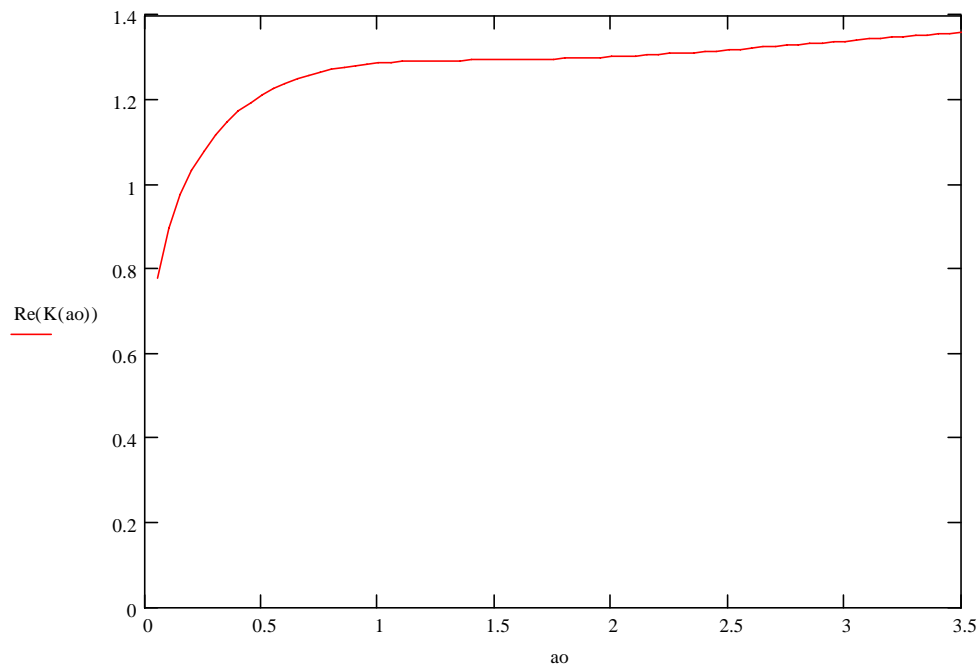
$$ao'(ao) := \frac{aoi}{\sqrt{1 + Di}}$$

$$bo'(ao) := \frac{aoi}{\eta \cdot \sqrt{1 + Di}}$$

$$T(ao) := \frac{4 \cdot K1(bo'(ao)) \cdot K1(ao'(ao)) + ao'(ao) \cdot K1(bo'(ao)) \cdot K0(ao'(ao)) + bo'(ao) \cdot K0(bo'(ao)) \cdot K1(ao'(ao))}{bo'(ao) \cdot K0(bo'(ao)) \cdot K1(ao'(ao)) + ao'(ao) \cdot K1(bo'(ao)) \cdot K0(ao'(ao)) + bo'(ao) \cdot ao'(ao) \cdot K0(bo'(ao)) \cdot K0(ao'(ao))}$$

$$K(ao) := -1 \cdot ao^2 \cdot T(ao)$$

$$ao := 0, 0.05..4$$



Real Part Inflection Point Determination

$$\text{fr}(\text{ao}) := \text{Re}(\text{K}(\text{ao}))$$

$$\text{gr}(\text{ao}) := \frac{d}{d\text{ao}} \text{fr}(\text{ao})$$

$$\text{ao} := 1.5$$

Given

$$\text{ao} \geq 0.0$$

$$\text{minRe}' := \text{Minimize}(\text{gr}, \text{ao}) \quad \text{minRe}' = 1.433$$

Real Part Curve Fitting by Least-Squares Approximation

$$N := 29$$

$$\text{aoi} := 1.0$$

$$\text{aof} := 3$$

$$i := 1..N$$

$$x_i := \text{aoi} + (\text{aof} - \text{aoi}) \cdot \frac{(i - 1)}{N - 1}$$

$$y_i := \text{fr}(x_i)$$

$$\alpha K := \frac{\sum_{i=1}^N y_i}{N}$$

$$\alpha M := 0$$

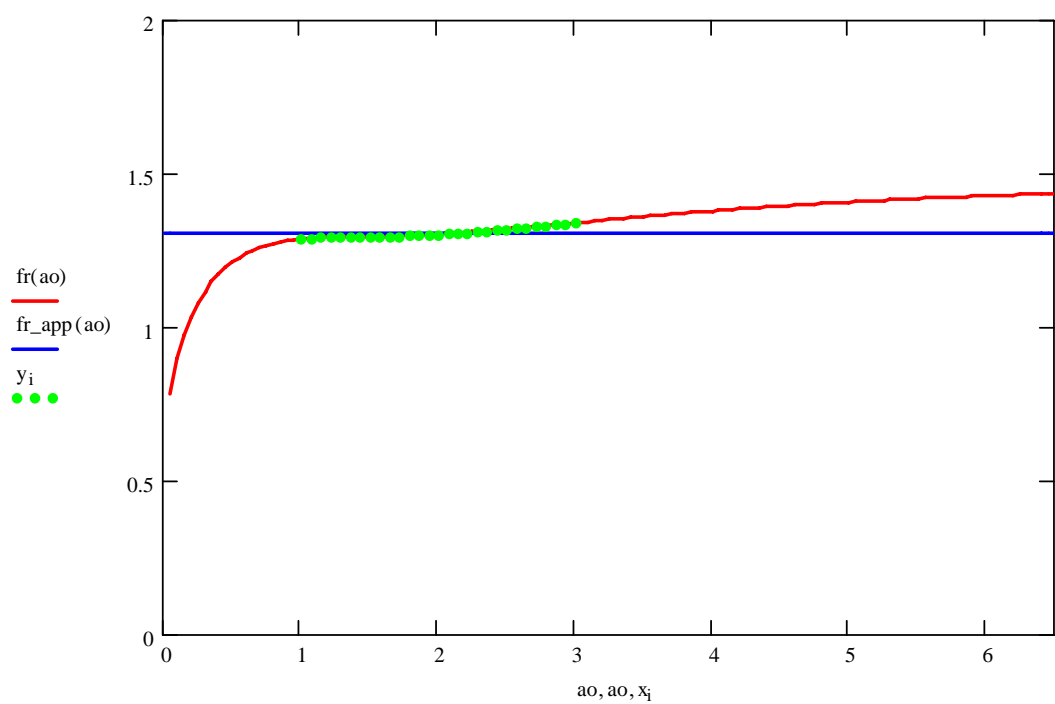
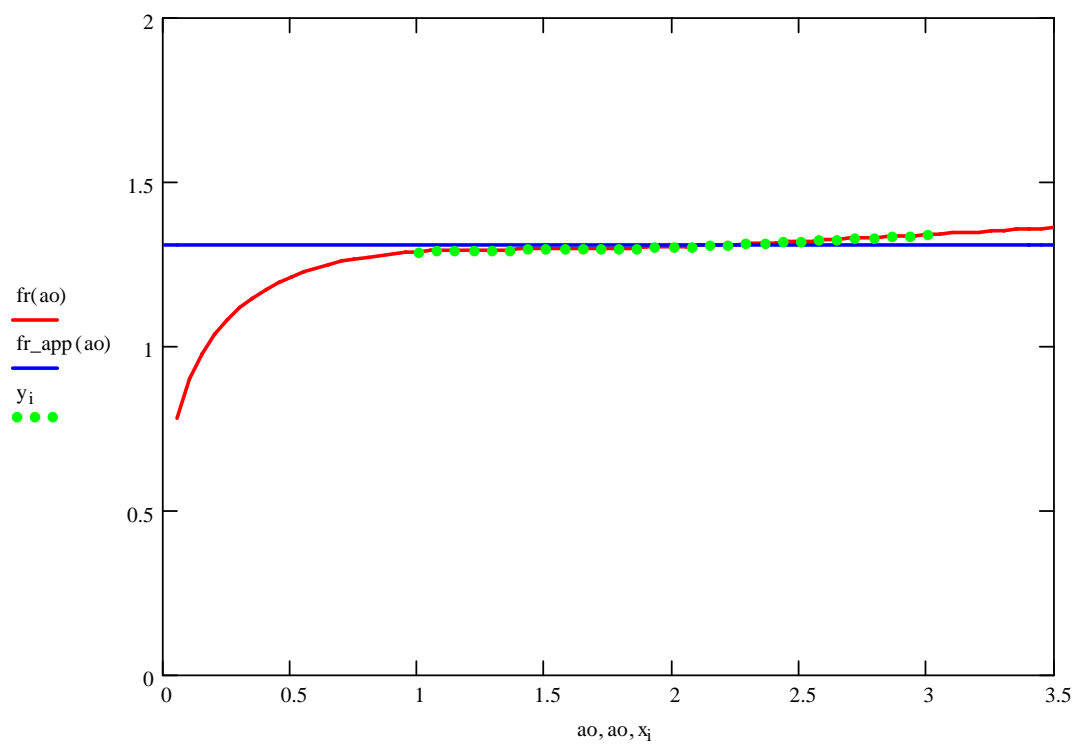
$$\alpha K = 1.3068585$$

$$\alpha M = 0$$

$$\text{fr_app}(\text{ao}) := \alpha K - \alpha M \cdot \text{ao}^2$$

$i := 1..N$

$\text{ao} := 0, 0.05..6.5$



Coefficient of Determination for the Real Part

$$y_m := \frac{\sum_{j=1}^N y_j}{N}$$

$$y_m = 1.307$$

$$i := 1..N$$

$$y_{a_i} := \text{fr_app}(x_i)$$

$$\text{RSS} := \sum_{j=1}^N (y_j - y_{a_j})^2$$

$$\text{RSS} = 6.731 \times 10^{-3}$$

$$\text{TSS} := \sum_{j=1}^N (y_j - y_m)^2$$

$$\text{TSS} = 6.731 \times 10^{-3}$$

$$R2 := 1 - \frac{\text{RSS}}{\text{TSS}}$$

$$R2 = 0$$

$$\text{SEE} := \sqrt{\frac{\sum_{j=1}^N (y_j - y_m)^2}{N - 1}}$$

$$\text{SEE} = 0.016$$

Standard error of estimate
(Sample Standard Deviation)

$$\text{CV} := \frac{\text{SEE}}{y_m}$$

$$\text{CV} = 0.012$$

coefficient of variation

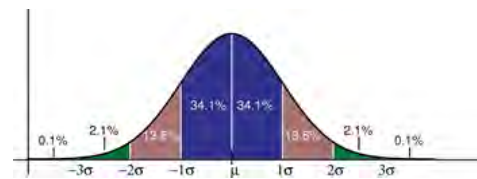
$$\text{RSD} := \text{CV} \cdot 100$$

$$\text{RSD} = 1.186$$

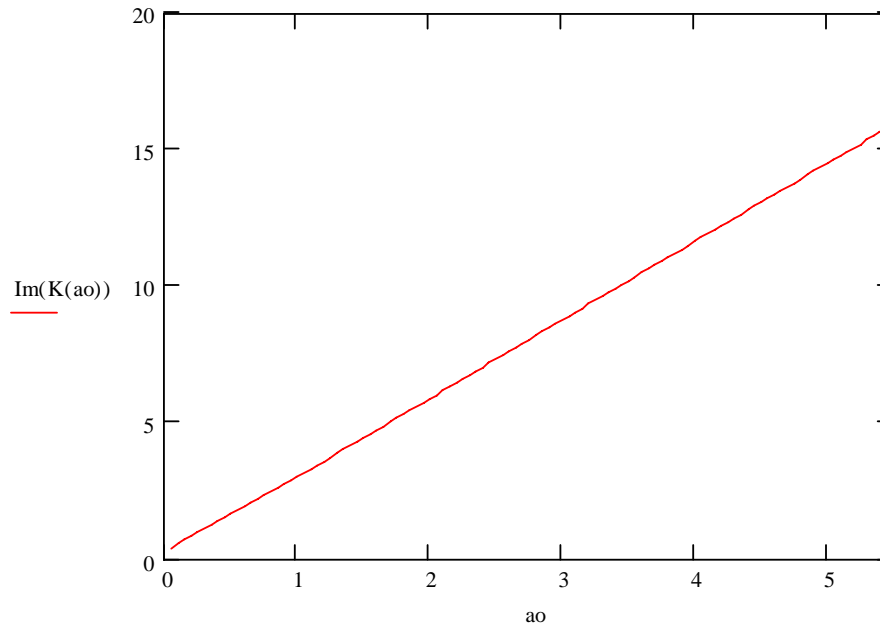
Relative Standard Deviation

$$\text{R2G} := 1 - \frac{3 \cdot \text{SEE}}{y_m}$$

$$\text{R2G} = 0.964$$



Dark blue is less than one standard deviation from the mean. For the normal distribution, this accounts for 68.27% of the set; while two standard deviations from the mean (blue and brown) account for 95.45%; and three standard deviations (blue, brown and green) account for 99.73%.



Imaginary Part Curve Fitting by Least-Squares Approximation

$$fi(ao) := \text{Im}(K(ao))$$

$$N := 30$$

$$x_1 := 0.0$$

$$y_1 := 0$$

$$i := 2..N$$

$$x_i := 0.1 \cdot (i - 1)$$

$$y_i := fi(x_i)$$

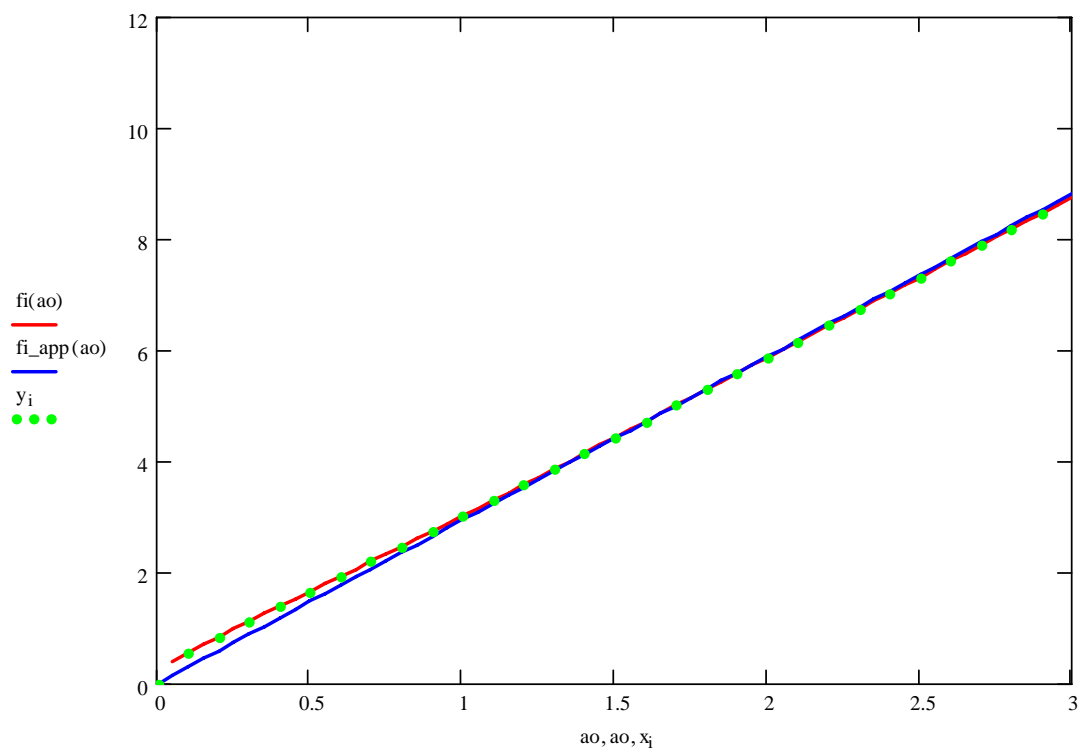
$$\alpha C := \frac{\sum_{i=1}^N (x_i \cdot y_i)}{\sum_{i=1}^N (x_i)^2}$$

$$\alpha C = 2.9405413$$

$$fi_app(ao) := \alpha C \cdot ao$$

$i := 1..N$

$ao := 0, 0.05..6.9$



Coefficient of Determination for the Imaginary Part

$$y_m := \frac{\sum_{j=1}^N y_j}{N}$$

$$i := 1..N$$

$$y_{a_i} := \text{fi_app}(x_i)$$

$$\text{RSS} := \sum_{j=1}^N (y_j - y_{a_j})^2$$

$$\text{TSS} := \sum_{j=1}^N (y_j - y_m)^2$$

$$R^2 := 1 - \frac{\text{RSS}}{\text{TSS}}$$

$$R^2 = 0.998$$

E Pile Element with Distributed Soil Parameters

E.1 Classical Beam Element

The derivation of the stiffness, mass, and dumping matrices for a pile element with distributed soil parameters is presented in this section. The element is shown in Figure E.1; the soil stiffness k_a per unit length, soil mass m_a per unit length, and soil damping coefficient c_a per unit length were obtained in Chapter 4.

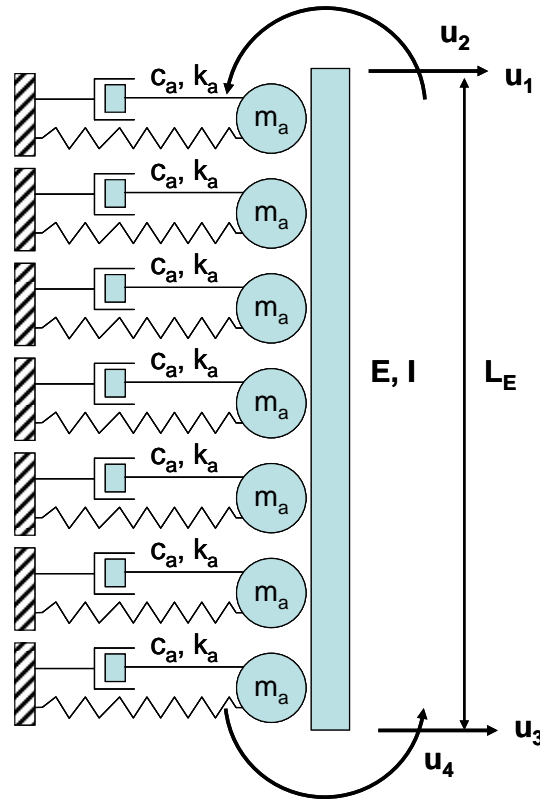


Figure E.1: Pile Element with Distributed Soil Parameters

The matrix will be derived by using the Finite Element Method (FEM) formulation based on the Virtual Work Principle. The four degrees of freedom (DOF) of the beam element are the two end displacements u_1 and u_3 and rotations u_2 and u_4 . In the FEM, the

displacements $v(x,t)$ within the element are expressed in terms of the end displacements and rotations $\{q\}$ through shape functions $[N]$:

$$v(x,t) = [\mathbf{N}] \{ \mathbf{q} \}$$

where

$$\{ \mathbf{q} \} = \begin{Bmatrix} u_1(t) \\ u_2(t) \\ u_3(t) \\ u_4(t) \end{Bmatrix}$$

It will be assumed that the shape functions for the classic beam theory (Bernoulli beam) are applicable. This shape functions are shown in Figure E.2, together with the element DOF.

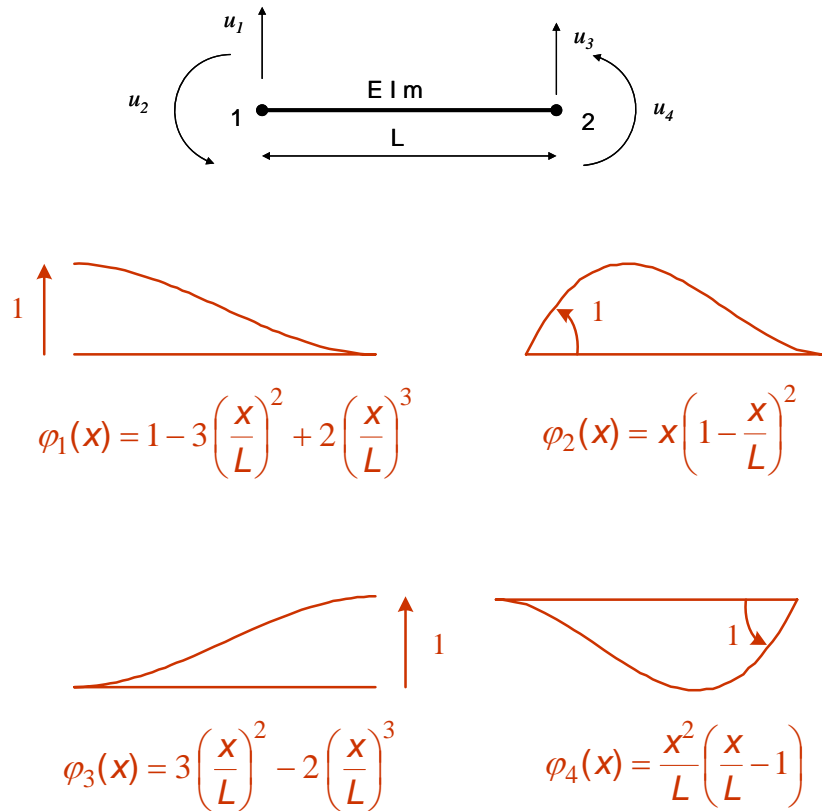


Figure E.2: Beam Element Shape Functions (Battini, 2006)

The Principle of Virtual Work for a dynamic structural system, also known as the generalized D’Alambert Principle, is:

$$\delta W_{int} - \delta W_{ext} - \delta W_{iner} = 0$$

where δW_{int} is the virtual work of the internal forces, δW_{ext} is the virtual work associated to the external forces, and δW_{iner} is the virtual work of the “inertial” forces, as defined by D’Alambert.

For a beam with a distributed force $f(x,t)$, the three virtual work expressions are:

$$\begin{aligned}\delta W_{int} &= \int_0^L E I v''(x,t) \frac{\delta v(x,t)}{dx} dx = \int_0^L E I v''(x,t) \frac{d(\delta v(x,t))}{dx^2} dx \\ \delta W_{ext} &= \int_0^L f(x,t) \delta v(x,t) dx \\ \delta W_{iner} &= - \int_0^L \bar{m} \ddot{v}(x,t) \delta v(x,t) dx\end{aligned}$$

where \bar{m} is the distributed mass of the beam per unit length, i.e. $\bar{m} = \rho A + m_a$, E is the elastic modulus, I the moment of inertia of the cross section, $v(x,t)$ is the transverse displacement, and $\delta v(x,t)$ is the virtual transverse displacement.

Introducing the FEM approximation:

$$\begin{aligned}v(x,t) &= [N(x)] \{q(t)\} \\ \delta v(x,t) &= [N(x)] \{\delta q(t)\} = \{\delta q(t)\}^T [N(x)]^T \\ v''(x,t) &= [N''(x)] \{q(t)\} \\ \delta v''(x,t) &= [N''(x)] \{\delta q(t)\} = \{\delta q(t)\}^T [N''(x)]^T\end{aligned}$$

The internal virtual work becomes:

$$\begin{aligned}\delta W_{\text{int}} &= \int_0^L E I v''(x,t) \delta v''(x,t) dx = \int_0^L E I \delta v''(x,t) v''(x,t) dx \\ \delta W_{\text{int}} &= \{\delta q(t)\}^T \left[\int_0^L E I [N''(x)]^T [N''(x)] dx \right] \{q(t)\}\end{aligned}$$

By defining the beam element stiffness matrix $[k_b]$ as:

$$[k_b] = \int_0^L E I [N''(x)]^T [N''(x)] dx$$

the internal virtual work results:

$$\delta W_{\text{int}} = \{\delta q(t)\}^T [k_b] \{q(t)\}$$

If the force $f(x,t)$ is due to the distributed spring and dampers, i.e. $f(x,t) = -k_a v(x,t) - c_a \dot{v}(x,t)$, the virtual work of the external forces is:

$$\delta W_{\text{ext}} = - \int_0^L k_a v(x,t) \delta v(x,t) dx - \int_0^L c_a \dot{v}(x,t) \delta v(x,t) dx$$

Introducing the FEM approximation shown previously, that for the velocity field results:

$$\begin{aligned}\dot{v}(x,t) &= [N(x)] \{\dot{q}(t)\} \\ \delta \dot{v}(x,t) &= [N(x)] \{\delta \dot{q}(t)\} = \{\delta \dot{q}(t)\}^T [N(x)]^T\end{aligned}$$

The external virtual work becomes:

$$\begin{aligned}\delta W_{\text{ext}} &= - \int_0^L k_a \delta v(x,t) v(x,t) dx - \int_0^L c_a \delta v(x,t) \dot{v}(x,t) dx \\ \delta W_{\text{ext}} &= - \{\delta q(t)\}^T \left[\int_0^L k_a [N(x)]^T [N(x)] dx \right] \{q(t)\} - \{\delta q(t)\}^T \left[\int_0^L c_a [N(x)]^T [N(x)] dx \right] \{\dot{q}(t)\}\end{aligned}$$

By defining the soil stiffness matrix $[k_s]$ and the soil damping matrix as $[c_s]$ as:

$$\begin{aligned} [k_s] &= \int_0^L k_a [N(x)]^T [N(x)] dx \\ [c_s] &= \int_0^L c_a [N(x)]^T [N(x)] dx \end{aligned}$$

the external virtual work results:

$$\delta W_{ext} = -\{\delta q(t)\}^T [k_s] \{q(t)\} - \{\delta q(t)\}^T [c_s] \{\dot{q}(t)\}$$

Finally, the acceleration field can be expressed in terms of the nodal coordinates as:

$$\begin{aligned} \ddot{v}(x,t) &= [N(x)] \{\ddot{q}(t)\} \\ \delta \ddot{v}(x,t) &= [N(x)] \{\delta \ddot{q}(t)\} = \{\delta \ddot{q}(t)\}^T [N(x)]^T \end{aligned}$$

Substituting these expressions into the equation of the virtual work of the inertial forces, it results:

$$\begin{aligned} \delta W_{iner} &= -\int_0^L \bar{m} \delta v(x,t) \ddot{v}(x,t) dx \\ \delta W_{iner} &= -\{\delta q(t)\}^T \left[\int_0^L \bar{m} [N(x)]^T [N(x)] dx \right] \{\ddot{q}(t)\} \end{aligned}$$

Introducing the consistent mass matrix $[M_E]$ for the beam element (which contribution is $[M_b]$) with added distributed soil mass (which contribution is $[M_s]$) as:

$$\begin{aligned} [M_E] &= \int_0^L \bar{m} [N(x)]^T [N(x)] dx = \int_0^L (\rho A + m_a) [N(x)]^T [N(x)] dx \\ [M_b] &= \int_0^L \rho A [N(x)]^T [N(x)] dx \\ [M_s] &= \int_0^L m_a [N(x)]^T [N(x)] dx \end{aligned}$$

the expression for the virtual work of the inertial forces becomes:

$$\delta W_{iner} = -\{\delta q(t)\}^T [M_E] \{\ddot{q}(t)\}$$

Considering the above mentioned nomenclature, the principle of virtual works results:

$$\delta W_{\text{int}} - \delta W_{\text{ext}} - \delta W_{\text{iner}} = 0$$

$$\{\delta q(t)\}^T \left[[k_b] \{q(t)\} + [k_s] \{q(t)\} + [c_s] \{\dot{q}(t)\} + [M_E] \{\ddot{q}(t)\} \right]$$

Since the virtual displacement $\{\delta q\}$, by definition, are arbitrary (as long as they are compatible with the support conditions), one obtains the equation of motion for the free vibrations of the element as:

$$[k_E] \{q(t)\} + [c_E] \{\dot{q}(t)\} + [M_E] \{\ddot{q}(t)\} = 0$$

where

$$[K_E] = [k_b] + [k_s] = \text{total element stiffness matrix}$$

$$[C_E] = [c_s] = \text{total element damping matrix}$$

$$[M_E] = [M_b] + [M_s] = \text{total element mass matrix}$$

E.1.1 Element Stiffness Matrix

The element stiffness matrix, that includes the contribution of the pile of modulus of elasticity E , cross sectional moment of inertia I , and length L_E , and the soil of distributed stiffness k_a , is computed as follows:

$$[K_E] = I \int_L [N']^T E [N'] dx + \int_L [N]^T k_a [N] dx$$

A listing of the Maple worksheet developed to compute the stiffness matrix is presented below:

```
> restart;
*****
*
* Shape Functions [Fi]
*****
*
> Fi := Vector(1..4):
Fi[1] := 1 - 3 * (x/L)^2 + 2 * (x/L)^3 :
Fi[2] := x * ( 1- x/L)^2 :
Fi[3] := 3 * (x/L)^2 - 2 * (x/L)^3 :
Fi[4] := x^2 / L * (x/L - 1) :

> Fi;
```

$$\begin{bmatrix} 1 - \frac{3x^2}{L^2} + \frac{2x^3}{L^3} \\ x \left(1 - \frac{x}{L} \right)^2 \\ 3 \frac{x^2}{L^2} - \frac{2x^3}{L^3} \\ \frac{x^2 \left(\frac{x}{L} - 1 \right)}{L} \end{bmatrix}$$


```

*****
*
* Matrix of Derivatives of the Shape Functions [B]
*****
*

> B := Matrix(1..1,1..4):

> with(student):
for j from 1 to 4 do
    B[1,j]:= diff(Fi[j],x$2):
end do:

> BT := Matrix(1..4, 1..1):
with(linalg):
BT := transpose(B):

> simplify(B);

$$\begin{bmatrix} -6\frac{L-2x}{L^3} & -2\frac{-3x+2L}{L^2} & 6\frac{L-2x}{L^3} & -2\frac{-3x+L}{L^2} \end{bmatrix}$$

*****
*
* Constitutive Matrix [E1]
*****
*

> E1 := Matrix(1,1):
E1[1,1] := E :
print(E1);


$$[E]$$

*****
*
* Stiffness Matrix [K]
*****
*

> dK1 := Matrix(1..4, 1..4):
with(linalg):
dk1 := multiply(BT,multiply(E1,B)):

> K1 := Matrix(1..4, 1..4):
with(student):
for i from 1 to 4 do
    for j from 1 to 4 do

```

```

      K1[i,j] := I * value(int(dk1[i,j], x = 0..L )) :
    end do:
end do:

> print(K1);

$$\begin{bmatrix} \frac{12 I E}{L^3} & \frac{6 I E}{L^2} & \frac{-12 I E}{L^3} & \frac{6 I E}{L^2} \\ \frac{6 I E}{L^2} & \frac{4 I E}{L} & \frac{-6 I E}{L^2} & \frac{2 I E}{L} \\ \frac{-12 I E}{L^3} & \frac{-6 I E}{L^2} & \frac{12 I E}{L^3} & \frac{-6 I E}{L^2} \\ \frac{6 I E}{L^2} & \frac{2 I E}{L} & \frac{-6 I E}{L^2} & \frac{4 I E}{L} \end{bmatrix}$$


> K2 := Matrix(1..4, 1..4):
with(student):
for i from 1 to 4 do
  for j from 1 to 4 do
    K2[i,j] := ka * value(int(Fi[i]*Fi[j], x = 0..L ))
  :
end do:
end do:

> print(K2);

$$\begin{bmatrix} \frac{13}{35} ka L & \frac{11}{210} ka L^2 & \frac{9}{70} ka L & -\frac{13}{420} ka L^2 \\ \frac{11}{210} ka L^2 & \frac{1}{105} ka L^3 & \frac{13}{420} ka L^2 & -\frac{1}{140} ka L^3 \\ \frac{9}{70} ka L & \frac{13}{420} ka L^2 & \frac{13}{35} ka L & -\frac{11}{210} ka L^2 \\ -\frac{13}{420} ka L^2 & -\frac{1}{140} ka L^3 & -\frac{11}{210} ka L^2 & \frac{1}{105} ka L^3 \end{bmatrix}$$


> K2R := simplify(K2 / (ka*L/420));

$$K2R := \begin{bmatrix} 156 & 22 L & 54 & -13 L \\ 22 L & 4 L^2 & 13 L & -3 L^2 \\ 54 & 13 L & 156 & -22 L \\ -13 L & -3 L^2 & -22 L & 4 L^2 \end{bmatrix}$$


>

```

E.1.2 Element Mass Matrix

The element mass matrix, that includes the contribution of the pile of density ρ and cross sectional area A , and the soil of distributed mass m_a , is computed as follows:

$$[M] = \int_0^L m [N]^T [N] dx$$

$$m = (\rho A + m_a) = \text{mass per unit length}$$

A listing of the Maple worksheet developed to compute the mass matrix is presented below:

```
> restart;
*****
* Shape Functions [Fi]
*****
> Fi := Vector(1..4):
Fi[1] := 1 - 3 * (x/L)^2 + 2 * (x/L)^3 :
Fi[2] := x * (1 - x/L)^2 :
Fi[3] := 3 * (x/L)^2 - 2 * (x/L)^3 :
Fi[4] := x^2 / L * (x/L - 1) :

> print (Fi);
```

$$\begin{bmatrix} 1 - \frac{3x^2}{L^2} + \frac{2x^3}{L^3} \\ x \left(1 - \frac{x}{L} \right)^2 \\ 3 \frac{x^2}{L^2} - \frac{2x^3}{L^3} \\ \frac{x^2 \left(\frac{x}{L} - 1 \right)}{L} \end{bmatrix}$$

```
*****
* Mass Matrix [ME]
*
*****
> ME := Matrix(1..4, 1..4):
with(student):
for i from 1 to 4 do
```

```

for j from 1 to 4 do
  ME[i,j] := (ro * A + ma) * value(int(Fi[i]*Fi[j], x = 0..L )) :
end do:
end do:

> print(ME);

```

$$\begin{bmatrix} \frac{13}{35}(ro A + ma) L & \frac{11}{210}(ro A + ma) L^2 & \frac{9}{70}(ro A + ma) L & -\frac{13}{420}(ro A + ma) L^2 \\ \frac{11}{210}(ro A + ma) L^2 & \frac{1}{105}(ro A + ma) L^3 & \frac{13}{420}(ro A + ma) L^2 & -\frac{1}{140}(ro A + ma) L^3 \\ \frac{9}{70}(ro A + ma) L & \frac{13}{420}(ro A + ma) L^2 & \frac{13}{35}(ro A + ma) L & -\frac{11}{210}(ro A + ma) L^2 \\ -\frac{13}{420}(ro A + ma) L^2 & -\frac{1}{140}(ro A + ma) L^3 & -\frac{11}{210}(ro A + ma) L^2 & \frac{1}{105}(ro A + ma) L^3 \end{bmatrix}$$

```

> MER := ME/((ro * A + ma)*L/420):
> simplify(MER);

```

$$\begin{bmatrix} 156 & 22 L & 54 & -13 L \\ 22 L & 4 L^2 & 13 L & -3 L^2 \\ 54 & 13 L & 156 & -22 L \\ -13 L & -3 L^2 & -22 L & 4 L^2 \end{bmatrix}$$

```

>

```

E.1.3 Element Damping Matrix

The element damping matrix that includes the contribution of the soil of distributed damping c_a , is computed as follows:

$$[C] = \int_0^L c [N]^T [N] dx$$

$c = (c_a) = \text{damping coefficient per unit length}$

The resulting damping matrix has the same form of the mass matrix, where $m_a L_E$ is replaced by $c_a L_E$.

E.2 Refined Beam Element

This section presents the derivation of the stiffness, mass, and dumping matrices for the refined pile element proposed by Deschapelles (2003) with distributed soil parameters. The element with its five DOF is displayed in Figure E.3. The soil stiffness k_a per unit length, soil mass m_a per unit length, and soil damping coefficient c_a per unit length were obtained in Chapter 4.

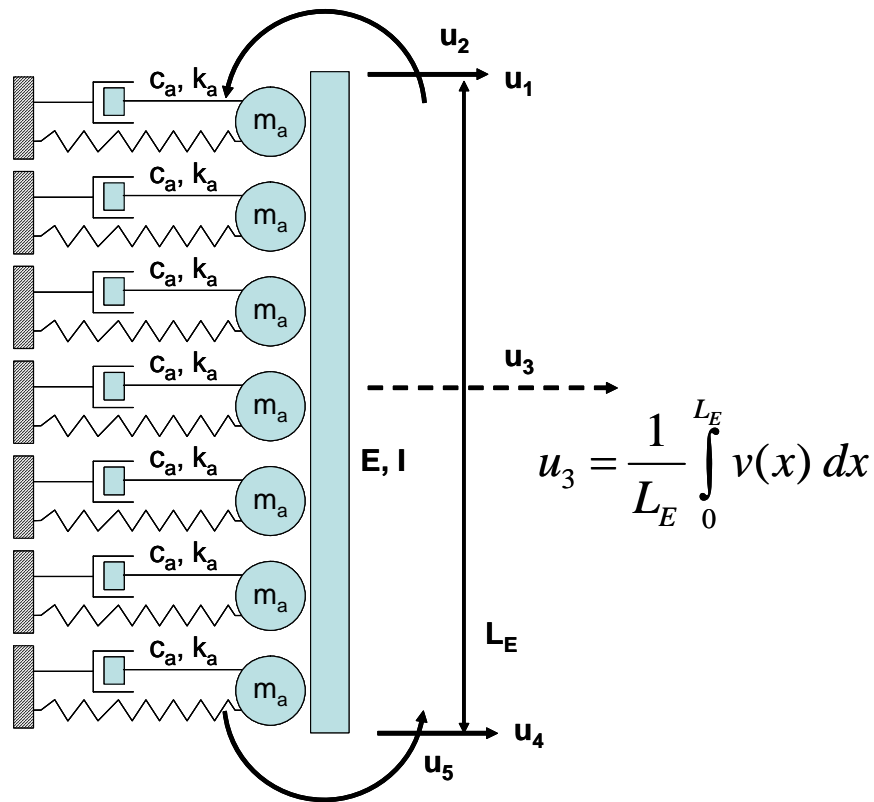


Figure E.3: Refined Pile Element with Distributed Soil Parameters

The advantages of this element, as reported by Deschapelles (2003) are:

- The nodal DOF in a conventional beam element are localized directions along which only concentrated forces or moments can be applied or computed. They are required to assure compatibility of deformed shape at nodal points, but do not provide “room” for distributed loads since such actions do not operate in specific

points. Distributed loads act over a finite element length, rather than over an infinitesimal point.

- Beam elements with distributed loads have bending moments with parabolic variation; considering the differential equation of a beam ($M/EI = d^2v/dx^2$), the transverse displacements should be represented by a 4th degree polynomial with 5 coefficients. Accordingly, 5 DOF should be used.

The shape functions for this element, considering a normalized coordinate $\xi = x / (L_E/2)$ and with the origin of coordinate axes located at the middle of the beam (as presented in Figure E.4), are presented in Figures E.5 to E.7. The shape functions for the nodal rotations (N2 and N5) should be multiplied by $L_E/2$.

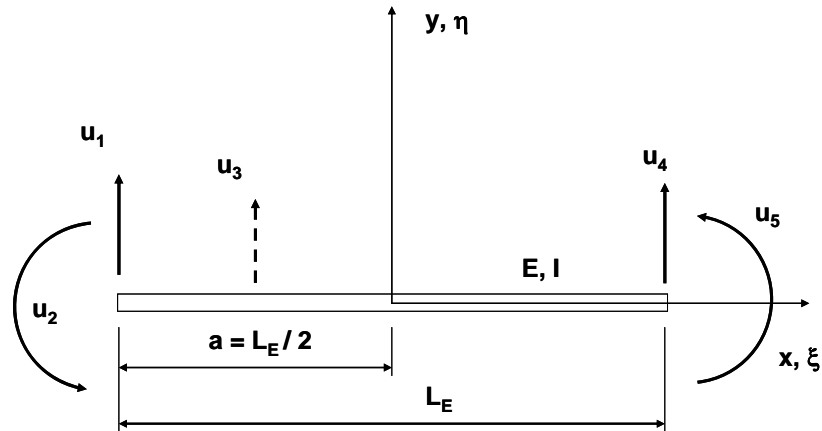
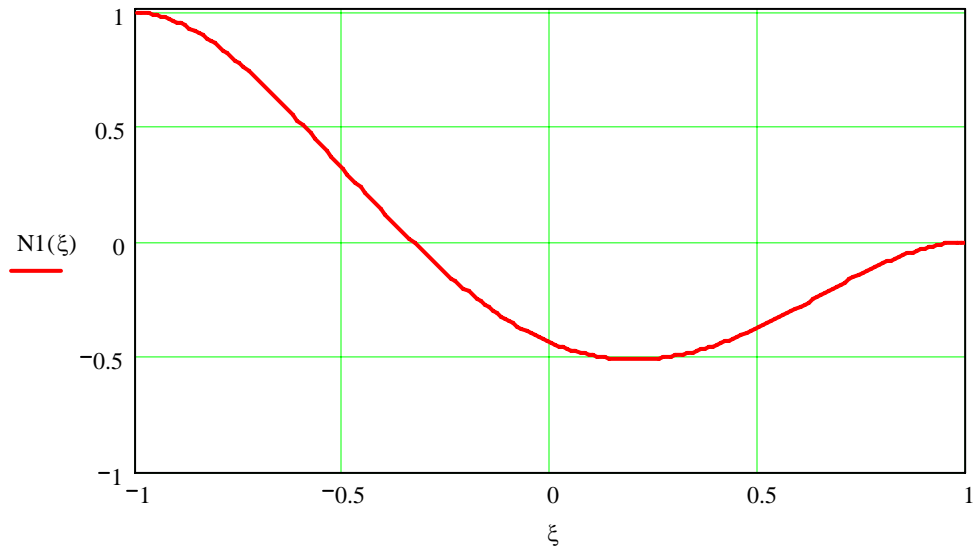


Figure E.4: Normalized Coordinate Sistem

First Shape Function

$$N1(\xi) := \frac{(-7 - 12 \cdot \xi + 30 \cdot \xi^2 + 4 \cdot \xi^3 - 15 \cdot \xi^4)}{16}$$

$$\int_{-1}^1 N1(\xi) d\xi = 0$$



Second Shape Function

$$N2(\xi) := \frac{(-1 - 4 \cdot \xi + 6 \cdot \xi^2 + 4 \cdot \xi^3 - 5 \cdot \xi^4)}{16}$$

$$\int_{-1}^1 N2(\xi) d\xi = 0$$

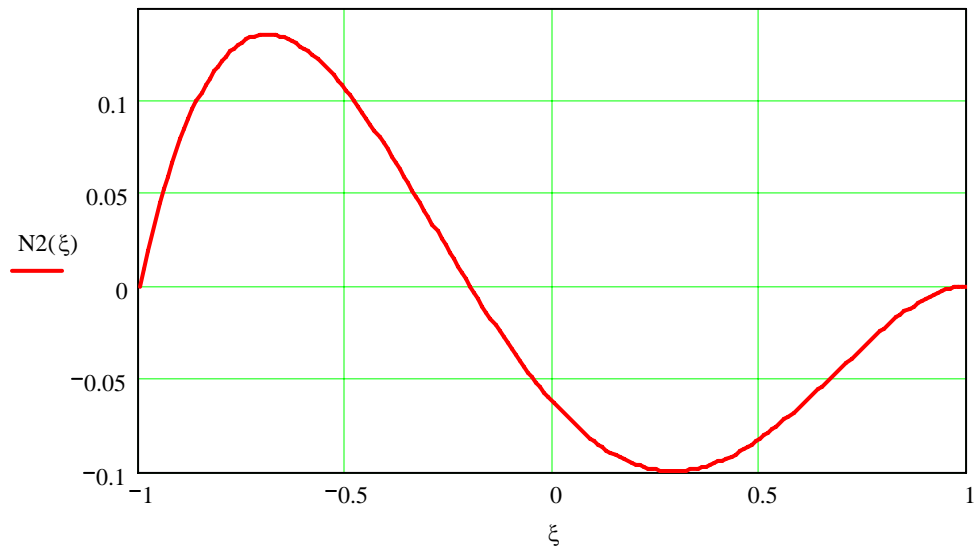
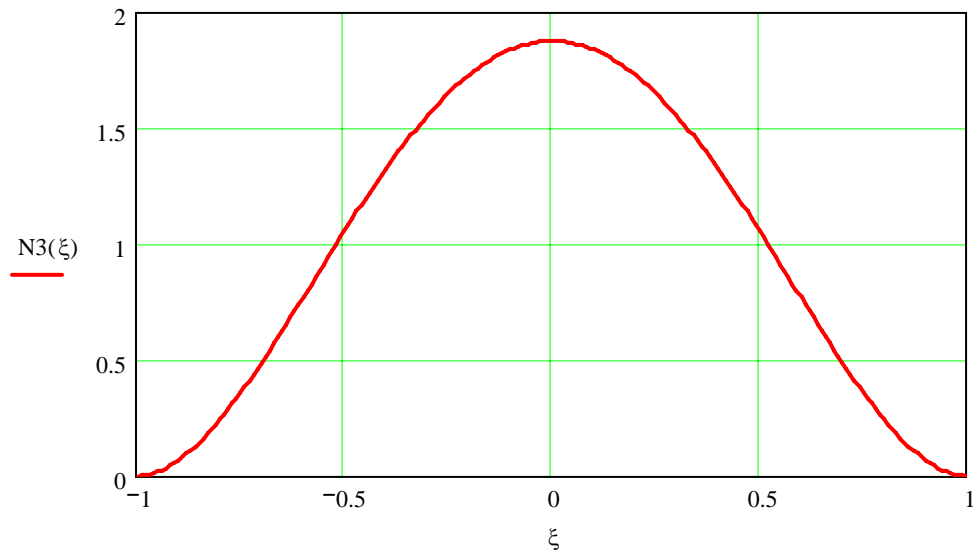


Figure E.5: Refined Beam Element Shape Functions - a

Third Shape Function

$$N3(\xi) := \frac{15 \cdot (1 - 2 \cdot \xi^2 + \xi^4)}{8}$$

$$\int_{-1}^1 N3(\xi) d\xi = 2$$



Fourth Shape Function

$$N4(\xi) := \frac{(-7 + 12 \cdot \xi + 30 \cdot \xi^2 - 4 \cdot \xi^3 - 15 \cdot \xi^4)}{16}$$

$$\int_{-1}^1 N4(\xi) d\xi = 0$$

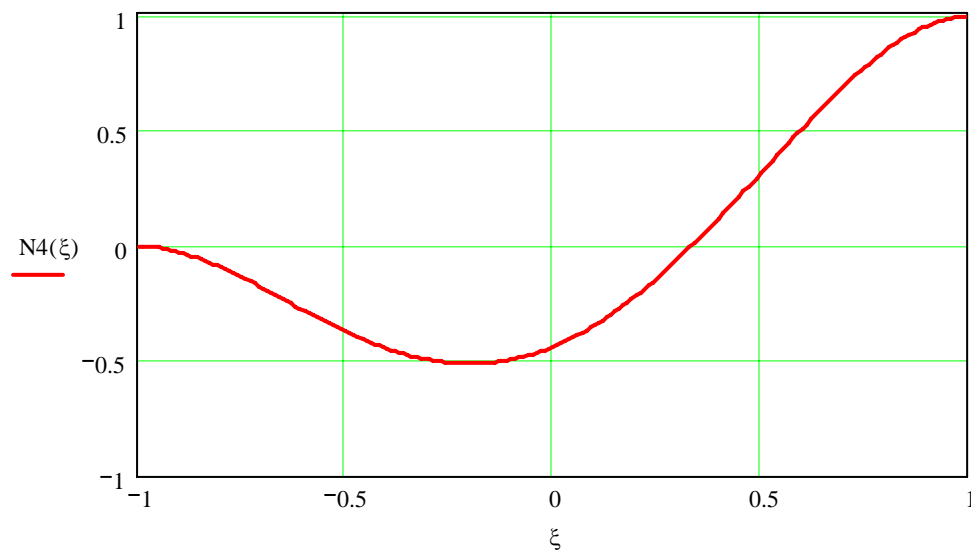


Figure E.6: Refined Beam Element Shape Functions - b

Fifth Shape Function

$$N5(\xi) := \frac{(1 - 4\xi - 6\xi^2 + 4\xi^3 + 5\xi^4)}{16}$$

$$\int_{-1}^1 N5(\xi) d\xi = 0$$

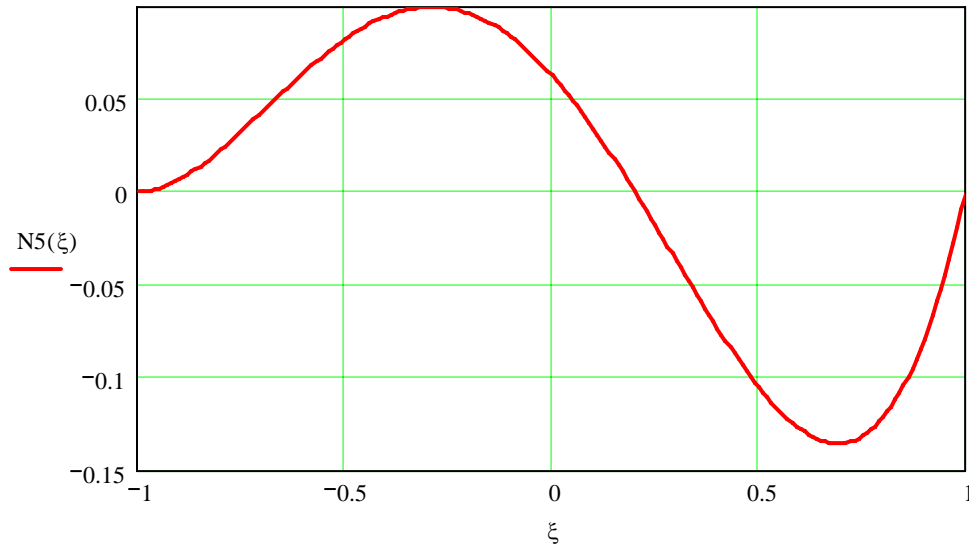


Figure E.7: Refined Beam Element Shape Functions - c

E.2.1 Refined Element Stiffness Matrix

The element stiffness matrix for a pile with modulus of elasticity E , cross sectional moment of inertia I , and length L_E , and that includes the contribution of the soil of distributed stiffness k_a , is computed as follows:

$$[K_E] = I \int_L [N']^T E [N'] dx + \int_L [N]^T k_a [N] dx$$

A listing of the Maple worksheet developed to compute the stiffness matrix is presented below:

```
> restart;
*****
*
* Shape Functions [Fi]
*****
*
> Fi := Vector(1..5):
Fi[1] := (-7 - 12 * x + 30 * x^2 + 4 * x^3 - 15 * x^4) /
16:
Fi[2] := L / 2 * (-1 - 4 * x + 6 * x^2 + 4 * x^3 - 5 *
x^4) / 16:
Fi[3] := ( 1 - 2 * x^2 + x^4 ) * 15 / 8 :
Fi[4] := (-7 + 12 * x + 30 * x^2 - 4 * x^3 - 15 * x^4) /
16:
Fi[5] := L / 2 * (1 - 4 * x - 6 * x^2 + 4 * x^3 + 5 *
x^4) / 16:

> Fi;
```

$$\begin{bmatrix} -\frac{7}{16} - \frac{3}{4}x + \frac{15}{8}x^2 + \frac{1}{4}x^3 - \frac{15}{16}x^4 \\ \frac{1}{32}L(-1 - 4x + 6x^2 + 4x^3 - 5x^4) \\ \frac{15}{8} - \frac{15}{4}x^2 + \frac{15}{8}x^4 \\ -\frac{7}{16} + \frac{3}{4}x + \frac{15}{8}x^2 - \frac{1}{4}x^3 - \frac{15}{16}x^4 \\ \frac{1}{32}L(1 - 4x - 6x^2 + 4x^3 + 5x^4) \end{bmatrix}$$

```
*****
*
* Matrix [B] with the derivatives of the Shape Functions
*****
*
> B := Matrix(1..1,1..5):

> with(student):
for j from 1 to 5 do
    B[1,j] := diff(Fi[j],x$2)* (2/L)^2:
```

end do:

```
> BT := Matrix(1..5, 1..1):
```

```
with(linalg):
```

```
BT := transpose(B):
```

```
> simplify(B);
```

$$\begin{bmatrix} -3 \frac{-5 - 2x + 15x^2}{L^2}, -\frac{3}{2} \frac{-1 - 2x + 5x^2}{L}, 30 \frac{-1 + 3x^2}{L^2}, -3 \frac{-5 + 2x + 15x^2}{L^2}, \\ \frac{3}{2} \frac{-1 + 2x + 5x^2}{L} \end{bmatrix}$$

```
*****
```

```
*
```

```
* Constitutive Matrix [E1]
```

```
*****
```

```
*
```

```
> E1 := Matrix(1,1):
```

```
E1[1,1] := E :
```

```
print(E1);
```

$[E]$

```
*****
```

```
*
```

```
* Stiffness Matrix [K]
```

```
*
```

```
*****
```

```
*
```

```
> dK1 := Matrix(1..5, 1..5):
```

```
with(linalg):
```

```
dk1 := multiply(BT,multiply(E1,B)):
```

```
> K1 := Matrix(1..5, 1..5):
```

```
with(student):
```

```
for i from 1 to 5 do
```

```
  for j from 1 to 5 do
```

```
    K1[i,j] := I * (L / 2) * value(int(dk1[i,j], x = -
```

```
1..1 )) :
```

```
  end do:
```

```
end do:
```

```
> print(K1);
```

$$\begin{bmatrix} \frac{192 I E}{L^3} & \frac{36 I E}{L^2} & \frac{-360 I E}{L^3} & \frac{168 I E}{L^3} & \frac{-24 I E}{L^2} \\ \frac{36 I E}{L^2} & \frac{9 I E}{L} & \frac{-60 I E}{L^2} & \frac{24 I E}{L^2} & \frac{-3 I E}{L} \\ \frac{-360 I E}{L^3} & \frac{-60 I E}{L^2} & \frac{720 I E}{L^3} & \frac{-360 I E}{L^3} & \frac{60 I E}{L^2} \\ \frac{168 I E}{L^3} & \frac{24 I E}{L^2} & \frac{-360 I E}{L^3} & \frac{192 I E}{L^3} & \frac{-36 I E}{L^2} \\ \frac{-24 I E}{L^2} & \frac{-3 I E}{L} & \frac{60 I E}{L^2} & \frac{-36 I E}{L^2} & \frac{9 I E}{L} \end{bmatrix}$$

```
> K1R:= simplify (K1/(3*E*I/L));
```

$$K1R := \begin{bmatrix} 64 \frac{1}{L^2} & 12 \frac{1}{L} & -120 \frac{1}{L^2} & 56 \frac{1}{L^2} & -8 \frac{1}{L} \\ 12 \frac{1}{L} & 3 & -20 \frac{1}{L} & 8 \frac{1}{L} & -1 \\ -120 \frac{1}{L^2} & -20 \frac{1}{L} & 240 \frac{1}{L^2} & -120 \frac{1}{L^2} & 20 \frac{1}{L} \\ 56 \frac{1}{L^2} & 8 \frac{1}{L} & -120 \frac{1}{L^2} & 64 \frac{1}{L^2} & -12 \frac{1}{L} \\ -8 \frac{1}{L} & -1 & 20 \frac{1}{L} & -12 \frac{1}{L} & 3 \end{bmatrix}$$

```
> K2 := Matrix(1..5, 1..5):
with(student):
for i from 1 to 5 do
  for j from 1 to 5 do
    K2[i,j] := ka *(L/2)* value(int(Fi[i]*Fi[j], x = -
1..1 )) :
  end do:
end do:

> print(K2);
```

$$\begin{bmatrix} \frac{8}{35} ka L & \frac{1}{60} ka L^2 & -\frac{3}{14} ka L & -\frac{1}{70} ka L & \frac{1}{210} ka L^2 \\ \frac{1}{60} ka L^2 & \frac{1}{630} ka L^3 & -\frac{1}{84} ka L^2 & -\frac{1}{210} ka L^2 & \frac{1}{1260} ka L^3 \\ -\frac{3}{14} ka L & -\frac{1}{84} ka L^2 & \frac{10}{7} ka L & -\frac{3}{14} ka L & \frac{1}{84} ka L^2 \\ -\frac{1}{70} ka L & -\frac{1}{210} ka L^2 & -\frac{3}{14} ka L & \frac{8}{35} ka L & -\frac{1}{60} ka L^2 \\ \frac{1}{210} ka L^2 & \frac{1}{1260} ka L^3 & \frac{1}{84} ka L^2 & -\frac{1}{60} ka L^2 & \frac{1}{630} ka L^3 \end{bmatrix}$$

> **K2R := simplify(K2 / (ka*L/1260));**

$$K2R := \begin{bmatrix} 288 & 21 L & -270 & -18 & 6 L \\ 21 L & 2 L^2 & -15 L & -6 L & L^2 \\ -270 & -15 L & 1800 & -270 & 15 L \\ -18 & -6 L & -270 & 288 & -21 L \\ 6 L & L^2 & 15 L & -21 L & 2 L^2 \end{bmatrix}$$

>

E.2.2 Refined Element Mass Matrix

The element mass matrix, that includes the contribution of the pile of density ρ and cross sectional area A , and the soil of distributed mass m_a , is computed as follows:

$$[M] = \int_0^L m [N]^T [N] dx$$

$$m = (\rho A + m_a) = \text{mass per unit length}$$

A listing of the Maple worksheet developed to compute the mass matrix is presented below:

> **restart;**

*

* Shape Functions [Fi]

*

```
> Fi := Vector(1..5):
```

```
Fi[1] := (-7 - 12 * x + 30 * x^2 + 4 * x^3 - 15 * x^4) / 16:
```

```
Fi[2] := L / 2 * (-1 - 4 * x + 6 * x^2 + 4 * x^3 - 5 * x^4) / 16:
```

```
Fi[3] := (1 - 2 * x^2 + x^4) * 15 / 8 :
```

```
Fi[4] := (-7 + 12 * x + 30 * x^2 - 4 * x^3 - 15 * x^4) / 16:
```

```
Fi[5] := L / 2 * (1 - 4 * x - 6 * x^2 + 4 * x^3 + 5 * x^4) / 16:
```

```
> print (Fi);
```

$$\begin{bmatrix} -\frac{7}{16} - \frac{3}{4}x + \frac{15}{8}x^2 + \frac{1}{4}x^3 - \frac{15}{16}x^4 \\ \frac{1}{32}L(-1 - 4x + 6x^2 + 4x^3 - 5x^4) \\ \frac{15}{8} - \frac{15}{4}x^2 + \frac{15}{8}x^4 \\ -\frac{7}{16} + \frac{3}{4}x + \frac{15}{8}x^2 - \frac{1}{4}x^3 - \frac{15}{16}x^4 \\ \frac{1}{32}L(1 - 4x - 6x^2 + 4x^3 + 5x^4) \end{bmatrix}$$

*

* Mass Matrix [ME]

*

*

```
> ME := Matrix(1..5, 1..5):
```

```
with(student):
```

```
for i from 1 to 5 do
```

```
  for j from 1 to 5 do
```

```
    ME[i,j] := (ro * A + ma) *(L/2)*
```

```
value(int(Fi[i]*Fi[j], x = -1..1 )) :
```

```
  end do:
```

```
end do:
```

```
> print(ME);
```

$$\begin{aligned}
& \left[\frac{8}{35} (ro A + ma) L, \frac{1}{60} (ro A + ma) L^2, -\frac{3}{14} (ro A + ma) L, -\frac{1}{70} (ro A + ma) L, \right. \\
& \left. \frac{1}{210} (ro A + ma) L^2 \right] \\
& \left[\frac{1}{60} (ro A + ma) L^2, \frac{1}{630} (ro A + ma) L^3, -\frac{1}{84} (ro A + ma) L^2, \right. \\
& \left. -\frac{1}{210} (ro A + ma) L^2, \frac{1}{1260} (ro A + ma) L^3 \right] \\
& \left[-\frac{3}{14} (ro A + ma) L, -\frac{1}{84} (ro A + ma) L^2, \frac{10}{7} (ro A + ma) L, \right. \\
& \left. -\frac{3}{14} (ro A + ma) L, \frac{1}{84} (ro A + ma) L^2 \right] \\
& \left[-\frac{1}{70} (ro A + ma) L, -\frac{1}{210} (ro A + ma) L^2, -\frac{3}{14} (ro A + ma) L, \right. \\
& \left. \frac{8}{35} (ro A + ma) L, -\frac{1}{60} (ro A + ma) L^2 \right] \\
& \left[\frac{1}{210} (ro A + ma) L^2, \frac{1}{1260} (ro A + ma) L^3, \frac{1}{84} (ro A + ma) L^2, \right. \\
& \left. -\frac{1}{60} (ro A + ma) L^2, \frac{1}{630} (ro A + ma) L^3 \right]
\end{aligned}$$

> **MER := ME/((ro * A + ma)*L/1260):**

> **simplify(MER);**

$$\begin{bmatrix} 288 & 21 L & -270 & -18 & 6 L \\ 21 L & 2 L^2 & -15 L & -6 L & L^2 \\ -270 & -15 L & 1800 & -270 & 15 L \\ -18 & -6 L & -270 & 288 & -21 L \\ 6 L & L^2 & 15 L & -21 L & 2 L^2 \end{bmatrix}$$

>

E.2.3 Refined Element Damping Matrix

The element damping matrix that includes the contribution of the soil of distributed damping c_a , is computed as follows:

$$[C] = \int_0^L c [N]^T [N] dx$$

$c = (c_a) = \text{damping coefficient per unit length}$

The resulting damping matrix has the same form of the mass matrix, where $m_a L_E$ is replaced by $c_a L_E$.

E.3 Analysis of Convergence to the Natural Frequency

In order to evaluate the appropriateness of the classical and the refined beam elements to perform dynamic analyses, the natural frequencies of a simple supported steel beam, W8x10, $L = 20$ ft, were computed using the classical beam element with consistent mass matrix and lumped mass matrix, the refined element proposed by Deschappelles with consistent mass matrix, and the exact solutions obtained considering the beam as a continuous (Humar, 2002).

Figures E.8 through E.10 present the first four natural frequencies of the system, and the convergence of the different models as the number of elements is increased. It is observed that the refined element proposed by Deschappelles gives a very good estimate of the first natural frequency with only one element, and converges to the exact values of the natural frequency for higher modes faster than the classical beam, as the number of elements “ne” used to discretize the beam is increased.

Section E3.1 through E.3.3 present the Matlab programs developed to compute the natural frequencies for each model, varying the number of elements.

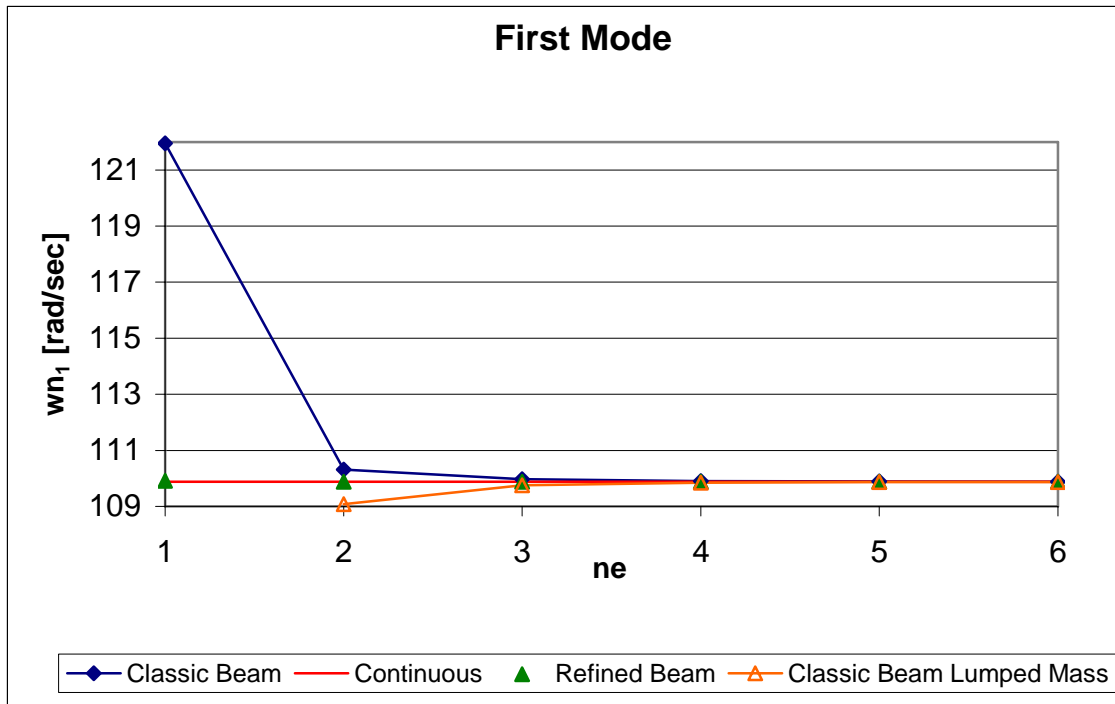


Figure E.8: First Natural Frequency vs Number of Elements (ne)

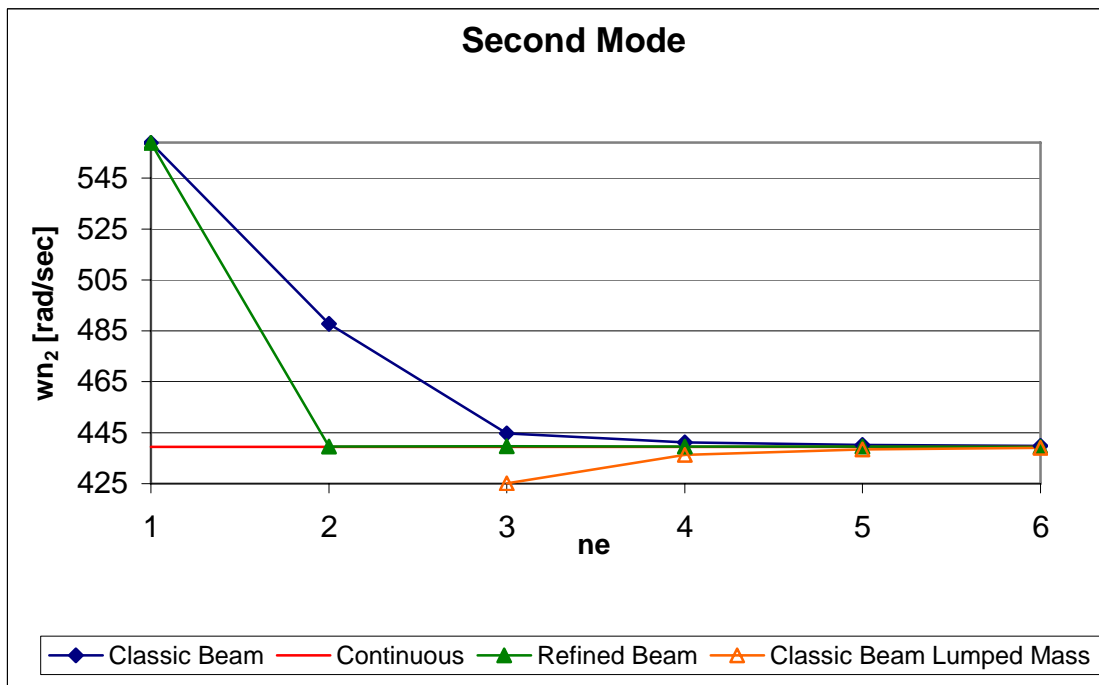


Figure E.9: Second Natural Frequency vs Number of Elements (ne)

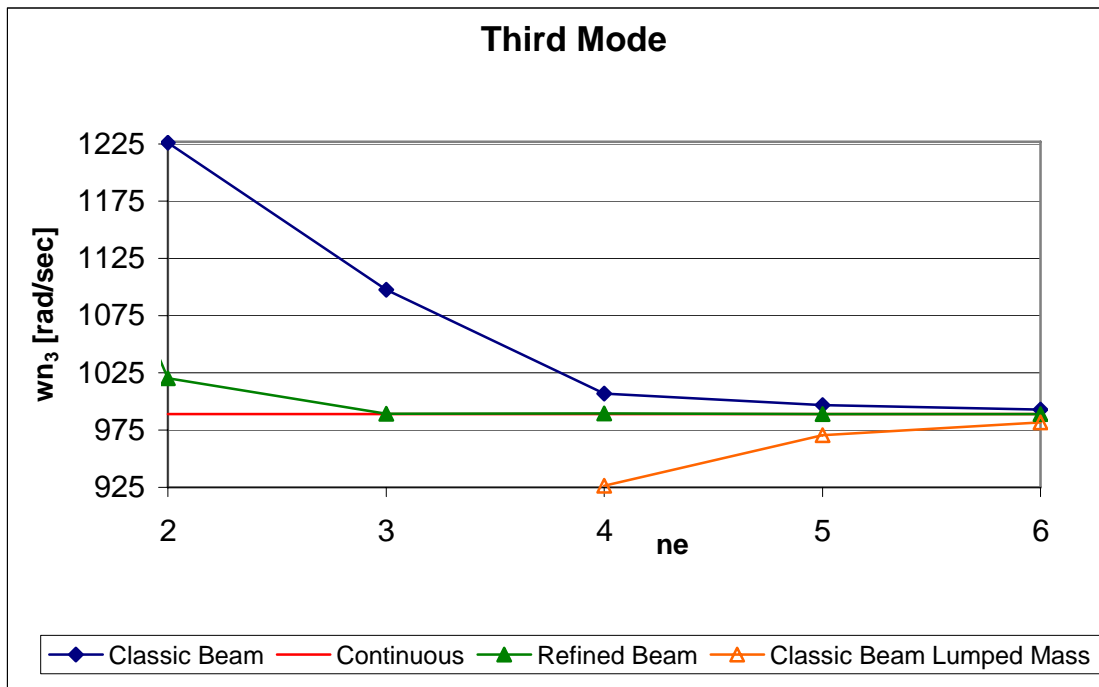


Figure E.10: Third Natural Frequency vs Number of Elements (ne)

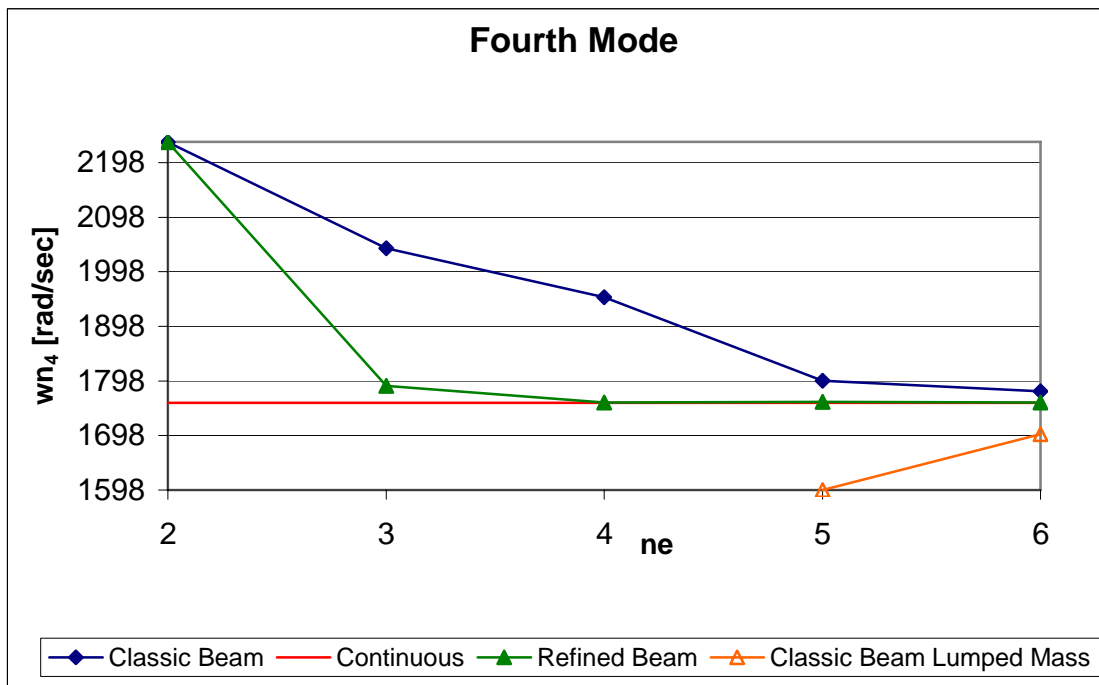


Figure E.11: Fourth Natural Frequency vs Number of Elements (ne)

E.3.1 Classical Beam Element with Lumped Mass Matrix

```

% *****
% BeamNatFreq.m
% Finite Element Program
% to obtain natural frequencies of a simple beam
% using classical and refined beam elements
% *****

% *****
% Clears window, variables, and graphs
% *****

clc;
clear all;
close all;

% *****
% Problem Data
% *****

g = 32.2;          % [ft/sec^2] gravity acceleration
                    % W8x10
A = 2.96;          % [in^2]
I = 30.8;          % [in^4]
L = 20.0;          % [ft]
E = 29000.0;       % [ksi]
gamma = 0.490;     % [kcf]

ne = 6;            % number elements
nm = 5;            % number of modes

% *****
% Parameters computation
% *****
L = L * 12;
rho = (gamma/12^3) / (g*12); % [pcf]
Le = L / ne ;

K = zeros(2*(ne+1), 2*(ne+1));
M = zeros(2*(ne+1), 2*(ne+1));

% BEAM ELEMENT STIFFNESS MATRIX

k1 = 4*E*I/Le;
k2 = 6*E*I/Le^2;
k3 = 12*E*I/Le^3;

Ke(1,1) = k3;
Ke(2,1) = k2;
Ke(3,1) = -k3;
Ke(4,1) = k2;

Ke(1,2) = k2;
Ke(2,2) = k1;
Ke(3,2) = -k2;
Ke(4,2) = k1/2;

Ke(1,3) = -k3;
Ke(2,3) = -k2;
Ke(3,3) = k3;
Ke(4,3) = -k2;

Ke(1,4) = k2;
Ke(2,4) = k1/2;
Ke(3,4) = -k2;
Ke(4,4) = k1;

% BEAM ELEMENT LUMPED MASS MATRIX

MB = rho * A * Le ;

Me(1,1) = MB / 2;
Me(2,1) = 0;
Me(3,1) = 0;

```

```

Me(4, 1) = 0;

Me(1, 2) = 0;
Me(2, 2) = 0;
Me(3, 2) = 0;
Me(4, 2) = 0;

Me(1, 3) = 0;
Me(2, 3) = 0;
Me(3, 3) = MB / 2;
Me(4, 3) = 0;

Me(1, 4) = 0;
Me(2, 4) = 0;
Me(3, 4) = 0;
Me(4, 4) = 0;

% *****
% Mass and Stiffness Matrices Assembling
% *****
for jj = 1 : ne
    dof(1) = jj * 2 - 1;
    dof(2) = jj * 2;
    dof(3) = jj * 2 + 1;
    dof(4) = jj * 2 + 2;
    for kk = 1 : 4
        for ll = 1 : 4
            row = dof(kk);
            col = dof(ll);
            K(row, col) = K(row, col) + Ke(kk, ll);
            M(row, col) = M(row, col) + Me(kk, ll);
        end
    end
end

% Boundary conditions
K
K(1, :) = []
K(:, 1) = []
K((ne+1)*2-2, :) = []
K(:, (ne+1)*2-2) = []

M
M(1, :) = []
M(:, 1) = []
M((ne+1)*2-2, :) = []
M(:, (ne+1)*2-2) = []

% *****
% Exact Beam Natural Frequencies
% *****
for jj = 1 : nm
    wex(jj) = (jj^2) * (pi^2) * sqrt(E*I / (rho*A*L^4));
    disp(wex(jj))
end

% *****
% Eigenvalues and Eigenvectors
% *****

[phi, lam] = eig(K, M);
wJ = sqrt(diag(lam));

% *****
% Ordena los autovalores y autovectores
% Calcula los periodos naturales
% *****
[wJ, id] = sort(wJ);
phi = phi(:, id);
Tj = 2*pi ./ wJ;
fj = 1 ./ Tj;

% *****
% Imprime en pantalla
% *****
for jj = 1 : ( (ne-1)*2 + 2 )

```

```

var1 = num2str(JJ);
var2 = num2str(wj(JJ));
var3 = num2str(fj(JJ));
var4 = num2str(Tj(JJ));
var5 = strcat( var1 , ',' , var2 , ',' , var3 , ',' , var4);
disp(var5)
end

```

E.3.2 Classical Beam Element with Consistent Mass Matrix

```

% *****
% BeamNatFreq.m
% Finite Element Program
% to obtain natural frequencies of a simple beam
% using classical and refined beam elements
% *****

% *****
% Clears window, variables, and graphs
% *****

clc;
clear all;
close all;

% *****
% Problem Data
% *****

g = 32.2;          % [ft/sec^2] gravity acceleration
                    % W8x10
A= 2.96;           %[in^2]
I = 30.8;          %[in^4]
L = 20.0;          %[ft]
E = 29000.0;       %[ksi]
gamma = 0.490;     %[kcf]

ne = 6;            % number elements
nm = 5;            % number of modes

% *****
% Parameters computation
% *****
L = L * 12;
rho = (gamma/12^3) / (g*12); %[pcf]
Le = L / ne ;

K = zeros(2*(ne+1), 2*(ne+1));
M = zeros(2*(ne+1), 2*(ne+1));

% BEAM ELEMENT STIFFNESS MATRIX

k1 = 4*E*I/Le;
k2 = 6*E*I/Le^2;
k3 = 12*E*I/Le^3;

Ke(1,1) = k3;
Ke(2,1) = k2;
Ke(3,1) = -k3;
Ke(4,1) = k2;

Ke(1,2) = k2;
Ke(2,2) = k1;
Ke(3,2) = -k2;
Ke(4,2) = k1/2;

Ke(1,3) = -k3;
Ke(2,3) = -k2;
Ke(3,3) = k3;
Ke(4,3) = -k2;

Ke(1,4) = k2;

```

```

Ke(2,4) = k1/2;
Ke(3,4) = -k2;
Ke(4,4) = k1;

% BEAM ELEMENT MASS MATRIX

MB = rho * A * Le ;

Me(1,1) = MB / 420 * 156;
Me(2,1) = MB / 420 * 22 * Le;
Me(3,1) = MB / 420 * 54;
Me(4,1) = - MB / 420 * 13 * Le;

Me(1,2) = MB / 420 * 22 * Le;
Me(2,2) = MB / 420 * 4 * Le^2;
Me(3,2) = MB / 420 * 13 * Le;
Me(4,2) = - MB / 420 * 3 * Le^2;

Me(1,3) = MB / 420 * 54;
Me(2,3) = MB / 420 * 13 * Le;
Me(3,3) = MB / 420 * 156;
Me(4,3) = - MB / 420 * 22 * Le;

Me(1,4) = - MB / 420 * 13 * Le;
Me(2,4) = - MB / 420 * 3 * Le^2;
Me(3,4) = - MB / 420 * 22 * Le;
Me(4,4) = MB / 420 * 4 * Le^2;

% *****
% Mass and Stiffness Matrices Assembling
% *****
for jj = 1 : ne
    dof(1) = jj * 2 - 1;
    dof(2) = jj * 2;
    dof(3) = jj * 2 + 1;
    dof(4) = jj * 2 + 2;
    for kk = 1 : 4
        for ll = 1 : 4
            row = dof(kk);
            col = dof(ll);
            K(row,col) = K(row,col) + Ke(kk,ll);
            M(row,col) = M(row,col) + Me(kk,ll);
        end
    end
end

% Boundary conditions
K
K(1,:) = []
K(:,1) = []
K((ne+1)*2-2,:) = []
K(:,(ne+1)*2-2) = []

M
M(1,:) = []
M(:,1) = []
M((ne+1)*2-2,:) = []
M(:,(ne+1)*2-2) = []

% *****
% Exact Beam Natural Frequencies
% *****
for jj = 1 : nm
    wex(jj) = (jj^2) * (pi^2) * sqrt(E*I / (rho*A*L^4));
    disp(wex(jj))
end

% *****
% Eigenvalues and Eigenvectors
% *****

[phi, lam] = eig(K,M);
wJ = sqrt(diag(lam));

% *****
% Ordena los autovalores y autovectores

```

```

% Calcula los periodos naturales
% *****
[wj, id]=sort(wj);
phi=phi(:,id);
Tj = 2*pi./wj;
fj = 1./Tj;

% *****
% Imprime en pantalla
% *****
for jj = 1 : ( (ne-1)*2 + 2 )
    var1 = num2str(jj);
    var2 = num2str(wj(jj));
    var3 = num2str(fj(jj));
    var4 = num2str(Tj(jj));
    var5 = strcat( var1 , ',' , var2 , ',' , var3 , ',' , var4);
    disp(var5)
end

```

E.3.3 Refined Beam Element with Consistent Mass Matrix

```

% *****
% Deschapel lesBeamNatFreq.m
% Finite Element Program
% to obtain natural frequencies of a simple beam
% using a refined beam elements
% *****

% *****
% Clears window, variables, and graphs
% *****

clc;
clear all;
close all;

% *****
% Problem Data
% *****

g = 32.2;          % [ft/sec^2] gravi ty accel erati on
                    % W8x10
A= 2.96;           %[in2]
I = 30.8;          %[in4]
L = 20.0;          %[ft]
E = 29000.0;       %[ksi]
gamma = 0.490;     %[kcf]

ne = 6;            % number elements
nm = 5;            % number of modes

% *****
% Parameters computation
% *****
L = L * 12;
rho = (gamma/12^3) / (g*12); %[pcf]
Le = L / ne ;

K = zeros(3*ne+2, 3*ne+2);
M = zeros(3*ne+2, 3*ne+2);

% BEAM ELEMENT STIFFNESS MATRIX

k1 = 3*64*E*I/Le^3;
k2 = 3*120*E*I/Le^3;
k3 = 3*56*E*I/Le^3;

k4 = 3*12*E*I/Le^2;
k5 = 3*8*E*I/Le^2;
k6 = 3*20*E*I/Le^2;

k7 = 3*3*E*I/Le;

```

```

k8 = 3*E*I/Le;

Ke(1,1) = k1;
Ke(2,1) = k4;
Ke(3,1) = -k2;
Ke(4,1) = k3;
Ke(5,1) = -k5;

Ke(1,2) = k4;
Ke(2,2) = k7;
Ke(3,2) = -k6;
Ke(4,2) = k5;
Ke(5,2) = -k8;

Ke(1,3) = -k2;
Ke(2,3) = -k6;
Ke(3,3) = 2*k2;
Ke(4,3) = -k2;
Ke(5,3) = k6;

Ke(1,4) = k3;
Ke(2,4) = k5;
Ke(3,4) = -k2;
Ke(4,4) = k1;
Ke(5,4) = -k4;

Ke(1,5) = -k5;
Ke(2,5) = -k8;
Ke(3,5) = k6;
Ke(4,5) = -k4;
Ke(5,5) = k7;

% BEAM ELEMENT MASS MATRIX

MB = rho * A * Le ;

Me(1,1) = MB / 1260 * 288;
Me(2,1) = MB / 1260 * 21 * Le;
Me(3,1) = - MB / 1260 * 270;
Me(4,1) = - MB / 1260 * 18;
Me(5,1) = MB / 1260 * 6 * Le;

Me(1,2) = MB / 1260 * 21 * Le;
Me(2,2) = MB / 1260 * 2 * Le^2;
Me(3,2) = - MB / 1260 * 15 * Le;
Me(4,2) = - MB / 1260 * 6 * Le;
Me(5,2) = MB / 1260 * Le^2;

Me(1,3) = - MB / 1260 * 270;
Me(2,3) = - MB / 1260 * 15 * Le;
Me(3,3) = MB / 1260 * 1800;
Me(4,3) = - MB / 1260 * 270;
Me(5,3) = MB / 1260 * 15 * Le;

Me(1,4) = - MB / 1260 * 18;
Me(2,4) = - MB / 1260 * 6 * Le;
Me(3,4) = - MB / 1260 * 270;
Me(4,4) = MB / 1260 * 288;
Me(5,4) = - MB / 1260 * 21 * Le;

Me(1,5) = MB / 1260 * 6 * Le;
Me(2,5) = MB / 1260 * Le^2;
Me(3,5) = MB / 1260 * 15 * Le;
Me(4,5) = - MB / 1260 * 21 * Le;
Me(5,5) = MB / 1260 * 2 * Le^2;

% *****
% Mass and Stiffness Matrices Assembling
% *****
for jj = 1 : ne
    dof(1) = jj * 3 - 2;
    dof(2) = jj * 3 - 1;
    dof(3) = jj * 3;
    dof(4) = jj * 3 + 1;
    dof(5) = jj * 3 + 2;
    for kk = 1 : 5
        for ll = 1 : 5

```



```

        row = dof(kk);
        col = dof(ll);
        K(row,col) = K(row,col) + Ke(kk,ll);
        M(row,col) = M(row,col) + Me(kk,ll);
    end
end

% Boundary conditions
K
K(1,:)=[]
K(:,1)=[]
K(3*ne,:)=[]
K(:,3*ne)=[]

M
M(1,:)=[]
M(:,1)=[]
M(3*ne,:)=[]
M(:,3*ne)=[]

% *****
% Exact Beam Natural Frequencies
% *****
for JJ = 1 : nm
    wex(JJ) = (JJ^2)*(pi^2)*sqrt(E*I/(rho*A*L^4));
    disp(wex(JJ))
end

% *****
% Eigenvalues and Eigenvectors
% *****

[phi, lam] = eig(K,M);
wJ = sqrt(diag(lam));

% *****
% Ordena los autovalores y autovectores
% Calcula los periodos naturales
% *****
[wJ, id]=sort(wJ);
phi=phi(:,id);
TJ = 2*pi./wJ;
fJ = 1./TJ;

% *****
% Imprime en pantalla
% *****
for JJ = 1 : ( 3*ne )
    var1 = num2str(JJ);
    var2 = num2str(wJ(JJ));
    var3 = num2str(fJ(JJ));
    var4 = num2str(TJ(JJ));
    var5 = strcat( var1 , ',' , var2 , ',' , var3 , ',' , var4);
    disp(var5)
end

```

F Programs for Approximate Model Verification

The Matlab programs (worksheets) developed to compute the frequency response function (FRF) or dynamic flexibility and the dynamic stiffness of the pile head, used to obtain the results of in Chapter 5, are listed in this appendix. The MathCad worksheets prepared to compare the approximate model to other models are also presented.

F.1 FRF Using Novak Plane Strain Soil Dynamic Stiffness

```
%----- Programa FRFNovak.m-----%
% Program to compute the dynamic flexibility of a pile head %
% using the dynamic stiffness proposed by Novak for the soil, who considers %
% the soil in plain-strain and the pile as a rigid circle of radius %
% ro embedded in an infinite medium. %
% Novak, Nogami and Aboul-Elia %
%-----%
clc; clear all; close all

% *****
% * PROBLEM DATA *
% *****

% SOIL DATA
Es = 1728000; % soil Young's elastic modulus [lb/ft^2]
nu = 0.40; % soil Poisson's ratio
D=0.0; % hysteretic damping ratio
sw = 110.0; % soil specific weight [pcf]

% PILE DATA
ro = 1.0; % pile radius
L = 30.0; % pile length
Ep = 518400000.0; % pile Young's modulus
pw = 150.0; % pile specific weight

% GENERAL DATA
ne = 15; % number of elements to discretize the
pile %
g = 32.2; % gravity acceleration [ft/sec^2]
FreqMax = 80; % maximum frequency [Hz]
NFreq = 240; % Number of frequency steps

% *****
% * PROBLEM ANALYSIS *
% *****

% GENERAL COMPUTATION
sm = sw/g; % density of soil [lb.s^2/ft^4]
G = Es/(2*(1+nu)); % soil shear elastic modulus [lb/ft^2]
Vs = sqrt(G/sm); % shear wave velocity [ft/sec]
eta = sqrt(2*(1-nu)/(1-2*nu)); % Novak Dynamic Stiffness parameter
Le = L/ne; % pile element length
pm = pw/g; % density of pile [lb.s^2/ft^4]

% ARRAYS DEFINITION
%
% The KDP, UP and FRFP variables refer to the system response without
% considering soil contribution (just the pile contribution).
%
KD = zeros(2*ne, 2*ne); % System dynamic stiffness matrix
KDP = zeros(2*ne, 2*ne); % Pile dynamic stiffness matrix
```

```

MT = zeros(2*ne, 2*ne);
KP = zeros(2*ne, 2*ne);
KS = zeros(2*ne, 2*ne);
Ke = zeros(4, 4);
F = zeros(2*ne);
U = zeros(2*ne);
UP = zeros(2*ne);
FRF = zeros(NFreq+1);
FRFM = zeros(NFreq+1);
FRFP = zeros(NFreq+1);
freq = zeros(NFreq+1);

% System mass matrix
% Pile Stiffness matrix
% Soil Dynamic Stiffness Matrix
% Pile element stiffness matrix
% Load vector
% System Displacement vector
% Pile Displacement vector
% FRF = top node displacement
% FRF Module top node displacement
% FRF Pile top node displacement
% Frequency data points

% UNIT LOAD ON TOP
F(1) = 1.0;

% PILE ELEMENT STIFFNESS MATRIX
Ip = pi*ro^4/4.;
Ap = pi*ro^2;

k1 = 4*Ep*Ip/Le;
k2 = 6*Ep*Ip/Le^2;
k3 = 12*Ep*Ip/Le^3;

Ke(1, 1) = k3;
Ke(2, 1) = k2;
Ke(3, 1) = -k3;
Ke(4, 1) = k2;

Ke(1, 2) = k2;
Ke(2, 2) = k1;
Ke(3, 2) = -k2;
Ke(4, 2) = k1/2;

Ke(1, 3) = -k3;
Ke(2, 3) = -k2;
Ke(3, 3) = k3;
Ke(4, 3) = -k2;

Ke(1, 4) = k2;
Ke(2, 4) = k1/2;
Ke(3, 4) = -k2;
Ke(4, 4) = k1;

% PILE STIFFNESS MATRIX
for jj = 1 : ne-1
    dof(1) = jj*2-1;
    dof(2) = jj*2;
    dof(3) = jj*2+1;
    dof(4) = jj*2+2;
    for kk = 1 : 4
        for ll = 1 : 4
            row = dof(kk);
            col = dof(ll);
            KP(row, col) = KP(row, col) + Ke(kk, ll);
        end
    end
end

dof(1) = ne*2-1;
dof(2) = ne*2;
for kk = 1 : 2
    for ll = 1 : 2
        row = dof(kk);
        col = dof(ll);
        KP(row, col) = KP(row, col) + Ke(kk, ll);
    end
end

% PILE MASS MATRIX
MT(1, 1) = pm*Ap*Le/2;
for jj = 2 : ne
    MT(2*jj-1, 2*jj-1) = pm*Ap*Le;
end

% FRF FUNCTION
ao = 0.3;

```

```

aoc = i*ao/sqrt(1+i*D);
boc = aoc/eta;
numer = 4*
bessel k(1, boc)*bessel k(1, aoc)+aoc*bessel k(1, boc)*bessel k(0, aoc)+boc*bessel k(0, boc)*
bessel k(1, aoc);
denom=
boc*bessel k(0, boc)*bessel k(1, aoc)+aoc*bessel k(1, boc)*bessel k(0, aoc)+boc*aoc*bessel k
(0, boc)*bessel k(0, aoc);
S03 =-pi *G*ao^2*numer/denom;

for JJ = 1 : NFreq+1

    freq(JJ) = FreqMax*(JJ -1)/NFreq;

    % SOIL DYNAMIC STIFFNESS
    w=freq(JJ)*2*pi;
    ao = w*ro/Vs;
    aoc = i*ao/sqrt(1+i*D);
    boc = aoc/eta;
    numer = 4*
bessel k(1, boc)*bessel k(1, aoc)+aoc*bessel k(1, boc)*bessel k(0, aoc)+boc*bessel k(0, boc)*
bessel k(1, aoc);
    denom=
boc*bessel k(0, boc)*bessel k(1, aoc)+aoc*bessel k(1, boc)*bessel k(0, aoc)+boc*aoc*bessel k
(0, boc)*bessel k(0, aoc);
    S =-pi *G*ao^2*numer/denom;
    if ao < 0.3
        S = i*i mag(S) + real (S03);
    end
    KS(1,1) = S*Le/2;
    for kk = 2 : ne
        KS(2*kk-1,2*kk-1) = S*Le;
    end

    % SYSTEM DYNAMIC STIFFNESS
    KD = KP + KS - w^2 * MT;
    KDP = KP - w^2 * MT;

    % FREQUENCY RESPONSE FUNCTION FRF
    U = KD\F;
    FRFM(JJ) = sqrt(real (U(1))^2+imag(U(1))^2);
    FRF(JJ) = U(1);

    UP = KDP\F;
    FRFP(JJ) = sqrt(real (UP(1))^2+imag(UP(1))^2);

end

figure; plot( freq,FRFM ); grid on; title('Pile FRF Using Novak Dynamic Stiffnes');
xlabel('Load frequency [Hz]'); ylabel('Module of the Dynamic Flexibility or FRF');

figure; plot( freq,FRFM, freq, FRFP ); grid on; title('Pile FRF Using Novak Dynamic
Stiffnes');
xlabel('Load frequency [Hz]'); ylabel('Module of the Dynamic Flexibility or FRF');

```

F.2 FRF Using Lumped Soil Dynamic Stiffness

```

%----- Programa FRFLumpedModel.m-----%
% Program to compute the dynamic flexibility of a pile head %
% using the equivalent lumped model obtained by regression of the %
% dynamic stiffness proposed by Novak for the soil, who considers %
% the soil in plain-strain and the pile as a rigid circle of radius %
% ro embedded in an infinite medium. %
% Novak, Nogami and Aboul-Elia %
%-----%
clc; clear all; close all

% *****
% * PROBLEM DATA *
% *****

% SOIL DATA
Es = 1728000; % soil Young's elastic modulus [lb/ft^2]
nu = 0.40; % soil Poisson's ratio
D=0.0; % hysteretic damping ratio
sw = 110.0; % soil specific weight [pcf]

% PILE DATA
ro = 1.0; % pile radius
L = 30.0; % pile length
Ep = 518400000.0; % pile Young's modulus
pw = 150.0; % pile specific weight

% GENERAL DATA
ne = 15; % number of elements to discretize the
pile %
g = 32.2; % gravity acceleration [ft/sec^2]
FreqMax = 200; % maximum frequency [Hz]
NFreq = 400; % Number of frequency steps

% Lumped model coefficients
ak = 1.3272671;
am = 0.0510557;
ac = 3.4246489;

% *****
% * PROBLEM ANALYSIS *
% *****

% GENERAL COMPUTATION
sm = sw/g; % density of soil [lb.s^2/ft^4]
G = Es/(2*(1+nu)); % soil shear elastic modulus [lb/ft]
Vs = sqrt(G/sm); % shear wave velocity [ft/sec]
eta = sqrt(2*(1-nu)/(1-2*nu)); % Novak Dynamic Stiffness parameter
Le = L/ne; % pile element length
pm = pw/g; % density of pile [lb.s^2/ft^4]

% ARRAYS DEFINITION
%
% The KDP, UP and FRFP variables refer to the system response without
% considering soil contribution (just the pile contribution).
%
KD = zeros(2*ne, 2*ne); % System dynamic stiffness matrix
KDP = zeros(2*ne, 2*ne); % Pile dynamic stiffness matrix

KP = zeros(2*ne, 2*ne); % Pile Stiffness matrix
KS = zeros(2*ne, 2*ne); % Soil Dynamic Stiffness Matrix
Ke = zeros(4, 4); % Pile element stiffness matrix

MP = zeros(2*ne, 2*ne); % Pile mass matrix
MS = zeros(2*ne, 2*ne); % Soil mass matrix
MT = zeros(2*ne, 2*ne); % System mass matrix

CS = zeros(2*ne, 2*ne); % Soil damping matrix

F = zeros(2*ne); % Load vector

U = zeros(2*ne); % System Displacement vector
UP = zeros(2*ne); % Pile Displacement vector

```

```

FRF = zeros(NFreq+1);
FRFM = zeros(NFreq+1);
FRFP = zeros(NFreq+1);
freq = zeros(NFreq+1);

% FRF = top node displacement
% FRF Module top node displacement
% FRF Pile top node displacement
% Frequency data points

% UNIT LOAD ON TOP
F(1) = 1000.0;

% Unit harmonic load on top of pile
% to obtain dynamic flexibility in
% [ft/Kip] units

% PILE ELEMENT STIFFNESS MATRIX
Ip = pi*ro^4/4.;
Ap = pi*ro^2;

% Pile cross section inertia
% Pile cross section area

k1 = 4*Ep*Ip/Le;
k2 = 6*Ep*Ip/Le^2;
k3 = 12*Ep*Ip/Le^3;

Ke(1,1) = k3;
Ke(2,1) = k2;
Ke(3,1) = -k3;
Ke(4,1) = k2;

Ke(1,2) = k2;
Ke(2,2) = k1;
Ke(3,2) = -k2;
Ke(4,2) = k1/2;

Ke(1,3) = -k3;
Ke(2,3) = -k2;
Ke(3,3) = k3;
Ke(4,3) = -k2;

Ke(1,4) = k2;
Ke(2,4) = k1/2;
Ke(3,4) = -k2;
Ke(4,4) = k1;

% PILE STIFFNESS MATRIX
for jj = 1 : ne-1
    dof(1) = jj*2-1;
    dof(2) = jj*2;
    dof(3) = jj*2+1;
    dof(4) = jj*2+2;
    for kk = 1 : 4
        for ll = 1 : 4
            row = dof(kk);
            col = dof(ll);
            KP(row,col) = KP(row,col) + Ke(kk,ll);
        end
    end
end

dof(1) = ne*2-1;
dof(2) = ne*2;
for kk = 1 : 2
    for ll = 1 : 2
        row = dof(kk);
        col = dof(ll);
        KP(row,col) = KP(row,col) + Ke(kk,ll);
    end
end

% PILE MASS MATRIX
MP(1,1) = pm*Ap*Le/2;
for jj = 2 : ne
    MP(2*jj-1, 2*jj-1) = pm*Ap*Le;
end

% SOIL STIFFNESS MATRIX, MASS MATRIX, AND DAMPING MATRIX
KS(1,1) = pi*G*ak*Le/2;
MS(1,1) = pi*ro^2*sm*am*Le/2;
CS(1,1) = pi*ro*G/Vs*ac*Le/2;
for jj = 2 : ne
    KS(2*jj-1, 2*jj-1) = pi*G*ak*Le;
    MS(2*jj-1, 2*jj-1) = pi*ro^2*sm*am*Le;

```

```

        CS(2*JJ-1,2*JJ-1) = pi*ro*G/Vs*ac*Le;
    end

    MT = MP + MS;

    % FRF FUNCTION
    for JJ = 1 : NFreq+1

        freq(JJ) = FreqMax*(JJ-1)/NFreq;
        w=freq(JJ)*2*pi;

        % SYSTEM DYNAMIC STIFFNESS
        KD = KP + KS + I * w * CS - w^2 * MT;
        KDP = KP - w^2 * MP;

        % FREQUENCY RESPONSE FUNCTION FRF
        U = KD\F;
        FRFM(JJ) = sqrt(real(U(1))^2+imag(U(1))^2);
        FRF(JJ) = U(1);

        UP = KDP\F;
        FRFP(JJ) = sqrt(real(UP(1))^2+imag(UP(1))^2);

    end

    figure; plot( freq,FRFM ); grid on; title('Pile FRF Using Novak Dynamic Stiffnes');
    xlabel('load frequency [Hz]'); ylabel('Module of the Dynamic Flexibility or FRF [ft/Kip]');

    figure; plot( freq,FRFM, freq, FRFP ); grid on; title('Pile FRF Using Novak Dynamic Stiffnes');
    xlabel('load frequency [Hz]'); ylabel('Module of the Dynamic Flexibility or FRF [ft/Kip]');

    figure; plot( freq, FRFP ); grid on; title('Pile FRF without Soil Contribution');
    xlabel('load frequency [Hz]'); ylabel('Module of the Dynamic Flexibility or FRF [ft/Kip]');

```

F.3 FRF Comparing Novak and Lumped Models

```

%----- Programa FRFNovakLumped.m-----%
% Program to compute the dynamic flexibility of a pile head %
% using the dynamic stiffness proposed by Novak for the soil, and %
% using the equivalent lumped model obtained by regression of the %
% dynamic stiffness proposed by Novak for the soil, who considers %
% the soil in plain-strain and the pile as a rigid circle of radius %
% ro embedded in an infinite medium. %
% Novak, Nogami and Aboul-Elia %
%-----%
clc; clear all; close all

% *****
% * PROBLEM DATA *
% *****

% SOIL DATA
Es = 1728000; % soil Young's elastic modulus [lb/ft^2]
nu = 0.40; % soil Poisson's ratio
D=0.0; % hysteretic damping ratio
sw = 110.0; % soil specific weight [pcf]

% PILE DATA
ro = 1.0; % pile radius
L = 30.0; % pile length
Ep = 518400000.0; % pile Young's modulus
pw = 150.0; % pile specific weight

% GENERAL DATA

```

```

ne = 15; % number of elements to discretize the
pile
g = 32.2; % gravity acceleration [ft/sec^2]
FreqMax = 200; % maximum frequency [Hz]
NFreq = 400; % Number of frequency steps

% Lumped model coefficients
ak = 1.3272671;
am = 0.0510557;
ac = 3.4246489;

% *****
% * PROBLEM ANALYSIS *
% *****

% GENERAL COMPUTATION
sm = sw/g; % density of soil [lb.s^2/ft^4]
G = Es/(2*(1+nu)); % soil shear elastic modulus [lb/ft]
Vs = sqrt(G/sm); % shear wave velocity [ft/sec]
eta = sqrt(2*(1-nu)/(1-2*nu)); % Novak Dynamic Stiffness parameter
Le = L/ne; % pile element length
pm = pw/g; % density of pile [lb.s^2/ft^4]

% ARRAYS DEFINITION
%
% The KDP, UP and FRFP variables refer to the system response without
% considering soil contribution (just the pile contribution).
%
KDN = zeros(2*ne, 2*ne); % Novak System dynamic stiffness matrix
KDL = zeros(2*ne, 2*ne); % Lumped System dynamic stiffness matrix
KDP = zeros(2*ne, 2*ne); % Pile dynamic stiffness matrix

KP = zeros(2*ne, 2*ne); % Pile Stiffness matrix
KS = zeros(2*ne, 2*ne); % Soil Dynamic Stiffness Matrix
KSL = zeros(2*ne, 2*ne); % Lumped Soil Dynamic Stiffness Matrix
Ke = zeros(4, 4); % Pile element stiffness matrix

MP = zeros(2*ne, 2*ne); % Pile mass matrix
MS = zeros(2*ne, 2*ne); % Lumped Soil mass matrix
MT = zeros(2*ne, 2*ne); % System mass matrix

CS = zeros(2*ne, 2*ne); % Lumped Soil damping matrix

F = zeros(2*ne); % Load vector

U = zeros(2*ne); % System Displacement vector
UL = zeros(2*ne); % Lumped Model Displacement vector
UP = zeros(2*ne); % Pile Displacement vector

FRF = zeros(NFreq+1); % FRF = top node displacement
FRFM = zeros(NFreq+1); % FRF Module top node displacement
FRFP = zeros(NFreq+1); % FRF Pile top node displacement
FRFL = zeros(NFreq+1); % Lumped FRF module top node displacement
freq = zeros(NFreq+1); % Frequency data points

% UNIT LOAD ON TOP
F(1) = 1000.0; % Unit harmonic load on top of pile
% to obtain dynamic flexibility in
% [ft/Kip] units

% PILE ELEMENT STIFFNESS MATRIX
Ip = pi*ro^4/4.; % Pile cross section inertia
Ap = pi*ro^2; % Pile cross section area

k1 = 4*Ep*Ip/Le;
k2 = 6*Ep*Ip/Le^2;
k3 = 12*Ep*Ip/Le^3;

Ke(1, 1) = k3;
Ke(2, 1) = k2;
Ke(3, 1) = -k3;
Ke(4, 1) = k2;

Ke(1, 2) = k2;
Ke(2, 2) = k1;
Ke(3, 2) = -k2;
Ke(4, 2) = k1/2;

```



```

Ke(1,3) = -k3;
Ke(2,3) = -k2;
Ke(3,3) = k3;
Ke(4,3) = -k2;

Ke(1,4) = k2;
Ke(2,4) = k1/2;
Ke(3,4) = -k2;
Ke(4,4) = k1;

% PILE STIFFNESS MATRIX
for jj = 1 : ne-1
    dof(1) = jj*2-1;
    dof(2) = jj*2;
    dof(3) = jj*2+1;
    dof(4) = jj*2+2;
    for kk = 1 : 4
        for ll = 1 : 4
            row = dof(kk);
            col = dof(ll);
            KP(row,col) = KP(row,col) + Ke(kk,ll);
        end
    end
end

dof(1) = ne*2-1;
dof(2) = ne*2;
for kk = 1 : 2
    for ll = 1 : 2
        row = dof(kk);
        col = dof(ll);
        KP(row,col) = KP(row,col) + Ke(kk,ll);
    end
end

% PILE MASS MATRIX
MP(1,1) = pm*Ap*Le/2;
for jj = 2 : ne
    MP(2*jj-1,2*jj-1) = pm*Ap*Le;
end

% LUMPED SOIL STIFFNESS MATRIX, MASS MATRIX, AND DAMPING MATRIX
KSL(1,1) = pi*G*ak*Le/2;
MS(1,1) = pi*ro^2*sm*am*Le/2;
CS(1,1) = pi*ro*G/Vs*ac*Le/2;
for jj = 2 : ne
    KSL(2*jj-1,2*jj-1) = pi*G*ak*Le;
    MS(2*jj-1,2*jj-1) = pi*ro^2*sm*am*Le;
    CS(2*jj-1,2*jj-1) = pi*ro*G/Vs*ac*Le;
end

MT = MP + MS;

% FRF FUNCTION
ao = 0.3;
aoc = i*ao/sqrt(1+i*D);
boc = aoc/eta;
numer = 4*
bessel k(1,boc)*bessel k(1,aoc)+aoc*bessel k(1,boc)*bessel k(0,aoc)+boc*bessel k(0,boc)*
bessel k(1,aoc);
denom=
boc*bessel k(0,boc)*bessel k(1,aoc)+aoc*bessel k(1,boc)*bessel k(0,aoc)+boc*aoc*bessel k
(0,boc)*bessel k(0,aoc);
S03 =-pi*G*ao^2*numer/denom;

for jj = 1 : NFreq+1
    freq(jj) = FreqMax*(jj-1)/NFreq;

    % SOIL DYNAMIC STIFFNESS
    w=freq(jj)*2*pi;
    ao = w*ro/Vs;
    aoc = i*ao/sqrt(1+i*D);
    boc = aoc/eta;
    numer = 4*
    bessel k(1,boc)*bessel k(1,aoc)+aoc*bessel k(1,boc)*bessel k(0,aoc)+boc*bessel k(0,boc)*
    bessel k(1,aoc);

```

```

denom=
boc*bessel k(0, boc)*bessel k(1, aoc)+aoc*bessel k(1, boc)*bessel k(0, aoc)+boc*aoc*bessel k
(0, boc)*bessel k(0, aoc);
S =-pi *G*ao^2*numer/denom;
if ao < 0.3
    S = i*imag(S) + real (S03);
end
KS(1, 1) = S*Le/2;
for kk = 2 : ne
    KS(2*kk-1, 2*kk-1) = S*Le;
end

% SYSTEM DYNAMIC STIFFNESS
KD = KP + KS - w^2 * MP;
KDP = KP - w^2 * MP;
KDL = KP + KSL + i * w * CS - w^2 * MT;

% FREQUENCY RESPONSE FUNCTION FRF
U = KD\F;
FRFM(JJ) = sqrt(real (U(1))^2+imag(U(1))^2);
FRF(JJ) = U(1);

UP = KDP\F;
FRFP(JJ) = sqrt(real (UP(1))^2+imag(UP(1))^2);

UL = KDL\F;
FRFL(JJ) = sqrt(real (UL(1))^2+imag(UL(1))^2);

end

figure; plot( freq,FRFM, freq, FRFL ); grid on; title('Pile FRF Using Lumped Model
and Novak Dynamic Stiffness');
xlabel('Load frequency [Hz]'); ylabel('Module of the Dynamic Flexibility or FRF
[ft/Kip]');

```

F.4 FRF Comparing Novak and Lumped Models for Different v

```

%----- Programa FRFNovakLumpedVariousnu.m-----%
% Program to compute the dynamic flexibility of a pile head %
% using the dynamic stiffness proposed by Novak for the soil, and %
% using the equivalent lumped model obtained by regression of the %
% dynamic stiffness proposed by Novak for the soil, who considers %
% the soil in plain-strain and the pile as a rigid circle of radius %
% ro embedded in an infinite medium. %
% Novak, Nogami and Aboul-Elia %
%-----%
clc; clear all; close all

% *****
% * PROBLEM DATA *
% *****

% SOIL DATA
Es = 1728000; % soil Young's elastic modulus[lb/ft^2]

nu = [0.499999, 0.48, 0.46, 0.44, 0.42, 0.40, 0.38, 0.36, 0.34, 0.32, 0.30, 0.28,
0.26, 0.24, 0.22, 0.20]; % soil Poisson's ratio

D=0.0; % hysteretic damping ratio
sw = 110.0; % soil specific weight [pcf]

% PILE DATA
ro = 1.0; % pile radius
L = 30.0; % pile length
Ep = 518400000.0; % pile Young's modulus
pw = 150.0; % pile specific weight

% GENERAL DATA

```

```

ne = 15; % number of elements to discretize the
pile
g = 32.2; % gravity acceleration [ft/sec^2]
FreqMax = 200; % maximum frequency [Hz]
NFreq = 400; % Number of frequency steps

% Lumped model coefficients
ak = [1.7213669, 1.4632669, 1.3691849, 1.3459197, 1.3354993, 1.3272671];
ak(7) = 1.3193269;
ak(8) = 1.3115302;
ak(9) = 1.3041138;
ak(10) = 1.2974948;
ak(11) = 1.3068585;
ak(12) = 1.3088585;
ak(13) = 1.3076619;
ak(14) = 1.304348;
ak(15) = 1.2996384;
ak(16) = 1.2940234;

am = [0.9653314, 0.4571463, 0.2348233, 0.1355508, 0.0825761, 0.0510557];
am(7) = 0.0310366;
am(8) = 0.0178041;
am(9) = 0.0088633;
am(10) = 0.0028022;
am(11) = 0.0;
am(12) = 0.0;
am(13) = 0.0;
am(14) = 0.0;
am(15) = 0.0;
am(16) = 0.0;

ac = [4.1074708, 4.3382529, 4.066384, 3.8045412, 3.5929876, 3.4246489];
ac(7) = 3.2890761;
ac(8) = 3.1780333;
ac(9) = 3.0855721;
ac(10) = 3.0074355;
ac(11) = 2.9405413;
ac(12) = 2.8826198;
ac(13) = 2.8319687;
ac(14) = 2.7872894;
ac(15) = 2.7475747;
ac(16) = 2.7120324;

% *****
% * PROBLEM ANALYSIS *
% *****

% GENERAL COMPUTATION
sm = sw/g; % density of soil [lb.s^2/ft^4]
Le = L/ne; % pile element length
pm = pw/g; % density of pile [lb.s^2/ft^4]

% ARRAYS DEFINITION
%
% The KDP, UP and FRFP variables refer to the system reponse without
% considering soil contribution (just the pile contribution).
%
KDN = zeros(2*ne, 2*ne); % Novak System dynamic stiffness matrix
KDL = zeros(2*ne, 2*ne); % Lumped System dynamic stiffness matrix
KDP = zeros(2*ne, 2*ne); % Pile dynamic stiffness matrix

KP = zeros(2*ne, 2*ne); % Pile Stiffness matrix
KS = zeros(2*ne, 2*ne); % Soil Dynamic Stiffness Matrix
KSL = zeros(2*ne, 2*ne); % Lumped Soil Dynamic Stiffness Matrix
Ke = zeros(4, 4); % Pile element stiffness matrix

MP = zeros(2*ne, 2*ne); % Pile mass matrix
MS = zeros(2*ne, 2*ne); % Lumped Soil mass matrix
MT = zeros(2*ne, 2*ne); % System mass matrix

CS = zeros(2*ne, 2*ne); % Lumped Soil damping matrix

F = zeros(2*ne); % Load vector

U = zeros(2*ne); % System Displacement vector
UL = zeros(2*ne); % Lumped Model Displacement vector
UP = zeros(2*ne); % Pile Displacement vector

```

```

FRF = zeros(NFreq+1);
FRFM = zeros(NFreq+1);
FRFP = zeros(NFreq+1);
FRFL = zeros(NFreq+1);
freq = zeros(NFreq+1);

% FRF = top node displacement
% FRF Module top node displacement
% FRF Pile top node displacement
% Lumped FRF module top node displacement
% Frequency data points

% UNIT LOAD ON TOP
F(1) = 1000.0;

% Unit harmonic load on top of pile
% to obtain dynamic flexibility in
% [ft/Kip] units

% PILE ELEMENT STIFFNESS MATRIX
Ip = pi*ro^4/4.;
Ap = pi*ro^2;

% Pile cross section inertia
% Pile cross section area

k1 = 4*Ep*Ip/Le;
k2 = 6*Ep*Ip/Le^2;
k3 = 12*Ep*Ip/Le^3;

Ke(1,1) = k3;
Ke(2,1) = k2;
Ke(3,1) = -k3;
Ke(4,1) = k2;

Ke(1,2) = k2;
Ke(2,2) = k1;
Ke(3,2) = -k2;
Ke(4,2) = k1/2;

Ke(1,3) = -k3;
Ke(2,3) = -k2;
Ke(3,3) = k3;
Ke(4,3) = -k2;

Ke(1,4) = k2;
Ke(2,4) = k1/2;
Ke(3,4) = -k2;
Ke(4,4) = k1;

% PILE STIFFNESS MATRIX
for jj = 1 : ne-1
    dof(1) = jj*2-1;
    dof(2) = jj*2;
    dof(3) = jj*2+1;
    dof(4) = jj*2+2;
    for kk = 1 : 4
        for ll = 1 : 4
            row = dof(kk);
            col = dof(ll);
            KP(row,col) = KP(row,col) + Ke(kk,ll);
        end
    end
end

dof(1) = ne*2-1;
dof(2) = ne*2;
for kk = 1 : 2
    for ll = 1 : 2
        row = dof(kk);
        col = dof(ll);
        KP(row,col) = KP(row,col) + Ke(kk,ll);
    end
end

% PILE MASS MATRIX
MP(1,1) = pm*Ap*Le/2;
for jj = 2 : ne
    MP(2*jj-1, 2*jj-1) = pm*Ap*Le;
end

for ii = 1 : 10
    % GENERAL COMPUTATIONS
    eta = sqrt(2*(1-nu(ii))/(1-2*nu(ii)));
    G = Es/(2*(1+nu(ii)));
    Vs = sqrt(G/sm);

    % Novak Dynamic Stiffness parameter
    % soil shear elastic modulus [lb/ft]
    % shear wave velocity [ft/sec]

```

```

% LUMPED SOIL STIFFNESS MATRIX, MASS MATRIX, AND DAMPING MATRIX
KSL(1,1) = pi * G * ak(11) * Le / 2;
MS(1,1) = pi * ro^2 * sm * am(11) * Le / 2;
CS(1,1) = pi * ro * G / Vs * ac(11) * Le / 2;
for jj = 2 : ne
    KSL(2*jj-1, 2*jj-1) = pi * G * ak(11) * Le;
    MS(2*jj-1, 2*jj-1) = pi * ro^2 * sm * am(11) * Le;
    CS(2*jj-1, 2*jj-1) = pi * ro * G / Vs * ac(11) * Le;
end

MT = MP + MS;

% FRF FUNCTION
ao = 0.3;
aoc = i * ao / sqrt(1 + i * D);
boc = aoc / eta;
numer = 4 *
bessel k(1, boc) * bessel k(1, aoc) + aoc * bessel k(1, boc) * bessel k(0, aoc) + boc * bessel k(0, boc) *
bessel k(1, aoc);
denom =
boc * bessel k(0, boc) * bessel k(1, aoc) + aoc * bessel k(1, boc) * bessel k(0, aoc) + boc * aoc * bessel k
(0, boc) * bessel k(0, aoc);
S03 = -pi * G * ao^2 * numer / denom;

for jj = 1 : NFreq + 1

    freq(jj) = FreqMax * (jj - 1) / NFreq;

    % SOIL DYNAMIC STIFFNESS
    w = freq(jj) * 2 * pi;
    ao = w * ro / Vs;
    aoc = i * ao / sqrt(1 + i * D);
    boc = aoc / eta;
    numer = 4 *
bessel k(1, boc) * bessel k(1, aoc) + aoc * bessel k(1, boc) * bessel k(0, aoc) + boc * bessel k(0, boc) *
bessel k(1, aoc);
    denom =
boc * bessel k(0, boc) * bessel k(1, aoc) + aoc * bessel k(1, boc) * bessel k(0, aoc) + boc * aoc * bessel k
(0, boc) * bessel k(0, aoc);
    S = -pi * G * ao^2 * numer / denom;
    if ao < 0.3
        S = i * imag(S) + real(S03);
    end
    KS(1,1) = S * Le / 2;
    for kk = 2 : ne
        KS(2*kk-1, 2*kk-1) = S * Le;
    end

    % SYSTEM DYNAMIC STIFFNESS
    KD = KP + KS - w^2 * MP;
    KDP = KP - w^2 * MP;
    KDL = KP + KSL + i * w * CS - w^2 * MT;

    % FREQUENCY RESPONSE FUNCTION FRF
    U = KD \ F;
    FRFM(jj) = sqrt(real(U(1))^2 + imag(U(1))^2);
    FRF(jj) = U(1);

    UP = KDP \ F;
    FRFP(jj) = sqrt(real(UP(1))^2 + imag(UP(1))^2);

    UL = KDL \ F;
    FRFL(jj) = sqrt(real(UL(1))^2 + imag(UL(1))^2);

end

var1 = strcat('nu = ', num2str(nu(11)), ' ');
var2 = strcat('FRF Lumped Model vs Novak Model - ', var1);
figure; plot(freq, FRFM, freq, FRFL); grid on; title(var2)
xlabel('load frequency [Hz]'); ylabel('Module of the Dynamic Flexibility or FRF
[ft/Kip]');

end

```

F.5 FRF Comparing Novak and Lumped Models for Different ro

```

%----- Programa FRFNovakLumpedVariousDo.m-----%
% Program to compute the dynamic flexibility of a pile head %
% using the dynamic stiffness proposed by Novak for the soil, and %
% using the equivalent lumped model obtained by regression of the %
% dynamic stiffness proposed by Novak for the soil, who considers %
% the soil in plain-strain and the pile as a rigid circle of radius %
% ro embedded in an infinite medium. %
% Novak, Nogami and Aboul-Elia %
%-----%
clc; clear all; close all

% *****
% * PROBLEM DATA *
% *****

% SOIL DATA
Es = 1728000; % soil Young's elastic modulus[lb/ft^2]
nu = 0.40; % soil Poisson's ratio
D=0.0; % hysteretic damping ratio
sw = 110.0; % soil specific weight [pcf]

% PILE DATA
for jj = 1 : 10
    roo(jj) = jj; % pile radius
end

L = 30.0; % pile length
Ep = 518400000.0; % pile Young's modulus
pw = 150.0; % pile specific weight

% GENERAL DATA
ne = 15; % number of elements to discretize the
pile %
g = 32.2; % gravity acceleration [ft/sec^2]
FreqMax = 200; % maximum frequency [Hz]
NFreq = 400; % Number of frequency steps

% Lumped model coefficients
ak = 1.3272671;
am = 0.0510557;
ac = 3.4246489;

% *****
% * PROBLEM ANALYSIS *
% *****

% GENERAL COMPUTATION
sm = sw/g; % density of soil [lb.s^2/ft^4]
G = Es/(2*(1+nu)); % soil shear elastic modulus[lb/ft]
Vs = sqrt(G/sm); % shear wave velocity [ft/sec]
eta = sqrt(2*(1-nu)/(1-2*nu)); % Novak Dynamic Stiffness parameter
Le = L/ne; % pile element length
pm = pw/g; % density of pile [lb.s^2/ft^4]

% ARRAYS DEFINITION
%
% The KDP, UP and FRFP variables refer to the system reponse without
% considering soil contribution (just the pile contribution).
%
KDN = zeros(2*ne,2*ne); % Novak System dynamic stiffness matrix
KDL = zeros(2*ne,2*ne); % Lumped System dynamic stiffness matrix
KDP = zeros(2*ne,2*ne); % Pile dynamic stiffness matrix

KP = zeros(2*ne,2*ne); % Pile Stiffness matrix
KS = zeros(2*ne,2*ne); % Soil Dynamic Stiffness Matrix
KSL = zeros(2*ne,2*ne); % Lumped Soil Dynamic Stiffness Matrix
Ke = zeros(4,4); % Pile element stiffness matrix

MP = zeros(2*ne,2*ne); % Pile mass matrix
MS = zeros(2*ne,2*ne); % Lumped Soil mass matrix
MT = zeros(2*ne,2*ne); % System mass matrix

```

```

CS = zeros(2*ne, 2*ne); % Lumped Soil damping matrix
F = zeros(2*ne); % Load vector
U = zeros(2*ne); % System Displacement vector
UL = zeros(2*ne); % Lumped Model Displacement vector
UP = zeros(2*ne); % Pile Displacement vector

FRF = zeros(NFreq+1); % FRF = top node displacement
FRFM = zeros(NFreq+1); % FRF Module top node displacement
FRFP = zeros(NFreq+1); % FRF Pile top node displacement
FRFL = zeros(NFreq+1); % Lumped FRF module top node displacement
freq = zeros(NFreq+1); % Frequency data points

% UNIT LOAD ON TOP
F(1) = 1000.0; % Unit harmonic load on top of pile
% to obtain dynamic flexibility in
% [ft/Kip] units

for ii = 1 : 10
    ro = roo(ii);

    % PILE ELEMENT STIFFNESS MATRIX
    Ip = pi * ro^4 / 4.; % Pile cross section inertia
    Ap = pi * ro^2; % Pile cross section area

    k1 = 4 * Ep * Ip / Le;
    k2 = 6 * Ep * Ip / Le^2;
    k3 = 12 * Ep * Ip / Le^3;

    Ke(1, 1) = k3;
    Ke(2, 1) = k2;
    Ke(3, 1) = -k3;
    Ke(4, 1) = k2;

    Ke(1, 2) = k2;
    Ke(2, 2) = k1;
    Ke(3, 2) = -k2;
    Ke(4, 2) = k1/2;

    Ke(1, 3) = -k3;
    Ke(2, 3) = -k2;
    Ke(3, 3) = k3;
    Ke(4, 3) = -k2;

    Ke(1, 4) = k2;
    Ke(2, 4) = k1/2;
    Ke(3, 4) = -k2;
    Ke(4, 4) = k1;

    % PILE STIFFNESS MATRIX
    for jj = 1 : ne-1
        dof(1) = jj * 2 - 1;
        dof(2) = jj * 2;
        dof(3) = jj * 2 + 1;
        dof(4) = jj * 2 + 2;
        for kk = 1 : 4
            for ll = 1 : 4
                row = dof(kk);
                col = dof(ll);
                KP(row, col) = KP(row, col) + Ke(kk, ll);
            end
        end
    end

    dof(1) = ne * 2 - 1;
    dof(2) = ne * 2;
    for kk = 1 : 2
        for ll = 1 : 2
            row = dof(kk);
            col = dof(ll);
            KP(row, col) = KP(row, col) + Ke(kk, ll);
        end
    end

    % PILE MASS MATRIX
    MP(1, 1) = pm * Ap * Le / 2;
    for jj = 2 : ne

```

```

        MP(2*JJ-1, 2*JJ-1) = pm*Ap*Le;
    end

    % LUMPED SOIL STIFFNESS MATRIX, MASS MATRIX, AND DAMPING MATRIX
    KSL(1,1) = pi*G*ak*Le/2;
    MS(1,1) = pi*ro^2*sm*am*Le/2;
    CS(1,1) = pi*ro*G/Vs*ac*Le/2;
    for jj = 2 : ne
        KSL(2*JJ-1, 2*JJ-1) = pi*G*ak*Le;
        MS(2*JJ-1, 2*JJ-1) = pi*ro^2*sm*am*Le;
        CS(2*JJ-1, 2*JJ-1) = pi*ro*G/Vs*ac*Le;
    end

    MT = MP + MS;

    % FRF FUNCTION
    ao = 0.3;
    aoc = i*ao/sqrt(1+i*D);
    boc = aoc/eta;
    numer = 4*
    besselk(1,boc)*besselk(1,aoc)+aoc*besselk(1,boc)*besselk(0,aoc)+boc*besselk(0,boc)*
    besselk(1,aoc);
    denom=
    boc*besselk(0,boc)*besselk(1,aoc)+aoc*besselk(1,boc)*besselk(0,aoc)+boc*aoc*besselk
    (0,boc)*besselk(0,aoc);
    S03 =-pi*G*ao^2*numer/denom;

    for JJ = 1 : NFreq+1

        freq(JJ) = FreqMax*(JJ-1)/NFreq;

        % SOIL DYNAMIC STIFFNESS
        w=freq(JJ)*2*pi;
        ao = w*ro/Vs;
        aoc = i*ao/sqrt(1+i*D);
        boc = aoc/eta;
        numer = 4*
        besselk(1,boc)*besselk(1,aoc)+aoc*besselk(1,boc)*besselk(0,aoc)+boc*besselk(0,boc)*
        besselk(1,aoc);
        denom=
        boc*besselk(0,boc)*besselk(1,aoc)+aoc*besselk(1,boc)*besselk(0,aoc)+boc*aoc*besselk
        (0,boc)*besselk(0,aoc);
        S =-pi*G*ao^2*numer/denom;
        if ao < 0.3
            S = i*imag(S) + real(S03);
        end
        KS(1,1) = S*Le/2;
        for kk = 2 : ne
            KS(2*kk-1, 2*kk-1) = S*Le;
        end

        % SYSTEM DYNAMIC STIFFNESS
        KD = KP + KS - w^2 * MP;
        KDP = KP - w^2 * MP;
        KDL = KP + KSL + i * w * CS - w^2 * MT;

        % FREQUENCY RESPONSE FUNCTION FRF
        U = KD\F;
        FRFM(JJ) = sqrt(real(U(1))^2+imag(U(1))^2);
        FRF(JJ) = U(1);

        UP = KDP\F;
        FRFP(JJ) = sqrt(real(UP(1))^2+imag(UP(1))^2);

        UL = KDL\F;
        FRFL(JJ) = sqrt(real(UL(1))^2+imag(UL(1))^2);

    end

    var1 = strcat('FRF Lumped vs Novac - ro = ', num2str(ro), ' [ft]');
    figure; plot(freq,FRFM,freq,FRFL); grid on; title(var1)
    xlabel('load frequency [Hz]'); ylabel('Module of the Dynamic Flexibility or FRF
    [ft/Kip]');

end

```


F.6 FRF Comparing Novak and Lumped Models for Different E

```

%----- Programa FRFNovakLumpedVariousE.m-----%
% Program to compute the dynamic flexibility of a pile head
% using the dynamic stiffness proposed by Novak for the soil, and
% using the equivalent lumped model obtained by regression of the
% dynamic stiffness proposed by Novak for the soil, who considers
% the soil in plain-strain and the pile as a rigid circle of radius
% ro embedded in an infinite medium.
% Novak, Nogami and Aboul-Elia
%-----%
clc; clear all; close all

% *****
% * PROBLEM DATA
% *****

% SOIL DATA
Es = [2000000, 6000000, 10000000, 14000000, 18000000, 22000000, 26000000, 30000000];
Es(9) = 34000000;
Es(10) = 38000000;

% soil Young's elastic modulus [lb/ft^2]

nu = 0.40;

% soil Poisson's ratio

D=0.0;
sw = 110.0;

% hysteretic damping ratio
% soil specific weight [pcf]

% PILE DATA
ro = 1.0;
L = 30.0;
Ep = 518400000.0;
pw = 150.0;

% pile radius
% pile length
% pile Young's modulus
% pile specific weight

% GENERAL DATA
ne = 15;
pile
g = 32.2;
FreqMax = 200;
NFreq = 400;

% number of elements to discretize the
% gravity acceleration [ft/sec^2]
% maximum frequency [Hz]
% Number of frequency steps

% Lumped model coefficients
ak = 1.3272671;
am = 0.0510557;
ac = 3.4246489;

% *****
% * PROBLEM ANALYSIS
% *****

% GENERAL COMPUTATION
sm = sw/g;
Le = L/ne;
pm = pw/g;

% density of soil [lb.s^2/ft^4]
% pile element length
% density of pile [lb.s^2/ft^4]

% ARRAYS DEFINITION
%
% The KDP, UP and FRFP variables refer to the system response without
% considering soil contribution (just the pile contribution).
%
KDN = zeros(2*ne, 2*ne);
KDL = zeros(2*ne, 2*ne);
KDP = zeros(2*ne, 2*ne);

% Novak System dynamic stiffness matrix
% Lumped System dynamic stiffness matrix
% Pile dynamic stiffness matrix

KP = zeros(2*ne, 2*ne);
KS = zeros(2*ne, 2*ne);
KSL = zeros(2*ne, 2*ne);
Ke = zeros(4, 4);

% Pile Stiffness matrix
% Soil Dynamic Stiffness Matrix
% Lumped Soil Dynamic Stiffness Matrix
% Pile element stiffness matrix

MP = zeros(2*ne, 2*ne);
MS = zeros(2*ne, 2*ne);
MT = zeros(2*ne, 2*ne);

% Pile mass matrix
% Lumped Soil mass matrix
% System mass matrix

```

```

CS = zeros(2*ne, 2*ne); % Lumped Soil damping matrix
F = zeros(2*ne); % Load vector
U = zeros(2*ne); % System Displacement vector
UL = zeros(2*ne); % Lumped Model Displacement vector
UP = zeros(2*ne); % Pile Displacement vector

FRF = zeros(NFreq+1); % FRF = top node displacement
FRFM = zeros(NFreq+1); % FRF Module top node displacement
FRFP = zeros(NFreq+1); % FRF Pile top node displacement
FRFL = zeros(NFreq+1); % Lumped FRF module top node displacement
freq = zeros(NFreq+1); % Frequency data points

% UNIT LOAD ON TOP
F(1) = 1000.0; % Unit harmonic load on top of pile
% to obtain dynamic flexibility in
% [ft/Kip] units

% PILE ELEMENT STIFFNESS MATRIX
Ip = pi*ro^4/4.; % Pile cross section inertia
Ap = pi*ro^2; % Pile cross section area

k1 = 4*Ep*Ip/Le;
k2 = 6*Ep*Ip/Le^2;
k3 = 12*Ep*Ip/Le^3;

Ke(1,1) = k3;
Ke(2,1) = k2;
Ke(3,1) = -k3;
Ke(4,1) = k2;

Ke(1,2) = k2;
Ke(2,2) = k1;
Ke(3,2) = -k2;
Ke(4,2) = k1/2;

Ke(1,3) = -k3;
Ke(2,3) = -k2;
Ke(3,3) = k3;
Ke(4,3) = -k2;

Ke(1,4) = k2;
Ke(2,4) = k1/2;
Ke(3,4) = -k2;
Ke(4,4) = k1;

% PILE STIFFNESS MATRIX
for jj = 1 : ne-1
    dof(1) = jj*2-1;
    dof(2) = jj*2;
    dof(3) = jj*2+1;
    dof(4) = jj*2+2;
    for kk = 1 : 4
        for ll = 1 : 4
            row = dof(kk);
            col = dof(ll);
            KP(row, col) = KP(row, col) + Ke(kk, ll);
        end
    end
end

dof(1) = ne*2-1;
dof(2) = ne*2;
for kk = 1 : 2
    for ll = 1 : 2
        row = dof(kk);
        col = dof(ll);
        KP(row, col) = KP(row, col) + Ke(kk, ll);
    end
end

% PILE MASS MATRIX
MP(1,1) = pm*Ap*Le/2;
for jj = 2 : ne
    MP(2*jj-1, 2*jj-1) = pm*Ap*Le;
end

```

```

for ii = 1 : 10

    % GENERAL COMPUTATIONS
    eta = sqrt(2*(1-nu)/(1-2*nu));          % Novak Dynamic Stiffness parameter
    G = Es(ii)/(2*(1+nu));                  % soil shear elastic modulus [lb/ft]
    Vs = sqrt(G/sm);                       % shear wave velocity [ft/sec]

    % LUMPED SOIL STIFFNESS MATRIX, MASS MATRIX, AND DAMPING MATRIX
    KSL(1,1) = pi*G*ak*Le/2;
    MS(1,1) = pi*ro^2*sm*am*Le/2;
    CS(1,1) = pi*ro*G/Vs*ac*Le/2;
    for jj = 2 : ne
        KSL(2*jj-1,2*jj-1) = pi*G*ak*Le;
        MS(2*jj-1,2*jj-1) = pi*ro^2*sm*am*Le;
        CS(2*jj-1,2*jj-1) = pi*ro*G/Vs*ac*Le;
    end

    MT = MP + MS;

    % FRF FUNCTION
    ao = 0.3;
    aoc = i*ao/sqrt(1+i*D);
    boc = aoc/eta;
    numer = 4*
    besselk(1,boc)*besselk(1,aoc)+aoc*besselk(1,boc)*besselk(0,aoc)+boc*besselk(0,boc)*
    besselk(1,aoc);
    denom=
    boc*besselk(0,boc)*besselk(1,aoc)+aoc*besselk(1,boc)*besselk(0,aoc)+boc*aoc*besselk
    (0,boc)*besselk(0,aoc);
    S03 = -pi*G*ao^2*numer/denom;

    for jj = 1 : NFreq+1

        freq(jj) = FreqMax*(jj-1)/NFreq;
        % SOIL DYNAMIC STIFFNESS
        w=freq(jj)^2*pi;
        ao = w*ro/Vs;
        aoc = i*ao/sqrt(1+i*D);
        boc = aoc/eta;
        numer = 4*
        besselk(1,boc)*besselk(1,aoc)+aoc*besselk(1,boc)*besselk(0,aoc)+boc*besselk(0,boc)*
        besselk(1,aoc);
        denom=
        boc*besselk(0,boc)*besselk(1,aoc)+aoc*besselk(1,boc)*besselk(0,aoc)+boc*aoc*besselk
        (0,boc)*besselk(0,aoc);
        S = -pi*G*ao^2*numer/denom;
        if ao < 0.3
            S = i*imag(S) + real(S03);
        end
        KS(1,1) = S*Le/2;
        for kk = 2 : ne
            KS(2*kk-1,2*kk-1) = S*Le;
        end

        % SYSTEM DYNAMIC STIFFNESS
        KD = KP + KS - w^2 * MP;
        KDP = KP - w^2 * MP;
        KDL = KP + KSL + i * w * CS - w^2 * MT;

        % FREQUENCY RESPONSE FUNCTION FRF
        U = KD\F;
        FRFM(jj) = sqrt(real(U(1))^2+imag(U(1))^2);
        FRF(jj) = U(1);

        UP = KDP\F;
        FRFP(jj) = sqrt(real(UP(1))^2+imag(UP(1))^2);

        UL = KDL\F;
        FRFL(jj) = sqrt(real(UL(1))^2+imag(UL(1))^2);
    end

    var1 = strcat(' E = ',num2str(Es(ii)), ' [psf]');
    var2 = strcat(' FRF Lumped Model vs Novak Model - ',var1);
    figure; plot(freq,FRFM,freq,FRFL); grid on; title(var2)
    xlabel('load frequency [Hz]'); ylabel('Module of the Dynamic Flexibility or FRF
    [ft/Kip]');
end

```

F.7 FRF Implemented in SAP

This section presents the models used to verify the application of SAP Link Element to model the Soil Spring-Dashpot lumped model. The relation between the Link element local axes and the global coordinate system is shown in Table F.1, and represented in Figure F.1.

Table F.1: Link Element DOF vs. Global DOF

Link Element DOF	Corresponding Global DOF
U1	U _z
U2	U _x
U3	U _y

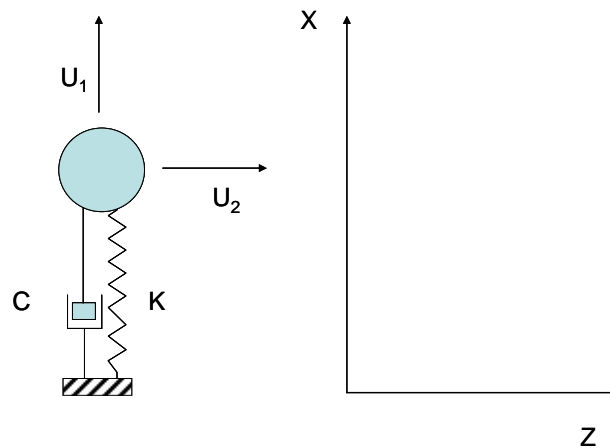


Figure F.1: Link Element DOF vs. Global Coordinates

F.7.1 SDOF System

A single degree of freedom (SDOF) system was first used to verify SAP Link Element local axis and behavior. The following problem will be analyzed:

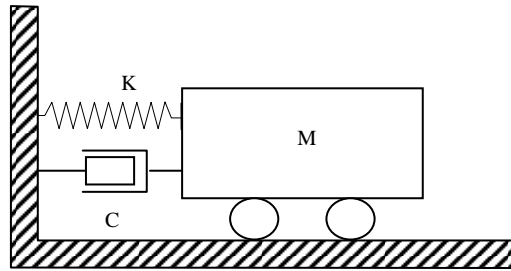


Figure F.2: SDOF Problem

The following is a listing of the MathCad worksheet developed to compute the SDOF response, and the problem data.

Problem Data

$$k := 40 \quad [\text{lb, in, sec}]$$

$$m := 0.1$$

$$c := 0.8$$

Solution

$$\omega_n := \sqrt{\frac{k}{m}} \quad \omega_n = 20$$

$$\xi := \frac{1}{2} \cdot c \cdot \frac{\omega_n}{k} \quad \xi = 0.2$$

$$\omega_d := \omega_n \cdot \sqrt{1 - \xi^2} \quad \omega_d = 19.596$$

$$\text{FRF}(\omega) := \frac{\left(\frac{1}{k}\right)}{\sqrt{\left[1 - \left(\frac{\omega}{\omega_n}\right)^2\right]^2 + \left(2 \cdot \xi \cdot \frac{\omega}{\omega_n}\right)^2}}$$

$$\text{FRF}(\omega_d) = 0.0635$$

$$\omega_1 := \omega_d$$

Given

$$\omega_1 \geq 0$$

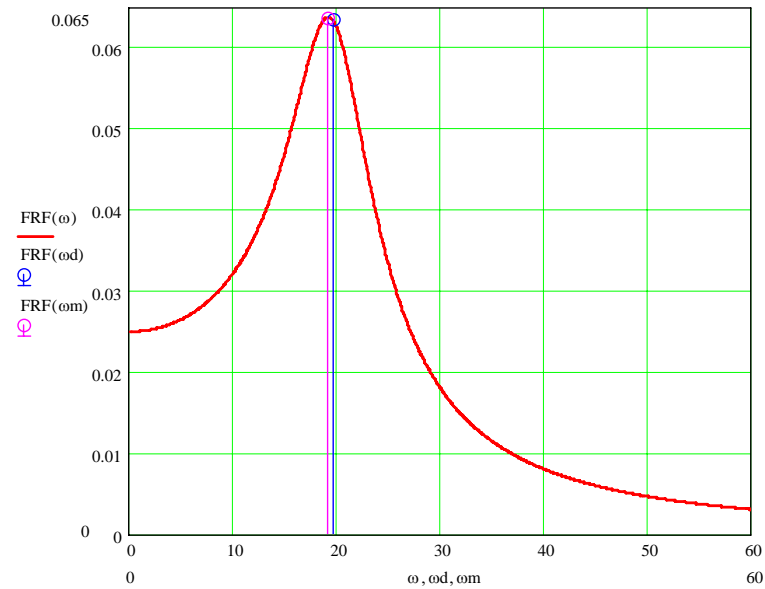
$$\omega_m := \text{Maximize}(\text{FRF}, \omega_1)$$

$$\omega_m = 19.183$$

$$\text{FRF}(\omega_m) = 0.0638$$

$$\text{FRF}(0) = 0.025$$

$$\text{FRF}(60) = 3.0904 \times 10^{-3}$$



The following figure presents the SAP model implementation, as a special point where the link element and the lumped mass were assigned.

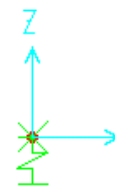
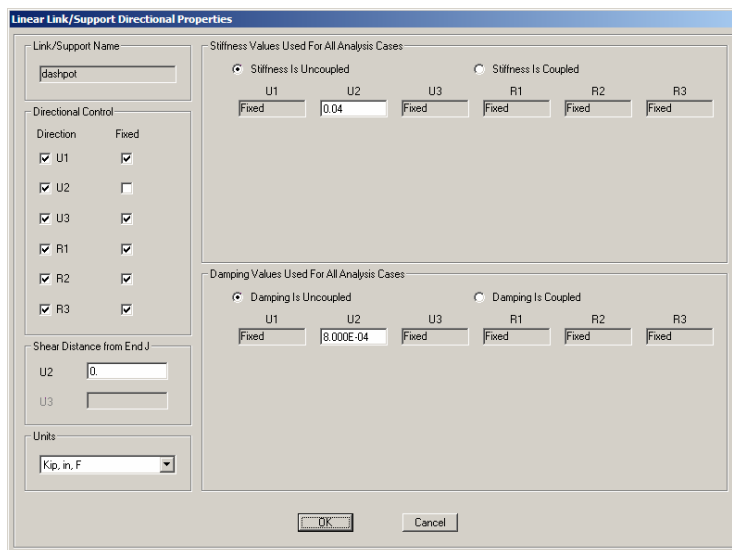


Figure F.3: SDOF System SAP Model

The following figure presents the results of SAP vs the ones obtained with a Matlab worksheet with the analytical response. There is a total agreement between both responses, indicating that the SAP model with Link elements is appropriate to model this type of systems.

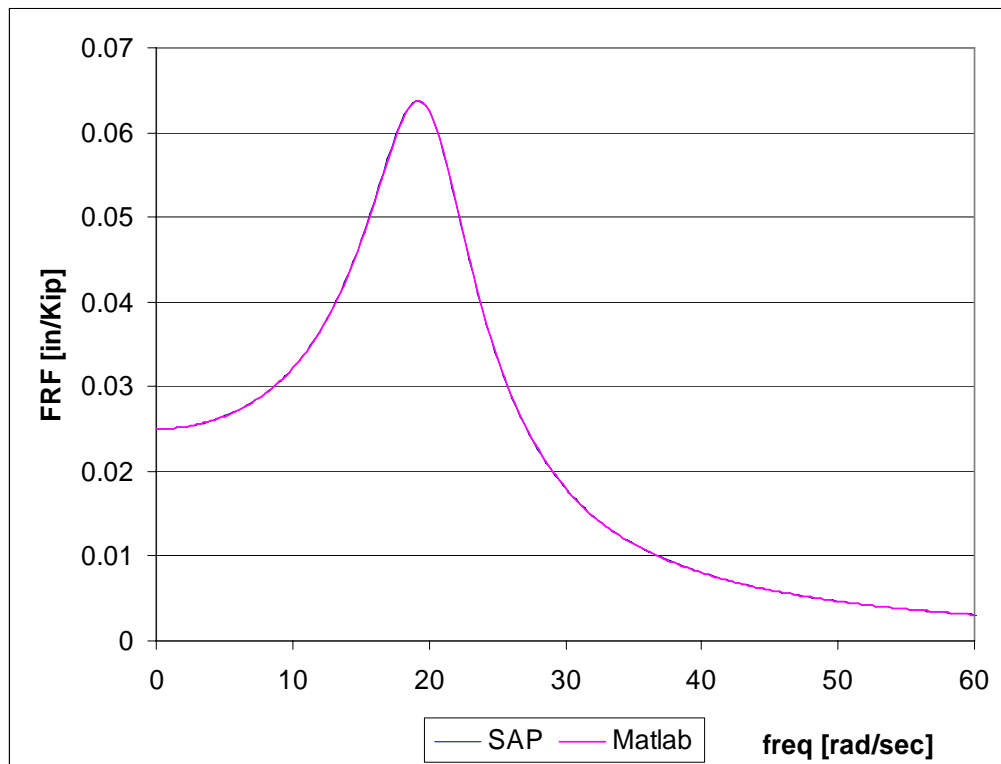


Figure F.4: SDOF Problem SAP Response vs. Analytical Response

F.7.2 Pile + Lumped Soil System

The following figure presents the link element parameters definition for the 1D model of the pile-soil system presented in Section 5.3, and the pile discretization adopted.

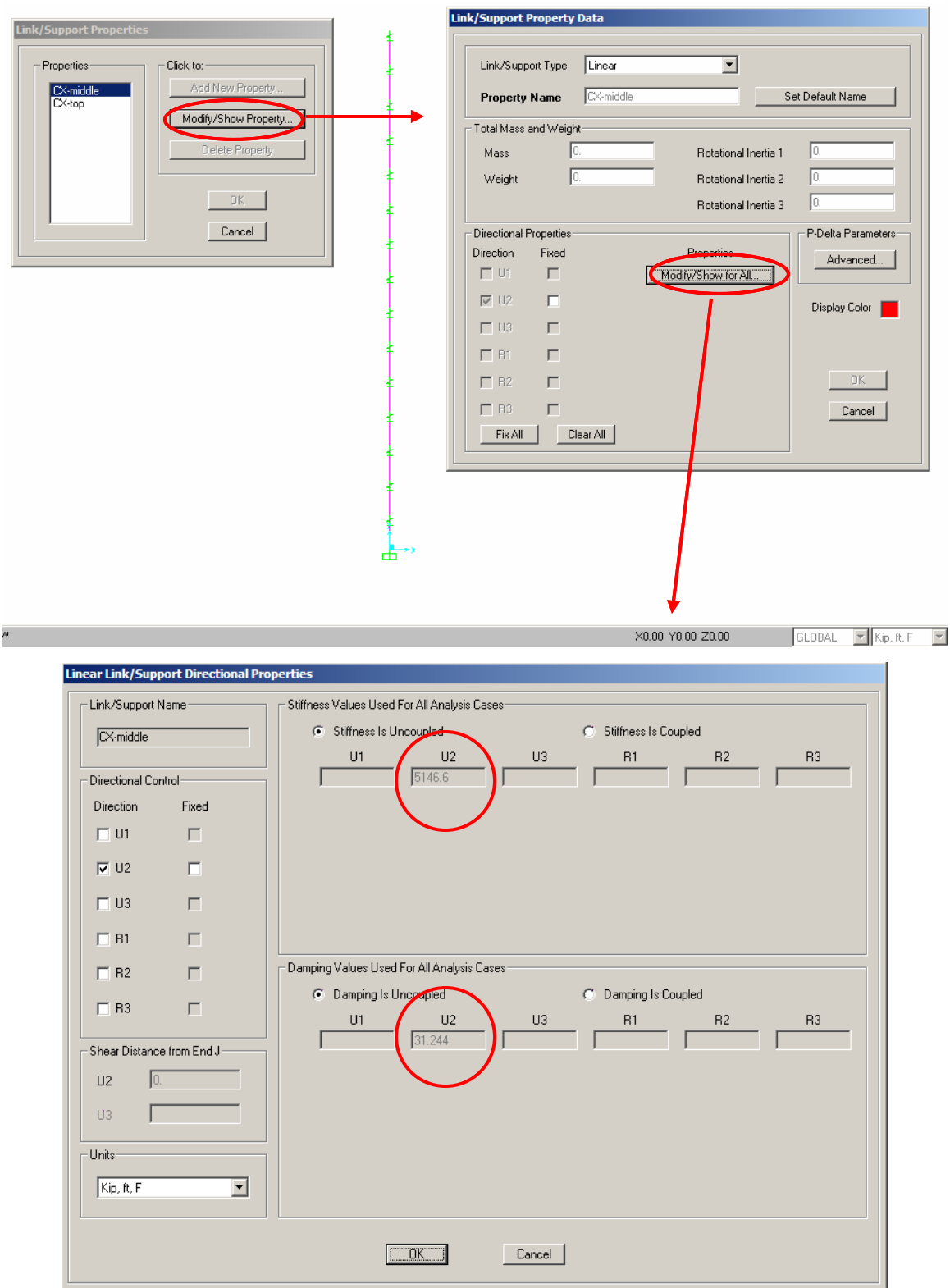


Figure F.5: SAP Link Element Definition for 1D Pile with Soil Model

F.8 Dynamic Stiffness of Pile Top for Di Napoli and Prato Test

```

%----- Programa FRFLumpedModel_DeNapoli.m-----%
% Program to compute the dynamic flexibility and dynamic stiffness of the pile %
% head tested by DeNapoli and Prato. The analysis uses the equivalent lumped %
% model obtained by regression of the dynamic stiffness proposed by Novak for %
% the soil, who considers the soil in plain-strain and the pile as a rigid %
% circle of radius ro embedded in an infinite medium. %
%-----%
clc; clear all; close all

% *****
% * PROBLEM DATA *
% *****

% SOIL DATA
Es = 288.0 * 10^6; % soil Young's elastic modulus [N/m^2]
nu = 0.31; % soil Poisson's ratio
sm = 1.55 * 10^3; % soil density [Kg/m3]

% PILE CAP DATA
Lpc = 0.3
Rpc = 0.25

% PILE DATA
ro = 0.15; % pile radius [m]
L = 2.7; % pile length [m]
Ep = 31000.0 * 10^6; % pile Young's modulus [Pa]
pm = 2.4 * 10^3; % pile density [Kg/m3]

% GENERAL DATA
nepc = 6;
ne = 54; % number of elements to discretize the
pile (5 cm length)
FreqMax = 150; % maximum frequency [Hz]
NFreq = 450; % Number of frequency steps

% Lumped model coefficients for nu=0.31
ak = 1.2947912;
am = 0.0005935;
ac = 2.9727406;

% *****
% * PROBLEM ANALYSIS *
% *****

% GENERAL COMPUTATION

G = Es/(2*(1+nu)); % soil shear elastic modulus [lb/ft]
Vs = sqrt(G/sm); % shear wave velocity [ft/sec]
eta = sqrt(2*(1-nu)/(1-2*nu)); % Novak Dynamic Stiffness parameter
nn = nepc + ne + 1; % number of nodes

% ARRAYS DEFINITION
%
% The KDP, UP and FRFP variables refer to the system response without
% considering soil contribution (just the pile contribution).
%
KD = zeros(2*nn, 2*nn); % System dynamic stiffness matrix

KP = zeros(2*nn, 2*nn); % Pile Stiffness matrix
KS = zeros(2*nn, 2*nn); % Soil Dynamic Stiffness Matrix
Ke = zeros(4, 4); % Pile element stiffness matrix

MP = zeros(2*nn, 2*nn); % Pile mass matrix
MS = zeros(2*nn, 2*nn); % Soil mass matrix
MT = zeros(2*nn, 2*nn); % System mass matrix

CS = zeros(2*nn, 2*nn); % Soil damping matrix

F = zeros(2*nn); % Load vector

U = zeros(2*nn); % System Displacement vector

```

```

UP = zeros(2*nn);
FRF = zeros(NFreq+1);
FRFM = zeros(NFreq+1);
FRFP = zeros(NFreq+1);
KDT = zeros(NFreq+1);
KDTR = zeros(NFreq+1);
KDTI = zeros(NFreq+1);
freq = zeros(NFreq+1);
% UNIT LOAD ON TOP
F(7) = 1000.0;

% PILE CAP ELEMENT STIFFNESS MATRIX
Le = Lpc/nepc;
Ip = pi*Rpc^4 / 4.;
Ap = pi*Rpc^2;
k1 = 4*Ep*Ip/Le;
k2 = 6*Ep*Ip/Le^2;
k3 = 12*Ep*Ip/Le^3;

Ke(1,1) = k3;
Ke(2,1) = k2;
Ke(3,1) = -k3;
Ke(4,1) = k2;

Ke(1,2) = k2;
Ke(2,2) = k1;
Ke(3,2) = -k2;
Ke(4,2) = k1/2;

Ke(1,3) = -k3;
Ke(2,3) = -k2;
Ke(3,3) = k3;
Ke(4,3) = -k2;

Ke(1,4) = k2;
Ke(2,4) = k1/2;
Ke(3,4) = -k2;
Ke(4,4) = k1;

% PILE CAP STIFFNESS MATRIX
for jj = 1 : nepc
    dof(1) = jj*2-1;
    dof(2) = jj*2;
    dof(3) = jj*2+1;
    dof(4) = jj*2+2;
    for kk = 1 : 4
        for ll = 1 : 4
            row = dof(kk);
            col = dof(ll);
            KP(row,col) = KP(row,col) + Ke(kk,ll);
        end
    end
end

% PILE CAP MASS MATRIX
MP(1,1) = pm*Ap*Le/2;
for jj = 2 : nepc
    MP(2*jj-1,2*jj-1) = pm*Ap*Le;
end
MP(2*ne+1,2*ne+1) = pm*Ap*Le/2;

% PILE ELEMENT STIFFNESS MATRIX
Le = L/ne;
Ip = pi*ro^4 / 4.;
Ap = pi*ro^2;
k1 = 4*Ep*Ip/Le;
k2 = 6*Ep*Ip/Le^2;
k3 = 12*Ep*Ip/Le^3;

```

% Pile Displacement vector
 % FRF = top node displacement
 % FRF Module top node displacement
 % FRF Pile top node displacement
 % Dynamic stiffness of pile top
 % Frequency data points
 % Unit harmonic load on top of pile
 % to obtain dynamic flexibility in
 % [m/KN] units
 % pile element length
 % Pile cross section inertia
 % Pile cross section area
 % pile element length
 % Pile cross section inertia
 % Pile cross section area

```

Ke(1,1) = k3;
Ke(2,1) = k2;
Ke(3,1) = -k3;
Ke(4,1) = k2;

Ke(1,2) = k2;
Ke(2,2) = k1;
Ke(3,2) = -k2;
Ke(4,2) = k1/2;

Ke(1,3) = -k3;
Ke(2,3) = -k2;
Ke(3,3) = k3;
Ke(4,3) = -k2;

Ke(1,4) = k2;
Ke(2,4) = k1/2;
Ke(3,4) = -k2;
Ke(4,4) = k1;

% PILE STIFFNESS MATRIX
for jj = 1 : ne
    dof(1) = nepc*2 + jj*2-1;
    dof(2) = nepc*2 + jj*2;
    dof(3) = nepc*2 + jj*2+1;
    dof(4) = nepc*2 + jj*2+2;
    for kk = 1 : 4
        for ll = 1 : 4
            row = dof(kk);
            col = dof(ll);
            KP(row,col) = KP(row,col) + Ke(kk,ll);
        end
    end
end

% PILE MASS MATRIX
MP(nepc*2+1, nepc*2+1) = MP(nepc*2+1, nepc*2+1) + pm*Ap*Le/2;
for jj = 2 : ne
    MP(nepc*2 + 2*jj-1, nepc*2 + 2*jj-1) = pm*Ap*Le;
end
MP(nepc*2 + 2*ne+1, nepc*2 + 2*ne+1) = pm*Ap*Le/2;

% SOIL STIFFNESS MATRIX, MASS MATRIX, AND DAMPING MATRIX
KS(nepc*2 + 1, nepc*2 + 1) = pi*G*ak*Le/2;
MS(nepc*2 + 1, nepc*2 + 1) = pi*ro^2*sm*am*Le/2;
CS(nepc*2 + 1, nepc*2 + 1) = pi*ro*G/Vs*ac*Le/2;

for jj = 2 : ne
    KS(nepc*2 + 2*jj-1, nepc*2 + 2*jj-1) = pi*G*ak*Le;
    MS(nepc*2 + 2*jj-1, nepc*2 + 2*jj-1) = pi*ro^2*sm*am*Le;
    CS(nepc*2 + 2*jj-1, nepc*2 + 2*jj-1) = pi*ro*G/Vs*ac*Le;
end

KS(nepc*2 + 2*ne+1, nepc*2 + 2*ne+1) = pi*G*ak*Le/2;
MS(nepc*2 + 2*ne+1, nepc*2 + 2*ne+1) = pi*ro^2*sm*am*Le/2;
CS(nepc*2 + 2*ne+1, nepc*2 + 2*ne+1) = pi*ro*G/Vs*ac*Le/2;

MT = MP + MS;

% FRF FUNCTION
for jj = 1 : NFreq+1
    freq(jj) = FreqMax*(jj-1)/NFreq;
    w=freq(jj)*2*pi;

    % SYSTEM DYNAMIC STIFFNESS
    KD = KP + KS + i * w * CS - w^2 * MT;

    % FREQUENCY RESPONSE FUNCTION FRF
    U = KD\F;
    FRFM(jj) = sqrt(real(U(7))^2+imag(U(7))^2);
    FRF(jj) = U(7);

```

```

KDT(JJ)= 1.0 / FRF(JJ);
KDTR(JJ) = real(KDT(JJ));
KDTI(JJ) = imag(KDT(JJ));

% to convert from KN to ton
KDT(JJ)= KDT(JJ)/10.;
KDTR(JJ) = KDTR(JJ)/10.;
KDTI(JJ) = KDTI(JJ)/10.;

var1 = num2str(JJ);
var2 = num2str(freq(JJ));
var3 = num2str(KDTR(JJ));
var4 = num2str(KDTI(JJ));
var5 = strcat( var1, ' ', var2, ' ', var3, ' ', var4);
% save ('FRF.txt', 'var1', 'var2', '-ASCII', '-append')
dl sp(var5)

end

figure; plot( freq, KDTR ); grid on; title('Real Part of KD Using Lumped Model');
xlabel('load frequency [Hz]'); ylabel('Module of the Dynamic Stiffness [ton/m]');

figure; plot( freq, KDTI ); grid on; title('Imaginary Part of KD Using Lumped Model');
xlabel('load frequency [Hz]'); ylabel('Module of the Dynamic Stiffness [ton/m]');

```

F.9 Damping Coefficient Comparison

Approximate Model vs Berger Coefficient of Damping

$$C_b = 2 \cdot d \cdot \rho \cdot (V_p + V_s) = 4 \cdot r \cdot \rho \cdot V_s \cdot \left(1 + \frac{V_p}{V_s} \right)$$

$$C_a = \alpha c \cdot \pi \cdot r \cdot \rho \cdot V_s$$

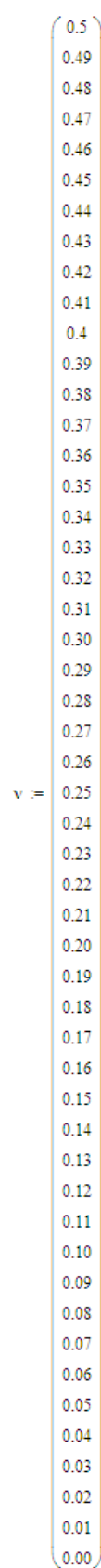
$$\frac{C_a}{C_b} = \frac{\alpha c \cdot \pi}{4 \cdot \left(1 + \frac{V_p}{V_s} \right)} = \frac{\alpha c \cdot \pi}{4 \cdot [1 + \sqrt{2(1 + \nu)}]}$$

$$V_p = \sqrt{\frac{E}{\rho}}$$

$$V_s = \sqrt{\frac{G}{\rho}}$$

$$G = \frac{E}{2 \cdot (1 + \nu)}$$

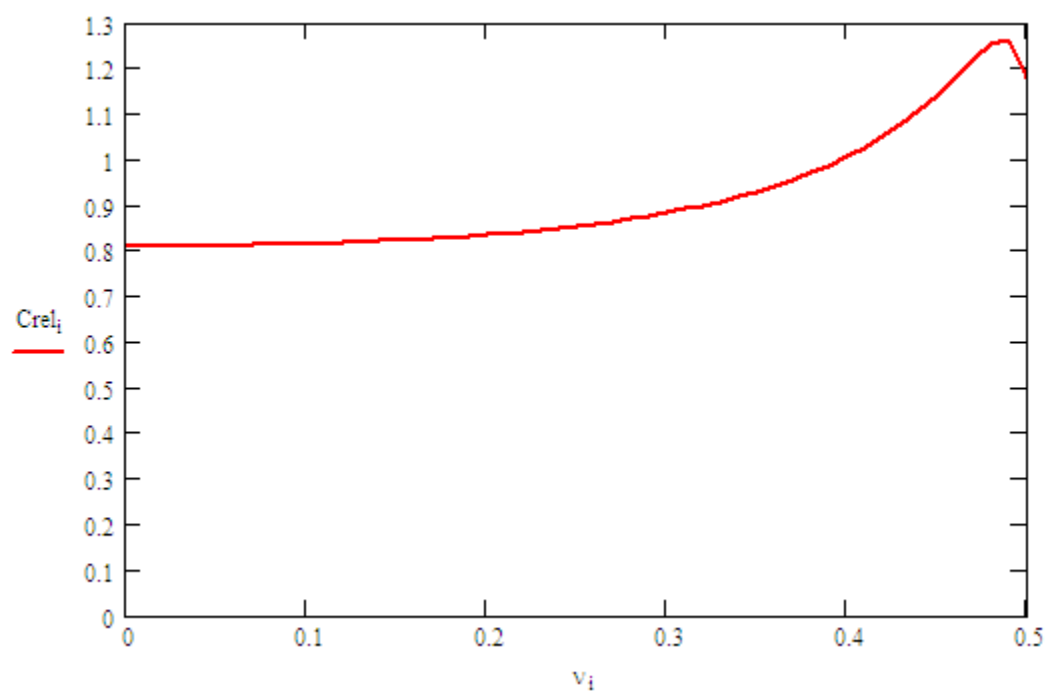
$$\alpha_{ci} := \begin{pmatrix} 4.10747 \\ 4.38920 \\ 4.33825 \\ 4.20948 \\ 4.06638 \\ 3.92941 \\ 3.80454 \\ 3.69268 \\ 3.59299 \\ 3.50411 \\ 3.42465 \\ 3.35334 \\ 3.28908 \\ 3.23091 \\ 3.17803 \\ 3.12978 \\ 3.08557 \\ 3.04493 \\ 3.00744 \\ 2.97274 \\ 2.94054 \\ 2.91058 \\ 2.88262 \\ 2.85647 \\ 2.83197 \\ 2.80895 \\ 2.78729 \\ 2.76687 \\ 2.74757 \\ 2.72932 \\ 2.71203 \\ 2.69562 \\ 2.68003 \\ 2.66519 \\ 2.65106 \\ 2.63758 \\ 2.62470 \\ 2.61240 \\ 2.60062 \\ 2.58934 \\ 2.57852 \\ 2.56814 \\ 2.55817 \\ 2.54859 \\ 2.53937 \\ 2.53049 \\ 2.52194 \\ 2.51370 \\ 2.50574 \\ 2.49806 \\ 2.49064 \end{pmatrix}$$



$i := 0..50$

$$Crel_i := \frac{\alpha c i_i \cdot \pi}{4 \cdot [1 + \sqrt{2(1 + v_i)}]}$$

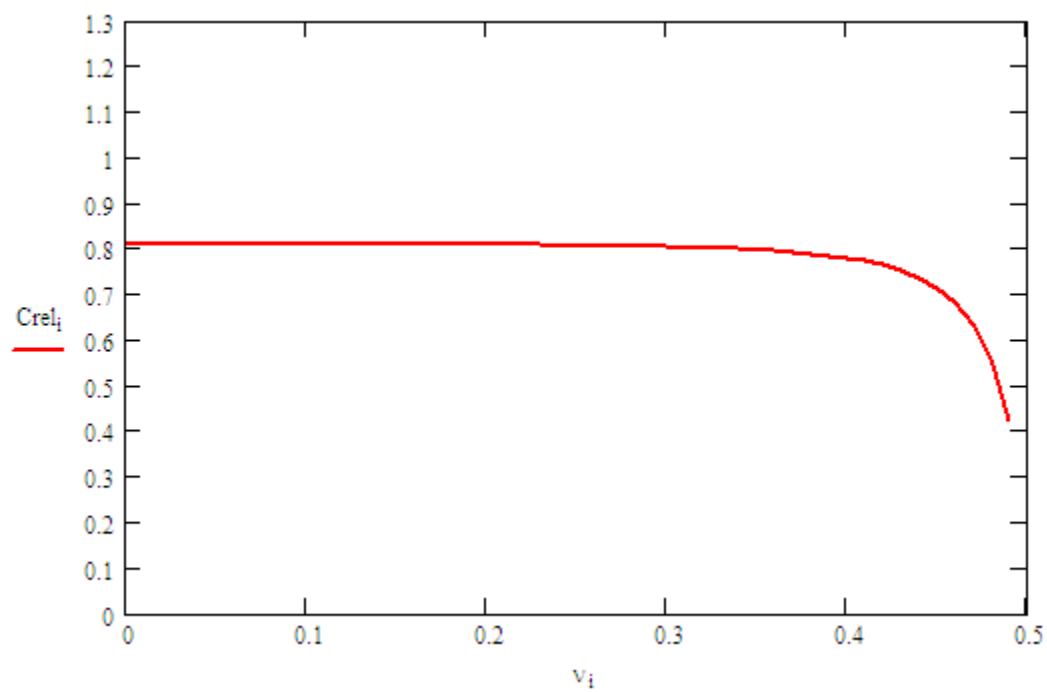
Crel = Ca/CBerger
Considering Vp of 1D case



$$i_x := 1..50$$

$$Crel_i := \frac{\alpha c i_i \cdot \pi}{4 \cdot \left[1 + \sqrt{\frac{2(1 - v_i)}{1 - 2 \cdot v_i}} \right]}$$

Crel = Ca/CBerger
Considering Vp of 3D case



F.10 Stiffness Coefficient Comparison

Approximate Model vs Vesic Subgrade Reaction Modulus

$$K_v = 0.65 \cdot \sqrt[12]{\frac{E_s \cdot d^4}{E_p \cdot I_p}} \cdot \frac{E_s}{1 - \nu^2}$$

$$E_p := 518400$$

$$3600 \cdot 144 = 5.184 \times 10^5$$

$$E_s := 1728$$

$$\nu_s := 0.4$$

$$\alpha k := 1.30686$$

$$K_{\text{vesic}}(E_s) := 2 \cdot 0.65 \cdot \sqrt[12]{\frac{E_s \cdot 64}{E_p \cdot \pi}} \cdot \left(\frac{E_s}{1 - \nu_s^2} \right)$$

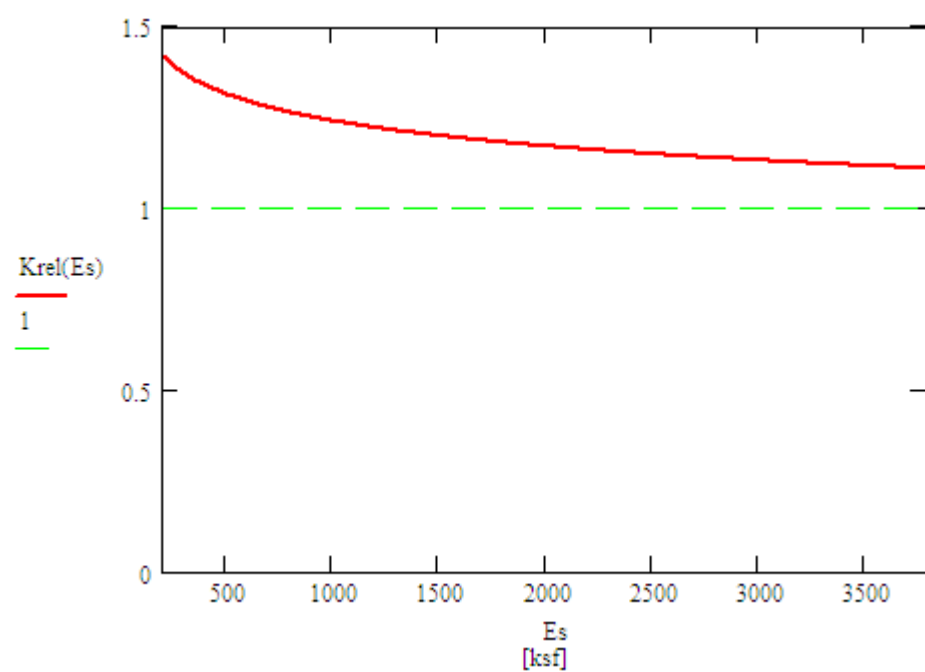
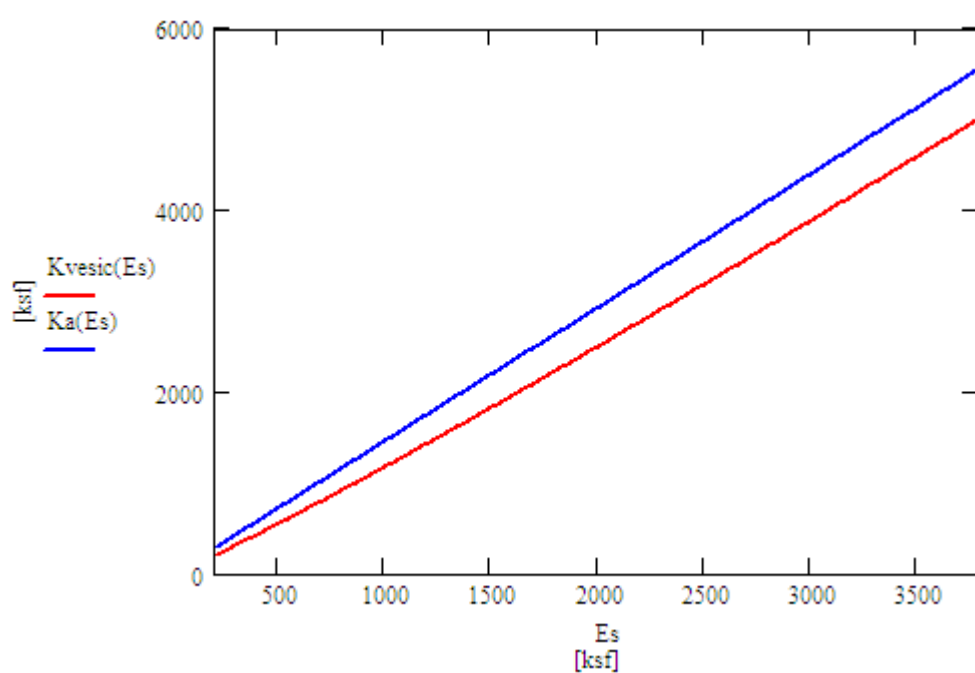
$$K_a(E_s) := \alpha k \cdot \left[\frac{E_s}{2 \cdot (1 + \nu_s)} \right] \cdot \pi$$

$$\frac{\alpha k \cdot \pi}{2 \cdot (1 + \nu_s)} = 1.466$$

$$2 \cdot 0.65 \cdot \sqrt[12]{\frac{E_s \cdot 64}{E_p \cdot \pi}} \cdot \left(\frac{1}{1 - \nu_s^2} \right) = 1.237$$

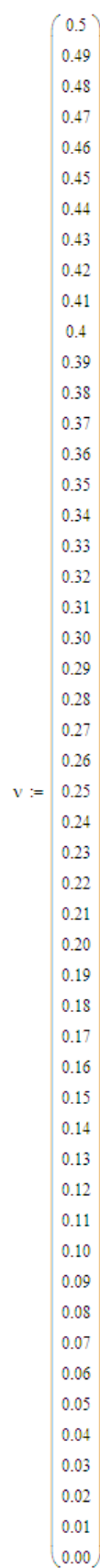
$$K_{\text{rel}}(E_s) := \frac{\alpha k \cdot \left[\frac{E_s}{2 \cdot (1 + \nu_s)} \right] \cdot \pi}{2 \cdot 0.65 \cdot \sqrt[12]{\frac{E_s \cdot 64}{E_p \cdot \pi}} \cdot \left(\frac{E_s}{1 - \nu_s^2} \right)}$$

$E_s := 200,210 \dots 3800$



$\alpha_{ki} :=$

1.72137
1.61062
1.46327
1.39946
1.36918
1.35437
1.34592
1.34015
1.33550
1.33130
1.32727
1.32329
1.31933
1.31540
1.31153
1.30775
1.30411
1.30067
1.29749
1.29479
1.30686
1.30834
1.30886
1.30858
1.30766
1.30622
1.30435
1.30213
1.29964
1.29692
1.29402
1.29099
1.28784
1.28461
1.28133
1.27800
1.27464
1.27127
1.26791
1.26454
1.26120
1.25787
1.25457
1.25131
1.24807
1.24488
1.24172
1.23861
1.23553
1.23251
1.22953



$$E_p := 518400$$

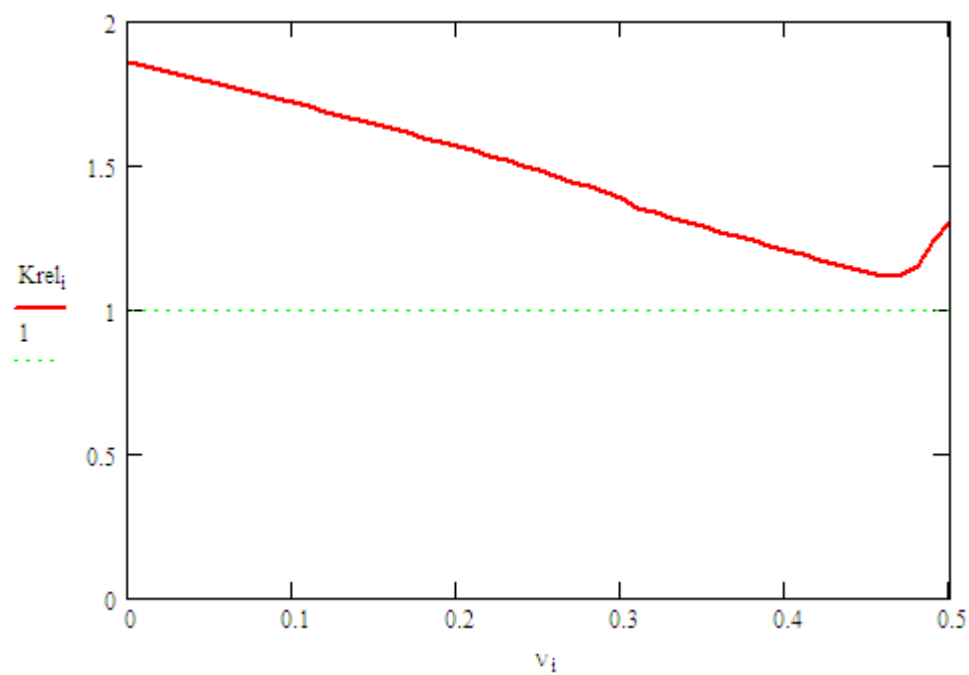
$$E_s := 1728$$

$$v_s := 0.3$$

$$i := 0..50$$

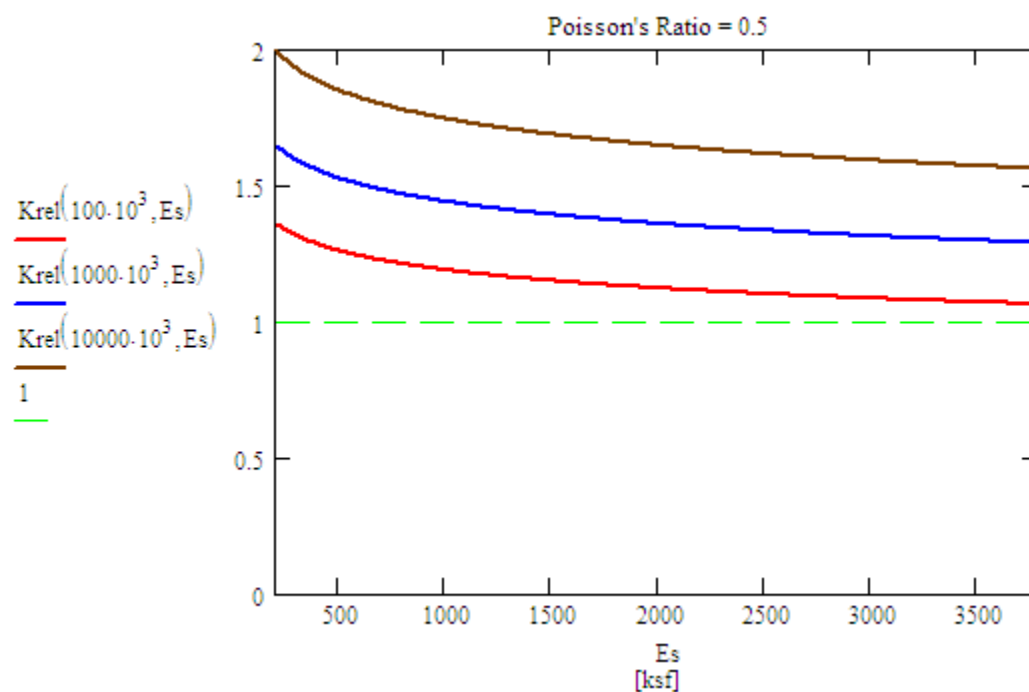
$$K_{rel,i} := \frac{\left[\frac{\alpha k_i \cdot \pi}{2 \cdot (1 + v_i)} \right]}{2 \cdot 0.65 \cdot \sqrt{\frac{E_s \cdot 64}{E_p \cdot \pi}} \cdot \left[\frac{1}{1 - (v_i)^2} \right]}$$

$$K_{rel} = K_a / K_{vesic}$$



$i := 0$

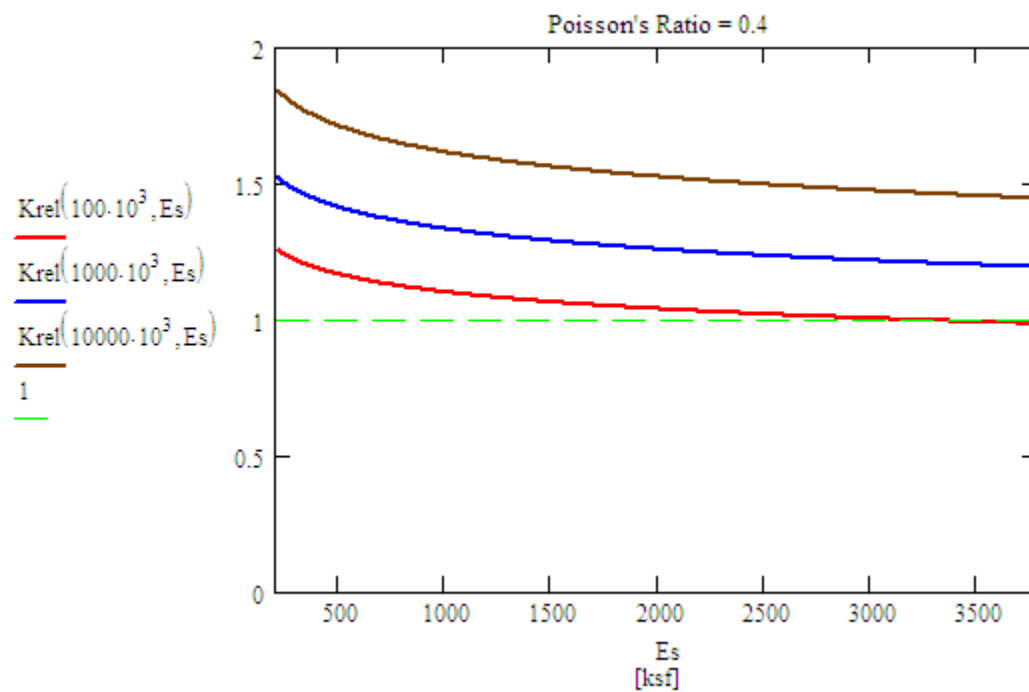
$$K_{rel}(E_p, E_s) := \frac{\left[\frac{\alpha k_i \pi}{2 \cdot (1 + \nu_i)} \right]}{\left[2 \cdot 0.65 \cdot \sqrt{\frac{E_s \cdot 64}{E_p \cdot \pi}} \cdot \left[\frac{1}{1 - (\nu_i)^2} \right] \right]}$$

 $E_s := 200, 210 \dots 3800$


$i := 10$

$$K_{rel}(E_p, E_s) := \frac{\left[\frac{\alpha k_i \pi}{2 \cdot (1 + \nu_i)} \right]}{\left[2 \cdot 0.65 \cdot \sqrt{\frac{E_s \cdot 64}{E_p \cdot \pi}} \cdot \left[\frac{1}{1 - (\nu_i)^2} \right] \right]}$$

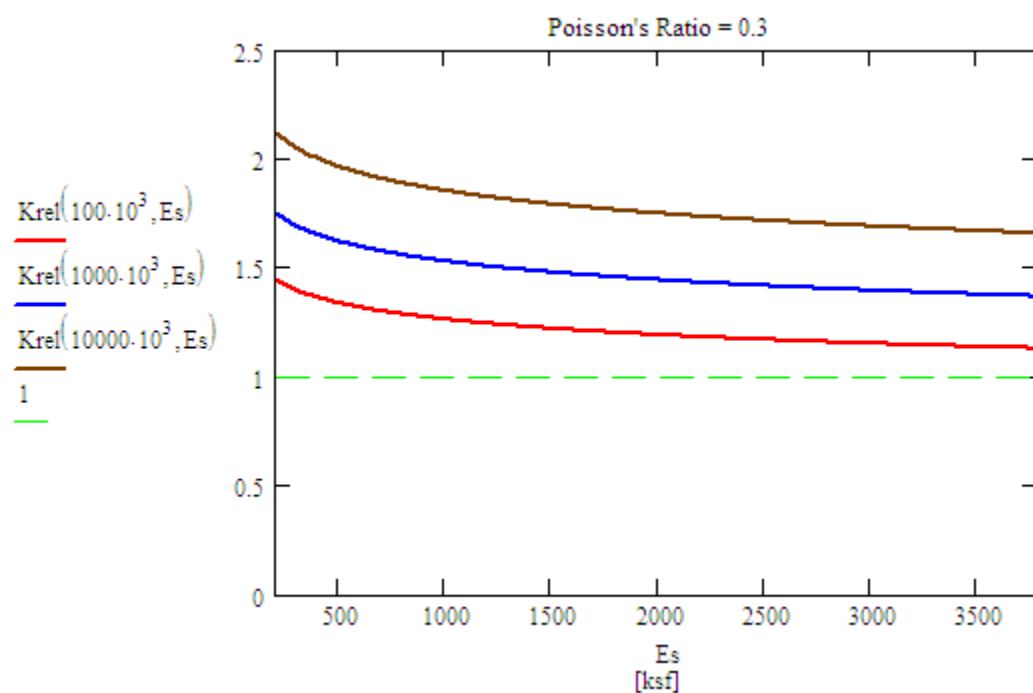
$E_s := 200, 210 \dots 3800$



$$i_s := 20$$

$$K_{rel}(E_p, E_s) := \frac{\left[\frac{\alpha k_{i1} \cdot \pi}{2 \cdot (1 + \nu_i)} \right]}{2 \cdot 0.65 \cdot \sqrt{\frac{E_s \cdot 64}{E_p \cdot \pi} \cdot \left[\frac{1}{1 - (\nu_i)^2} \right]}}$$

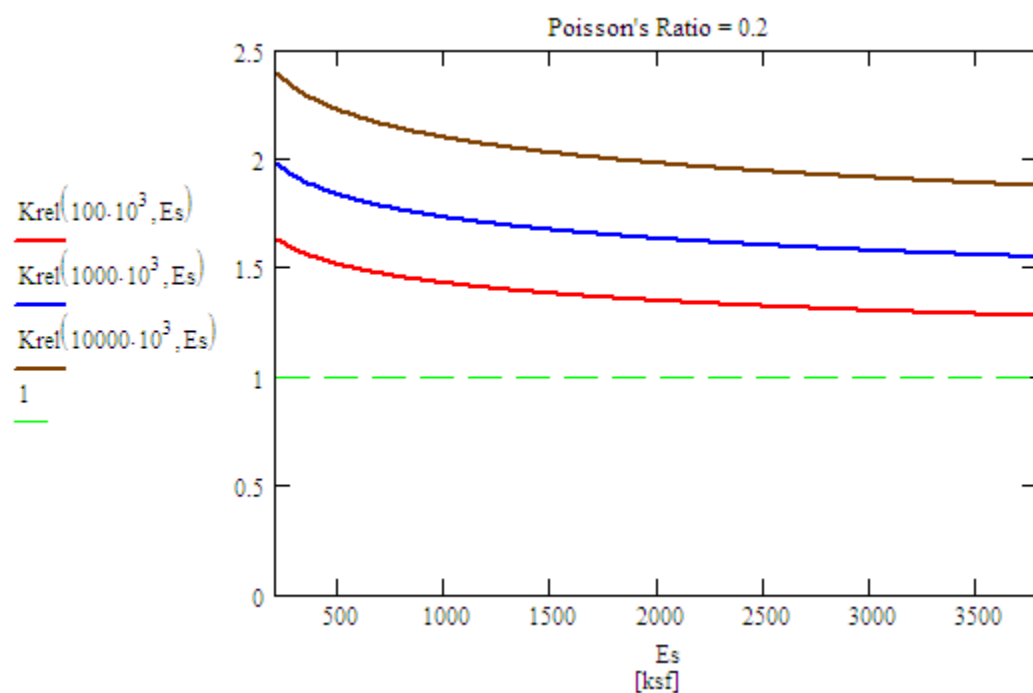
$$E_s := 200, 210 \dots 3800$$



$$i_s := 30$$

$$K_{rel}(E_p, E_s) := \frac{\left[\frac{\alpha k_{i1} \cdot \pi}{2 \cdot (1 + \nu_i)} \right]}{2 \cdot 0.65 \cdot \sqrt{\frac{E_s \cdot 64}{E_p \cdot \pi} \cdot \left[\frac{1}{1 - (\nu_i)^2} \right]}}$$

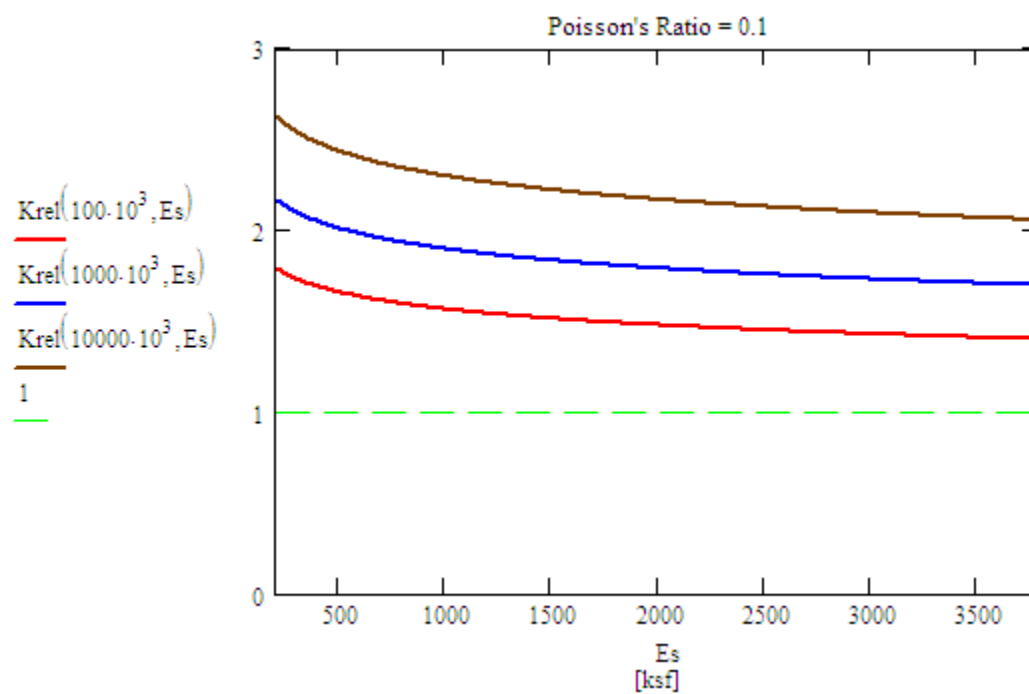
$$E_s := 200, 210 \dots 3800$$



$i := 40$

$$K_{rel}(E_p, E_s) := \frac{\left[\frac{\alpha k_i \cdot \pi}{2 \cdot (1 + \nu_i)} \right]}{\left[2 \cdot 0.65 \cdot \sqrt{\frac{E_s \cdot 64}{E_p \cdot \pi}} \cdot \left[\frac{1}{1 - (\nu_i)^2} \right] \right]}$$

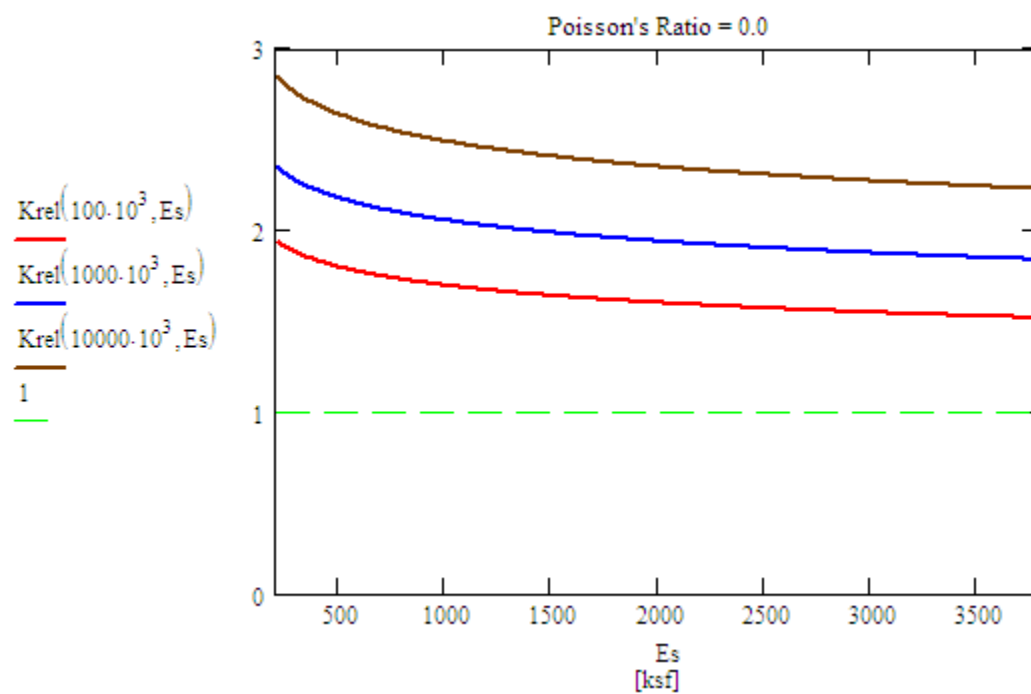
$E_s := 200,210..3800$



$i := 50$

$$K_{rel}(E_p, E_s) := \frac{\left[\frac{\alpha k_i \pi}{2 \cdot (1 + \nu_i)} \right]}{\left[2 \cdot 0.65 \cdot \sqrt{\frac{E_s \cdot 64}{E_p \cdot \pi}} \cdot \left[\frac{1}{1 - (\nu_i)^2} \right] \right]}$$

$E_s := 200,210..3800$



G Influence of Pile Stiffness on the FRF of Pile Head

The Matlab program (worksheet) developed to compute the frequency response function (dynamic flexibility) of the pile head, used to obtain the results of in Chapter 6, is listed in this appendix. The program varies the pile radius and obtains the FRF of the pile head considering the soil with the lumped model, and considering the pile alone (without soil contribution)

G.1 FRF Comparing Pile Alone and Pile + Soil for Different Radius

```
%----- Programa FRFLumpedVariousDo.m-----%
% Program to compute the dynamic flexibility of a pile head %
% using the equivalent lumped model obtained by regression of the %
% dynamic stiffness proposed by Novak for the soil, who considers %
% the soil in plain-strain and the pile as a rigid circle of radius %
% ro embedded in an infinite medium (Novak, Nogami and Aboul-Ella ). %
% The effect of different radius is computed %
%-----%
clc; clear all; close all

% *****
% * PROBLEM DATA
% *****

% SOIL DATA
Es = 1728000; % soil Young's elastic modulus[lb/ft^2]
nu = 0.40; % soil Poisson's ratio
D=0.0; % hysteretic damping ratio
sw = 110.0; % soil specific weight [pcf]

% PILE DATA
for jj = 1 : 10
    roo(jj) = jj; % pile radius
end

L = 30.0; % pile length
Ep = 518400000.0; % pile Young's modulus
pw = 150.0; % pile specific weight

% GENERAL DATA
ne = 15; % number of elements to discretize the
pile %
g = 32.2; % gravity acceleration [ft/sec^2]
FreqMax = 400; % maximum frequency [Hz]
NFreq = 800; % Number of frequency steps

% Lumped model coefficients
ak = 1.3272671;
am = 0.0510557;
ac = 3.4246489;

% *****
% * PROBLEM ANALYSIS
% *****

% GENERAL COMPUTATION
sm = sw/g; % density of soil [lb.s^2/ft^4]
G = Es/(2*(1+nu)); % soil shear elastic modulus[lb/ft]
Vs = sqrt(G/sm); % shear wave velocity [ft/sec]
eta = sqrt(2*(1-nu)/(1-2*nu)); % Novak Dynamic Stiffness parameter
```

```

Le = L/ne; % pile element length
pm = pw/g; % density of pile [lb.s^2/ft^4]

% ARRAYS DEFINITION
%
% The KDP, UP and FRFP variables refer to the system reponse without
% considering soil contribution (just the pile contribution).
%
KDN = zeros(2*ne, 2*ne); % Novak System dynamic stiffness matrix
KDL = zeros(2*ne, 2*ne); % Lumped System dynamic stiffness matrix
KDP = zeros(2*ne, 2*ne); % Pile dynamic stiffness matrix

KP = zeros(2*ne, 2*ne); % Pile Stiffness matrix
KS = zeros(2*ne, 2*ne); % Soil Dynamic Stiffness Matrix
KSL = zeros(2*ne, 2*ne); % Lumped Soil Dynamic Stiffness Matrix
Ke = zeros(4, 4); % Pile element stiffness matrix

MP = zeros(2*ne, 2*ne); % Pile mass matrix
MS = zeros(2*ne, 2*ne); % Lumped Soil mass matrix
MT = zeros(2*ne, 2*ne); % System mass matrix

CS = zeros(2*ne, 2*ne); % Lumped Soil damping matrix

F = zeros(2*ne); % Load vector

U = zeros(2*ne); % System Displacement vector
UL = zeros(2*ne); % Lumped Model Displacement vector
UP = zeros(2*ne); % Pile Displacement vector

FRF = zeros(NFreq+1); % FRF = top node displacement
FRFM = zeros(NFreq+1); % FRF Module top node displacement
FRFP = zeros(NFreq+1); % FRF Pile top node displacement
FRFL = zeros(NFreq+1); % Lumped FRF module top node displacement
freq = zeros(NFreq+1); % Frequency data points

% UNIT LOAD ON TOP
F(1) = 1000.0; % Unit harmonic load on top of pile
% to obtain dynamic flexibility in
% [ft/Kip] units

for ii = 1 : 10

    ro = roo(ii);

    % PILE ELEMENT STIFFNESS MATRIX
    Ip = pi *ro^4/4. ; % Pile crossm section inertia
    Ap = pi *ro^2; % Pile cross section area

    k1 = 4*Ep*Ip/Le;
    k2 = 6*Ep*Ip/Le^2;
    k3 = 12*Ep*Ip/Le^3;

    Ke(1, 1) = k3;
    Ke(2, 1) = k2;
    Ke(3, 1) = -k3;
    Ke(4, 1) = k2;

    Ke(1, 2) = k2;
    Ke(2, 2) = k1;
    Ke(3, 2) = -k2;
    Ke(4, 2) = k1/2;

    Ke(1, 3) = -k3;
    Ke(2, 3) = -k2;
    Ke(3, 3) = k3;
    Ke(4, 3) = -k2;

    Ke(1, 4) = k2;
    Ke(2, 4) = k1/2;
    Ke(3, 4) = -k2;
    Ke(4, 4) = k1;

    % PILE STIFFNESS MATRIX
    for jj = 1 : ne-1
        dof(1) = jj *2-1;
        dof(2) = jj *2;
        dof(3) = jj *2+1;
        dof(4) = jj *2+2;
        for kk = 1 : 4

```

```

        for ll = 1 : 4
            row = dof(kk);
            col = dof(ll);
            KP(row, col) = KP(row, col) + Ke(kk, ll);
        end
    end
end

dof(1) = ne*2-1;
dof(2) = ne*2;
for kk = 1 : 2
    for ll = 1 : 2
        row = dof(kk);
        col = dof(ll);
        KP(row, col) = KP(row, col) + Ke(kk, ll);
    end
end

% PILE MASS MATRIX
MP(1, 1) = pm*Ap*Le/2;
for jj = 2 : ne
    MP(2*jj-1, 2*jj-1) = pm*Ap*Le;
end

% LUMPED SOIL STIFFNESS MATRIX, MASS MATRIX, AND DAMPING MATRIX
KSL(1, 1) = pi*G*ak*Le/2;
MS(1, 1) = pi*ro^2*sm*am*Le/2;
CS(1, 1) = pi*ro*G/Vs*ac*Le/2;
for jj = 2 : ne
    KSL(2*jj-1, 2*jj-1) = pi*G*ak*Le;
    MS(2*jj-1, 2*jj-1) = pi*ro^2*sm*am*Le;
    CS(2*jj-1, 2*jj-1) = pi*ro*G/Vs*ac*Le;
end

MT = MP + MS;

% FRF FUNCTION

for jj = 1 : NFreq+1

    freq(jj) = FreqMax*(jj-1)/NFreq;
    w=freq(jj)*2*pi;

    % SYSTEM DYNAMIC STIFFNESS
    KDP = KP - w^2 * MP;
    KDL = KP + KSL + i * w * CS - w^2 * MT;

    % FREQUENCY RESPONSE FUNCTION FRF
    UP = KDP\F;
    FRFP(jj) = sqrt(real(UP(1))^2+i mag(UP(1))^2);

    UL = KDL\F;
    FRFL(jj) = sqrt(real(UL(1))^2+i mag(UL(1))^2);

end

var1 = strcat('FRF Pile Alone vs Pile + Soil - ro = ', num2str(ro), ' [ft]');
figure; plot(freq, FRFL, '-b', freq, FRFP, '-r'); grid on; title(var1);
xlabel('load frequency [Hz]'); ylabel('Module of the Dynamic Flexibility or FRF [ft/Kip]');
end

```

H Influence of Radiation Damping on the FRF of Pile Head

The Matlab program (worksheet) developed to compute the frequency response function (dynamic flexibility) of the pile head, used to obtain the results of in Chapter 6, is listed in this appendix. The program varies the soil equivalent lumped damping coefficient and obtains the FRF of the pile head considering the soil with the lumped model.

H.1 FRF Comparing Pile Alone and Pile + Soil for Different Ca

```
%----- Programa FRFLumpedVariousC.m-----%
% Program to compute the dynamic flexibility of a pile head
% using the dynamic stiffness proposed by Novak for the soil, and
% using the equivalent lumped model obtained by regression of the
% dynamic stiffness proposed by Novak for the soil, who considers
% the soil in plain-strain and the pile as a rigid circle of radius
% ro embedded in an infinite medium.
% Novak, Nogami and Aboul-Elia
%-----%
clc; clear all; close all

% *****
% * PROBLEM DATA
% *****

% SOIL DATA
Es = 1728000;
nu = 0.40;
D=0.0;
sw = 110.0;

% PILE DATA
ro = 1;
L = 30.0;
Ep = 518400000.0;
pw = 150.0;

% GENERAL DATA
ne = 15;
pile
g = 32.2;
FreqMax = 400;
NFreq = 800;

% Lumped model coefficients
ak = 1.3272671;
am = 0.0510557;
ac = 3.4246489;

% *****
% * PROBLEM ANALYSIS
% *****

% GENERAL COMPUTATION
sm = sw/g;
G = Es/(2*(1+nu));
Vs = sqrt(G/sm);
eta = sqrt(2*(1-nu)/(1-2*nu));
Le = L/ne;
pm = pw/g;

% ARRAYS DEFINITION

% soil Young's elastic modulus[lb/ft^2]
% soil Poisson's ratio
% hysteretic damping ratio
% soil specific weight [pcf]

% pile radius
% pile length
% pile Youngs' modulus
% pile specific weight

% number of elements to discretize the
% gravity acceleration [ft/sec^2]
% maximum frequency [Hz]
% Number of frequency steps

% density of soil [lb.s^2/ft^4]
% soil shear elastic modulus[lb/ft]
% shear wave velocity [ft/sec]
% Novak Dynamic Stiffness parameter
% pile element length
% density of pile [lb.s^2/ft^4]
```

```

%
% The KDP, UP and FRFP variables refer to the system reponse without
% considering soil contribution (just the pile contribution).
%
KDN = zeros(2*ne, 2*ne); % Novak System dynamic stiffness matrix
KDL = zeros(2*ne, 2*ne); % Lumped System dynamic stiffness matrix
KDP = zeros(2*ne, 2*ne); % Pile dynamic stiffness matrix

KP = zeros(2*ne, 2*ne); % Pile Stiffness matrix
KS = zeros(2*ne, 2*ne); % Soil Dynamic Stiffness Matrix
KSL = zeros(2*ne, 2*ne); % Lumped Soil Dynamic Stiffness Matrix
Ke = zeros(4, 4); % Pile element stiffness matrix

MP = zeros(2*ne, 2*ne); % Pile mass matrix
MS = zeros(2*ne, 2*ne); % Lumped Soil mass matrix
MT = zeros(2*ne, 2*ne); % System mass matrix

CS = zeros(2*ne, 2*ne); % Lumped Soil damping matrix

F = zeros(2*ne); % Load vector

U = zeros(2*ne); % System Displacement vector
UL = zeros(2*ne); % Lumped Model Displacement vector
UP = zeros(2*ne); % Pile Displacement vector

FRF = zeros(NFreq+1); % FRF = top node displacement
FRFM = zeros(NFreq+1); % FRF Module top node displacement
FRFP = zeros(NFreq+1); % FRF Pile top node displacement
FRFL = zeros(NFreq+1); % Lumped FRF module top node displacement
freq = zeros(NFreq+1); % Frequency data points

% UNIT LOAD ON TOP
F(1) = 1000.0; % Unit harmonic load on top of pile
% to obtain dynamic flexibility in
% [ft/Kip] units

% PILE ELEMENT STIFFNESS MATRIX
Ip = pi*ro^4/4.; % Pile cross section inertia
Ap = pi*ro^2; % Pile cross section area

k1 = 4*Ep*Ip/Le;
k2 = 6*Ep*Ip/Le^2;
k3 = 12*Ep*Ip/Le^3;

Ke(1,1) = k3;
Ke(2,1) = k2;
Ke(3,1) = -k3;
Ke(4,1) = k2;

Ke(1,2) = k2;
Ke(2,2) = k1;
Ke(3,2) = -k2;
Ke(4,2) = k1/2;

Ke(1,3) = -k3;
Ke(2,3) = -k2;
Ke(3,3) = k3;
Ke(4,3) = -k2;

Ke(1,4) = k2;
Ke(2,4) = k1/2;
Ke(3,4) = -k2;
Ke(4,4) = k1;

% PILE STIFFNESS MATRIX
for jj = 1 : ne-1
    dof(1) = jj*2-1;
    dof(2) = jj*2;
    dof(3) = jj*2+1;
    dof(4) = jj*2+2;
    for kk = 1 : 4
        for ll = 1 : 4
            row = dof(kk);
            col = dof(ll);
            KP(row, col) = KP(row, col) + Ke(kk, ll);
        end
    end
end

```



```

end

dof(1) = ne*2-1;
dof(2) = ne*2;
for kk = 1 : 2
    for ll = 1 : 2
        row = dof(kk);
        col = dof(ll);
        KP(row, col) = KP(row, col) + Ke(kk, ll);
    end
end

% PILE MASS MATRIX
MP(1,1) = pm*Ap*Le/2;
for jj = 2 : ne
    MP(2*jj-1, 2*jj-1) = pm*Ap*Le;
end

% LUMPED SOIL STIFFNESS MATRIX, MASS MATRIX, AND DAMPING MATRIX
KSL(1,1) = pi*G*ak*Le/2;
MS(1,1) = pi*ro^2*sm*am*Le/2;
CS(1,1) = pi*ro*G/Vs*ac*Le/2;
for jj = 2 : ne
    KSL(2*jj-1, 2*jj-1) = pi*G*ak*Le;
    MS(2*jj-1, 2*jj-1) = pi*ro^2*sm*am*Le;
    CS(2*jj-1, 2*jj-1) = pi*ro*G/Vs*ac*Le;
end

MT = MP + MS;

% FRF FUNCTION
for ii = 1 : 6
    for jj = 1 : NFreq+1
        freq = FreqMax*(jj-1)/NFreq;
        w=freq*2*pi;

        % SYSTEM DYNAMIC STIFFNESS
        KDL = KP + KSL + i * w * CS * (2*ii-2)/10 - w^2 * MT;

        % FREQUENCY RESPONSE FUNCTION FRF
        UL = KDL\F;
        FRFL(ii, jj) = sqrt(real(UL(1))^2+imag(UL(1))^2);
    end
end

end

for jj = 1 : NFreq+1
    freq = FreqMax*(jj-1)/NFreq;
    x(jj) = freq;
    y1(jj) = FRFL(1, jj);
    y2(jj) = FRFL(2, jj);
    y3(jj) = FRFL(3, jj);
    y4(jj) = FRFL(4, jj);
    y5(jj) = FRFL(5, jj);
    y6(jj) = FRFL(6, jj);
end

var1 = 'FRF Pile + Soil - Different Damping';
figure; plot(x, y1, x, y2, x, y3, x, y4, x, y5, x, y6); grid on; title(var1);
xlabel('load frequency [Hz]'); ylabel('Module of the Dynamic Flexibility or FRF [ft/Kip]');
legend('c = 0.0', 'c = 0.2 ca', 'c = 0.4 ca', 'c = 0.6 ca', 'c = 0.8 ca', 'c = 1.0 ca');

```

I Influence of the Soil Mass Distribution

The Matlab programs (worksheets) developed to compute the frequency response function (dynamic flexibility) of the Spring-Mass system and the pile head, used to obtain the results of in Section 6.3, are listed in this appendix.

I.1 FRF For a System with Springs in Series

```
%----- Programa FRFDistributedMass.m-----%
% Program to compute the dynamic flexibility of a SDOF
% with different number of springs in series (but same stiffness)
% And different mass distribution
%-----%
clc; clear all; close all

% *****
% * PROBLEM DATA
% *****

% Model Data
ks = 1000. *(1+0.05i); % spring stiffness
m = 10.; % mass
ma = 50.; % added mass

FreqMax = 10;
NFreq = 1000;

% *****
% * PROBLEM ANALYSIS
% *****

% ARRAYS DEFINITION

K = zeros(10,10);
M1 = zeros(10,10);
M2 = zeros(10,10);
KD1 = zeros(10,10);
KD2 = zeros(10,10);

F = zeros(10); % Load vector

U1 = zeros(10); % System Displacement vector
U2 = zeros(10);

FRF1 = zeros(NFreq+1); % FRF SDOF
FRF2 = zeros(NFreq+1); % FRF Series springs, lumped mass
FRF3 = zeros(NFreq+1); % FRF Series springs, distributed mass
freq = zeros(NFreq+1); % Frequency data points

% UNIT LOAD ON TOP
F(1) = 1.0;

% STIFFNESS MATRIX
for jj = 1 : 9
    dof(1) = jj;
    dof(2) = jj+1;
    for kk = 1 : 2
        for ll = 1 : 2
            row = dof(kk);
            col = dof(ll);
            K(row,col) = K(row,col) + ks*10*(-1)^(kk+ll);
        end
    end
end
```

```

        end
    end
    K(10,10)=K(10,10)+ks*10;
    K

% MASS MATRIX
M1(1,1)=m+ma;
M2(1,1)=m;
for jj = 1 : 10
    M2(jj,jj) = M2(jj,jj) + ma/10;
end
M1
M2

% FRF FUNCTION
for JJ = 1 : NFreq+1
    freq(JJ) = FreqMax*(JJ-1)/NFreq;
    w=freq(JJ)*2*pi;

    % SYSTEM DYNAMIC STIFFNESS
    KD1 = K - w^2 * M1;
    KD2 = K - w^2 * M2;

    % FREQUENCY RESPONSE FUNCTION FRF
    U1 = KD1\F;
    U2 = KD2\F;

    FRF1(JJ) = sqrt(real(1/(ks-w^2*m))^2+imag(1/(ks-w^2*m))^2);
    FRF2(JJ) = sqrt(real(U1(1))^2+imag(U1(1))^2);
    FRF3(JJ) = sqrt(real(U2(1))^2+imag(U2(1))^2);

    var1 = num2str(JJ);
    var2 = num2str(freq(JJ));
    var3 = num2str(FRF1(JJ));
    var4 = num2str(FRF2(JJ));
    var5 = num2str(FRF3(JJ));
    var6 = strcat( var1 , ',' , var2 , ',' , var3 , ',' , var4 , ',' , var5);

    disp(var6)
end

figure; plot( freq,FRF1, freq, FRF2, freq, FRF3 ); grid on; title('FRF Multiple Springs');
xlabel('load frequency [Hz]'); ylabel('Module of the Dynamic Flexibility or FRF [L/F]');

```

I.2 FRF For a System with Springs in Parallel

```

%----- Programa FRFDistributedMassWithParallelSpring.m-----%
% Program to compute the dynamic flexibility of a SDOF %
% with different number of springs in series (but same stiffness) %
% And different mass distribution %
% And a parallel spring to provide alternate path to the waves %
%-----%
clc; clear all; close all

% *****
% * PROBLEM DATA *
% *****

% Model Data
ks = 1000.*(1+0.05i); % spring stiffness
m = 10.; % mass
ma = 50.; % added mass

FreqMax = 6;
NFreq = 1000;

```

```

nss = 2; % number of series springs
nps = 6; % number of parallel springs

% *****
% * PROBLEM ANALYSIS *
% *****

% ARRAYS DEFINITION

K2 = zeros(1,1);
K3 = zeros(2*nss-1+nps, 2*nss-1+nps);

M2 = zeros(1,1);
M3 = zeros(2*nss-1+nps, 2*nss-1+nps);

KD2 = zeros(1,1);
KD3 = zeros(2*nss-1+nps, 2*nss-1+nps);

F2 = zeros(1); % Load vector
F3 = zeros(2*nss-1+nps);

U2 = zeros(1); % System Displacement vector
U3 = zeros(2*nss-1+nps);

FRF1 = zeros(NFreq+1); % FRF SDOF
FRF2 = zeros(NFreq+1); % FRF SDOF with Lumped Added Mass
FRF3 = zeros(NFreq+1); % FRF Series Springs and Parallel,
Distributed Added Mass

freq = zeros(NFreq+1); % Frequency data points

% UNIT LOAD ON TOP
F2(1) = 1.0;
F3(nss) = 1.0;

% STIFFNESS MATRIX

K2(1,1) = ks;

K3(1,1) = ks*nss/2;
K3(2*nss-1, 2*nss-1) = ks*nss/2;
for jj = 2 : (2*nss-1)
    dof(1) = jj-1;
    dof(2) = jj;
    for kk = 1 : 2
        for ll = 1 : 2
            row = dof(kk);
            col = dof(ll);
            K3(row,col) = K3(row,col) + ks*nss/2*(-1)^(kk+ll);
        end
    end
end
for jj = 1 : nps
    dof(1) = nss-1;
    dof(2) = 2*nss-1+jj;
    for kk = 1 : 2
        for ll = 1 : 2
            row = dof(kk);
            col = dof(ll);
            K3(row,col) = K3(row,col) + ks*nss/(2*(nps+1))*(-1)^(kk+ll);
        end
    end
    dof(1) = 2*nss-1+jj;
    dof(2) = nss+1;
    for kk = 1 : 2
        for ll = 1 : 2
            row = dof(kk);
            col = dof(ll);
            K3(row,col) = K3(row,col) + ks*nss/(2*(nps+1))*(-1)^(kk+ll);
        end
    end
end

% MASS MATRIX

```

```

M2(1,1)=m+ma;

M3(nss,nss)=m;
for jj = 1 : (2*nss-1+nps)
    M3(jj,jj) = M3(jj,jj) + ma/(2*nss-1+nps);
end

% FRF FUNCTION
for jj = 1 : NFreq+1
    freq(jj) = FreqMax*(jj-1)/NFreq;
    w=freq(jj)*2*pi;

    % SYSTEM DYNAMIC STIFFNESS
    KD2 = K2 - w^2 * M2;
    KD3 = K3 - w^2 * M3;

    % FREQUENCY RESPONSE FUNCTION FRF
    U2 = KD2\F2;
    U3 = KD3\F3;

    FRF1(jj) = sqrt(real(1/(ks-w^2*m))^2+imag(1/(ks-w^2*m))^2);
    FRF2(jj) = sqrt(real(U2(1))^2+imag(U2(1))^2);
    FRF3(jj) = sqrt(real(U3(nss))^2+imag(U3(nss))^2);

    var1 = num2str(jj);
    var2 = num2str(freq(jj));
    var3 = num2str(FRF1(jj));
    var4 = num2str(FRF2(jj));
    var5 = num2str(FRF3(jj));
    var6 = strcat( var1 , ',' , var2 , ',' , var3 , ',' , var4 , ',' , var5);

    disp(var6)
end

figure; plot( freq,FRF1, freq, FRF2, freq, FRF3); grid on; title('FRF Multiple Springs');
xlabel('load frequency [Hz]'); ylabel('Module of the Dynamic Flexibility or FRF [L/F]');

```

I.3 FRF For a Pile-Soil System with Springs in Series

```

%----- Programa FRFPileSoilDistributedMass.m-----%
% Program to compute the dynamic flexibility of a pile head %
% using the equivalent lumped model obtained by regression of the %
% dynamic stiffness proposed by Novak for the soil. %
% Then representing the soil as a series of springs and a distributed %
% mass among spring nodes %
% %
%-----%
clc; clear all; close all

% *****
% * PROBLEM DATA *
% *****

% SOIL DATA
Es = 1728000*(1+0.05i); % soil Young's elastic modulus[lb/ft^2]
nu = 0.40; % soil Poisson's ratio
D=0.0; % hysteretic damping ratio
sw = 110.0; % soil specific weight [pcf]

% PILE DATA
ro = 1.0; % pile radius
L = 30.0; % pile length
Ep = 518400000.0*(1+0.05i); % pile Young's modulus
pw = 150.0; % pile specific weight

% GENERAL DATA

```

```

ne = 15; % number of elements to discretize the
pile %
g = 32.2; % gravity acceleration [ft/sec^2]
FreqMax = 100; % maximum frequency [Hz]
NFreq = 1000; % Number of frequency steps

nss = 10; % number of series springs
ma = 20*20*sw/5; % Soil mass to be added, from 3D FEM
analysis % with partial soil mass

% Lumped model coefficients
ak = 1.3272671;
am = 0.0510557;
ac = 3.4246489;

% *****
% * PROBLEM ANALYSIS *
% *****

% GENERAL COMPUTATION
sm = sw/g; % density of soil [lb.s^2/ft^4]
G = Es/(2*(1+nu)); % soil shear elastic modulus[lb/ft]
Vs = sqrt(G/sm); % shear wave velocity [ft/sec]
Le = L/ne; % pile element length
pm = pw/g; % density of pile [lb.s^2/ft^4]

% ARRAYS DEFINITION
%
% The KDP, UP and FRFP variables refer to the system reponse without
% considering soil contribution (just the pile contribution).
%
KD = zeros(2*ne, 2*ne); % System dynamic stiffness matrix
KDP = zeros(2*ne, 2*ne); % Pile dynamic stiffness matrix

KP = zeros(2*ne, 2*ne); % Pile Stiffness matrix
KS = zeros(2*ne, 2*ne); % Soil Dynamic Stiffness Matrix
Ke = zeros(4, 4); % Pile element stiffness matrix

MP = zeros(2*ne, 2*ne); % Pile mass matrix
MS = zeros(2*ne, 2*ne); % Soil mass matrix
MT = zeros(2*ne, 2*ne); % System mass matrix

CS = zeros(2*ne, 2*ne); % Soil damping matrix

F = zeros(2*ne); % Load vector

U = zeros(2*ne); % System Displacement vector
UP = zeros(2*ne); % Pile Displacement vector

FRF = zeros(NFreq+1); % FRF = top node displacement
FRFM = zeros(NFreq+1); % FRF Module top node displacement
FRFP = zeros(NFreq+1); % FRF Pile top node displacement
freq = zeros(NFreq+1); % Frequency data points

% DOF = 2*ne + (nss-1)*ne
KSSS = zeros((nss+1)*ne, (nss+1)*ne);
MSSS = zeros((nss+1)*ne, (nss+1)*ne);
KPSS = zeros((nss+1)*ne, (nss+1)*ne);
MPSS = zeros((nss+1)*ne, (nss+1)*ne);
KDSS = zeros((nss+1)*ne, (nss+1)*ne);
FSS = zeros((nss+1)*ne);
USS = zeros((nss+1)*ne);
FRFSS = zeros(NFreq+1);

% UNIT LOAD ON TOP
F(1) = 1000.0; % Unit harmonic load on top of pile
% to obtain dynamic flexibility in
% [ft/Kip] units

FSS(1) = 1000.0;

% PILE ELEMENT STIFFNESS MATRIX
Ip = pi*ro^4/4.; % Pile cross section inertia
Ap = pi*ro^2; % Pile cross section area

k1 = 4*Ep*Ip/Le;

```

```

k2 = 6*Ep*Ip/Le^2;
k3 = 12*Ep*Ip/Le^3;

Ke(1,1) = k3;
Ke(2,1) = k2;
Ke(3,1) = -k3;
Ke(4,1) = k2;

Ke(1,2) = k2;
Ke(2,2) = k1;
Ke(3,2) = -k2;
Ke(4,2) = k1/2;

Ke(1,3) = -k3;
Ke(2,3) = -k2;
Ke(3,3) = k3;
Ke(4,3) = -k2;

Ke(1,4) = k2;
Ke(2,4) = k1/2;
Ke(3,4) = -k2;
Ke(4,4) = k1;

% PILE STIFFNESS MATRIX
for jj = 1 : ne-1
    dof(1) = jj*2-1;
    dof(2) = jj*2;
    dof(3) = jj*2+1;
    dof(4) = jj*2+2;
    for kk = 1 : 4
        for ll = 1 : 4
            row = dof(kk);
            col = dof(ll);
            KP(row,col) = KP(row,col) + Ke(kk,ll);
            KPSS(row,col) = KPSS(row,col) + Ke(kk,ll);
        end
    end
end

dof(1) = ne*2-1;
dof(2) = ne*2;
for kk = 1 : 2
    for ll = 1 : 2
        row = dof(kk);
        col = dof(ll);
        KP(row,col) = KP(row,col) + Ke(kk,ll);
        KPSS(row,col) = KPSS(row,col) + Ke(kk,ll);
    end
end

% PILE MASS MATRIX
MP(1,1) = pm*Ap*Le/2;
MPSS(1,1) = pm*Ap*Le/2;
for jj = 2 : ne
    MP(2*jj-1,2*jj-1) = pm*Ap*Le;
    MPSS(2*jj-1,2*jj-1) = pm*Ap*Le;
end

% SOIL STIFFNESS MATRIX, MASS MATRIX, AND DAMPING MATRIX
KS(1,1) = pi*G*ak*Le/2;
MS(1,1) = pi*ro^2*sm*am*Le/2;
CS(1,1) = pi*ro*G/Vs*ac*Le/2;

MSSS(1,1) = ma * Le/2 / (ne*nss);

for jj = 2 : ne
    KS(2*jj-1,2*jj-1) = pi*G*ak*Le;
    MS(2*jj-1,2*jj-1) = pi*ro^2*sm*am*Le;
    CS(2*jj-1,2*jj-1) = pi*ro*G/Vs*ac*Le;

    MSSS(2*jj-1,2*jj-1) = ma * Le / (ne*nss);
end

for ll = 1 : ne
    if (ll < 2)
        Ls = Le/2;
    end
end

```

```

else
    Ls = Le;
end

KSSS(ne*2+ (nss-1)*(ll-1)+ 1, ne*2+ (nss-1)*(ll-1)+ 1) = nss *pi *G*ak*Ls;

for jj = 2 : nss;
    dof(1) = ne*2+ (nss-1)*(ll-1)+ (jj-1);
    if (jj < nss)
        dof(2) = dof(1)+1;
    else
        dof(2) = (ll-1)*2+1;
    end

    for kk = 1 : 2
        for ll = 1 : 2
            row = dof(kk);
            col = dof(ll);
            KSSS(row, col) = KSSS(row, col) + nss *pi *G*ak*Ls*(-1)^(kk+ll);
        end
    end

    MSSS(dof(1), dof(1)) = MSSS(dof(1), dof(1)) + ma * Ls / (ne*nss);
end
end

MT = MP + MS;

% FRF FUNCTION
for jj = 1 : NFreq+1
    freq(jj) = FreqMax*(jj-1)/NFreq;
    w=freq(jj)*2*pi;

    % SYSTEM DYNAMIC STIFFNESS
    KD = KP + KS + I * w * CS - w^2 * MT;
    KDP = KP - w^2 * MP;
    KDSS = KPSS + KSSS - w^2 * (MPSS+MSSS);

    % FREQUENCY RESPONSE FUNCTION FRF
    U = KD\F;
    FRFM(jj) = sqrt(real(U(1))^2+imag(U(1))^2);
    FRF(jj) = U(1);

    UP = KDP\F;
    FRFP(jj) = sqrt(real(UP(1))^2+imag(UP(1))^2);

    USS = KDSS\FSS;
    FRFSS(jj) = sqrt(real(USS(1))^2+imag(USS(1))^2);

    var1 = num2str(jj);
    var2 = num2str(freq(jj));
    var3 = num2str(FRFM(jj));
    var4 = num2str(FRFSS(jj));
    var5 = strcat( var1, ', ', var2, ', ', var3, ', ', var4);
    % save ('FRF.txt', 'var1', 'var2', '-ASCII', '-append')
    disp(var5)
end

% figure; plot( freq,FRFM ); grid on; title('FRF Using Lumped Model')
% xlabel('load frequency [Hz]'); ylabel('Module of the Dynamic Flexibility or FRF [ft/Kip]');

figure; plot( freq,FRFM, freq, FRFSS ); grid on; title('FRF Lumped Model vs Series of Springs and Masses')
xlabel('load frequency [Hz]'); ylabel('Module of the Dynamic Flexibility or FRF [ft/Kip]');

% figure; plot( freq, FRFP ); grid on; title('FRF Pile Alone')
% xlabel('load frequency [Hz]'); ylabel('Module of the Dynamic Flexibility or FRF [ft/Kip]');

```


I.4 FRF For a Pile-Soil System with Springs in Parallel

```

%----- Programa FRFPileSoilDistributedMassParallel.m -----%
% Program to compute the dynamic flexibility of a pile head %
% using the equivalent lumped model obtained by regression of the %
% dynamic stiffness proposed by Novak for the soil. %
% Then representing the soil as a two series springs and a set of %
% parallel springs, and a distributed mass among spring nodes %
% %
%-----%
clc; clear all; close all

% *****
% * PROBLEM DATA *
% *****

% SOIL DATA
Es = 1728000*(1+0.05i); % soil Young's elastic modulus [lb/ft^2]
nu = 0.40; % soil Poisson's ratio
D=0.0; % hysteretic damping ratio
sw = 110.0; % soil specific weight [pcf]

% PILE DATA
ro = 1.0; % pile radius
L = 30.0; % pile length
Ep = 518400000.0*(1+0.05i); % pile Young's modulus
pw = 150.0; % pile specific weight

% GENERAL DATA
ne = 15; % number of elements to discretize the
pile %
g = 32.2; % gravity acceleration [ft/sec^2]
FreqMax = 100; % maximum frequency [Hz]
NFreq = 1000; % Number of frequency steps

nss = 2; % number of series springs
nps = 10; % number of parallel springs
ma = 20*20*sw; % Soil mass to be added, from 3D FEM
analysis % with partial soil mass

% Lumped model coefficients
ak = 1.3272671;
am = 0.0510557;
ac = 3.4246489;

% *****
% * PROBLEM ANALYSIS *
% *****

% GENERAL COMPUTATION
sm = sw/g; % density of soil [lb.s^2/ft^4]
G = Es/(2*(1+nu)); % soil shear elastic modulus [lb/ft]
Vs = sqrt(G/sm); % shear wave velocity [ft/sec]
Le = L/ne; % pile element length
pm = pw/g; % density of pile [lb.s^2/ft^4]

% ARRAYS DEFINITION
%
% The KDP, UP and FRFP variables refer to the system reponse without
% considering soil contribution (just the pile contribution).
%
KD = zeros(2*ne, 2*ne); % System dynamic stiffness matrix
KDP = zeros(2*ne, 2*ne); % Pile dynamic stiffness matrix

KP = zeros(2*ne, 2*ne); % Pile Stiffness matrix
KS = zeros(2*ne, 2*ne); % Soil Dynamic Stiffness Matrix
Ke = zeros(4, 4); % Pile element stiffness matrix

MP = zeros(2*ne, 2*ne); % Pile mass matrix
MS = zeros(2*ne, 2*ne); % Soil mass matrix
MT = zeros(2*ne, 2*ne); % System mass matrix

CS = zeros(2*ne, 2*ne); % Soil damping matrix

F = zeros(2*ne); % Load vector

```

```

U = zeros(2*ne); % System Displacement vector
UP = zeros(2*ne); % Pile Displacement vector

FRF = zeros(NFreq+1); % FRF = top node displacement
FRFM = zeros(NFreq+1); % FRF Module top node displacement
FRFP = zeros(NFreq+1); % FRF Pile top node displacement
freq = zeros(NFreq+1); % Frequency data points

TD0F = 2*ne + ((nss-1)*2+ nps)*ne; % Total DOF
TSN = (nss-1)*2+ nps + 1; % Total Spring Nodes per Layer
KSPS = zeros(TD0F, TD0F);
MSPS = zeros(TD0F, TD0F);
KPPS = zeros(TD0F, TD0F);
MPPS = zeros(TD0F, TD0F);
KDPS = zeros(TD0F, TD0F);
FPS = zeros(TD0F);
UPS = zeros(TD0F);
FRFPS = zeros(NFreq+1);

% UNIT LOAD ON TOP
F(1) = 1000.0; % Unit harmonic load on top of pile
% to obtain dynamic flexibility in
% [ft/Kip] units

FPS(1) = 1000.0;

% PILE ELEMENT STIFFNESS MATRIX
Ip = pi*ro^4/4.; % Pile cross section inertia
Ap = pi*ro^2; % Pile cross section area

k1 = 4*Ep*Ip/Le;
k2 = 6*Ep*Ip/Le^2;
k3 = 12*Ep*Ip/Le^3;

Ke(1,1) = k3;
Ke(2,1) = k2;
Ke(3,1) = -k3;
Ke(4,1) = k2;

Ke(1,2) = k2;
Ke(2,2) = k1;
Ke(3,2) = -k2;
Ke(4,2) = k1/2;

Ke(1,3) = -k3;
Ke(2,3) = -k2;
Ke(3,3) = k3;
Ke(4,3) = -k2;

Ke(1,4) = k2;
Ke(2,4) = k1/2;
Ke(3,4) = -k2;
Ke(4,4) = k1;

% PILE STIFFNESS MATRIX
for jj = 1 : ne-1
    dof(1) = jj*2-1;
    dof(2) = jj*2;
    dof(3) = jj*2+1;
    dof(4) = jj*2+2;
    for kk = 1 : 4
        for ll = 1 : 4
            row = dof(kk);
            col = dof(ll);
            KP(row,col) = KP(row,col) + Ke(kk,ll);
            KPPS(row,col) = KPPS(row,col) + Ke(kk,ll);
        end
    end
end

dof(1) = ne*2-1;
dof(2) = ne*2;
for kk = 1 : 2
    for ll = 1 : 2
        row = dof(kk);
        col = dof(ll);

```

```

        KP(row,col) = KP(row,col) + Ke(kk,ll);
        KPPS(row,col) = KPPS(row,col) + Ke(kk,ll);
    end
end

% PILE MASS MATRIX
MP(1,1) = pm*Ap*Le/2;
MPPS(1,1) = pm*Ap*Le/2;
for jj = 2 : ne
    MP(2*jj-1,2*jj-1) = pm*Ap*Le;
    MPPS(2*jj-1,2*jj-1) = pm*Ap*Le;
end

% SOIL STIFFNESS MATRIX, MASS MATRIX, AND DAMPING MATRIX
KS(1,1) = pi *G*ak*Le/2;
MS(1,1) = pi *ro^2*sm*am*Le/2;
CS(1,1) = pi *ro*G/Vs*ac*Le/2;
for jj = 2 : ne
    KS(2*jj-1,2*jj-1) = pi *G*ak*Le;
    MS(2*jj-1,2*jj-1) = pi *ro^2*sm*am*Le;
    CS(2*jj-1,2*jj-1) = pi *ro*G/Vs*ac*Le;
end

% SOIL AS PARALLEL SPRINGS AND MASSES
for ll = 1 : ne
    if (ll < 2)
        Ls = Le/2;
    else
        Ls = Le;
    end
    ksref = pi *G*ak*Ls*nss/2;
    mref = ma*Ls/TSN;

    %first two series springs nss = 2
    dof(1) = 2*ne + (2+nps)*(ll-1)+1 ;
    dof(2) = (ll-1)*2+1;
    for kk = 1 : 2
        for ll = 1 : 2
            row = dof(kk);
            col = dof(ll);
            KSPS(row,col) = KSPS(row,col) + ksref;
        end
    end
    KSPS(dof(1),dof(1)) = KSPS(dof(1),dof(1)) + ksref;
    MSPS(dof(1),dof(1)) = MSPS(dof(1),dof(1)) + mref;
    MSPS(dof(2),dof(2)) = MSPS(dof(2),dof(2)) + mref;

    %second two series springs
    dof(1) = 2*ne + (2+nps)*(ll-1)+2 ;
    dof(2) = (ll-1)*2+1;
    for kk = 1 : 2
        for ll = 1 : 2
            row = dof(kk);
            col = dof(ll);
            KSPS(row,col) = KSPS(row,col) + ksref;
        end
    end
    KSPS(dof(1),dof(1)) = KSPS(dof(1),dof(1)) + ksref;
    MSPS(dof(1),dof(1)) = MSPS(dof(1),dof(1)) + mref;

    %set of parallel springs
    for jj = 1 : nps
        dof(1) = 2*ne + (2+nps)*(ll-1)+1;
        dof(2) = 2*ne + (2+nps)*(ll-1)+2+jj;
        for kk = 1 : 2
            for ll = 1 : 2
                row = dof(kk);
                col = dof(ll);
                KSPS(row,col) = KSPS(row,col) + ksref/(nps+1);
            end
        end
        MSPS(dof(2),dof(2)) = MSPS(dof(2),dof(2)) + mref;

        dof(1) = 2*ne + (2+nps)*(ll-1)+2;
        dof(2) = 2*ne + (2+nps)*(ll-1)+2+jj;
        for kk = 1 : 2

```

```

        for ll = 1 : 2
            row = dof(kk);
            col = dof(ll);
            KSPS(row, col) = KSPS(row, col) + ksref/(nps+1);
        end
    end
end

end

MT = MP + MS;

% FRF FUNCTION
for JJ = 1 : NFreq+1

    freq(JJ) = FreqMax*(JJ-1)/NFreq;
    w=freq(JJ)*2*pi;

    % SYSTEM DYNAMIC STIFFNESS
    KD = KP + KS + I * w * CS - w^2 * MT;
    KDP = KP - w^2 * MP;
    KDPS = KP + KS - w^2 * (MPPS+MSPS);

    % FREQUENCY RESPONSE FUNCTION FRF
    U = KD\F;
    FRFM(JJ) = sqrt(real(U(1))^2+imag(U(1))^2);
    FRF(JJ) = U(1);

    UP = KDP\F;
    FRFP(JJ) = sqrt(real(UP(1))^2+imag(UP(1))^2);

    UPS = KDPS\FPS;
    FRFPS(JJ) = sqrt(real(UPS(1))^2+imag(UPS(1))^2);

    var1 = num2str(JJ);
    var2 = num2str(freq(JJ));
    var3 = num2str(FRFM(JJ));
    var4 = num2str(FRFP(JJ));
    var5 = strcat( var1, ' ', var2, ' ', var3, ' ', var4);
    % save ('FRF.txt', 'var1', 'var2', '-ASCII', '-append')
    disp(var5)

end

% figure; plot( freq,FRFM ); grid on; title('FRF Using Lumped Model')
% xlabel('load frequency [Hz]'); ylabel('Module of the Dynamic Flexibility or FRF [ft/Kip]');

figure; plot( freq,FRFM, freq, FRFPS ); grid on; title('FRF Lumped Model vs Series of Springs and Masses')
xlabel('load frequency [Hz]'); ylabel('Module of the Dynamic Flexibility or FRF [ft/Kip]');

% figure; plot( freq, FRFP ); grid on; title('FRF Pile Alone')
% xlabel('load frequency [Hz]'); ylabel('Module of the Dynamic Flexibility or FRF [ft/Kip]');

```

I.5 FRF For a Pile-Soil System with Single Spring

```

%----- Programa FRFPileSoilLumpedMass.m-----%
% Program to compute the dynamic flexibility of a pile head %
% using the equivalent lumped model obtained by regression of the %
% dynamic stiffness proposed by Novak for the soil. %
% Then representing the soil as a single spring and a and a lumped %
% mass among pile nodes %
%-----%
clc; clear all; close all

```

```

% *****
% * PROBLEM DATA *
% *****

% SOIL DATA
Es = 1728000*(1+0.05i); % soil Young's elastic modulus[lb/ft^2]
nu = 0.40; % soil Poisson's ratio
D=0.0; % hysteretic damping ratio
sw = 110.0; % soil specific weight [pcf]

% PILE DATA
ro = 1.0; % pile radius
L = 30.0; % pile length
Ep = 518400000.0*(1+0.05i); % pile Young's modulus
pw = 150.0; % pile specific weight

% GENERAL DATA
ne = 15; % number of elements to discretize the
pile %
g = 32.2; % gravity acceleration [ft/sec^2]
FreqMax = 100; % maximum frequency [Hz]
NFreq = 1000; % Number of frequency steps

nss = 10; % number of series springs
ma = 20*20*sw/5; % Soil mass to be added, from 3D FEM
analysis % with partial soil mass

% Lumped model coefficients
ak = 1.3272671;
am = 0.0510557;
ac = 3.4246489;

% *****
% * PROBLEM ANALYSIS *
% *****

% GENERAL COMPUTATION
sm = sw/g; % density of soil [lb.s^2/ft^4]
G = Es/(2*(1+nu)); % soil shear elastic modulus[lb/ft]
Vs = sqrt(G/sm); % shear wave velocity [ft/sec]
Le = L/ne; % pile element length
pm = pw/g; % density of pile [lb.s^2/ft^4]

% ARRAYS DEFINITION
%
% The KDP, UP and FRFP variables refer to the system response without
% considering soil contribution (just the pile contribution).
%
KD = zeros(2*ne, 2*ne); % System dynamic stiffness matrix
KDP = zeros(2*ne, 2*ne); % Pile dynamic stiffness matrix

KP = zeros(2*ne, 2*ne); % Pile Stiffness matrix
KS = zeros(2*ne, 2*ne); % Soil Dynamic Stiffness Matrix
Ke = zeros(4, 4); % Pile element stiffness matrix

MP = zeros(2*ne, 2*ne); % Pile mass matrix
MS = zeros(2*ne, 2*ne); % Soil mass matrix
MT = zeros(2*ne, 2*ne); % System mass matrix

CS = zeros(2*ne, 2*ne); % Soil damping matrix

F = zeros(2*ne); % Load vector

U = zeros(2*ne); % System Displacement vector
UP = zeros(2*ne); % Pile Displacement vector

FRF = zeros(NFreq+1); % FRF = top node displacement
FRFM = zeros(NFreq+1); % FRF Module top node displacement
FRFP = zeros(NFreq+1); % FRF Pile top node displacement
freq = zeros(NFreq+1); % Frequency data points

% DOF = 2*ne + (nss-1)*ne
KSLS = zeros(2*ne, 2*ne);
MSLS = zeros(2*ne, 2*ne);
KPLS = zeros(2*ne, 2*ne);
MPLS = zeros(2*ne, 2*ne);

```

```

KDLS = zeros(2*ne, 2*ne);
FLS = zeros(2*ne, 2*ne);
ULS = zeros(2*ne, 2*ne);
FRFLS = zeros(NFreq+1);

% UNIT LOAD ON TOP
F(1) = 1000.0; % Unit harmonic load on top of pile
                % to obtain dynamic flexibility in
                % [ft/Kip] units

FLS(1) = 1000.0;

% PILE ELEMENT STIFFNESS MATRIX
Ip = pi*ro^4/4.; % Pile cross section inertia
Ap = pi*ro^2;    % Pile cross section area

k1 = 4*Ep*Ip/Le;
k2 = 6*Ep*Ip/Le^2;
k3 = 12*Ep*Ip/Le^3;

Ke(1,1) = k3;
Ke(2,1) = k2;
Ke(3,1) = -k3;
Ke(4,1) = k2;

Ke(1,2) = k2;
Ke(2,2) = k1;
Ke(3,2) = -k2;
Ke(4,2) = k1/2;

Ke(1,3) = -k3;
Ke(2,3) = -k2;
Ke(3,3) = k3;
Ke(4,3) = -k2;

Ke(1,4) = k2;
Ke(2,4) = k1/2;
Ke(3,4) = -k2;
Ke(4,4) = k1;

% PILE STIFFNESS MATRIX
for jj = 1 : ne-1
    dof(1) = jj*2-1;
    dof(2) = jj*2;
    dof(3) = jj*2+1;
    dof(4) = jj*2+2;
    for kk = 1 : 4
        for ll = 1 : 4
            row = dof(kk);
            col = dof(ll);
            KP(row,col) = KP(row,col) + Ke(kk,ll);
            KPLS(row,col) = KPLS(row,col) + Ke(kk,ll);
        end
    end
end

dof(1) = ne*2-1;
dof(2) = ne*2;
for kk = 1 : 2
    for ll = 1 : 2
        row = dof(kk);
        col = dof(ll);
        KP(row,col) = KP(row,col) + Ke(kk,ll);
        KPLS(row,col) = KPLS(row,col) + Ke(kk,ll);
    end
end

% PILE MASS MATRIX
MP(1,1) = pm*Ap*Le/2;
MPSS(1,1) = pm*Ap*Le/2;
for jj = 2 : ne
    MP(2*jj-1, 2*jj-1) = pm*Ap*Le;
    MPLS(2*jj-1, 2*jj-1) = pm*Ap*Le;
end

% SOIL STIFFNESS MATRIX, MASS MATRIX, AND DAMPING MATRIX
KS(1,1) = pi*G*ak*Le/2;

```

```

MS(1,1) = pi*ro^2*sm*am*Le/2;
CS(1,1) = pi*ro*G/Vs*ac*Le/2;

MSLS(1,1) = ma * Le/2;

for jj = 2 : ne
    KS(2*jj-1, 2*jj-1) = pi * G * ak * Le;
    MS(2*jj-1, 2*jj-1) = pi * ro^2 * sm * am * Le;
    CS(2*jj-1, 2*jj-1) = pi * ro * G / Vs * ac * Le;

    MSLS(2*jj-1, 2*jj-1) = ma * Le;
    KSLS(2*jj-1, 2*jj-1) = pi * G * ak * Le;
end

MT = MP + MS;

% FRF FUNCTION

for jj = 1 : NFreq+1

    freq(jj) = FreqMax*(jj-1)/NFreq;
    w=freq(jj)*2*pi;

    % SYSTEM DYNAMIC STIFFNESS
    KD = KP + KS + I * w * CS - w^2 * MT;
    KDP = KP - w^2 * MP;
    KDLS = KPLS + KSLS - w^2 * (MPLS+MSLS);

    % FREQUENCY RESPONSE FUNCTION FRF
    U = KD\F;
    FRFM(jj) = sqrt(real(U(1))^2+imag(U(1))^2);
    FRF(jj) = U(1);

    UP = KDP\F;
    FRFP(jj) = sqrt(real(UP(1))^2+imag(UP(1))^2);

    ULS = KDLS\FLS;
    FRFLS(jj) = sqrt(real(ULS(1))^2+imag(ULS(1))^2);

    var1 = num2str(jj);
    var2 = num2str(freq(jj));
    var3 = num2str(FRFM(jj));
    var4 = num2str(FRFLS(jj));
    var5 = strcat( var1, ',', var2, ',', var3, ',', var4);
    % save ('FRF.txt', 'var1', 'var2', '-ASCII', '-append')
    disp(var5)

end

% figure; plot( freq,FRFM ); grid on; title('FRF Using Lumped Model')
% xlabel('load frequency [Hz]'); ylabel('Module of the Dynamic Flexibility or FRF [ft/Kip]');

figure; plot( freq,FRFM, freq, FRFLS ); grid on; title('FRF Lumped Model vs Series of Springs and Masses')
xlabel('load frequency [Hz]'); ylabel('Module of the Dynamic Flexibility or FRF [ft/Kip]');

% figure; plot( freq, FRFP ); grid on; title('FRF Pile Alone')
% xlabel('load frequency [Hz]'); ylabel('Module of the Dynamic Flexibility or FRF [ft/Kip]');

```